Università degli studi di Napoli Federico II

Ph.D. Thesis

in

Information Technology and Electrical Engineering

C-ITS services and advanced vehicle control for complex traffic scenarios

Angelo Coppola

Tutor

Prof. Stefania Santini

Co-Tutor

Anita Fiorentino, Stellantis Group

Coordinator

Prof. Daniele Riccio

XXXIV Cycle

Scuola Politecnica e delle Scienze di Base

Department of Information Technology
and Electrical Engineering (DIETI)

"It is the nature of science that answers automatically pose new and more subtle question"

Isaac Asimov

ABSTRACT

The deployment of innovative, fully automated C-ITS connected mobility services is expected to mitigate traffic congestion - making cities and human settlements safe, resilient, sustainable - and decrease the number of road accidents. However, the spread of automated and connected vehicles into existing traffic poses specific and new problems regarding reliability and effectiveness, particularly concerning interactions with other vehicles and with other actors. Furthermore, automated driving systems must be suitably designed to be resilient to both the uncertainties of V2X (Vehicle-to-Vehicle or Vehicle-to-Infrastructure) communication and drivers to ensure sufficient reliability and robustness in any traffic situation in the real world. Within this framework, this thesis deals with the following challenges: *i*) develop innovative, reliable and resilient C-ITS strategies for cooperation between vehicles and between vehicles and infrastructures, based on V2X communication; *ii*) test and validate C-ITS strategies in complex and realistic traffic conditions. In the light of the first goal, different control strategies addressing many various issues are proposed for both urban and extra-urban traffic scenarios as well as for both mixed and fully-autonomous traffic flows. To achieve goal 2, a novel Integrated Simulation Environment, named Mixed Traffic Simulator (MiTraS), for the assessment and evaluation of C-ITS services is proposed. It embeds different interacting simulation tools within a holistic view of the co-simulation approach to be as realistic as possible.

Contents

1 Introduction **3**
1.1 Motivation and Contributions 3
1.2 Thesis Outline 8

2 Cooperative Intelligent Transport Systems and Services **13**
2.1 The European Framework 15
2.1.1 Italian Roadmap for C-ITS 21
2.2 Advanced Driver-Assistance Systems 22
2.3 C-ITS Services 25
2.4 Communication Standard 29
2.4.1 DSRC-Based V2X 30
2.4.2 Cellular V2X 32
2.4.3 Comparison between Cellular and Non-Cellular V2X Technologies 33
2.5 Testing and Validation Methods 33
2.5.1 Field Operational Test 34
2.5.1.1 Real-World Traffic Testing 34
2.5.1.2 Closed Area Testing 36
2.5.2 Virtual Testing 38

3 Cooperative Driving Systems **43**
3.1 Modelling of Connected Autonomous Vehicles 47
3.1.1 Agent Dynamics 48
3.1.1.1 Longitudinal Models 49
3.1.1.2 Longitudinal-Lateral Models 52
3.1.2 Communication Topology 55

3.1.3 Formation Geometry 59
3.1.4 Distributed Controller 62
3.2 Consensus and Synchronisation in Networked Dynamical Systems 64
3.2.1 Stability of Continuous-Time Systems 65
3.2.2 Integral Inequalities 66

4 Integrated Simulation Environment 67
4.1 Existing Virtual Testing Environments 69
4.1.1 Microscopic Traffic Simulators 69
4.1.2 Physics-Based Simulators 70
4.1.3 Integrated Simulation Environment 71
4.2 Proposed Integrated Simulation Environment 72
4.2.1 The Role of SUMO 73
4.2.2 The Role of MATLAB/Simulink 74
4.2.3 Co-Simulation Procedure 74
4.3 Modeling 75
4.3.1 Vehicle Model 75
4.3.2 Consumption Models 79
4.3.2.1 Fuel Consumption Model 79
4.3.2.2 Power-Based Energy Consumption Estimation Model 80

5 Development and Testing of a Green Light Optimal Speed Advisory Service Under Different Working Conditions 83
5.1 Green Light Optimal Speed Advisory System 84
5.2 Related Works on GLOSA System 85
5.3 GLOSA Algorithm 90
5.4 Testing Methodology 91
5.4.1 Testing Scenario 92
5.4.2 Traffic Conditions 93
5.4.3 TLS Cycle Duration 95
5.4.3.1 Communication Distance 96
5.4.4 Minimum Speed 96
5.4.5 Traffic Signal Phase Condition 97
5.5 Numerical Analysis 97
5.5.1 Consumption-Related Results 98

5.5.1.1 Validation of Consumption Computing Methods . . . 98
5.5.1.2 Analysis of S-GLOSA Improvement . . . 101
5.5.1.3 Effects of Different Conditions on System Performance - Endothermic Engine . . . 101
5.5.1.4 Effects of Different Conditions on System Performance - Electric Engine . . . 102
5.5.2 Mobility-Related Results . . . 104
5.5.2.1 Analysis of S-GLOSA Improvement . . . 105
5.5.2.2 Effects of Different Conditions on System Performance . . . 105
5.6 Significance of Results . . . 107
5.7 Concluding Remark . . . 111

6 Combined Energy-Oriented Path Following and Collision Avoidance Approach for Autonomous Electric Vehicles via Nonlinear Model Predictive Control 115
6.1 Multiple-Objective Control Problem . . . 116
6.2 Combined Energy-Oriented Path Following and Collision Avoidance Approach . . . 117
6.2.1 Nonlinear Ego-Vehicle Dynamics . . . 118
6.3 Control Design . . . 119
6.3.1 ACC Controller Design . . . 119
6.3.2 NMPC Controller . . . 119
6.3.2.1 Energy Consumption Model for Control Purpose . . . 122
6.4 Numerical Analysis . . . 122
6.4.1 Car-Following and Path-Following Results . . . 125
6.4.2 Energy Consumption Results . . . 126
6.5 Concluding Remarks . . . 127

7 Decentralized Cooperative Crossing at Unsignalized Intersections via Vehicle-to-Vehicle Communication in Mixed Traffic Flows 129
7.1 Cooperative Crossing at Intersection in Mixed Traffic . . . 130
7.2 Unsignalised Intersection Crossing . . . 134
7.2.1 CHV Dynamics . . . 135
7.2.2 CAV Dynamics . . . 137

7.3 Cooperative Distributed Control Protocol for CAV in a Mixed-Traffic Flow . . . 139
7.3.1 Cooperative Time-to-Intersection-Based Longitudinal Controller . . . 140
7.3.2 Lateral Control . . . 146
7.4 Numerical Analysis . . . 147
7.4.1 Case Study . . . 148
7.4.2 Mobility Performance . . . 149
7.4.3 Safety Performance . . . 155
7.5 Concluding Remarks . . . 157

8 Distributed Robust PID-like Control for Heterogeneous Nonlinear Uncertain Autonomous Vehicles Platoon: Design, Analysis and Cooperative manoeuvres Evaluation 159
8.1 Tracking Issues in Cooperative Driving Systems . . . 160
8.2 Cooperative Tracking . . . 164
8.2.1 Nonlinear Longitudinal Uncertain Vehicle Dynamics Model for Control Design . . . 165
8.3 Robust Nonlinear Platooning Control Protocol . . . 169
8.3.1 Closed-Loop Vehicular Network . . . 170
8.4 Stability Analysis . . . 171
8.5 Numerical Analysis . . . 178
8.5.1 Driving Scenario and Manoeuvres . . . 178
8.5.1.1 Platoon Formation and Maintenance . . . 179
8.5.1.2 Leader-Tracking . . . 180
8.5.1.3 Join in-the-middle Manoeuvre . . . 180
8.5.1.4 Leave from-the-middle Manoeuvre . . . 181
8.5.2 Simulation Results . . . 183
8.5.2.1 Platoon Formation and Maintenance . . . 183
8.5.2.2 Leader Tracking for Trapezoidal Speed Profile . . . 185
8.5.2.3 Join in-the-middle Manoeuvre . . . 187
8.5.2.4 Leave from-the-middle Manoeuvre . . . 189
8.5.3 Robustness with respect to Communication Delays 191
8.6 Concluding Remarks . . . 193

9 Distributed Fixed-Time Leader-Tracking Control for Heterogeneous Uncertain Autonomous Connected Vehicles Platoons 195

9.1 Leader-Tracking Control Issues . . . 196
9.2 Mathematical Preliminaries on Fixed-Time . . . 197
9.3 Platooning Control Problem in Fixed-Time . . . 199
9.4 Distributed Fixed-Time Platooning Control . . . 200
9.4.1 Control Design . . . 200
9.4.2 Stability Analysis . . . 202
9.5 Numerical Analysis . . . 204
9.5.1 Leader-Predecessor-Follower Topology Scenario . . 207
9.5.2 Random Topology Scenario . . . 208
9.6 Concluding Remarks . . . 209

10 Distributed Nonlinear Model Predictive Control for Connected Autonomous Electric Vehicles Platoon with Distance-Dependent Air-Drag Formulation 211

10.1 Energy-Saving Challenge in Platooning Applications . . . 212
10.2 E-Platoon Modelling and Control Objectives . . . 215
10.2.1 Nonlinear Longitudinal EV Model . . . 215
10.3 Design of Distributed Distance-Based Nonlinear Model Predictive Control . . . 217
10.4 Numerical Analysis . . . 221
10.4.1 DNMPC vs Pure Diffusive Controller . . . 224
10.5 Concluding Remarks . . . 225

11 Conclusions 231

A Terminology 235

A.1 Autonomous vs. Automated Vehicle . . . 235
A.2 Platooning . . . 236
A.3 Virtual Environment Components . . . 236

B Typical Architecture of Automated/Autonomous Cars 239

B.1 Vehicle Equipment . . . 239
B.1.1 Proprioceptive Sensors . . . 239
B.1.2 Exteroceptive Sensors . . . 241
B.1.3 Computational Units and Actuators . . . 242

B.1.4 Communication Systems 243
B.2 Perception System 243
B.3 Decision Making System 244

List of Acronyms **247**

List of Abbreviations **253**

Bibliography **254**

List of Figures

2.1 Cooperative Intelligent Transportation Systems (C-ITS) scenario: road users communicate information each other. 15
2.2 Exemplar communication paradigm for automated/autonomous car. 16
2.3 European C-ITS framework. 18
2.4 SAE level of automation. 20
2.5 Advanced Driver Assistance Systems (ADAS) and exploited automated technologies. 24
2.6 C-ITS services and relative features. 27
2.7 Awareness Driving example. 28
2.8 Sensing Driving example. 28
2.9 Cooperative Driving example. 29
2.10 Use cases and Quality of Service (QoS) requirements of Vehicle-to-Everything (V2X) applications. 30
2.11 Feature comparison between 802.11bd and 802.11p. 32
2.12 An overall comparison of 802.11p, 802.11bd, LTE V2X, and NR V2X based on common features. 34

3.1 Cooperative driving systems. 44
3.2 The architecture for the cooperative driving of autonomous/automated vehicles. 45
3.3 Schematic representation of autonomous connected vehicles platoons from networked control systems perspective [1]. 48
3.4 Vehicle 2-DOF bicycle model. 52

3.5 Non linear 3 DOF bicycle model. 54
3.6 Exemplar platoon communication topologies: (a) Predecessor-Following (P-F), (b): Leader-Predecessor-Following (L-P-F); (c): Bidirectional-Leader-Predecessor (B-L-F); (d): All-to-All (Broadcast, BR); (e): Platoon of $N+1$ vehicles. 56

4.1 Integrated Simulation Environment MiTraS 75
4.2 Air-Drag Reduction of Passenger Cars [2] 80
4.3 The slipstream effect [3] 81
4.4 Battery Model [4] 82

5.1 Simulation Network: (**a**) SUMO network capture; (**b**) corridor layout; (**c**) altitude profile. 94
5.2 Average flow vs. average density from all the detectors in the appraised network area. 95
5.3 Distribution of fuel consumption among simulations sorted w.r.t.: (a) travel time [s]; (b) stop time [s]. 99
5.4 Distribution of energy consumption among simulations sorted w.r.t.: (a) travel time [s]; (b) stop time [s]. 99
5.5 Comparison of the distribution of consumption outputs between external models and SUMO built-in models. Histogram of: (a) fuel consumption [l/km]; (b) energy consumption [kWh/km]. 100
5.6 Comparison of the distribution of consumption outputs between GLOSA and no GLOSA cases. Histogram of: (a) fuel consumption [l/km]; (b) energy consumption [kWh/km]. 101
5.7 Input-output relationship for endothermic engine. Boxplot of FC w.r.t.: (a) TLS cycle duration [s]; (b) traffic condition; (c) phase condition [s]; (d) communication distance [m]; (e) minimum speed [m/s]. 103
5.8 Input-output relationship for electric engine. Boxplot of EC w.r.t.: (a) TLS cycle duration [s]; (b) traffic condition; (c) phase condition [s]; (d) communication distance [m]; (e) minimum speed [m/s]. 104

5.9 Comparison of mobility indexed distribution between GLOSA and no GLOSA cases. Histogram of: (a) travel time [s]; (b) stop time [s]. 106
5.10 Boxplot of input-output relationship for TT w.r.t.: (a) TLS cycle duration [s]; (b) traffic condition; (c) phase condition [s]; (d) communication distance [m]; (e) minimum speed [m/s]. 107
5.11 Boxplot of input-output relationship for ST w.r.t.: (a) TLS cycle duration [s]; (b) traffic condition; (c) phase condition [s]; (d) communication distance [m]; (e) minimum speed [m/s]. 108

6.1 Cured Road for the appraised simulation scenario. 124
6.2 3-D snapshot of all three vehicles within the simulation scenario. 125
6.3 Ego-Vehicle motion under the action of the proposed double-layer control architecture. Time history of: a) Ego-vehicle speed; b) inter-vehicle distance w.r.t. the preceding; c) lateral deviation error; d) yaw error. 125

7.1 Unsignalised Intersection Crossing Problem: a) example of Two-lane four-way unsignalised intersection; b) conflict points for the two-lane four-way intersection. The dashed circle is the Cooperative Zone (CZ), while the red zone is the Conflicting Area (CA). 136
7.2 Definition of the intersection crossing sequence leveraging the Virtual Platoon control concept: a) example of a mixed traffic flow composed by $M = 2$ autonomous vehicles and $N = 3$ human-driven vehicles approaching the intersection; b) virtual crossing sequence definition on the basis of the TTI of each incoming vehicle. 140
7.3 Desired reference speed ${v_{kj}}^{\star}(t)$ (see Eq. (7.15)) computed as a function of the difference $\Delta_{TTI_{kj}}$ between the Time-to-Intersection of the CAV k and of the vehicle j. 145
7.4 Example of the left-turning manoeuvre allowing to compute the value assumed by of R_{dx} and R_{sx} in Fig. 7.3 . . 145

7.5 Trend of the Throughput as function of both the traffic demand and CAVs penetration rate for: a) the *Deterministic Desired Driving Speed* scenario; b) the *Stochastic Desired Driving Speed* scenario. 151

7.6 Trend of the Average Speed and the Speed Variance as function of both the traffic demand and CAVs penetration rate for: a) the *Deterministic Desired Driving Speed* scenario; b) the *Stochastic Desired Driving Speed* scenario. 151

7.7 Time histories of the trajectories of both CAVs and CHVs approaching the unsignalized intersection for the scenario A-V considering: (a) 20% of CAVs penetration rate; (b) 60% of CAVs penetration rate. 152

7.8 Comparison among the CAVs and CHVs accelerations for the scenario A-V: (a) boxplot; (b) histogram of 20% of CAVs penetration rate; (c) histogram of 40% of CAVs penetration rate; (d) histogram of 60% of CAVs penetration rate. 153

7.9 Comparison among the CAVs and CHVs accelerations for the other scenarios under investigation: (a) boxplot for the scenario A-I; (b) boxplot for the scenario A-II; (c) boxplot for the scenario A-III; (d) boxplot for the scenario A-IV. 154

7.10 Comparison among the CAVs and CHVs accelerations for the scenario B-V: (a) boxplot; (b) histogram of 20% of CAVs penetration rate; (c) histogram of 40% of CAVs penetration rate; (d) histogram of 60% of CAVs penetration rate. 155

7.11 Comparison among the CAVs and CHVs accelerations for the other scenarios under investigation: (a) boxplot for the scenario B-I; (b) boxplot for the scenario B-II; (c) boxplot for the scenario B-III; (d) boxplot for the scenario B-IV. 156

7.12 Trend of the Collisions Number as function of both the traffic demand and CAVs penetration rate for: a) the *Deterministic Desired Driving Speed* scenario; b) the *Stochastic Desired Driving Speed* scenario. 156

8.1 Altitude profile for the appraised road network. 179

8.2 Evolution of the communication topology in the *join in the middle* manoeuvre: (a) communication topology $\bar{\mathcal{G}}_1$; (b) communication topology $\bar{\mathcal{G}}_2$; (c) communication topology $\bar{\mathcal{G}}_3$; (d) communication topology $\bar{\mathcal{G}}_4$. 180

8.3 Evolution of the communication topology in the *leave from-the-middle* manoeuvre: (a) communication topology $\bar{\mathcal{G}}_4$; (b) communication topology $\bar{\mathcal{G}}_3$; (c) communication topology $\bar{\mathcal{G}}_2$; (d) communication topology $\bar{\mathcal{G}}_1$. 182

8.4 Platoon Formation and Maintenance performances. Robustness analysis via the Monte Carlo Method. Time history of: (a) vehicles position $p_i(t)$; (b) vehicles position errors computed $p_i(t)-p_0(t)-d_{i0}$; (c) vehicles inter-vehicle distance computed $p_i(t)-p_{i-1}(t)$; (d) vehicles speed $v_i(t)$; (e) vehicles acceleration $a_i(t)$; (f) vehicles jerk $\dot{a}_i(t)$; 184

8.5 Leader Tracking performance for trapezoidal speed profile. Robustness analysis via the Monte Carlo Method. Time history of: (a) vehicles positions $p_i(t)$; (b) vehicles speed $v_i(t)$; (c) vehicles acceleration $a_i(t)$; (d) vehicles position errors computed $p_i(t)-p_0(t)-d_{i0}$; (e) vehicles speed errors computed $v_i(t)-v_0(t)$; (f) vehicles inter-vehicle distance computed $p_i(t)-p_{i-1}(t)$; (g) vehicles jerk $\dot{a}_i(t)$. 186

8.6 *Join in-the-middle* manoeuvre performances. Robustness analysis via the Monte Carlo Method. Time history of: (a) vehicles position $p_i(t)$; (b) inter-vehicle distance computed as $p_i(t)-p_{i-1}(t)$; (c) vehicles position $p_i(t)$ vs predecessor-follower gap distance for vehicle 4; (d) vehicles speed $v_i(t)$; (e) vehicles jerk $\dot{a}_i(t)$. 188

8.7 *Leave from-the-middle* manoeuvre performances. Robustness analysis via the Monte Carlo Method. Time history of: (a) vehicles position $p_i(t)$; (b) vehicles inter-vehicle distance computed $p_i(t)-p_{i-1}(t)$; (c) vehicles speed $v_i(t)$; (d) vehicles jerk $\dot{a}_i(t)$. 190

8.8 Leader Tracking performance for trapezoidal speed profile in presence of time-varying communication delays. Robustness analysis via the Monte Carlo Method. Time history of: (a) vehicles speed $v_i(t)$; (b) vehicles speed errors computed $v_i(t) - v_0(t)$; (c) vehicles inter-vehicle distance computed $p_i(t) - p_{i-1}(t)$; (d) vehicles acceleration $a_i(t)$; (e) vehicles jerk $\dot{a}_i(t)$; (f) communication delays $\tau_{ij}(t)$. 192

9.1 Exemplar platoon of five heterogeneous vehicles plus a leader connected via the L-P-F topology. 205
9.2 Exemplar platoon of five heterogeneous vehicles plus a leader connected via a Random topology. 205
9.3 Leader-tracking performance under the control in (9.13). Leader-Predecessor-Follower topology scenario. Time history of: (a) sliding surface $\sigma_i(t)$ $(i = 1, 2, 3, 4, 5)$; (b) position error $\tilde{p}_i(t) = p_i(t) - p_0(t) - d_{i0}$ $(i = 1, 2, 3, 4, 5)$; (c) vehicles velocity $v_i(t)$ $(i = 0, 1, 2, 3, 4, 5)$. 206
9.4 Leader-tracking performance under the control in (9.13). Random topology scenario. Time history of: (a) sliding surface $\sigma_i(t)$ $(i = 1, 2, 3, 4, 5)$; (b) position error $\tilde{p}_i(t) = p_i(t) - p_0(t) - d_{i0}$ $(i = 1, 2, 3, 4, 5)$; (c) vehicles velocity $v_i(t)$ $(i = 0, 1, 2, 3, 4, 5)$. 207

10.1 Energy-oriented optimal spacing policy for the EV i. . . . 220
10.2 *basic* scenario. Tracking performances. Time history of: a) Energy-optimal leader speed profile; b) vehicles speed $v_i(t)$; c) vehicles acceleration $a_i(t)$; d) inter-vehicle distances $\bar{d}_{i,i-1}(t)$ 223
10.3 *Energy-oriented* scenario. Tracking performances. Time history of: a) vehicles longitudinal position $p_i(t)$; b) vehicles speed $v_i(t)$; c) vehicles acceleration $a_i(t)5$; d) inter-vehicle distances $\tilde{d}_{i,i-1}(t)$; e) Comparison between inter-vehicle distances $\bar{d}_{i,i-1}(t)$ and $\tilde{d}_{i,i-1}$ in *basic* and *energy-oriented* scenarios. 227
10.4 Computational load in *energy-oriented* scenario and *basic-scenario* with controller (10.11). 228

10.5 Tracking performances with the classic distributed diffusive control in (10.11). Time history of: *a*) vehicles speed $v_i(t)$; *b*) inter-vehicle distances $d_{i,i-1}(t)$; *c*) Comparison between inter-vehicle distances $d_{i,i-1}(t)$ and $\tilde{d}_{i,i-1}(t)$ in *basic* and *energy-oriented* scenarios. 229

A.1 Exemplary scheme of a Use-Case 237

B.1 Overview of the typical architecture of the automation system of automated/autonomous vehicle. 240

List of Tables

5.1 Comparison of GLOSA research works 86
5.2 Ego-Vehicle Model Parameters 93
5.3 ANOVA results for the endothermic engine 102
5.4 ANOVA results for electric engine 105
5.5 ANOVA results for travel time 107
5.6 ANOVA results for stop time 109
5.7 Comparison of linear regression models for consumption and mobility KPIs. 110

6.1 Ego-Vehicle Controllers Parameters. 123
6.2 Cost function weights for each considered operating configuration. 123
6.3 Energy consumption results for each operating condition and energy reduction w.r.t. baseline scenario. 126

7.1 Dynamic Parameters for each CAV vehicle type 147
7.2 Demand Patterns 148
7.3 CAV Controllers Parameters ($\forall k = N+1, \ldots, N+M$) . . 148
7.4 Mobility Performance 150
7.5 Safety Performance 155

8.1 Heterogeneous Nonlinear Vehicle Parameters 178
8.2 $\mathcal{H}_\sigma$ matrices for the topologies related to the *join in-the-middle* manoeuvre. 181
8.3 $\mathcal{H}_\sigma$ matrices for the topologies related to the *leave from-the-middle* manoeuvre. 182

8.4 Control Parameters for *join in-the-middle* and *leave from-the-middle* manoeuvres. 182

9.1 Vehicle and Control parameters. 205
9.2 Simulation parameters for the L-P-F topology scenario. . 208
9.3 Simulation parameters for Random topology scenario. . . 209

10.1 Heterogeneous Nonlinear Vehicles Parameters 221
10.2 Percentage of energy saving in $[kWh/km]$ under Energy-Oriented Architecture compared to *basic* scenario. 222
10.3 Percentage of energy saving in $[kWh/km]$ under Energy-Oriented Architecture compared to *basic* scenario with proportional controller. 222

List of Algorithms

1 GLOSA Algorithm executed when the Ego-Vehicle enters the communication range of upstream TLS i 91

2 On-board computation of the minimum gap $\overline{D}_{k,j}$ for the k-th CAV approaching the CA (see (7.13)). 142

CHAPTER 1

Introduction

1.1 Motivation and Contributions

The transformation towards the so-called *Smart Roads* is underway in complete harmony with the governance and management of innovation in the transportation sector across Europe, with particular reference to the European C-ITS platform, the GEAR 2030 initiative, the communication of the European Commission (EC) dated 30-11-2016 [1] and the *Smart Road Decree* signed by the Government Italian in March 2018. The process mentioned above involves the development and exploitation of key technologies for enabling innovative and automated driving functions and applications, as well as the design of demonstration scenarios in which automated driving capabilities are tested in different use cases. The main idea is to promote the innovation and application of automated driving technology in the road transport sector, as well as of new transportation services, so to build a intelligent road transport environment. It is of great significance for enhancing road safety, improving traffic flow, reducing traffic congestion, improving the efficiency in using energy sources, and reducing pollutant emissions. New fully automated C-ITS connected mobility services can also reduce the overall level of traffic congestion to make cities and human settlements safe, resilient, sustainable and

[1] `https://eur-lex.europa.eu/legal-content/EN/TXT/PDF/?uri=CELEX:52016DC0766&from=EN`

decrease the number of deaths and injuries caused by road accidents. A particularly demanding challenge concerns the introduction of automated vehicles into existing traffic: this poses specific and new problems in terms of reliability and effectiveness, particularly concerning interactions both with other vehicles (regardless of the degree of automation) and with other actors of traffic scenario (e.g., pedestrians, public vehicles or cyclists). Furthermore, automated driving systems must be suitably designed to be resilient to both the uncertainties, arising from V2X communication and vehicles, and drivers to ensure sufficient reliability and robustness in any traffic situation in the real world.
Hence, it seems clear that, to promote the widespread deployment of C-ITS services on the market, research still has to provide new effective solutions to overcome the several challenges in the transportation field. To this end, a key point is the qualitative and quantitative evaluation of driving systems performance and their effects. The design and validation methods should demonstrate the behavioural skills that an automated vehicle should perform during, for instance, normal operation, the performance during accident prevention situations and the performance of fallback strategies. It is possible to verify that safety requirement is always satisfied, quantify potential advantages, and evaluate issues to optimise the connected, cooperative, and automated driving functions.
Hence, in light of the above discussion, the main objective of this thesis is twofold

1. Research and develop innovative C-ITS strategies for cooperation between vehicles and between vehicles and infrastructures, based on V2X communication and enabled by the digital transformation of road infrastructures. This aim includes the development of reliable and resilient control architectures to increase the performance of automated and connected driving in urban and extra-urban scenarios.

2. Test and validate proposed strategies in several different complex traffic contexts, both urban and extra-urban. In so doing, it is possible to deploy flexible and adaptable C-ITS services to any type of situation (e.g. manoeuvres, formation and dissolution of vehicle fleets, automatic crossing of intersections in the presence or

absence of traffic lights) so to ensure safety driving conditions, also under mixed traffic situations.

To achieve goal 1, different control strategies addressing as many issues are proposed for urban and extra-urban traffic scenarios. Indeed, automated/autonomous connected vehicles can drive better in restricted conditions such as on roads with clear lane markings, clear weather, visible road signs, and controlled speed limits. This kind of road is more like a highway than an urban one, where more unexpected situations can occur due to a more challenging external environment. Hence, it is essential to address the specific problems of both traffic environments.
One of the main open challenges regarding the urban environment is the optimisation of crossing manoeuvres at intersections, which could be signalised or unsignalised. However, traffic flows will be composed of a mix of connected and autonomous vehicles and human-driven vehicles for a relatively long time, creating very complex traffic scenarios and interactions.
Firstly, a Green Light Optimal Speed Advisory (GLOSA) algorithm aiming at reducing both waiting time and *stop&go* phenomena at urban signalised intersection is proposed. By leveraging Traffic Light Signals (TLSs) information shared via wireless communication, the algorithm computes, as long as it is possible, an optimal speed profile to cross the intersection without coming to a complete stop. The effectiveness of the proposed algorithm is tested under different road conditions by varying several road variables, i.e. traffic signal phase condition, engine type, traffic condition, TLSs cycle duration, communication distance and minimum achievable speed. In this case, one controlled vehicle, travelling along a single route through a real-world city centre including many TLSs, is equipped with the GLOSA algorithm, while other cars are human-driven.
Another open issue in the urban environment is the cooperative crossing of unsignalised intersection. Most of the existing studies on unsignalised intersections crossing assume the presence of only fully autonomous vehicles [5, 6, 7]. However, as previously mentioned, mixed traffic will likely be the prevailing traffic condition in the next 10 or 20 years. In this framework, a cooperative fully-distributed control protocol for Connected and Automated/Autonomous Vehicles (CAVs), augmenting the Adaptive Cruise Control (ACC) action based on proximity sensors

measurements, with an additional networked protocol exploiting Vehicle-to-Vehicle (V2V) information to estimate the Time-to-Intersection of all incoming vehicles within the communication range, is proposed. This collaborative action adapts the CAVs motion at the intersection to avoid collisions with other vehicles and reduce stop and waiting time.
Besides the intersection crossing, another crucial challenge in the urban environment is to accomplish different driving tasks at the same time such as, for instance, avoiding collisions with obstacles and tracking a path along a curved road. To handle both issues simultaneously, a double layer control architecture combines the classical ACC with the multi-objective Nonlinear Model Predictive Controller (NMPC) approach, able to drive the vehicle along a predefined path while keeping a safe distance from the predecessor and ensuring energy-saving consumption, is proposed. Moreover, since in urban environments a vehicle might follow routes where several turning manoeuvres, the losses during cornering manoeuvres are explicitly taken into account [8].
Regarding extra-urban traffic scenarios, three cooperative driving applications of platooning are considered. The first one addresses the leader-tracking control problem for uncertain heterogeneous nonlinear autonomous vehicles platoon sharing state information through a vehicular communication network and performing the cooperative manoeuvre. Indeed, tracking ability plays a crucial role in platooning applications during normal operations, platooning manoeuvres, or emergency actions. In this perspective, the robustness concerning uncertain nonlinear dynamics is vital when implementing cooperative driving applications: mismatches between the actual plant and its control-oriented model could strongly affect the performance of a designed control protocol and, hence, the expected behaviour of the vehicle. Another critical issue is related to vehicle communication topology: it may not be maintained fixed due to communication constraints, environmental disturbances, or platooning manoeuvres. Hence, there is the need to investigate the performance of vehicle platoon control under switching topologies when some communication links among vehicles within the platoon are created and/or disrupted. To this aim, a robust distributed Proportional-Integral-Derivative (PID)-like control protocol is proposed, which ensures that all vehicles within the platoon robustly track the leader behaviour despite the presence of both unknown parameters uncertainties and network

switching. The control strategy weights the vehicles state information via proportional action, augmented with an additional integral action on the position state information so to improve steady-state and robustness performances. Each vehicle is described via a nonlinear dynamical system accounting for the effect of the air-drag reduction due to platooning and time-varying uncertainties depending on the different driving conditions in which the platoon is currently involved.

The second application considers the problem of achieving the consensus with a fixed settling time for a heterogeneous uncertain autonomous vehicles platoon. To this end, by exploiting the Integral Sliding Mode (ISM) approach and the Lyapunov theory, a distributed control strategy ensures the leader-tracking in a finite settling time, independent from any initial condition of the vehicle, while counteracting heterogeneity and unknown external disturbances, is proposed.

The last one addresses the problem of simultaneously achieving leader-tracking and energy-saving goals for a heterogeneous autonomous connected fully electric vehicles platoon. To this end, by embedding a distance-dependent air drag formulation into the vehicle model, an energy-saving oriented Distributed Nonlinear Model Predictive Controller (DNMPC) able to guarantee the following three-fold control objective is proposed: *i*) ensure that each vehicle tracks the energy-oriented optimised leader speed profile, assumed to be directly or indirectly known by each vehicle within the platoon; *ii*) compute, at time instant, the optimal variable inter-vehicle distance from the vehicle ahead by considering safety constraints, as well as the electric power saving requirement and distance-dependent air-drag formulation; guarantee the minimisation of the required battery power, thus achieving energy saving objective.

To achieve goal 2, a novel Integrated Simulation Environment, named MiTraS, for assessing and evaluating C-ITS services, from the individual level to the large-scale network level, is proposed. It embeds different interacting simulation tools within a holistic view of the co-simulation approach to be as realistic as possible. Namely, the MATLAB/Simulink is exploited to model high-fidelity vehicle dynamics, develop the proposed control strategies, and emulate heterogeneous time-varying delays associated with each active communication link. Furthermore, by leveraging the Automated Driving Toolbox, it is possible to obtain a 3D representation of the road environment and, as a consequence, to simulate

on-board ranging sensors such as camera, radar, and lidar. On the other side, Simulation of Urban Mobility (SUMO) is embedded to provide a realistic traffic environment and emulate the human-driver behaviour, i.e. to account for unplanned but realistic events such as congestion, slower or faster vehicles ahead, lane changes manoeuvres and, generally, to face up with different drivers behaviours. Hence, it is possible to enable virtual testing in complex, stochastic and reproducible traffic scenarios. Moreover, it is worth noting that the proposed virtual environment is built up in a modular framework, which allows users to replace or modify each component according to their needs.
The proposed Integrated Simulation Environment is, thus, exploited to assess the performance of all the proposed control strategies under different traffic conditions.

1.2 Thesis Outline

The thesis is structured as follows.

- In Chapter 2, C-ITS concept and relative services are introduced, providing also an overview of the European framework, communication standards and testing and validation methods.

- In Chapter 3, after presenting the cooperative driving systems, a description of how to model them as networked control systems is provided. Moreover, some useful concepts and definitions, in the general context of networked control systems, are summarised for the sake of clarity.

- In Chapter 4 is introduced and described the proposed Integrated Simulation Environment. The results of this chapter are demonstrated in the following publications [9, 10] and in the on-going work presented in Chapter 7.

- Chapter 5 focuses focuses on developing a GLOSA service and its assessment via an enhanced testing approach exploiting the Mixed Traffic Simulator (MiTraS) Integrated Simulation Environment. The proposed approach can be used to cover several aspects that usually are not considered (traffic signal phase condition), rarely considered (electric engine), or considered in a non-integrated way (traffic condition, TLSs cycle duration, communication distance, and minimum speed). To prove the effectiveness of the proposed approach, a controlled vehicle, equipped with a GLOSA system, travelling along a single route through a city centre including many TLSs, is considered. Numerical results confirm that the proposed Integrated Simulation Environment can give valuable insights and suggestions to enhance the design of a GLOSA service aiming to improve both mobility and environmental performance. Moreover, the outcome shows that the considered traffic factors affect system performance in a very different way The results of this chapter are demonstrated in the following publications [11, 10].

- Chapter 6 addresses the problem of computing an eco-driving speed profile for an autonomous electric vehicle travelling along a curved road while ensuring path following/car following functionalities. To this end, a double-layer control architecture combining the classical Adaptive Cruise Control with a NMPC is proposed. The latter is designed to drive the vehicle along a predefined path while guaranteeing safety and improving energy performance. The appraised control-oriented design model is non-linear, and the energy consumption one explicitly accounts for the cornering effects, which can not be neglected when a vehicle travels along a curved urban road. Numerical results confirm the effectiveness of the proposed control architecture and disclose its ability to guarantee energy saving. The results of this chapter are demonstrated in the following publication [12].

- In Chapter 7, a cooperative fully-distributed control protocol for CAVs is proposed to deal with the open challenge of decentralised crossing at unsignalised intersections for mixed traffic flows, composed of Connected Human-driven Vehicles (CHVs) and CAVs. The proposed control action augments the classical ACC action with an additional networked protocol exploiting V2V information for the cooperative evaluation of the Time-to Intersection of all incoming vehicles within the communication range. This further collaborative action automatically adapts the CAVs motion at the intersection, avoiding collisions with other cars and reducing stop and waiting times. The analysis is carried out for an exemplary two-lane four-way unsignalised road intersection considering several traffic demands levels, several CAVs penetration rates, and the presence of variable delays affecting the wireless communication network. The extensive simulation analysis confirms how the inclusion of CAVs, equipped with the proposed control algorithm, within the mixed traffic flow improves both safety and mobility performances of the intersection. Note that, the content of this chapter is in the on-going work presented in Chapter 7. Moreover, the early development can be found in the following publication [13].

- Chapter 8 deals with the leader-tracking control problem for uncertain heterogeneous nonlinear autonomous vehicles platoon sharing information through a vehicular communication network and performing cooperative manoeuvres in extra-urban scenarios. The nonlinear vehicle dynamic is affected by time-varying parameters uncertainties, explicitly considering the air-drag reduction. At the same time, the variation of V2V links, due to cooperative manoeuvres, are modelled via switching into the communication network topology. To this end, a novel robust distributed PID-like control protocol is proposed, ensuring that all vehicles within the platoon robustly track the leader behaviour despite the presence of both unknown parameters uncertainties and network switching. The stability of the proposed control strategy is analytically proven by leveraging the Lyapunov theory. Sufficient stability conditions are expressed as a set of feasible Linear Matrix Inequalities (LMIs) whose solution allows the proper tuning of the robust control gains. The effectiveness of the approach is evaluated via the MiTraS Integrated Simulation Environment. The exhaustive simulation analysis, involving the Monte Carlo method, considers different cooperative platooning manoeuvres and confirms the theoretical derivation. Note that, the content of this chapter is in the ongoing work presented in Chapter 8.

- In Chapter 9 the problem of achieving leader-tracking in a fixed-time while dealing, at the same time, with heterogeneity and unknown external disturbance for a platoon of autonomous and connected vehicles is addressed. To deal with it, by exploiting the ISM approach and the Lyapunov theory, a novel distributed fixed-time control protocol is proposed. This latter is able to: *i*) counteract the vehicles heterogeneity and unknown external disturbances; *ii*) guarantee the leader-tracking in a fixed settling time whose estimation only depends on the proper choice of the control gains, and not on any vehicles initial conditions. The simulation analysis, carried out in two different driving scenarios, confirms the effectiveness of the theoretical derivation. The results of this chapter are demonstrated in the following publication [14].

- In Chapter 10 the energy-saving challenge for a platoon of heterogeneous autonomous, connected, fully-electric vehicles is addressed. Specifically, a cooperative driving control strategy ensures the leader tracking performance while keeping a variable energy-oriented inter-vehicle distance between adjacent vehicles is designed. To this aim, by considering a distance-dependent air drag coefficient, a novel DNMPC, whose cost function aims to ensure leader tracking performances and optimised the inter-vehicle distance to reduce energy consumption, is designed. Extensive simulation analyses, carried out exploiting MiTraS and involving a comparative analysis with respect to the classical Constant Time Gap (CTG) spacing policy, are performed to confirm the capability of the DNMPC in guaranteeing energy saving. The results of this chapter are demonstrated in the following publications [15, 16].

- In Chapter 11 conclusions are drawn.

CHAPTER 2

Cooperative Intelligent Transport Systems and Services

Owing to the ever-increasing number of vehicles and their usage, modern societies with well-planned road management systems and sufficient infrastructures for transportation still face the problem of traffic congestion. This issue results in travel time loss, enormous societal and economic costs, and an increasing environmental impact [17]. Several solutions have been adopted to give new answers to traffic-related open issues in past decades. Some of these rely on the enhancement or on the construction of new infrastructures (like roads, highways, ports, airports, and so on); some others rely on the enhancement of the vehicular safety systems (like airbags or safety belts). However, building new infrastructures requires several expensive actions with an increased environmental impact drawback [18]. For these reasons, solutions allowing more efficient use of the existing infrastructure are aimed.
Among these solutions, the so-called C-ITS refers to transport systems where two or more Intelligent Transportation Systems (ITS) sub-systems (vehicles, infrastructure devices, pedestrians, and cyclists) cooperate. This way enables and provides a service that offers better quality and an enhanced service level, compared to the same ITS service provided by only

one of the ITS sub-systems. Within this framework, road actors became smart agents, and reliable communication between them is required to share helpful information to enhance the quality of the travel experience. With specific regard to automated/autonomous connected vehicles, they can interact and cooperate with other vehicles, motorcycles, bicycles, pedestrians, and other road-users, as well as with Internet-of-Things (IoT) services, to improve safety and increase their effectiveness The communication paradigm for automated/autonomous car is shown in Fig. 2.2, in which is possible to note that the automated/autonomous car communicates with both the infrastructure and its neighbours. Connected car technology is realised through Vehicular-ad-hoc-networks (VANETs) where vehicles on the road communicate with each other, with the infrastructure and with the environment through different underlying wireless communication technologies, such as Dedicated Short Range Communications (DSRC) and Cellular Vehicle-to-Everything (C-V2X). In general line, the wireless data exchange among several different road actors and ITS stations and related functions are referred as V2X communication services; these services are also known as V2V, Vehicle-to-Infrastructure (V2I), Vehicle-to-Pedestrian (V2P) or Vehicle-to-Network (V2N) communications communications based on involved actors. V2X services can support vehicles to help them obtain more information and promote the innovation and application of automated driving technology, contributing to building an intelligent transport system and promoting the development of new modes and new forms of automobiles and transportation services [19].
Note that, in the rest of the thesis, only vehicles and infrastructures are going to be taken into account as actors; accordingly, only V2V and V2I services are going to be treated.
In a cooperative road traffic scenario, cooperative V2X communication units are deployed in vehicles and road traffic infrastructure and exchange data via a wireless communication network. Multiple times per second, On-Board unit (OBU) mounted in the vehicles share data such as position, speed, driving direction, and event-triggered messages about notable events (e.g., emergency braking, a vehicle defect, or a slippery road detected). On the other hand, traffic infrastructure, equipped with Road-Side unit (RSU), inform, e.g., about signal phases of traffic lights, speed limits, or road works congestion level. The native purpose of

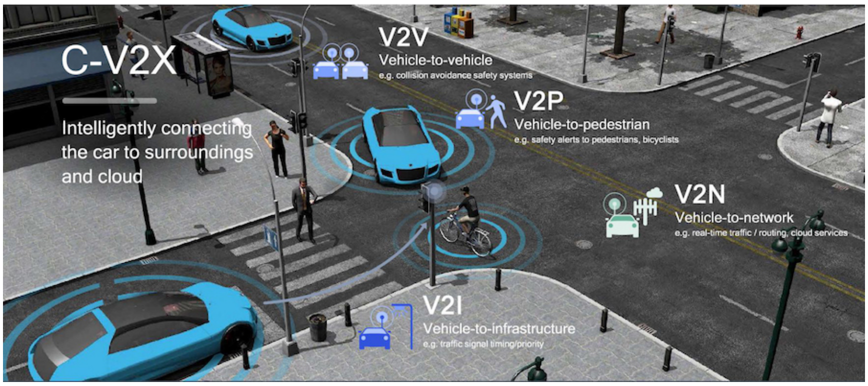

Figure 2.1: C-ITS scenario: road users communicate information each other.

such technologies is to improve road safety helping the driver avoid critical road safety situations: as depicted in Fig. 2.1, vehicles and infrastructure cooperate in perceiving potentially dangerous situations across an ample space and time horizon [20]. Moreover, use of V2X technologies is assumed to enormously enhance both traffic congestion and driving comfort [21, 22]. Indeed, services such as providing information about traffic light signal phases and their predicted changes or barriers on the route in real-time support smooth and comfortable travelling. Finally, they can also improve the environmental footprint of transport systems through in-vehicle technologies (e.g., eco-driving) and more intelligent and innovative transportation management at the network level. Indeed, avoiding intense acceleration/deceleration manoeuvres can reduce fuel/energy consumption with favoured effects on lowering noise and emissions.

2.1 The European Framework

The development and implementation of C-ITS services are part of a broader process of transforming the road environment. In particular, the concept of Smart Road has been introduced: an intelligent road environment enabling communication and interconnection among actors moving along it. In a Smart Road, to facilitate flows and transport, weather and traffic detection systems must be implemented so that

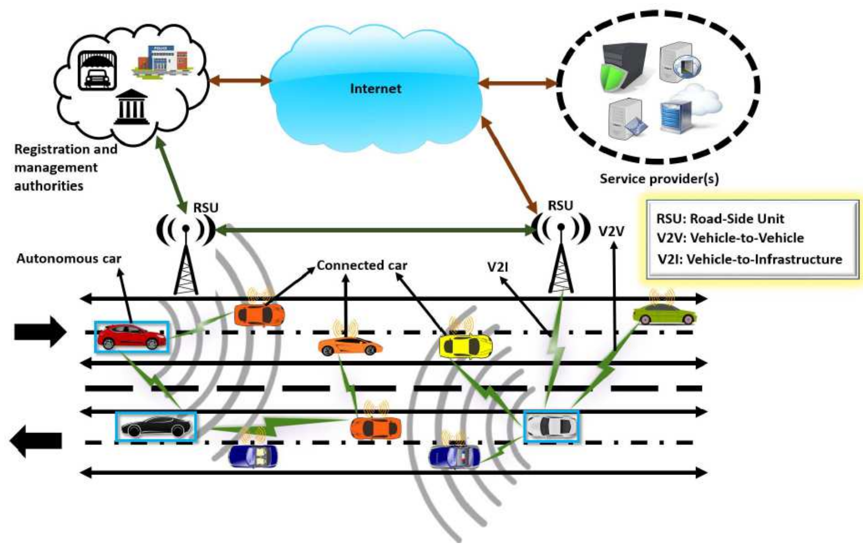

Figure 2.2: Exemplar communication paradigm for automated/autonomous car.

travellers can request information on road conditions, traffic, or other particular situations in real-time. Furthermore, the Smart Road aim to provide: services for diverting traffic flow in the event of accidents; suggestions of alternative trajectories; speed interventions to avoid traffic situations; management of accesses, parking lots, and supplies; timely interventions in case of emergencies. The digital transformation towards Smart Roads needs to be in complete harmony with the governance and management processes of innovation in the sector in progress in Europe. Indeed, Smart Road is intertwined with the developments taking place in the field of cooperation between vehicles and transport infrastructures and in the development of connected driving solutions and increasing levels of automation. The idea of an intelligent road is designed to adapt to a network vision: the digital transformation process will be gradually applied, first to road infrastructures of the Trans-European Network-Transport (TEN-T) and new infrastructures or pre-existing infrastructural sections connecting elements of the TEN- network.

In this framework, the EC is making significant efforts in developing and deploying C-ITS services based on V2X communication, setting up a reference framework for supporting Cooperative, Connected and

Automated Mobility (CCAM) policies [1]. The European Union (EU) framework for supporting C-ITS services development, shown in Fig. 2.3, highlights the complexity of the matter. Above all, C-ITS strategies aim to develop a shared vision throughout the EU to combine the different stakeholders efforts. To this end, in 2010 the European Parliament and the Council released Directive 2010/40/EU [2] on the framework for the deployment of ITS in the field of road transport and for interfaces with other modes of transport. It defined the following priority areas of intervention: optimal use of road, traffic and mobility data; continuity of ITS traffic and freight management services; ITS applications for road safety and transport safety; the connection between vehicles and road infrastructure V2X. Specific features to be respected are associated with each sector to ensure compatibility, inter-operability, and continuity of the ITS services, which are key components for disseminating and using in all member countries. Then, in early 2014 the EC set up the C-ITS Platform, conceived as a cooperative framework to develop a shared vision for the inter-operable deployment of C-ITS in the EU. During the first stage (2016), it provided policy recommendations for developing a road-map and implementation strategy C-ITS in the EU, identifying potential solutions for some crucial cross-cutting issues, as well as identified consolidated C-ITS services from a technological point of view. During the second stage (2017), it further developed a shared vision on the inter-operable implementation of C-ITS towards cooperative, connected, and automated mobility CCAM in the European Union. In 2016, the Member States and the Commission launched the C-Roads Platform [3] to link and coordinate C-ITS deployment across the Union. The main aim of the Platform is to develop harmonised and standardised guidelines and specifications, taking into consideration the recommendations issued by the C-ITS platform, linking all the C-ITS projects within Europe and the subsequent operation of the *day-1* C-ITS services and. in the end, planning cross-member evaluations and tests between member states. In this context, particular attention is paid to the inter-operability problem of the infrastructural network of member states participating in the C-Roads initiative: pilot

[1] `https://www.ccam.eu/`

[2] `https://eur-lex.europa.eu/legal-content/EN/TXT/PDF/?uri=CELEX:32010L0040&from=IT`

[3] `https://www.c-roads.eu/platform.html`

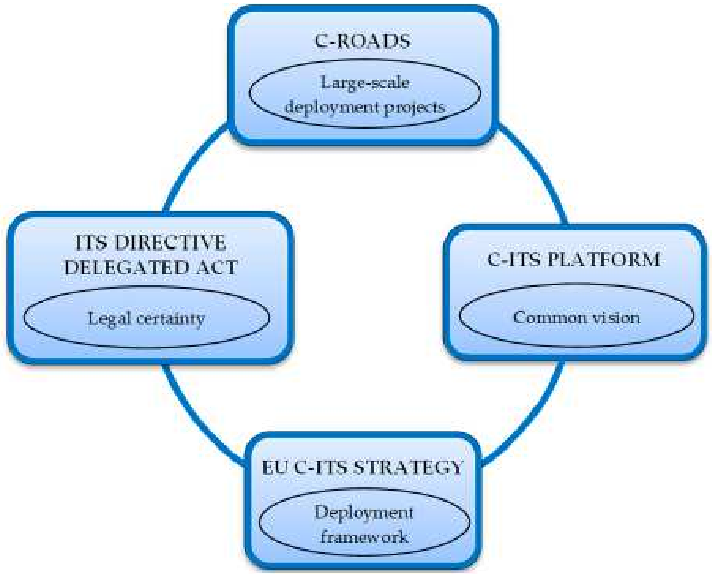

Figure 2.3: European C-ITS framework.

installations need to be harmonised in the light of cross-border interoperability based on cooperation within the C-Roads platform. Individual experts participating in individual pilots and appointed by the members of the C-Roads Steering Committee collaborate within a series of working groups to prepare the recommendations. In addition, members of the pilot activities and C-Roads working groups actively contribute to the work of the C-ITS platform.

Finally, in March 2019 was released a delegated act supplementing Directive 2010/40/EU [4]. This new regulation concerning C-ITS will enter into force and be directly applicable in all Member States if the European Parliament or the Council of the EU do not object to it.

Within the European initiative for the promotion of C-ITS, a key role is being played by the Car2Car Communication Consortium (C2C-CC) [5]. C2C-CC, founded in 2002 by a group of car-makers, today comprises 74 members among car-makers, Original Equipment Manufacturers (OEMs),

[4] `https://ec.europa.eu/transparency/documents-register/detail?ref=C(2019)1789&lang=en`

[5] `https://www.car-2-car.org/`

first-and second-tier suppliers, technology suppliers, and research organizations.
Furthermore, it is worth noting that the Society of Automotive Engineers (SAE) has established a similar evolution pattern, based on different levels of increasing automation. More specifically, the SAE J3016 [6] document defines six levels (from 0 to 5) to classify the degree of automation of the individual systems (see also Fig. 2.4):

1. Level 0: there are no automated driving functions. The driver performs the longitudinal control of the vehicle (i.e., maintaining speed, accelerating, and braking) and the lateral control (i.e.steering). There are no systems that intervene, only those that produce warnings.

2. Level 1: a system can assume either longitudinal or lateral vehicle control while the driver continuously performs other tasks. He can enable some safety functions such as ACC and lane centering.

3. partial automation since the driver can now demand both tasks (longitudinal and lateral control) to the system in specific use cases. The driver continuously monitors the vehicle and the traffic during the journey, and at all times, they must be in a position to resume control of the vehicle immediately.

4. Level 3: the system independently recognizes its limits, that is, the point at which its functions can no longer cope with the environmental conditions. The vehicle requests the driver to resume the task of driving. The driver no longer has to monitor the longitudinal and lateral control of the vehicle continuously. However, he must resume driving when the system signals him to do so, with some extra time in reserve.

5. Level 4 (limited self-driving automation): the driver can hand over the entire task of driving to the system in specific use cases. These scenarios refer to the type of road, the speed range, and the environmental conditions.

[6] https://www.sae.org/standards/content/j3016_202104/

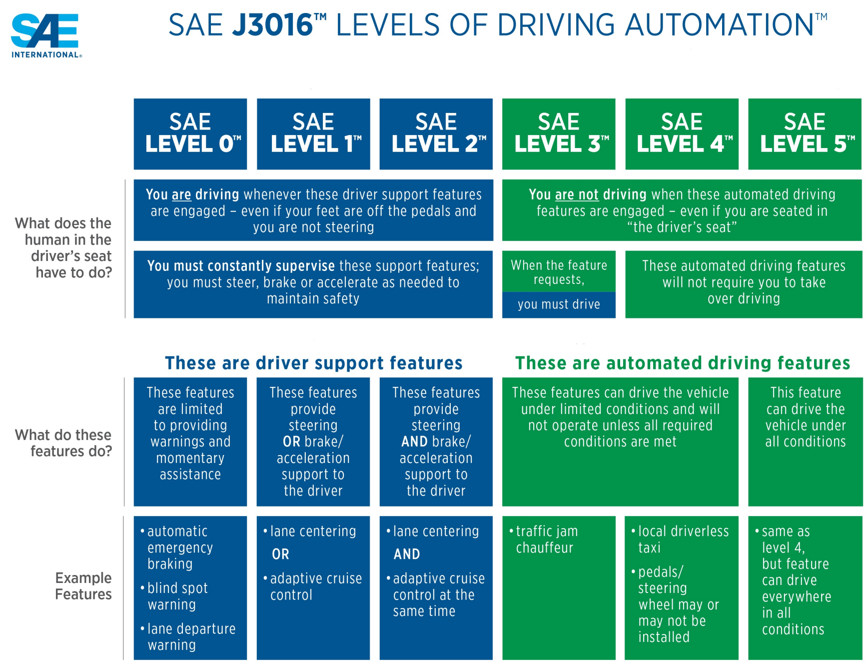

Figure 2.4: SAE level of automation.

6. Level 5 (full self-driving automation): the vehicle can completely independently perform the task of driving in full on all types of roads, in all speed ranges and under all environmental conditions.

However, a specific correspondence between the two cases evolution phases has not been established yet. As of December 2021, vehicles operating at Level 3 SAE and above remain a marginal portion of the market. Waymo became the first service provider to offer driver-less taxi rides to the general public in a part of Phoenix, Arizona in 2020 [7]. However, while there is no driver in the car, the vehicles still have remote human overseers. Up to now, Honda [8] and Mercedes-Benz [9] are

[7] https://arstechnica.com/cars/2020/10/waymo-finally-launches-an-actual-public-driverless-taxi-service/
[8] https://global.honda/newsroom/news/2021/4210304eng-legend.html
[9] https://www.fleetnews.co.uk/news/manufacturer-news/2021/12/09/mercedes-benz-self-driving-car-technology-approved-for-use

the only two manufacturers to provide a legally approved Level 3 vehicle. Finally, it is worth citing the extensive consultation process undertaken by the Commission through several working groups called upon to analyze the current situation and provide valuable recommendations for the future. An appropriate instance of this is establishing the High Level Group (HLG) Gear 2030 in 2015. The outcome of such a consultation process provides some valuable suggestions to address the main challenges and opportunities offered by cooperative driving in the runup to 2030 and beyond [10].

2.1.1 Italian Roadmap for C-ITS

In recent years, the Italian government has been paying great attention to the issue of Smart Roads, promoting a policy aimed at standardizing and homogenizing practices, being first and foremost the guarantor of the creation and optimal management of the Italian road network. To this end, following all the European directives in Sec. 2.1, in 2018 was released by the Italian Ministry of Infrastructure and Transport (MIT) the so-called *Smart Road Decree* to foster the digital transformation process aimed to introduce: traffic observation and monitoring platforms, data and information processing models and provide advanced services to infrastructure managers, to the public administration and road users, so to create a technological ecosystem able to guarantee the inter-operability between new infrastructures and vehicles generation. Summarizing, this digital transformation process is finalized to:

- enhance traffic management systems by exploiting real-time traffic congestion conditions;
- enhance road safety and security by introducing innovative services enabled by new technologies.
- ensure inter-operability with new generation vehicles and the commissioning of C-ITS services, starting with those called *day-1* by the European C-ITS platform.

[10] `https://www.etsi.org/deliver/etsi_tr/102600_102699/102638/01.01.01_60/tr_102638v010101p.pdf`

2.2 Advanced Driver-Assistance Systems

The revolution affecting transport engineering and the car makers industry is closely linked to the introduction of autonomous and automated driving systems, which facilitate the role of drivers, leading to increased safety since human error is one of the leading causes of road accidents. Driving automation began with introducing the so-called ADAS. ADAS are vehicle-based intelligent safety systems that could enhance road safety by minimising human error. Indeed, they exploit automated technology, such as sensors and cameras (see Fig. 2.5), to detect nearby obstacles or driver errors and respond accordingly. Safety features are required to avoid accidents and collisions by offering technologies that alert the driver to problems, implementing safeguards, and taking control of the vehicle if necessary. Adaptive features may automate lighting, provide adaptive cruise control, assist in avoiding collisions, alert drivers to possible obstacles, assist in lane departure and lane centering. Commonly available ADAS are:

- Cruise Control (CC) maintains a specific speed pre-determined by the drive.
- Adaptive cruise control (ACC) can maintain a desired speed and distance from a forward vehicle. ACC systems with stop and go functions can stop entirely and accelerate back to the specified speed
- Anti-lock Braking System (ABS) restores traction to a car tires by regulating the brake pressure when the vehicle begins to skid and assists drivers who may lose control of their vehicle.
- Electronic stability control (ESC) can lessen the speed of the car and activate individual brakes to prevent understeer and oversteer.
- Automatic parking entirely takes control of parking functions, including steering, braking, and acceleration, to assist drivers in parking. Currently, the driver must still be aware of the vehicleâ€™s surroundings and be willing to control it if required.
- Backup camera provides real-time video information regarding the location of a vehicle and its surroundings.

- Blind spot monitor involves cameras that monitor the blind spots of the driver and notify the driver if any obstacles come close to the vehicle.
- Collision avoidance system (pre-crash system) uses small radar detectors, typically placed near the front of the car, to determine the distance to nearby obstacles and notify the driver of potential car crash situations.
- Driver drowsiness detection aims to prevent collisions due to driver fatigue.
- Driver monitoring system is designed to monitor the alertness of the driver.
- Emergency driver assistant facilitates emergency counteract measures if the driver falls asleep or does not perform any driving action after a defined length of time.
- Forward Collision Warning (FCW) monitors the speed of the vehicle and the vehicle in front of it, and the open distance around the vehicle.
- Intersection assistants use two radar sensors in the front bumper and sides of the car to monitor any oncoming vehicles at intersections, highway exits, or car parks.
- Hill-start or hill-holder helps prevent a vehicle from rolling backward down a hill when starting from a stopped position.
- Lane Centering assists the driver in keeping the vehicle centered in a lane.
- Lane Departure Warning (LDW) alerts the driver when they partially merge into a lane without using their turn signals.
- Lane change assistance helps the driver through a safe completion of a lane change by using sensors to scan the vehicle surroundings and monitor the driver blind spots.

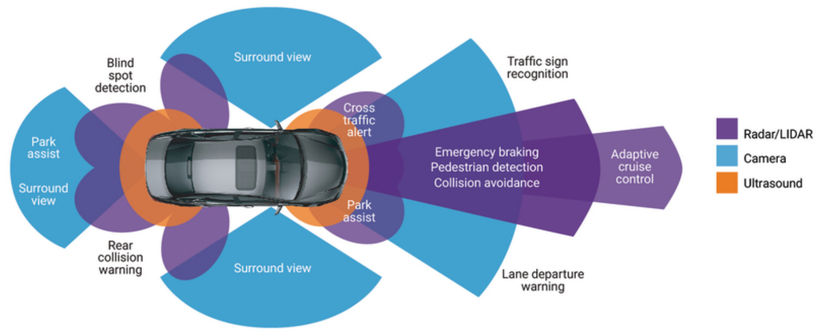

Figure 2.5: ADAS and exploited automated technologies.

- Traffic Sign Recognition (TSR) systems can recognise common traffic signs, such as a stop sign or a turn ahead sign, through image processing techniques.

Sensor-based systems offer varying degrees of assistance to the driver (see Appendix B for an overview of the typical architecture of the automation system of automated-driving cars). However, in their current form, such vehicles are not yet capable of providing complete and cost-effective self-driving experiences [23]. To this aim, car manufacturers have developed ADAS integrated with V2X communication device so to enable additional interactions from/to other sources/destinations different from the Ego-Vehicle-only platform and, hence, overcome shortcomings of this latter approach. For this reason, more V2X applications that will increase safety and traffic efficiency are expected to emerge in the foreseeable future [19]. Examples of communication-induced improvements are: V2V systems allow vehicles to exchange information with each other about their current position and upcoming hazards that are, for instance, beyond the line-of-sight; V2I systems occur when the vehicle takes information about street signs, TLSs status and road traffic congestion; V2X systems occur when the vehicle monitors its environment and takes in information about possible obstacles or pedestrians in its path.

2.3 C-ITS Services

The EC divides the C-ITS services according to the degree of technological maturity. So-called *day 1* C-ITS services, which focus on exchanging information enhancing foresighted driving, are considered technologically mature, highly beneficial, and should be deployed quickly so that end-users and society can benefit from them as soon as possible. Some services of *day 1* list are reported below:

- Emergency Vehicle Approaching (EVA): aims at alerting about the presence of approaching emergency vehicles before the siren or light bar on-board the vehicle is audible or visible, thus allowing vehicles to have more time to clear the road and, consequently, reducing the number of unsafe manoeuvres. This is a critical service for safety.

- Slow or Stationary Vehicle(s): alerts approaching drivers in the event of slowdowns or vehicles which have stopped/failed during the journey. It is a critical service for safety; however, it can also benefit traffic efficiency.

- Traffic Jam ahead Warning (TJW): alerts drivers about queues near a traffic jam. This service can be handy when, for example, the tail is hidden (e.g., behind a hill or curve). It is a critical service for safety, but it can also benefit traffic efficiency.

- Road Works Warning (RWW): informs drivers about current road works and related restrictions. It is a critical safety service, but it can also improve traffic efficiency.

- Weather Conditions (WTC): aims to provide accurate and up-to-date local weather information. It is handy in dangerous and visually tricky weather conditions such as black ice or strong wind gusts.

- In-Vehicle Signage (VSGN): aims to provide preliminary information on relevant road signs in the environment surrounding the vehicle, thus increasing driver awareness. This is a critical service for safety.

- In-Vehicle Speed limit (VSPD): informs drivers about speed limits, either continuously or at a specific event (for example, in the vicinity of road signs). It is a critical service for safety; however, it can also benefit traffic efficiency.

- Shockwave Damping (SWD): aims to mitigate the occurrence of shockwave traffic to make the flow of vehicular traffic more smooth.

- Green Light Optimal Speed Advisory (GLOSA)/ Time To Green (TTG): provides speed advice to drivers approaching traffic lights, thus reducing the number of sudden accelerations or braking accidents. The optimisation of vehicle movement benefits traffic efficiency, vehicle operation (fuel economy), and the environment.

- Cooperative Collision Risk Warning (CCRW): aims to minimise the risk of collision when overtaking or merging with traffic. This is a critical service for safety.

- Infotainment services: provides different types of information to drivers. They can be further outlined as follows: Information on refueling and charging stations for electric vehicles (iFuel); Off-road parking information (Pinfo); Road and Parking Management (Pmang); Information about Park & Ride (P&ride); Traffic Information and Smart Routing.

The second group of C-ITS services is called the *day 1.5*: these are services for which full specifications or standards might not be entirely ready for large-scale deployment, even though they are considered to be generally mature. Some services of *day 1.5* list are reported below:

- Vulnerable Road user protection.

- On street parking management & information.

- Off street parking information.

- Park & Ride information.

- Connected & Cooperative navigation into and out of the city (1st and last mile, parking, route advice, coordinated traffic lights).

- Traffic information & Smart routing.

C-ITS services	Involved interlocutors		Standardised messages				Communication technology		Priority in deployment	
	V2I	V2V	CAM	DENM	SPaT	MAP	ETSI-G5	Cellular	Day 1	Day 1.5
EBL		x		x			x		x	
EVA		x	x	x			x		x	
SSV		x	x	x			x		x	
TJW		x		x			x		x	
HLN	x	x		x		x	x		x	
RWW	x		x	x		x	x	x	x	
WTC	x	x	x	x			x	x	x	
VSGN	x		x		x	x	x	x	x	
VSPD	x		x		x	x	x	x	x	
PVD	x		x		x		x	x	x	
SWD	x		x				x	x	x	
GLOSA/TTG	x		x	x	x	x	x		x	
SigV	x		x	x	x	x	x		x	
TSP	x			x	x	x	x		x	
Infotainment[1]	x		x				x	x		x
LZM	x		x				x	x		x
ZAC	x		x				x	x		x
VRU	x	x		x	x		x			x
CCRW		x		x			x			x
MCA		x		x			x			x
WWD	x			x		x	x			x
CCN	x	x	x	x	x	x	x	x		x

Figure 2.6: C-ITS services and relative features.

A wider and detailed list of C-ITS services and relative features is reported in Fig. 2.6.
A more general classification of C-ITS services is given by CAR 2 CAR Communication Consortium: *day 1* services focus on exchanging information enhancing foresighted driving; *day 2* services improve the service quality and share perception and awareness information; *day 3+* adds further sophisticated services like sharing intentions, supporting negotiation and cooperation that paves the way towards cooperative accident free automated driving. Moreover, the Consortium divides the C-ITS services based on three use cases:

- The exchange of status data via cooperative V2X communication, e. g. the position, speed, driving direction, or special events like a vehicle defect, enables a set of information and warning services. They support road users in driving with foresight and get aware of potential risks which are not yet visible to them. Examples are Intersection Collision Warning, Emergency Vehicle Warning, Dangerous Situation Warning, Stationary Vehicle Warning, Traffic Jam warning, Pre-/Postcrash Warning.

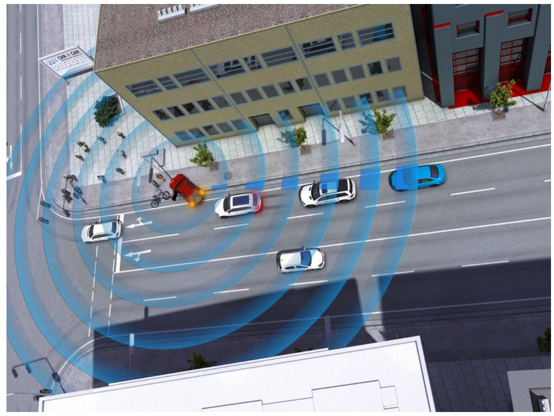

Figure 2.7: Awareness Driving example.

- Sensing Driving: on top of status data, cooperative V2X capable road users can share observations gained by sensors and advanced environmental information. This way, other traffic participants are warned against dangers they cannot perceive themselves yet; non-communicating road users are taken into account and protected in different traffic situations. Examples are (Fig. 2.8): Overtaking Warning, Extended Intersection Collision Warning, Vulnerable Road User Warning, Cooperative Adaptive Cruise Control, Long-term Road Works Warning, Special Vehicle Prioritisation.

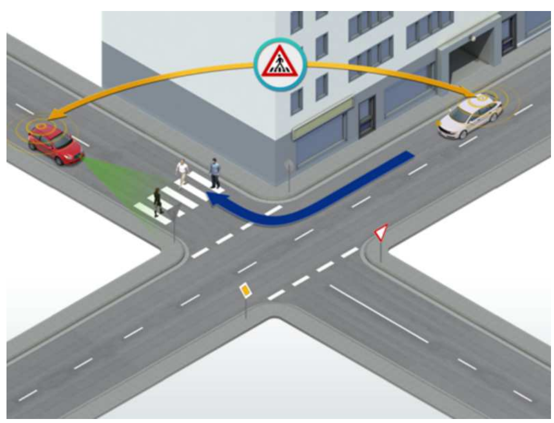

Figure 2.8: Sensing Driving example.

- Cooperative Driving (Fig. 2.9): in addition to status and sensor data, cooperative V2X road users can also provide intention data, allowing them to interact intelligently and coordinate their behaviour even in complex traffic situations. The prediction of the expected behaviour of all road users is an essential requirement for the long-term goal of highly automated and autonomous driving. Examples are: (Static or dynamic) Platooning, Area reservation, Cooperative Merging, Cooperative Lane Change, Cooperative Overtaking.

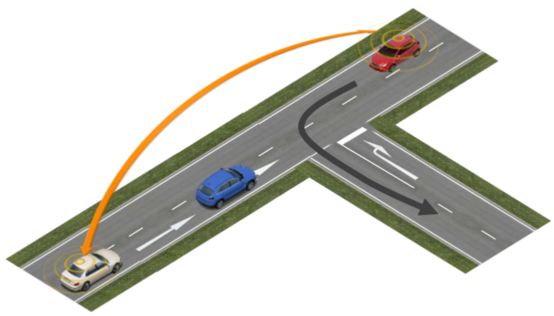

Figure 2.9: Cooperative Driving example.

2.4 Communication Standard

C-ITS services described in Sec. 2.3 needs to be supported by both standardised messages and suitable communication technologies which, hence, enable their development. The two wireless technologies that support connected vehicles are DSRC and C-V2X [24, 25].
The DSRC and C-V2X communication technologies are capable of providing the vehicle safety applications within the message requirements of 1 $[Hz]$ to 10 $[Hz]$ periodicity and end-to-end latency of $50 - 100$ $[ms]$. However, as vehicles become more advanced and, as they evolve towards intelligent and autonomous vehicles, the Quality of Service (QoS) requirements of V2X become more stringent. Thus, the existing V2X technologies need to evolve to enhance the reliability in advanced V2X use-cases for intelligent and autonomous vehicles. They should satisfy ultra-low latency, safety, and security enhancements beyond what the existing V2X applications have achieved based on basic safety applications

Use Case	Communication Mode	Pyaload (Bytes)	Max. Delay (msec)	Datarate (Mbps)	Minimum Range (m)	Reliability
Advanced driving	V2V, V2I	300–12,000	3∼100 ms	10–50	360–500	90–99.999
Remote driving	V2N	-	5 ms	UL:25/DL:1	-	99.999
Vehicle platooning	V2V, V2I	50–6000	10∼500 ms	50–65	80–350	90–99.99
Extended sensors	V2V, V2I, V2P	1600	3∼100 ms	10–1000	50–1000	90–99.999

Figure 2.10: Use cases and Quality of Service (QoS) requirements of V2X applications.

[26]. Some advanced V2X applications and their QoS requirements are listed in Fig. 2.10.

2.4.1 DSRC-Based V2X

The standardisation work of the DSRC has been carried out by: *i*) Institute of Electrical and Electronic Engineers (IEEE), a worldwide association of professionals to promote publications, conferences, and technological standards; *ii*) European Telecommunications Standards Institute (ETSI), the international body responsible for setting and issuing standards in the field of telecommunications across Europe. It is short-range communication technology, exploiting the 5.9 $[GHz]$ frequency band for data exchange, and relying on the IEEE 802.11p standard for its physical (PHY) and medium access control (MAC) layers. DSRC uses a MAC protocol that is simple, well-characterised, and capable of distributed operations. ETSI G5 DSRC allows the transmission of the following messages:

- Cooperative Awareness Messages (CAM): single-hop messages, sent with an adaptive frequency of $1-10$ $[Hz]$, including information such as location, type, and direction; they are periodically transmitted from each C-ITS agent to each nearest single-hop with a specific frequency.

- Decentralized Environmental Notification Message (DENM): multi-hop warning messages generated by ITS and C-ITS applications to warn neighbouring vehicles of potential dangers.

- Signal Phase and Timing Message (SPaT): include information about signal phase and timing of TLSs, the status of traffic controller, prediction of duration and phases, and permissions linked to manoeuvres instead to lanes.
- Map Data message (MAP): include information about the road network topology.

The considered communication technology enables cooperative awareness applications such as vehicle warning, vehicle traffic management, and emergency brake lighting. DSRC performance is adequate for most vehicle safety applications requiring end-to-end latency around 100 [ms] as long as the vehicle density assumes low values [27]. However, the adoption of DSRC in vehicles has been delayed due to its poor scalability and communication challenges imposed by high-mobility environments. Indeed, its performance degrades if the vehicle density increases due to packet collisions from the simultaneous transmission, the hidden node problem, and weakness in the physical layer (i.e., radio technology). Hence, since intelligent vehicle connectivity requirements and applications are growing exponentially, DSRC cannot get closer to the ever-increasing needs of such applications due to its limitation in satisfying all of the specifications of future V2X requirements. Moreover, the infrastructure of DSRC needs RSUs, taking a massive amount of time and money for global implementation. To overcome the issues in terms of MAC throughput, inter-operability, Doppler shift, and so on, the IEEE 802.11 Next Generation V2X Study Group is developing the IEEE 802.11bd [11]. Fig. 2.11 summarises the advancements in 802.11bd over 802.11p.
Moreover, the 802.11bd should be able to meet the following requirements: *i*) coexistence, i.e., it must coexist with 802.11p; *ii*) inter-operability, i.e., devices, information systems, or applications should be inter-operable in such a way that 802.11p devices can detect and decode at least one of the transmission modes from 802.11bd devices and vice-versa; *iii*) fairness, i.e., the 802.11bd and 802.11p standards must have fair communication and access capabilities in co-channel configurations; *iv*) backward compatibility, i.e., at least one mode of 802.11bd must be inter-operable with 802.11p.

[11] `https://www.ieee802.org/11/Reports/tgbd_update.htm`

Features/ Mechanisms	802.11bd	802.11p
Frequency band	5.9 GHz/ 60 GHz	5.9 GHz
Sub-carrier spacing	312.5 KHz/ 156.25 KHz/ 78.125 KHz	156.25 KHz
Channel coding	LDPC	BCC
Re-transmission	Congestion dependent	None
Cyclic Prefix (CP)	1.6 us and 3.2 us	1.6 us
Spatial streams	Multiple	One
Relative vehicle speed	500 km/hr	252 km/h
Doppler shift counter measures	High density midambles	None

Figure 2.11: Feature comparison between 802.11bd and 802.11p.

2.4.2 Cellular V2X

More recent V2X communication exploits cellular networks, i.e. the C-V2X technology developed by the 3^{rd} Generation Partnership Project (3GPP) based on V2X RAT in release 14, which gives the highest priority for modifications of radio access suitable for V2X. Long-Term Evolution (LTE) for vehicles has been introduced as in-vehicle networks as an alternative to DSRC for ITS and C-ITS services. More recently, in 3GPP release 15 the V2X functionalities were expanded to support 5G; hence C-V2X technology will offer superior performance to support connected vehicles communicate with transport infrastructure, leading to less congestion, reduced emissions, and a smoother driving experience. The standard introduced two types of communications: network communications using the Uu interface (the radio interface between the user equipment and the enodeB) and direct communications using the sidelink channel over the PC5 interface. Network communications operate over licensed spectrum, and messages are relayed to vehicle user equipment (UEs) using evolved node B (eNodeB). In contrast, direct communications occur in the $5.9\,[GHz]$ spectrum, allowing vehicles to exchange information directly. While 3GPP defines the data transport features that enable V2X, it does not include V2X semantic content. Still, it proposes the usage of DSRC standards like CAM and DENM over 3GPP V2X data transport features [12]. Multiple industry organisations, such as the 5G Automotive Association (5GAA), promote C-V2X due to its advantages over DSRC: 4G+/5G can be used for basic safety

[12] `https://www.3gpp.org/release-15`

applications, does not suffer from the problem of shadowing (elements such as buildings, trees, and walls that are common in urban environments constitute an obstacle to high frequency communications), improve Non-Line of Sight (NLoS) capabilities and has been proved to be more reliable, as well as more cost-effective and easier to deploy [28]. Moreover, C-V2X is intrinsically less disturbed as cellular networks operate within a controlled and licensed spectrum, and, not least, it enables the V2N communication, which does not exist in 802.11p based V2X networks.
The so-called 5G New Radio (5G NR) standard is currently under development to meet ultra-reliable and ultra-low latency requirements, which are particularly useful for autonomous driving applications. Incorporating a mobile network provider for V2N will facilitate frequencies beyond ITS, with high service quality in low bands and millimetre waves in 5G. Since C-V2X is already standardised and commercial deployments are underway [29], NR V2X will not replace it, but it aims to provide support and ensure all V2X applications in C-V2X efficiently. To ensure that 5G NR provide unified support for all V2X applications, it should be capable of supporting both advanced V2X applications and basic safety applications that are supported by present-day C-V2X.

2.4.3 Comparison between Cellular and Non-Cellular V2X Technologies

In a V2V scenario, one of the key challenges to realise ultra-reliable connectivity is the high Doppler shift. NR V2X can better handle the Doppler shifts, and as a result, it can outperform IEEE 802.11bd based on reliability [29]. The salient features described above make NR V2X more reliable, efficient, and flexible than other technologies. A comparative overview, including all standard features of 802.11p, 802.11bd, LTE V2X, and NR V2X are given in Fig. 2.12

2.5 Testing and Validation Methods

The increasing complexity of C-ITS systems requires efficient and effective ways to test and evaluate them to guarantee safety, quantify possible advantages and evaluate arising issues. Design and validation

Features	802.11p	802.11bd	LTE V2X	NR V2X
Base technology	802.11a/n	IEEE802.11n/ac	4G/LTE	5GNR
Radio bands	5.9 GHz	5.9 GHz,60 GHz	5.9 GHz	5.9 GHz~52.6 GHz including mmWave
Channel coding	BCC	LDPC	Data:Turbo coding Control:Convolution coding	Data:LDPC Control: Polar coding
Subcarrier spacing	156.25 KHz	312.5 KHz,156.25 KHz,78.15 KHz	15 KHz	Sub-6 GHz:15,30,60 KHz mmWave:60, 120 KHz
Retransmission	None	Congestion dependent	Blind	HARQ-based
Modes	Broadcast	Broadcast, groupcast	Broadcast	Broadcast, groupcast, unicast
PHY layer	N/A	OFDM	SC-FDMA	SC-FDMA, OFDM
Interoperability	N/A	Yes	N/A	Non co-channel
mmWave support	N/A	Yes	N/A	Yes

Figure 2.12: An overall comparison of 802.11p, 802.11bd, LTE V2X, and NR V2X based on common features.

methods should demonstrate the behavioural competencies an automated/autonomous vehicle would be expected to perform during a routine operation, the performance during crash avoidance situations, and the performance of fallback strategies. Test approaches may include a combination of simulation, test track, and on-road testing [30].

2.5.1 Field Operational Test

Field Operational Test (FOT)s are the most realistic validation methods, as they are held with the prototype vehicle in public or confined areas. The high degree of reality requires more effort and thus comes at a higher cost. Traditionally, manufacturers have always sought to reduce the amount of testing in FOTs as much as possible. There are two main types of FOTs: real-world and closed area.

2.5.1.1 Real-World Traffic Testing

Test drives in real-world traffic are performed on public roads to test the capabilities and compliance with the safety requirements of an automated/autonomous vehicle. In addition to the apparent advantage of driving in a natural, targeted environment, it has many disadvantages. The first drawback is the low repeatability of test conditions, which are non-reproducible. Secondly, the car must be fully functional, so these tests must be carried out at the end of product development, extending the development time. Test drives can cause danger to other users and the driver himself, so it is required to avoid testing immature systems. Also, testing on public roads is inconvenient and time-consuming, as every hardware or software modification requires returning to the site of the company. The strengths of this testing methodology are summarised below:

- High environmental validity: allows for validation of the vehicle in its intended Operational Design Domain (ODD)(s) and the diverse conditions these may present.
- Can be used to test scenarios elements, such as weather and infrastructure (e.g., bridges, tunnels), that are unavailable through track testing.
- May be used to validate the simulation and track-testing by comparing an acADAS performance within a simulation and track test with its performance in a real-world environment when executing the same scenario.
- Can be used to assess aspects of the acADAS performance related to its interaction with other road users, e.g., maintaining the flow of traffic, being considerate and courteous to other vehicles.
- Allows model, single software, and tool-chain validation.

The weaknesses of this testing methodology are summarised below:

- Limited controllability: public-road scenarios afford a limited amount of control over ODD conditions.
- Limited reproducibility: public-road scenarios are difficult to replicate precisely in different locations.
- Restricted repeatability: public-road scenarios are challenging to repeat precisely over multiple iterations.

- Limited scalability: public-road scenarios may not scale up sufficiently.
- Costly, but not as expensive as track testing, requires many resources, and is time-consuming.
- Safety risks: on-road testing could subject test personnel and the public to significant risks of unsafe behaviour.

2.5.1.2 Closed Area Testing

Closed area testing area on-field test carried out in closed areas specially adapted for testing. This kind on test methodology allows the physical vehicles to be tested through a limited set of realistic scenarios (based on the test track geometries, dimensions, size, and ODDs to evaluate either subsystems or the fully assembled system. These external inputs and conditions can be controlled or measured during a test. This method allows testing the vehicle with less danger than what is likely posed within real-world tests. However, operating on test tracks can be resource-intensive; therefore, testing on a test track will be based on selected known critical scenarios. The strengths of this testing methodology are summarised below:

- Controllability: allows for control over many of the test elements, including certain ODD aspects.
- Fidelity: involves functional, physical ADS-equipped vehicles, real obstacles, and environmental conditions.
- Reproducibility: scenarios can be replicated in different locations by different testing entities.
- Repeatability: allows for multiple iterations of tests to be run in the same fashion, with the same inputs and initial conditions.
- Efficiency: compared to real-world testing, closed-course testing can accelerate exposure to known rare events or safety-critical scenarios by setting them up as explicitly designed test scenarios. Road testing, by contrast, could be an inefficient way to test less co manifesting by chance.

- can be used to validate the quality of the simulation tool-chain by comparing the performance of an acADAS within a simulation test with its performance on a test track when executing the same scenario.

The weaknesses of this testing methodology are summarised below:

- Time effort: can take a significant amount of time to set up and execute.
- Cost Effort: may require a large number of personnel and specialised test equipment (e.g., obstacle objects, measurement devices, safety driver).
- Limited variability: facility infrastructure and conditions may be challenging to modify to account for a wide variety of test elements (e.g., ODD conditions). They are restricted to their geometries, dimensions, size, and ODD limitations such as weather conditions, time of day, number, and type of other traffic agents.
- Safety risks: physical vehicles and obstacles represent a potentially uncertain and hazardous environment for the test participants.
- Representativeness: even with its increased fidelity, it is not possible to replicate at all the clutter or real-world environment.

Artificial Cities Artificial cities are fake cities purposely built to perform testing of AD. Such cities exist, among others, in South Korea (K-city) [31] or in the USA (Mcity) [13]. For instance, Mcity consists of 40 building facades, a tunnel, a bridge, a four-lane highway, mechanical pedestrians, standard road markings, and traffic lights. Testing in such conditions has many advantages, such as testing in states that do not threaten other road users. Moreover, all test conditions are almost reproducible except for weather conditions. A significant advantage is the possibility of any environment configuration, for example, by changing signs or traffic lights. Despite all these advantages, this method still has some drawbacks, including a degree of danger to the driver during the tests. Furthermore, building such a city is very expensive and time-consuming, and the car itself must still be fully functional.

[13] `https://mcity.umich.edu/our-work/mcity-test-facility/`

Test Track A cheaper alternative is testing on test tracks (or empty squares). Individual obstacles are placed on the track to validate a given safety-purpose designed system, e.g., emergency braking. This kind of testing is probably the most popular because it is the cheapest and fastest to implement. It is often the initial phase before testing in road traffic.

Semi-Virtual Tests It is common to combine a virtual test drive with a real one. In the beginning, the entire real track is mapped into the simulation. Then, a test car equipped with a high-accuracy Differential GPS (DGPS) sends its location to the simulator, which sends back the environment data. This information is sent directly to the ECU of the radar, and the active safety system is triggered. The test is carried out on a real track where there are no road users, while from the perspective of the car, it is driving along the same track simultaneously with other cars. Often, in such an environment the driver is equipped with goggles, in which elements generated by the simulator augment the reality. Another approach to semi-virtual tests is to drive on an empty track where the driver is equipped with VR goggles displaying the completely virtual test drive. The advantage of this approach is that the driver experiences all of the relevant forces while conducting a virtual test drive []. Semi-virtual tests often require the presence of a driver in the car, which can be dangerous, especially when the vehicle is a prototype. This risk can be avoided by replacing the driver with actuators that can be controlled remotely.

2.5.2 Virtual Testing

Virtual testing is a powerful approach to assessing the performance of automated/autonomous systems under diverse and complex conditions prohibitive for conventional physical testing. Virtual testing includes replacing one or more physical elements characterised in a scenario-based test with a simulation model. The goal of such virtualisation is to resemble, to a sufficient extent, the original physical elements. For instance, in automotive applications, virtual testing is used to reproduce the driving environment (and the objects therein) that interact with either the entire system (e.g., a full vehicle and a C-ITS system), a subsystem (e.g., an actuator or a hardware controller), or a component (e.g., a sensor). In this perspective, virtual testing expands the scope

of physical testing to account for the diversity of traffic. Indeed, such an approach allows cost-effectively assessing systems performance across ranges of variables and arrays of scenarios. Furthermore, it enables results of limited physical tests to be supplemented by verifiable data covering variations on the physical test scenario and the coverage of safety-critical scenarios. All these advantages reduce the burden on physical tests (offsetting their weaknesses) to improve the efficiency of the overall assessment process. Hence, speed and flexibility requirements in analysing real-world events to verify performance against real-world events and, if necessary, support modifications to improve performance are ensured. Another significant advantage is the possibility to assess performance boundaries of automated/autonomous systems: through methods of randomisation and compositions, it is possible to challenge the system with unexpected, unplanned scenarios, and thus increases the confidence in the performance of the system under investigation when challenged with low probability events. Moreover, virtual testing has the significant advantage of allowing the safe verification of specific requirements, also in conditions characterised by vast uncertainty, without the risk of real accidents and crashes (or incipient collisions) such as during autonomous manoeuvring [32].
Virtual testing is particularly indicated to test the C-ITS services under safety-critical scenarios that would be difficult and unsafe to reproduce on test tracks or public roads. Hence, through this approach is possible to get confidence about the C-ITS service based on the virtual tests and validation that was performed by the developer in an agile, controllable, predictable, repeatable, and efficient manner.
The simulation tool-chain used for virtual testing may result in different approaches. Before introducing these latter, it is worth noting that the interaction between the system under the test and the environment can either be an open or closed-loop:

- Open-loop virtual tests: virtual objects actions are data-driven only, and the information is not self-corrected based on feedback from the output.

- Closed-loop virtual test: a feedback loop that continuously sends information from the closed-loop controller to the C-ITS service. Within these test systems, the behaviour of the digital objects could react in different ways depending on the action of the system under test.

Model-in-the-Loop In Model-in-the-Loop (MiL) approach, the designed system is a model created in a modelling tool, e.g., in MATLAB/Simulink. By employing generic components, a general, high-level system model is created. As a result, it is possible to design the system without entering the implementation details. Testing the model involves providing a set of simulated signals and checking its response.

Software-in-the-Loop In Software-in-the-Loop (SiL) approach, the implementation of the developed model is evaluated on general-purpose computing systems. This step can use a complete software implementation close to the final one. SIL testing is used to describe a test methodology, where executable code such as algorithms (or even an entire controller strategy) is tested within a modelling environment that can help prove or test the software. Such an approach brings with it some risks: *i*) if the computer program is compiled with a different compiler, the machine code may be slightly different from a machine code compiled with a dedicated compiler; *ii*) during execution on the final hardware, such programs can behave differently.

Hardware-in-the-Loop Hardware-in-the-Loop (HiL) involves the final hardware of a specific vehicle sub-system running the final software with input and output connected to a simulation environment to perform virtual testing. HIL testing provides a way of replicating sensors, actuators, and mechanical components that connects all the I/O of the Electronic Control Units (ECU) being tested long before the final system is integrated. This is probably the most common type of testing in the automotive industry, because usually the manufacturer of the designed device is responsible for only one device and has no access to other cooperating devices. The main drawback is that the device is not tested in the real environment with other real ECUs, with real power supplies, etc. Therefore, there is a chance that the device will not work correctly in a real environment.

Vehicle-in-the-Loop Vehicle-in-the-Loop (ViL) is a fusion environment of a real testing vehicle in the real-world and a virtual objects. It can reflect vehicle dynamics at the same level as the real-world, and it can be operated on a vehicle test bed or a test track. This testing method is often possible to meet the terms of testing in the open and closed-loop.

Driver-in-the-Loop Driver-in-the-Loop (DiL) is typically conducted in a driving simulator to test the human-automation interaction design. DiL has components for the driver to operate and communicate with the virtual environment.
Since they are based on the utilisation of physical hardware, all described methods (except SiL and MiL) have to be conducted in real-time, resulting in complications regarding their scalability.
Strengths of this testing methodology are summarised below:

- Controllability: it affords an unmatched ability to control many aspects of a test. Agility: allows for system changes to be reevaluated immediately.
- Efficiency: many tests can be run concurrently in a relatively short amount of time (also in MIL and SIL approaches).
- Cost effectiveness at test execution: the running costs connected to its use are considerably lower than those required by physical testing.
- Wide scenario coverage: compared to other testing methods, virtual testing allows a wider exploration of safety-critical scenarios.
- Data gathering and analysis: offers a convenient and error-free platform for data gathering and analysis of the system performance.
- Repeatability and replicability: simulation affords the re-execution of the same virtual test without deviations due to stochastic phenomena. Faults in the functioning of the ADS can thus be identically replicated at any moment.

The weaknesses of this testing methodology are summarised below:

- Lower environmental fidelity/reliability: it is challenging and likely impossible for models to completely reproduce the environment, responses, and behaviour of the vehicle, other road users, etc., in the real world.
- Risk of over-reliance: without proper consideration of models intrinsic limitations, a risk exists to put too much emphasis on virtual testing results without sufficient proof of their validity by physical testing.
- Expensive software life-cycle: the availability of a simulation model to execute virtual testing requires covering specific aspects of the software life-cycle, which can be costly and time-consuming.

It is worth noting that virtual simulation approaches have been recognised as a key component to foster the development of connected and autonomous driving technologies on public roads according to the recent technical literature (see e.g. [33]). Moreover, as a matter of fact, in the automotive industry 80% improvements of automated vehicles comes from simulation, according to Krafcik, CEO of Waymo (see [34] and [35]). In addiction, the importance of using simulations to provide a broader and robust assessment of advanced technologies and innovating solution aiming at improving passenger autonomous car safety is also highlighted in the Euro NCAP 2025 Roadmap (2018) [14] and clearly emerges from the guideline documents of the European Commission [15] [16]. According to this trend, some Nations regulate the testing activities of automated/autonomous vehicles via virtual simulations before on-road tests, both on test roads and public ones, as in the case of the Italian *Smart Road Decree.* [17] stating that autonomous vehicles need to perform virtual experiments of at least $3000\,[Km]$ for each simulated use-case, before going on the Italian roads.Along this line, theoretical results in the automated driving field are usually validated via integrated virtual simulation platforms, e.g., see the very recent results in [35, 36].

[14] `https://cdn.euroncap.com/media/30700/euroncap-roadmap-2025-v4.pdf`

[15] `https://publications.jrc.ec.europa.eu/repository/handle/JRC119345`

[16] `https://ec.europa.eu/growth/content/guidelines-exemption-procedure-eu-approval-automated-vehicles_en`

[17] `https://www.gazzettaufficiale.it/eli/id/2018/04/18/18A02619/sg`

CHAPTER 3

Cooperative Driving Systems

Cooperative driving systems, one of the C-ITS services, exploit the wireless communication in addition to status and sensor data so to enable V2X road users to communicate with each other, hence providing intention data, allowing them to interact intelligently and to coordinate their behaviour even in complex traffic situations. The prediction of the expected behaviour of all road users is an essential requirement for the long-term goal of highly automated and autonomous driving. Only the cooperative driving systems relating to vehicles will be dealt with in the following.

The idea of vehicles cooperating via wireless communication dates back to the 1980s [37] when California PATH program was established to study and develop vehicle-highway cooperation and communication systems [38, 39]. The basic idea is to enable the communication and the cooperation among neighbouring vehicles to safely reduce their mutual distance, hence increasing the road capacity, and suppress traffic shock-waves, hence reducing fuel consumption [40].

To allow communication among nearby vehicles or between vehicles and nearby fixed roadside equipment, different architectural solution for creating vehicular networks were proposed. Such architectures have to guarantee two primary communication paradigm:

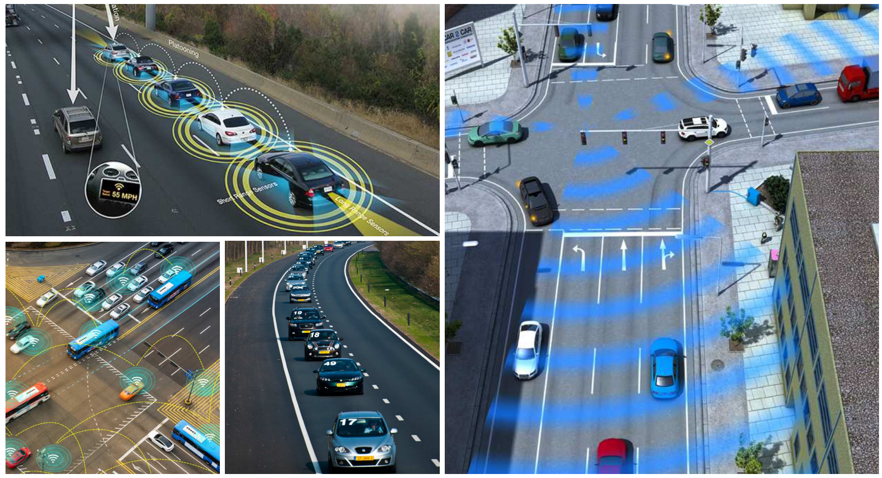

Figure 3.1: Cooperative driving systems.

- a pure wireless V2V , allowing vehicular communication with no infrastructure support;
- an hybrid V2I architecture that does not rely on fixed infrastructure in a constant manner, but can exploit it for improved performance and service access when it is available.

The V2I architecture implicitly includes V2V communication. The communication between vehicles or between vehicles and road infrastructure enable vehicles and infrastructure to form a cooperative system where the users exchange information and cooperate to improve the quality of the travel experience. In *cooperative driving systems* vehicles are organised as a platoon, i.e., a set of vehicles that, to reach a common objective, share information about their state information (position, velocity, acceleration, consumption, emission, etc.) or communicate with a road side infrastructure through a wireless communication network as in Sec. 2.4 (see Fig. 3.1). The core of such cooperative driving systems is a set of algorithms deployed on the vehicles and controlling their motion based on the behaviour of the surrounding vehicles so to achieve an inter-vehicle separation (smaller than the one guaranteed by human drivers, but safe) while increasing road capacity and decreasing, at the same time, traffic congestion [41, 42, 43]. Another benefit, originated by cooperation, is that the aerodynamic drag is reduced (especially for heavy-duty vehicles) thereby increasing fuel economy and, consequently, lowering pollutants emissions [44, 45]. The cooperative driving systems are characterised by distributed, hierarchical control to achieve these objectives. The high-level control structure takes decisions and computes set point for the lower level controller that acts on the throttle and brake systems. As an exemplary case, one can consider the architecture shown in Fig. 3.2 [46], where is possible to distinguish five layers: network layer, link layer, coordination, and planning layer, regulation layer, and physical layer. The aforementioned layer have the following functions:

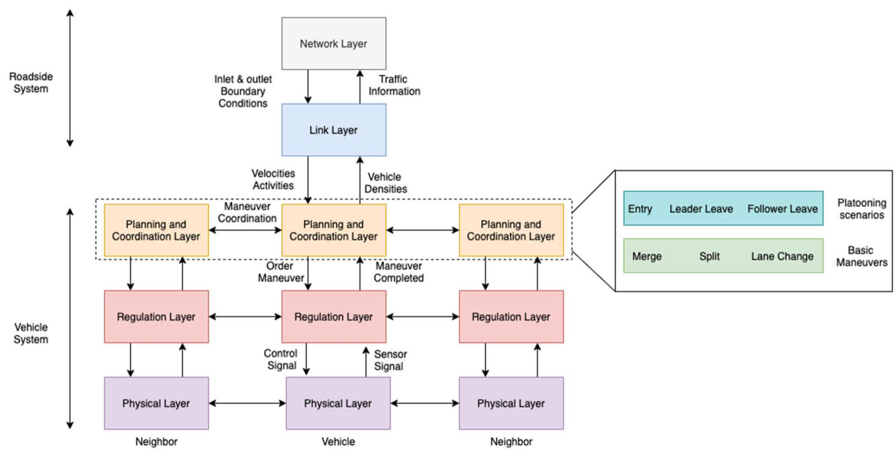

Figure 3.2: The architecture for the cooperative driving of autonomous/automated vehicles.

1. Network Layer: controls the traffic flow at the network level. It optimises the capacity of the whole set of roads and the average travel time for each vehicle and reduces transient congestion;

2. Link Layer: controls the link traffic flow to achieve its total capacity and minimise the travel time of vehicles and traffic congestion. Each link communicates with the neighbouring links and transfers the traffic flow between links. Links are divided into multiple sections, where aggregated vehicle density, speed, and flows are measured.

3. Coordination and Planning Layer: determines the intents of the different vehicles in the platoon, such as join, split and change lane

manoeuvres. This layer performs a structured data exchange via communication protocols with the neighbouring vehicles to safely execute such a manoeuvre.

4. Regulation Layer: it deals with the vehicle's lateral and longitudinal control. It receives the commands from the coordination layer and translates them into steering, throttle, and braking inputs to the on-board vehicle's actuators. It uses various continuous-time feedback control laws to generate inputs for the vehicle's actuators to execute the desired manoeuvres. This layer handles two longitudinal control tasks: maintaining specified velocity and inter-vehicle spacing and efficiently and safely performing manoeuvres outputted by the coordination and planning layer for the platoon leader or free agents.

5. Physical Layer: it consists of the local physical components which include local sensors, various lateral and longitudinal guidance, steering and brake control systems, and transmission and engine.

The criteria of the movement come from the traffic control layer. The traffic control layer has two parts: the physical part, which includes the infrastructure-based ITS equipment like sign boards, traffic signals, and the road-vehicle communications, and a logical part that contains common sense, laws, rules, manners, and ethics in the human society. Within the two parts, a criterion that must be common to neighbouring vehicles will be found and sent to the vehicle management layer in each vehicle. The cooperative control strategies that drive the collective behaviour of vehicles platoon are usually deployed on the regulation layer and network/link layer of the architecture in Fig. 3.2.
The control strategy precursors of the cooperative driving system introduced by the automotive industry is the ACC system. The ACC is considered to be the successor of the conventional CC. A vehicle with CC can maintain a pre-selected speed if no vehicle is upfront. The ACC is a radar-based system that is designed to enhance driving comfort and convenience by relieving the driver of the need to adjust speed to match that of a preceding vehicle continually. The system slows down the speed when it approaches a vehicle with a lower speed, and the system increases the speed to the level of speed previous set when the vehicle upfront accelerates or disappears (e.g., by changing lanes) [47]. Recently, V2V

communication has pushed the ACC system into a more sophisticated system, called Cooperative Adaptive Cruise Control (CACC). Each vehicle within the cooperative driving system is equipped with on-board sensors measuring position, velocity, acceleration. Such a set of measurements requires Inertial Measurement Unit (IMU), Global Positioning Systems (GPS), and radars, commonly available on vehicles. Each vehicle is also equipped with wireless V2V communication hardware to share information with its neighbours and receive reference signals. Thanks to the information of neighbours vehicles, CACC controller will be able to anticipate problems better, enabling it to be safer, smoother, and more reliable in response. In CACC, wireless communication is used by the controller to regulate speed and distance between vehicles, ensuring that any changes in speed by the driver in front of you are immediately registered in the cooperative vehicle. However, most of the CACC controller presented in the literature does not cope with communication failure/impairments, network delay, and security vulnerabilities. A flexible control system, re-configurable based on the actual communication capabilities, has to be designed to overcome these issues. In this sight, cooperative driving can be represented as a networked control system where the vehicles are controlled by handling their state information and networked information received from neighbouring vehicles through the communication network [48, 49, 50] in which the time-delays are explicitly modelled to give a more realistic representation of the cooperative driving systems [51, 52].

3.1 Modelling of Connected Autonomous Vehicles

Formation control of autonomous, connected vehicles is one of the typical problems addressed in the context of networked multi-agent systems (e.g., for the flight formation of autonomous aerial vehicles [53]). It follows that a multi-agent system has been naturally proposed as an alternative modelling approach to easily handle the coordination of ground vehicles (cars) and to manage platoon tasks (e.g. see [54, 55, 48, 56, 49, 57, 51, 58, 59] and references therein).

By leveraging this networked control system paradigm, a platoon composed of multiple connected and automated vehicles is represented as

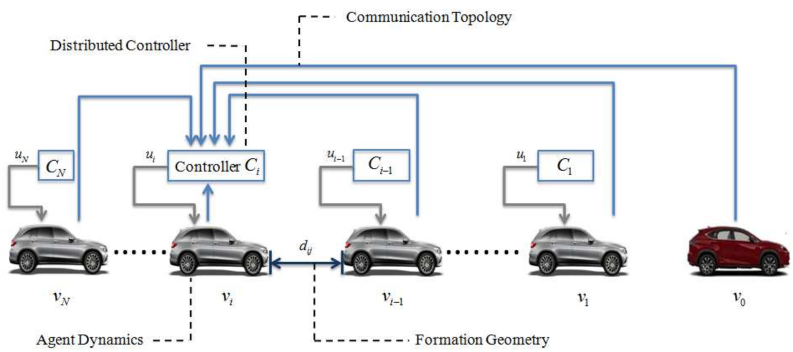

Figure 3.3: Schematic representation of autonomous connected vehicles platoons from networked control systems perspective [1].

a one-dimensional network of dynamical agents, in which each agent only uses its neighboured information to control its motion locally. At the same time, it aims to achieve specific global coordination with all other agents. This framework is schematically represented in Fig. 3.3 as the composition of the following main interrelated components: *a*) agent dynamics, that model the longitudinal dynamics of each vehicle; *b*) communication topology, which indicates how and if an agent obtains information about other agents depending on the active communication links *c*) formation geometry, which defines the desired spacing between adjacent vehicles in a platoon; *d*) distributed collaborative control that is implemented at the single-vehicle level and depends on both the state variables of the vehicle itself (measured on-board) and information received from neighboured vehicles through the communication topology.

3.1.1 Agent Dynamics

Each agent can be thought of as a generic non-linear control system of the form:

$$\dot{x}_i(t) = f_i(x_i(t)) + g_i(x_i(t))u_i(t), \tag{3.1}$$

where $x_i(t) \in \mathcal{R}^n$ is the state of the system and $u_i(t) \in \mathcal{R}^m$ the control inputs.

The complex mathematical form of multi-body vehicle models demands a simultaneous solution of the combined differential and/or algebraic equations, thus introducing convergent issues with an increased computational burden. However, while designing control requirements, these bulky models are rarely used in their raw form, owing to the inherent complexity in analysis and design. Accordingly, simplified versions of the vehicle models are widely used. Both pure longitudinal and complete (considering both longitudinal and lateral motion) control-oriented vehicle models, presented in the following, can be used for simulation studies performed during vehicle design or performance analysis.

Before introducing the several control-oriented vehicle models, it is worth noting that multiple vehicles are involved in cooperative driving applications. Thus a feature for the agent dynamics is homogeneity.

Definition 1. *A platoon of connected autonomous vehicles is homogeneous if all vehicles share identical dynamics; otherwise, it is heterogeneous.*

3.1.1.1 Longitudinal Models

The behaviour of each vehicle within the vehicular network is described by its longitudinal dynamics. These latter are inherently nonlinear due to some salient non-linearities involved in the power-train system, e.g., engine, drive-line, brake system, aerodynamics drag, tire friction, gravitational force [60].

For control design purpose, the following assumptions are usually made to obtain a concise model for cooperative driving control [61]: *i*) the longitudinal tire slip is negligible; *ii*)the vehicle body is rigid and symmetric; *iii*) the influence of pitch and yaw motions are negligible; *iv*) the driving and braking torques are controllable inputs.

Under the assumption mentioned above, the simplified resulting longitudinal dynamics for each i-th vehicle, still nonlinear, are described as follows [48] ($\forall i = 1, \cdots, N$, being N the number of the vehicle within the vehicular network):

$$\begin{aligned}
\dot{p}_i(t) &= v_i(t),\\
F_i(t) &= \Big(m_i\dot{v}_i(t) + mgsin(\theta_i(t)) + mgcos(\theta_i(t))\frac{C_r}{1000}(c_1 v_i(t) + c_2)\\
&\quad + \frac{\rho_{air}}{2}C_{D_i}A_{f_i}v_i^2(t)\Big)\frac{r_i}{\eta_i}\\
\dot{F}_i(t) &= \frac{F_{des,i}(t)}{T_i} - \frac{F_i(t)}{T_i},
\end{aligned} \tag{3.2}$$

where p_i $[m]$, v_i $[m/s]$ are the position and the speed of the i-th vehicle that are measured with respect to a road reference frame; m_i $[kg]$, ρ_{air} $[kg/m^3]$, $C_{D,i}$ $A_{f,i}$ $[m^2]$, g $[m/s^2]$, η_i, r_i $[m]$ are the mass, the air density, the aerodynamics drag coefficient, the front area, the gravitational acceleration, the mechanical efficiency of drive-line and the wheel radius for the i-th vehicle, respectively; the parameters C_r, c_1 and c_2 are related to the rolling resistance force and vary on basis of the road surface condition and the type of the vehicle tire; $F_i(t)$ $[N]$ denotes the actual driving/brake force; T_i $[s]$ is is the characteristic time constant of the drive-train depending upon specific features of the vehicle; $F_{des,i}(t)$ $[N]$ is the desired driving/brake force, i.e. the control input, that has to be imposed to vehicle dynamic in order to reach a specific control objective. However, control performance are difficult to analytically analyse for nonlinear models [61]. To this aim, linear models are more frequently used to formulate tractable problems. The most commonly used models for describing the i-th vehicle behaviour are:
paragraphSingle Integrator Model
The single integrator model is the simplest model for vehicle dynamics, where the vehicle speed is taken as the control input $u_i(t)$ and the position $p_i(t)$ is the only state variable [62], i.e.

$$\dot{p}_i(t) = u_i(t). \tag{3.3}$$

Second-Order Model One improvement compared to single integrator model is to consider the vehicle dynamic as a point mass, described by the following second-order dynamics[63]:

$$\begin{aligned}\dot{p}_i(t) &= v_i(t),\\ \dot{v}_i(t) &= \frac{1}{m_i}u_i(t),\end{aligned} \tag{3.4}$$

where p_i $[m]$, v_i $[m/s]$ are the position and the speed of the i-th vehicle; m_i $[kg]$ is the mass of the vehicle i; $u_i(t)$ $[m/s^2]$ is the control input, i.e. the desired acceleration that has to be imposed to the vehicle dynamic so to achieve the desired control objective.
Note that, although commonly exploited, the assumption of directly controlling the acceleration of the vehicle still does not capture some features of the internal vehicle dynamics, e.g., the inertial delay in power-train dynamics, and might lead to instability in real-world driving conditions [64].

Third-Order Model The third-order model is introduced to take into account the power-train dynamics of the vehicle. It is obtained by converting the nonlinear model (3.2) into a linear one for controller design via a feedback linearization technique [64]. Specifically, the control input $F_{des,i}(t)$ is selected as [61]

$$\begin{aligned}F_{des,i}(t) = \frac{r_{w,i}}{\eta_i}\Big(&C_{D,i}A_{f,i}v_i(t)(2T_i\dot{v}_i(t) + v_i(t)) + mgsin(\theta_i)\\ &+ mgcos(\theta_i)\frac{C_r}{1000}(c_1v_i(t) + c_2)\Big)\end{aligned} \tag{3.5}$$

where $u_i(t)$ is the new input after linearization. Then, the following linear model is obtained for vehicle longitudinal dynamics [65]:

$$T_i\dot{a}_i(t) + a_i(t) = u_i(t), \tag{3.6}$$

where $a_i(t)$ $[m/s^2]$ denotes the acceleration of vehicle i.
Considering the state space representation of model (3.6), the third order model for each vehicle is obtained as:

$$\dot{x}_i = Ax_i + Bu_i(t) \tag{3.7}$$

where $x_i(t) = [r_i(t)\ v_i(t)\ a_i(t)]^\top \in \mathbb{R}^3$ represents the i-th vehicle state vector $(i = 1, \cdots, N)$ (being r_i [m] and v_i [m/s] and a_i [m/s^2] the i-th

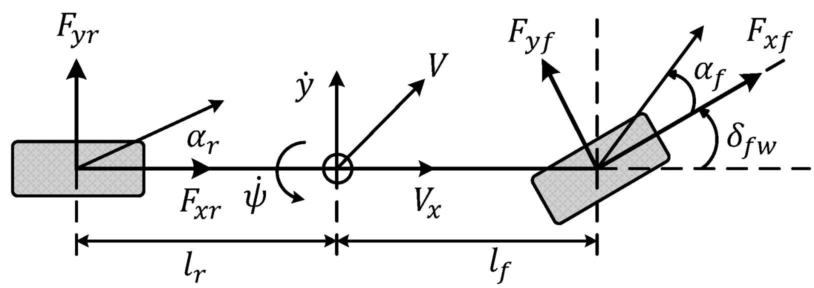

Figure 3.4: Vehicle 2-DOF bicycle model.

vehicle position, velocity and acceleration, measured with respect to road reference frame); $A \in \mathbb{R}^{3\times3}$ and $B \in \mathbb{R}^{3\times1}$ have the following expression:

$$A = \begin{bmatrix} 0 & 1 & 0 \\ 0 & 0 & 1 \\ 0 & 0 & -\frac{1}{T_i} \end{bmatrix}, \; B = \begin{bmatrix} 0 \\ 0 \\ \frac{1}{T_i} \end{bmatrix}. \tag{3.8}$$

3.1.1.2 Longitudinal-Lateral Models

Complete models are applicable for representing general longitudinal and lateral vehicle dynamics. The most commonly used models for describing the i-th vehicle behaviour are described in the following.

2-DOF Linear Bicycle Model The bicycle model is one of the most frequently used form of vehicle representation, owing to its simplicity and lesser computational requirements. For control design requirements not requiring critical dynamics analysis, this simplified model is of great applications [66].

The bicycle model, shown in Fig. 3.4, has 2 Degree-of-Freedom (DOF), i.e. yaw rate and lateral sliding angle.

The dynamic model has been formulated neglecting roll, bounce, and pitch with the following assumptions considered during the design: *i*) front, and rear tires lateral sliding and steering angles are neglected; *ii*) the longitudinal velocity remains almost constant; *iii*) a linear relationship is assumed to exist between the lateral forces of the tire and the sliding angle; *iv*) the front wheel is the guiding wheel. Accordingly, the dynamics of body slip angle (β) and yaw rate ($\dot{\psi}$ $[rad/s]$) representing the model can be obtained as

$$
\begin{aligned}
\dot{\beta}_i =& -2\frac{c^*_{f,i}+c^*_{r,i}}{m_i V_{x,i}}\beta_i + \Big(-1+2\frac{l_{r,i}c^*_{f,i}-l_{f,i}c^*_{r,i}}{m_i V^2_{x,i}}\Big)\psi_i + 2\frac{c^*_{f,i}}{m_i V_{x,i}}\delta_{f,i},\\
\dot{\psi}_i =& \Big(2\frac{l_{r,i}c^*_{f,i}-l_{f,i}c^*_{r,i}}{I_{z,i}}\Big)\beta_i + \Big(-2\frac{l^2_{r,i}c^*_{f,i}-l^2_{f,i}c^*_{r,i}}{I_{z,i}V_{x,i}}\Big)\psi_i + 2\frac{l_{f,i}c^*_{f,i}}{I_{z,i}}\delta_{f,i},
\end{aligned}
\tag{3.9}
$$

where subscript f and r stand for front and rear axle, respectively; $c^*_{f,i}$ $[N/rad]$ and $c^*_{r,i}$ $[N/rad]$ are nominal lateral stiffness; $l_{f,i}$ $[m]$ and $l_{r,i}$ $[m]$ are the distance of front and wheels from centre of gravity; $m_i[kg]$ is the mass of the vehicle; $V_{x,i}$ $[m/s]$ is the longitudinal speed; ψ_i $[rad]$ is the yaw angle; $I_{z,i}$ $[m\ N\ s]$ is the car inertia; $\delta_{f,i}$ $[rad]$ is the front steering wheel angle.
The tire lateral forces in terms of friction coefficient can be expressed in terms of friction coefficient μ:

$$
\begin{aligned}
F_{f,i} &= \alpha_{f,i}c^*_{f,i} = \alpha_{f,i}c_{f,i}\mu,\\
F_{r,i} &= \alpha_{r,i}c^*_{r,i} = \alpha_{r,i}c_{r,i}\mu,
\end{aligned}
\tag{3.10}
$$

where $c_{f,i}$ $[N/rad]$ and $c_{r,i}$ $[N/rad]$ are front and rear tire cornering stiffness, respectively.
According to [60], the desired yaw angle $\phi_{des,i}$ $[rad]$ can be expressed as

$$
\phi_{des,i} = arctan\left(\frac{\dot{Y}_{des,i}}{\dot{X}_{des,i}}\right),
\tag{3.11}
$$

being $\dot{X}_{des,i}$ $[m/s]$ and $\dot{Y}_{des,i}$ $[m/s]$ the longitudinal and lateral desired speeds, respectively, while $X_{des,i}$ $[m]$ and $Y_{des,i}$ $[m]$ are the desired global position coordinates. The trajectory of the centre of gravity in an absolute inertial frame could be calculated as

$$
\begin{aligned}
\dot{X}_i =& V_{x,i}cos\phi_{des,i} - V_{y,i}sin\phi_{des,i},\\
\dot{Y}_i =& V_{x,i}sin\phi_{des,i} + V_{y,i}cos\phi_{des,i}.
\end{aligned}
\tag{3.12}
$$

In spite of the simplicity of the bicycle model, it is seldom used for intricate control designs. Indeed, when used for vehicle operations involving hefty

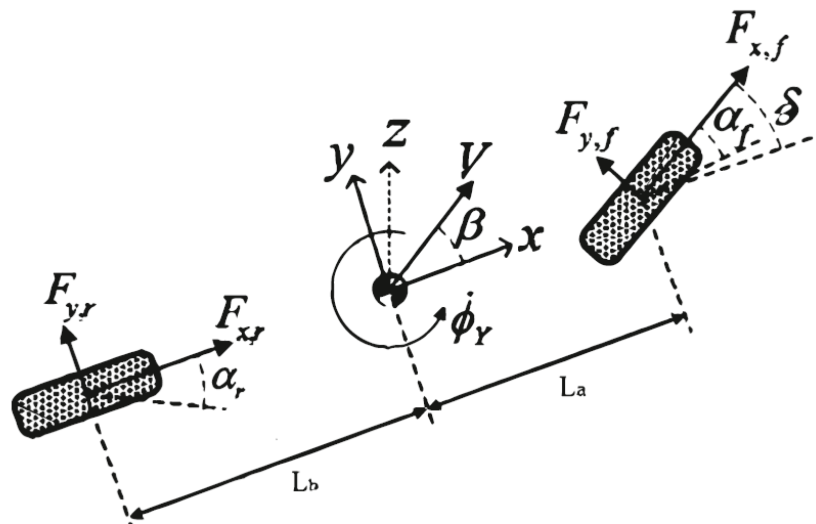

Figure 3.5: Non linear 3 DOF bicycle model.

lateral speeding, the linearized bicycle model predicted responses will vary considerably from the actual vehicle response. To this reason, in those case a nonlinear model reflecting the nonlinear attributes will be a better choice.

Non-linear Bicycle Model The model is formulated with the assumption that the vehicle mass is completely in the vehicle rigid base. From Fig. 3.5, the dynamic equations for the nonlinear bicycle model can be obtained as follows:

$$\begin{aligned} m_i(\dot{V}_{x,i} - V_{y,i}r_i) &= \sum F_{x,\star,i}, \\ (\dot{V}_{y,i} - V_{x,i}r_i) &= \sum F_{x,\star,i}, \\ I_{z,i}\dot{r}_i &= F_{y,f,i}l_{f,i} - F_{y,r,i}l_{r,i}, \\ r &= \dot{\psi} \end{aligned} \tag{3.13}$$

where $\star \in (f, r)$ indicates the front and rear axes; $F_{x,\star,i}$ $[N]$ and $F_{y,\star,i}$ $[N]$ represent the forces along x and y axis, respectively, computed as function of longitudinal tire force $F_{w,x,\star,i}$ $[N]$, lateral force $F_{w,y,\star,i}$ $[N]$ and the wheel steer angle $\delta_{f,i}$, as

$$\begin{aligned} F_{y,\star,i} &= F_{w,x,\star,i} \sin \delta_{\star,i} + F_{w,y,\star,i} \cos \delta_{\star,i}, \\ F_{x,\star,i} &= F_{w,x,\star,i} \cos \delta_{\star,i} - F_{w,y,\star,i} \sin \delta_{\star,i}. \end{aligned} \tag{3.14}$$

Considering drive moment $T_{w,d,\star,i}$ $[Nm]$ and braking moment $T_{w,b,\star.i}$ $[Nm]$ applying on each wheel, the rotational motion can be derived as

$$I_{z,i}\dot{\omega}_{w,i} = T_{w,d,\star,i} - F_{x,w,\star,i} r_{w,i} - T_{w,b,\star.i}, \tag{3.15}$$

where $r_{w,i}$ $[m]$ is the wheel radius. Again, the trajectory of the centre of gravity in an absolute inertial frame can be computed as in (3.12).

3.1.2 Communication Topology

The communication topology in cooperative driving applications indicates how each vehicle obtains information about its neighbouring vehicles. More specifically, it describes the data used by local on-board vehicles controller and thus strongly influences the collective behaviour of vehicles platoon. Early-stage cooperative driving applications were mainly based on radars and sensors to acquire information about the surrounding environment [67]. This implies that each vehicle could obtain, at most, information coming from its preceding and follower vehicles. In this case, the following communication topologies arise:

1. Predecessor-Follower (P-F). Each vehicle can exchange information only with its preceding vehicle;

2. Bidirectional (B-F). Each vehicle can exchange information with its preceding and follower vehicles.

More recently, the development of reliable wireless vehicular communication, leveraging V2V and/or V2I connectivity, has allowed the exchange of more information among vehicles and between a vehicle and the road infrastructure. Therefore new communication topologies, depicted in Fig. 3.6, are emerging in cooperative driving applications such as [68]:

1. Leader-Predecessor-Follower (L-P-F). Each vehicle can communicate with its preceding vehicle and the leading vehicle;

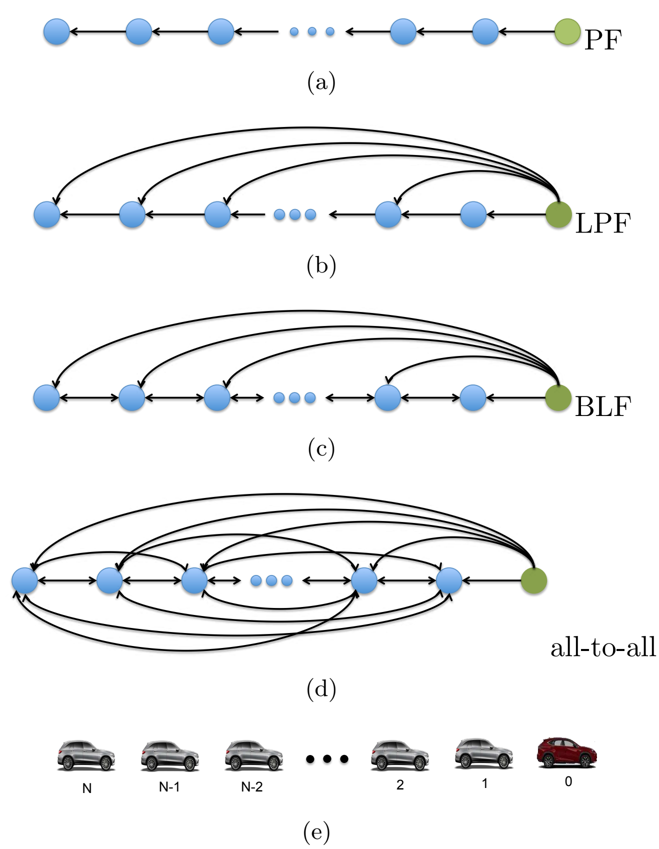

Figure 3.6: Exemplar platoon communication topologies: (a) Predecessor-Following (P-F), (b): Leader-Predecessor-Following (L-P-F); (c): Bidirectional-Leader-Predecessor (B-L-F); (d): All-to-All (Broadcast, BR); (e): Platoon of $N+1$ vehicles.

2. Bidirectional-Leader-Follower (B-L-F). Each vehicle can exchange information with its preceding vehicle, its follower vehicle and the leading vehicle;

3. All-to-All (Broadcast, BR). Each vehicle exchange information with all the other vehicles in platoon.

The network communication structure can be modelled by a graph where every vehicle is a node. Hence, a network of N vehicles is represented as a directed graph (digraph) $\mathcal{G} = (\mathcal{V}, \mathcal{E}, \mathcal{A})$ of order N characterised by the set of nodes $\mathcal{V} = \{1, \ldots, N\}$ and the set of edges $\mathcal{E} \subseteq \mathcal{V} \times \mathcal{V}$. The topology of the graph is associated to an adjacency matrix with non negative elements $\mathcal{A} = [\alpha_{ij}]_{N\times N}$. The adjacency matrix $\mathcal{A}$ is a matrix whose elements are 1 if and only if exists an edge from vertex i to vertex j. In what follows, it as assumed that $\alpha_{ij} = 1$ in the presence of a communication link from vehicle j to vehicle i, otherwise $\alpha_{ij} = 0$. Moreover, $\alpha_{ii} = 0$ (i.e., self-edges (i, i) are not allowed unless otherwise indicated).

In some situations, however, it is useful to represent edges as having strength, weight, or value, usually a real number. They are called weighted networks, and the adjacency matrix will not have elements equal to 1 or 0. Furthermore, it is possible to talk of delayed networks if the communication between agents, i.e., each network link, is affected by time-delay even though an own non-delayed dynamics characterise the agent. To analytically describe this situation, it is possible to define for each edge $(i, j) \in \mathcal{E}$ a function $\tau_{i,j}(t)$ that model the communication delay among agent i and agent j. Indeed, the assumption that a communication time-delay between agents is a very realistic assumption for many real systems such as the World Wide Web. In reality, communication is not instantaneous, but the exchanged information is affected by time-delays, although sometimes negligible.

The presence of edge $(i, j) \in \mathcal{E}$ means that vehicle i can obtain information from vehicle j, but not necessarily *vice-versa*. The degree of a vertex (also called degree matrix) i by Δ_i in a graph is, hence, defined as the number of edges connected to it. In general Δ_i is so calculated:

$$\Delta_i = \sum_{j=1, j\neq i}^{N} \alpha_{i,j}. \tag{3.16}$$

Furthermore, it is possible to introduce the diagonal matrix $\Delta \in \mathcal{R}^{N\times N}$ whose diagonal element are the vertex degrees:

$$\Delta = \begin{bmatrix} \Delta_1 & 0 & ... & 0 \\ 0 & \Delta_2 & ... & 0 \\ ... & ... & ... & ... \\ 0 & 0 & ... & \Delta_n \end{bmatrix}. \tag{3.17}$$

Thanks to the degree matrix Δ and to the adjacency matrix $\mathcal{A}$, another important matrix, called Laplacian matrix $L \in \mathcal{R}^{N\times N}$ can be defined:

$$L = \Delta - \mathcal{A} \tag{3.18}$$

For construction, the Laplacian matrix has zero row-sum, hence, at least one eigenvalue will be zero.
In the rest of the thesis, when dealing with cooperative applications, N vehicles plus a leader, taken as an additional agent labelled with the index zero (node 0), are considered. Hence, an augmented directed graph $\mathcal{G}_{N+1}$ to model the resulting network topology is used. To model the resulting graph $\mathcal{G}$, the pinning matrix [69] $\mathcal{P} = \text{diag}\{p_1, p_2, ..., p_N\}$ is considered, such that $p_i = 1$ when the leader information is directly available for the $i - th$ agent/vehicle, 0 otherwise. In so doing, the communication graph is described via the matrix $\mathcal{H} = \mathcal{L} + \mathcal{P} \in \mathbb{R}^{N\times N}$.
Moreover, in what follows, according to [70, 71] the following assumption is assumed to be held.

Assumption 1 ([70])**.** *The communication graph $\mathcal{G}$ contains a directed spanning tree with the leader as the root.* ▲

In so doing, node 0 is assumed to be *globally reachable* in $\mathcal{G}_{N+1}$. Thus there exists a path in $\mathcal{G}_{N+1}$ from every node i in $\mathcal{G}$ to node 0 [72]. Note that, in the typical network topologies for cooperative applications, shown in Fig. 3.6, the leader is always globally reachable (see [73] and reference therein).

Digraph Propriety A directed network or directed graph also called a *digraph* for short, is a network in which each edge has a direction, pointing from one vertex to another. Such edges are themselves called directed edges and can be represented by lines with arrows on them. An example of a directed network is the World Wide Web, in which hyperlinks run in one direction from one web page to another. Conversely, a graph is defined undirected if each edge has not a direction. A digraph is strongly connected if there is a path from every node to every other node. A strong component of a digraph is an induced sub-graph that is maximal, which is subject to being strongly connected. A directed tree is a digraph in which every node has exactly one parent node except for one node, called the root, which has no parent and has a directed path to every other node. It is possible to say that j is reachable from node i if a path exists from node i to node j. A node is globally reachable if it is reachable from any other node in the graph. The Laplacian matrix is a symmetric matrix with zero row-sum and real spectrum in the undirected graph. For a digraph, the Laplacian matrix is so defined:

$$L = [l_{i,j}] = \begin{cases} l_{i,i} = \sum_{j=1, j\neq i}^{N} \alpha_{i,j} & \\ l_{i,j} = -\alpha_{i,j} & i \neq j \end{cases} \tag{3.19}$$

3.1.3 Formation Geometry

Formation geometry defines the desired inter-vehicle spacing between adjacent vehicles in cooperative driving applications. There are several policies for formation geometry employed in cooperative driving, which can be classified into some groups based on their characteristics [74].

Constant Spacing Policy Constant Spacing Policy (CSP) [63, 75] keeps a constant inter-vehicle spacing between two adjacent vehicles, independent of both vehicle velocity and driving environment. This spacing policy can be simply expressed as

$$D_{des} = d_0, \tag{3.20}$$

where D_{des} $[m]$ denotes the desired inter-vehicle spacing and d_0 $[m]$ represents a fixed positive constant. The computation load of the CSP is low, and it provides high traffic capacity if a small d_0 is chosen.

Time Headway/Time Gap based Spacing Policy Time Headway-based spacing policies are based on the computation of a time-based reference distance. In some works the phrase *time gap* is employed instead of *time headway.* The time gap is the period during which the rear bumper of the preceding vehicle and the front bumper of the host vehicle passes a fixed position on the road. In contrast, the time headway refers to the period during which the front bumper of the preceding vehicle and the front bumper of the host vehicle passes a fixed position on the road. In this case., the desired inter-vehicle spacing varies with vehicle velocity, which is more likely per driver behaviours, but has a limit on achievable traffic capacity. The first Time Headway/Time Gap based spacing policy was proposed based on the kinematic relationship between the preceding and host vehicles [76]:

$$D_{des} = d_0 + vh + c(v^2 - v_p^2), \tag{3.21}$$

where c $[s^2/m]$ is a constant coefficient; v $[m/s]$ is the speed of the host vehicle; v_p $[m/s]$ is the speed of the preceding vehicle; h $[s]$ is the constant inter-vehicle time-headway or time-gap distance. For tight vehicle following conditions, i.e. v is close to v_p, relation in (3.21) simplifies to the so-called Constant Time Headway (CTH) or CTG policy [48, 49, 67]:

$$D_{des} = d_{st} + vh, \tag{3.22}$$

where $d_0 = d_{st}$ $[m]$ represents the fixed constant standstill distance. The CTH is consistent with the driving intuition of slowing down as the inter-vehicle spacing decreases, its computation load is low and the value of h can be easily changed. For these reasons, the CTH/CTG spacing policy has become the most common spacing policy in both academia and automotive industry [77]. However, the CTH/CTG spacing policy is not suitable for high density traffic conditions since: *i*) it reduces traffic throughput as the inter-vehicle spacing increases [78] ; *ii*) it can not guarantee the traffic flow stability [77]. To overcome the first issue, Yanakiev [79] developed a Variable Time-Headway (VTH) (or Variable Time-Gap (VTG)), where h is computed as:

$$h = sat(h_0 + c_h v_r) = \begin{cases} h_{max}, & \text{if } h_0 + c_h v_r \geq h_{max}, \\ h_0 + c_h v_r, & \text{if } h_{min} < h_0 + c_h v_r < h_{max}, \\ h_{min}, & \text{otherwise}, \end{cases} \tag{3.23}$$

being h_0 $[s]$ and c_h $[s^2/m]$ constant, while h_{max} $[s]$ and h_{mim} $[s]$ are the maximum and minimum values of time-headway/time-gap.
The exploitation of nonlinear function of vehicle velocity [80, 81, 58] to compute the desired inter-vehicle distance can allow balancing the traffic flow stability and traffic capacity compared with CTH/CTG in (3.22) and VTH/VTG in (3.23). For instance, to decrease the inter-vehicle spacing, a speed parameter can be introduced in (3.22):

$$D_{des} = d_{st} + v(h - v^{\star}), \tag{3.24}$$

where v^{star} $[m/s]$ is a reference speed, shared by all vehicles in the platoon, that can be chosen as the speed of the lead vehicle, the minimum speed in the platoon or according to the following relation []:

$$v^{\star} = \begin{cases} 0, & \text{if } e_1 < S_1, \\ \bar{v^{\star}}, & \text{if } S_1 \geq e_1 \leq S_2, \\ V_{max}, & \text{if } e_1 > S_2, \end{cases} \tag{3.25}$$

where S_1 and S_2 are two positive constants; V_{max} $[m/s]$ denotes the maximum speed in the platoon; e_i $[m]$ is defined as $e_i = d_i - d_0$; $\bar{v^{\star}}$ $[m/s]$ takes the following form:

$$\bar{v^{\star}} = \frac{V_{max}}{2}\Big[1 - cos(\pi\frac{e_i - S_1}{S_2 - S_1})\Big]. \tag{3.26}$$

Constant Safety Factor Spacing Policy Constant Safety Factors (CSF) spacing policy aim to improve safety and minimise the possibility of collisions. Indeed, it can be obtained by analysing the emergency braking process, and is usually expressed as [82]:

$$D_{des} = k\frac{v^2}{2b_{max}}, \tag{3.27}$$

being k a safety factor and b_{max} $[m/s^2]$ the maximum deceleration of the host vehicle. A modified CSF policy was proposed in [83]:

$$D_{des} = d_0 + \sigma v + \frac{v^2}{2b_{max}}, \tag{3.28}$$

where σ $[s]$ is the time delay of the vehicle longitudinal control system. CSF policy can achieve traffic flow stability but operates with a higher emphasis on safety and is very conservative safety-wise.

Human Driving Behaviour Spacing Policy Human Driving Behavior (HDB) aims to enhance comfort and customer acceptance, apart from stability and safety, by considering the characteristics of human drivers. Usually, it is expressed in a quadratic form derived from recorded data of several human drivers [84]:

$$D_{des} = d_{st} + Tv + Gv^2, \tag{3.29}$$

where T and G are the coefficients determined by curve fitting, and approximately related by $G = -0.0246T + 0.010819$. The drawback of this spacing policy is that the traffic flow stability can not be guaranteed [83].

3.1.4 Distributed Controller

The distributed controllers are implemented at the single-vehicle level and depend on both the state variables of the vehicle itself (measured on board) and the information received from neighbouring vehicles through the communication topology to achieve specific global coordination.
For example, the coupling between nodes can be modelled as:

$$u_i(t) = \sigma \sum_{j=1, j\neq i}^{N} \alpha_{i,j} h(x_i(t), x_j(t)), \tag{3.30}$$

where σ is the coupling gain, $\alpha_{i,j}$ model the presence/absence of coupling between agents in the network and $h(x_i(t), x_j(t))$ refers to the particular protocol used.
The controller design strongly depends on the performances that the designer would achieve in cooperative driving applications. The priority for cooperative driving application is to guarantee internal stability, i.e., the networked closed-loop system needs to be asymptotically stable. In addition to the internal stability, other performances metrics include:

- String stability [85]. A vehicles platoon is string stable if the disturbances are attenuated when propagating downstream along the string of vehicles.
- Stability margin [86]. The stability margin is the real part of the least stable eigenvalue that characterises the convergence speed to the desired behaviour.
- Coherence behaviour [87]. It is quantified as the H_2 norm of the closed-loop system, capturing the robustness of the vehicle platoon compared to exogenous disturbances.

The majority of distributed controllers are linear for the easiness of comprehensive theoretical analysis, and the convenience of hardware implementation [88].

However, there are several major drawbacks with this linear design methods. For instance, it is not able to deal with the non-linearity, the uncertainties and the constraints. Most of existing work exploiting linear design methods compensate nonlinear behaviour via some feed-forward control actions, which suffer from well-known difficulty due to the exact knowledge or the real-time measuring of the various characteristic parameters [89, 90, 91], or additional state-observer for their compensation [19, 92]. However, control protocols purposely designed for copying with platoon non-linearities are usually designed under the main restrictive assumption of neglecting uncertainties affecting the vehicles dynamics. The robustness concerning uncertain nonlinear dynamics is crucial when implementing in practice cooperative driving applications since there exist a lot of mismatches between the actual plant and its control-oriented model that inevitably arise due to different environmental conditions, parameter variations, and unmodeled dynamics.
Nevertheless, the robustness with respect to uncertain nonlinear dynamics is crucial when implementing in practice cooperative driving applications. Indeed, there are a lot of mismatches between the actual plant and its control-oriented model that inevitably arise due to different environmental conditions, parameter variations, and unmodeled dynamics. Another critical issue within the platooning driving paradigm is related to communication topology among vehicles: it may not be maintained fixed due to communication constraints, environmental disturbances or platooning manoeuvres (e.g. create, merge and disengage platoons). Hence, there is the need to investigate the performance of vehicle platoon control also under switching topologies when some communication links among the vehicles within the platoon are created and/or disrupted. An emerging challenge is the achievement of both leader-tracking and energy-saving performance simultaneously. Therefore, more recently, advanced control methods have been introduced into cooperative driving control for achieving better performances. For example, Sliding Mode Control (SMC) [64] and H_∞ [93] controller for dealing with string stability, Model Predictive Controller (MPC) and Distributed Model Predictive Controller (DMPC) approaches to handle vehicle non-linearities and constraints as well as achieve multiple objectives at same time [94, 89], and robust control to deal with heterogeneous uncertain nonlinear dynamics [95].
Traditionally, control algorithms are usually designed based on an implicit

assumption of unlimited computation resources, non-delayed sensing and actuation, unlimited bandwidth, and perfect communication environments. However, computation and communication resources are limited and often shared between multiple applications (such as subsystems, agents, nodes, and other processes). Thus, the development of real-time distributed control algorithms in cooperative driving applications should be realised and reevaluated by integrating communication, computation, and control to achieve the desired control performance through local, asynchronous, distributed, and cooperative actions. Therefore, another crucial performance metric that has to be considered in cooperative driving control strategy design is the resiliency and the robustness to the unavoidable communication impairments introduced by the wireless vehicular network.

3.2 Consensus and Synchronisation in Networked Dynamical Systems

In networks of agents (or dynamical systems), consensus means to reach an agreement regarding a certain quantity of interest that depends on the state of all agents. A consensus algorithm (or protocol) is an interaction rule that specifies the information exchange between an agent and all of its neighbours on the network [96]. Every agent exploit the same algorithm and take decision thanks to the local available information and those that receive from the other agents.
Consider a network of agents interested in reaching a consensus via local communication with their neighbours on a graph $\mathcal{G} = (\mathcal{V}, \mathcal{E}, \mathcal{A})$ that represent the agent connection. By reaching a consensus, the state of the considered system asymptotically converges to a constant agreement value, i.e.:

$$\lim_{t \longrightarrow \infty} x_i(t) = \bar{x} \ \forall i \in \mathcal{V} \tag{3.31}$$

being $\bar{x}$ the collective decision of the group.
Most early works on networked dynamical systems address consensus problem without considering the presence of a leader node, so all nodes are commanded to converge toward a not prescribed common evolution. Synchronisation, in the sense of cooperative tracking, has been then studied by adding a leader that imposes the desired behaviour to a group

of agents to achieve the command trajectory (e.g., see [97], [98] and references therein). According to [99], it is possible to claim that the networked dynamical systems achieve synchronisation if

$$\lim_{t\to\infty} \|x_i(t) - x_0(t)\| = 0, \quad i = 1, \dots N, \tag{3.32}$$

where $x_i = (x_{i1}, x_{i2}, \dots, x_{in})^T \in \mathbb{R}^n$ are the state variables of node i and $x_0 = (x_{01}, x_{02}, \dots, x_{0n})^T \in \mathbb{R}^n$ are the reference state variables of the leader node. The hyperplane:

$$\mathcal{S} = \left\{ \left[x_1^\top(t), x_2^\top(t), ..., x_N^\top(t) \right]^\top \in \mathcal{R}^{N\times N} : x_i(t) = x_j(t) = x_0(t) \right\}$$

for $i, j = 1, 2, ..., N$ is said to be the synchronisation manifold of the networked dynamical systems.

3.2.1 Stability of Continuous-Time Systems

In what follow some useful results about stability of linear system are recalled.
Consider the familiar linear state equation:

$$\dot{x}(t) = Ax(t). \tag{3.33}$$

For this class of systems, the following result hold:

Theorem 1. *(Lyapunov stability for linear systems) Consider a linear system in the form of (3.33) and let $A \in \mathcal{R}^{N\times N}$. The following statements are equivalent:*

- *all the eigenvalues of A have negative real part;*
- *for all matrices $Q = Q^\top > 0$ there exists an unique solution $P = P^\top > 0$ to the following (Lyapunov) equation:*

$$AP^\top + PA = -Q \tag{3.34}$$

3.2.2 Integral Inequalities

In this section, some useful integral inequalities have been retrieved. Above all, the Hadamard inequality, valid for convex functions only, is recalled:

Lemma 1. *(Hadamard Inequality) [100] Let $f : I \subseteq \mathcal{R} \to \mathcal{R}$ be a convex mapping defined on the interval I of real numbers, then the following inequality holds:*

$$\frac{1}{b-a}\int_a^b f(x)dx \leq \frac{f(a)+f(b)}{2}, \tag{3.35}$$

being $a, b \in I$ with $a < b$.

The following integral inequality is known as the Jensen Inequality, which plays an important role in the stability problem of time-delay systems:

Lemma 2. *(Jensen Inequality) [101] For any constant matrix $\Theta = \Theta^\top > 0 \in \mathcal{R}^{N\times N}$, scalar $h : h(t) > 0$, and vector function $x(.) : [-h, 0] \longrightarrow \mathcal{R}^n$ such that the following integral is defined, then*

$$h\int_{t-h}^{t} \eta^\top(s)\Theta\eta(s)ds \geqslant \int_{t-h}^{t} \eta^\top(s)ds\Theta\int_{t-h}^{t} \eta(s)ds. \tag{3.36}$$

Moreover, the following useful integral inequality are recalled:

Lemma 3. *[102] For any generic positive definite matrix Ξ it holds*

$$2a^\top c \leq a^\top \Xi a + c^\top \Xi^{-1} c. \tag{3.37}$$

CHAPTER 4

Integrated Simulation Environment

The development of fully automated/autonomous driving functions requires accurate verification and testing to guarantee high safety levels in different traffic scenarios. However, classical road and field tests are often demanding to carry out due to several drawbacks (see Sec. 2.5.1 for more detail): *i*) may require a great monetary and temporal effort; *ii*) the achievement of broad test coverage (i.e., vary a large number of parameters values in a wide range) is commonly not possible or easy or cost-efficient; for instance, a limited number of vehicles is usually involved in the experiments, with specific characteristics and mechanical features; hence it is not possible to perform sensitivity analysis w.r.t. vehicles heterogeneity and uncertainty [32, 103]; *iii*) repeatability and replicability of a given driving scenario are limited since the control of the scenario itself is limited due to unavoidable stochastic phenomena (e.g., see the well-known problem of repeated reconstruction of identical road conditions) [104]; *iv*) variability is limited due to infrastructure (geometries, dimensions) and conditions (weather conditions, time of day) [105]; *v*) safety is not always completely guaranteed [106].
Within this context, virtual simulation approaches have been recognised as a key component to foster the development of connected and autonomous driving technologies on public roads according to the recent

technical literature (see, e.g., [33]) since they are needed to perform comprehensive, short-time and cost-effective performance assessment of connected and autonomous vehicles. Moreover, virtual testing has the significant advantage of allowing the safe verification of specific requirements, also in conditions characterised by extensive uncertainty, without the risk of accidents and crashes (or incipient collisions) [32]. Car manufacturers nowadays make extensive use of simulation platforms to the point that, according to Krafcik, CEO of Waymo (see [34] and [35]), about 80% of improvements of automated vehicles comes from simulation. In addition, the importance of using simulations to provide a broader and robust assessment of advanced technologies and innovating solutions aiming at improving passenger autonomous car safety is also highlighted in the Euro NCAP 2025 Roadmap (2018) [1]. It also emerges from the guideline documents of the European Commission [2] [3]. According to this trend, some Nations regulate the testing activities of automated/autonomous vehicles via Virtual Simulations before on-road tests, both on test roads and public ones, as in the case of the *Italian Smart Road Decree* [4] stating that autonomous vehicles need to perform virtual experiments of at least 300000 $[km]$ for each simulated use-case, before going on the Italian roads.
The researchers involved in developing simulation platforms for autonomous/automated driving functions evaluation and validation can be divided into two main groups: automotive engineers and transportation engineers. Those two groups approach the problem from very different angles. Traffic engineers exploit simulation platforms able to simulate background traffic, even in large-scale networks, but with simplified vehicle dynamics and controllers; this could compromise the authenticity of the simulation. On the other hand, automotive engineers focus more on the enabling of the technology and aim at developing platforms that are most realistic and accurate in terms of vehicle dynamics, sensors, and control logic; however, these platforms are typically unable to simulate realistic background traffic conditions in which autonomous/automated vehicles will be involved when commercialised.

[1] https://cdn.euroncap.com/media/30700/euroncap-roadmap-2025-v4.pdf

[2] https://publications.jrc.ec.europa.eu/repository/handle/JRC119345

[3] https://ec.europa.eu/growth/content/guidelines-exemption-procedure-eu-approval-automated-vehicles_en

[4] https://www.gazzettaufficiale.it/eli/id/2018/04/18/18A02619/sg

In this context, a novel *Integrated Simulation Environment* should be developed for autonomous/automated driving functions evaluation and validation. The platform should be able to: *i*) simulate various background traffic conditions, road geometries, and traffic control schemes; *ii*) model and emulate the detailed dynamics of CAVs; *iii*) account for the effects of the on-board ranging sensors (e.g., camera, radar); *iv*) mimic V2X communication.

4.1 Existing Virtual Testing Environments

Existing simulation platforms can be categorised into three types: *microscopic traffic simulators*, *physics-based simulators* and *integrated platforms.*

4.1.1 Microscopic Traffic Simulators

Traditional microscopic traffic simulators have been developed to emulate the time variability of traffic phenomena starting from the dynamics of each single vehicle [107]. Usually, the main components of a traffic simulator are: *i*) transport network to define road topology; *ii*) traffic demand; *iii*) models for regulating the vehicle driving behavior (e.g., car-following and lane-changing). Some typical simulators include VISSIM [108], Aimsun [109], MATSim [110], which are popular commercial solutions, and the open-source SUMO [111]. They are widely used to estimate road infrastructure level of service, design, and implementation of traffic management solutions and compare the performances of different road design solutions. Moreover, some researchers (e.g., [112]) focused on the applicability of traffic micro-simulators to estimate vehicle emission based on real-world data from an expressway, but, due to systematic error, they did not provide a realistic driving behaviour to estimate both consumption and pollutant emissions of the vehicle. From the early 2000s, such simulators have also been used to assess the impact of ADAS systems (e.g., ACC, Intelligent Speed Assistance (ISA), or overtaking assistants) on traffic efficiency as the penetration rate, vehicle fleet, road infrastructure, and surrounding driver behaviour vary [113]. More recently, following the development of communication technologies, traffic micro-simulators have also been used to test information systems and

V2X-based systems [52, 114].
However, this approach presents several drawbacks. Above all, these platforms represent both vehicles and control systems in an over-simplified way. Indeed, each vehicle is modelled as a simple point mass, and its behaviour is described only via its kinematic motion. For instance, the behaviour of a single vehicle following another is represented through a car-following model, which simplifies a controller (e.g., CACC or ACC) or the human-driver behaviour and vehicle dynamics into a single model. Hence, the vehicle models embedded in these simulators do not guarantee the high fidelity vehicle dynamics requirement, which is crucial for autonomous/automated driving simulation and validation. Moreover, despite some micro-simulation tools that allow on-board functionalities to be embedded via an application programming interface, they are usually too simplified models of the real ones, resulting in a non-realistic representation of the vehicle behaviour in traffic scenarios.

4.1.2 Physics-Based Simulators

Typical automotive development process focuses on a highly detailed representation of vehicle dynamics, actuators, control logic, on-board sensors, communication devices, and so on [115].
Existing commercial virtual testing solutions, such as IPG CarMaker [116], VIRES VTD [117], dspace ASM [118], PreScan [119]and CarSim [120], focus mainly on the motion of a single-vehicle with detailed dynamics and equipped with on-board sensors. By leveraging graphics engines, they build up ideal 2D/3D traffic scenarios, which combine road sections, infrastructure components, weather conditions, and light sources. However, these tools allow only a simplified representation of surrounding vehicles behaviour, consisting of pre-loaded and predefined driving trajectories, given as a simulation input. Moreover, commercial solutions are costly and require powerful hardware to run. Currently, only the latest version of VIRES VTD allows the emulation of multi-ego vehicles scenarios to the best of the author knowledge.
To reduce monetary cost and unnecessary dependencies, open-source solutions can be alternatively used. For example, TORCS [121] is a car simulation platform for racing game neglecting road traffic elements (e.g., intersections and traffic rules), while CoInCar-Sim [122] focuses on cooperative motion planning of vehicles with SAE4+ automation

level; however, it does not integrate detailed vehicle dynamics or realistic traffic conditions. CARLA [123], AirSim [124] and Udacity [125] are, instead, devoted to the testing of different ranging sensors (e.g., camera and radar) and/or machine learning since they allow to create and render high-resolution 3D traffic environment based on a game engine. The main issue of such simulators is that when a high-fidelity simulation is required, correct mathematical representation of subsystems in models or software is imperative to achieve realistic calculations [126]. Finally, it is worth noting that MATLAB recently extended with the Automated Driving Toolbox, which provides algorithms and tools for designing and testing ADAS and autonomous driving systems also within a simplified 3D environment, which enables vision systems simulation [126].

4.1.3 Integrated Simulation Environment

Although single simulators described in 4.1.1 and 4.1.2 can explore several functions of autonomous/automated driving, the complexity of the traffic scenarios is still challenging. Hence, some integrated simulation environments have recently been developed to combine and fully take advantage of existing single simulators.

To investigate the interaction between traffic mobility and V2X communication, a feasible solution is to integrate traffic simulator with network simulator. Common vehicular network simulators are TraNS [127], iTETRIS [128] and Veins [129]. TraNS combines SUMO and NS-2 networking simulator [130], while iTETRIS integrates SUMO and NS-3 [131], and Veins couples SUMO with OMNET++ [132]. These integrated simulators have been widely applied in system validations such as platoon-based cooperative driving [133] and communication optimization [134].

Some *physics-based commercial simulators* can interact with external software so to improve their capabilities. For instance, IPG CarMaker, VIRES VTD, dSPACE, Prescan, and rFpro [135], which is a commercial game engine, allow populating the virtual test environment with realistic road users moved by SUMO or PTV VISSIM. Similarly, the integrated use of AIMSUM, CARSIM, and Passenger Car and Heavy Duty Emission Model to estimate pollutant emissions is proposed in [136]. Despite the presence of both high fidelity vehicle dynamics and a realistic surrounding

traffic environment, the use of commercial tools remains too expensive and not light-weighted.
To reduce monetary cost and unnecessary dependencies, as well as to improve the flexibility to any different developers requirements, some in-house solutions have been developed during recent years. Most of them are light-weighted and based on MATLAB/Simulink environment, hence allowing to customize both vehicle dynamics and control algorithms [137, 138, 139], but mainly focus on single CAV control. More recently, a comprehensive simulation platform for conventional, connected, and automated driving was proposed in [36] by combining SUMO, Omnet++, and Webots [140], which allows modelling of both autonomous/automated and conventional vehicles.

4.2 Proposed Integrated Simulation Environment

Motivated by the need to develop a simulation platform to enhance the autonomous/automated driving evaluation and validation process, a new integrated virtual simulation environment, named Mixed Traffic Simulator (MiTraS), is developed. It embeds different interacting simulation tools within a holistic view of the co-simulation approach. Namely, it leverages the MATLAB/Simulink features for modelling the autonomous/automated vehicle dynamics, developing a customized control strategy, i.e., longitudinal and lateral dynamics of CAVs, communications topology, and the emulation of heterogeneous systems time-varying delays associated with each active communication link. Furthermore, integrating the Automated Driving Toolbox, it can be easily obtained a 3D representation of the road scenario and, as a consequence, it is possible to simulate camera, radar, and lidar. On the other side, the virtual platform exploits SUMO for reproducing human-driver behaviour and traffic scenarios in realistic conditions (also by selecting road network type, road rules, and so on). Exploiting SUMO, MiTraS accounts for unplanned but realistic events such as congestion, slower or faster vehicles ahead, lane changes, and, generally, to face up with different drivers behaviours. Hence, by integrating the simulation tools mentioned above, it is possible to enable virtual testing in complex, stochastic and reproducible traffic scenarios. The primary needs to build up MiTraS are: *i*) no powerful hardware required to run; *ii*) no commercial software is required except for MATLAB; *iii*) flexibility and easy adaptation to different developers requirements; *iv*) possibility to improve each component independently thanks to the modular structure; *v*) the simultaneous control of several CAVs; *vi*) the emulation of large-scale traffic, also mixed-traffic conditions; *vii*) the assessment of the performance of autonomous vehicles in a wide range of realistic traffic scenarios; *viii*) the repeatability and replicability, since it is possible to re-execute the same test without deviations due to stochastic phenomena and faults in the functioning of a system can thus be identically replicated at any moment. The key components of MiTraS, as well as the allowable features, are detailed in the following.

4.2.1 The Role of SUMO

Simulation of Urban MObility (SUMO) [111] is an open-source, highly portable, microscopic traffic simulator designed to emulate road traffic systems. SUMO allows modeling each vehicle individually, i.e., it is characterised by its own ID, route, position, speed, and it moves within the traffic flow according to built-in car-following models or external inputs computed, as in this case, in MATLAB/Simulink environment.
To simulate a traffic scenario, several elements are needed. The most important ones are network data (e.g., roads and footpaths), possible additional traffic infrastructure (e.g., traffic lights), and traffic demand. The information related to these elements is contained in specific XML files. Further and in-depth details on the functionality, simulation models, tools, and the workflow with traffic simulations can be found in [141].

Network Setup SUMO networks consist of nodes and unidirectional edges representing, for instance, streets, waterways, tracks, and so on. Each edge has a specific geometry (a series of line segments) and consists of one or more lanes. Attributes such as width, speed limit, and access permissions are modelled as constant along a lane. Moreover, SUMO networks include detailed information regarding possible movements at intersections and the corresponding right of way rules used to determine the dynamic simulation behaviour.

Demand Modelling In SUMO, traffic demand can be defined as individual trips, flows, or routes. The basic information should include departure time, origin, destination, and transport mode. Once traffic demand is generated, traffic assignment can be executed for understanding the traffic state of the investigated network. SUMO embeds different traffic assignment methods: User Equilibrium, Stochastic User Equilibrium, or the fastest route at a given departure time.

4.2.2 The Role of MATLAB/Simulink

The MATLAB/Simulink environment plays a key role in the proposed virtual testing platform performing the following main tasks: *i*) modelling and emulating the detailed dynamics of CAVs; *ii*) emulating the on-board ranging sensors (e.g., camera, radar); *iii*) emulating the V2V communication infrastructure; *iv*) controlling the CAVs; *v*) reproduce the road traffic simulation in a 3D environment.
Tasks *ii*) and *v*) are accomplished by leveraging the Automated Driving Toolbox of MATLAB, i.e., a tool for the designing and testing of ADAS and autonomous driving systems that provides ranging sensors models and allows the 3D visualisation. This latter is realized by importing the road network from SUMO via OpenDrive files. The heterogeneous time-varying delays affecting the information shared via the V2V communication paradigm are emulated as stochastic variables with a uniform discrete distribution within the typical range that can be observed in vehicular network delays during normal operating conditions in practice [142].

4.2.3 Co-Simulation Procedure

To enable co-simulation, the SUMO Traffic Control Interface (TRACI) 4MATLAB is exploited, allowing to connect SUMO and MATLAB in a server-client architecture [143]. All the necessary TraCI4MATLAB commands are coded within S-Function level 2 within Simulink. An overview of this interface architecture is depicted in Figure 4.1. The following co-simulation procedure briefly summarises how SUMO interacts with the MATLAB/Simulink environment. Before enabling this interaction, the following preliminary actions are required: *i*) define the traffic demand, the set of CAVs, the set of CHVs, vehicles routes, as

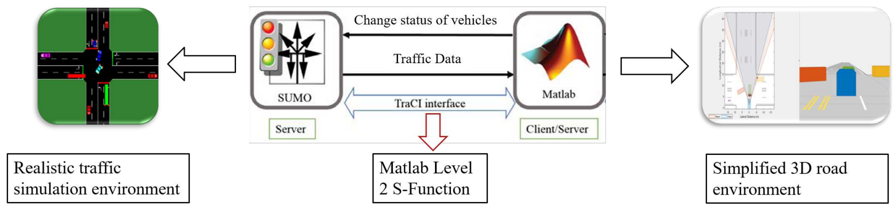

Figure 4.1: Integrated Simulation Environment MiTraS

well as initial conditions for each vehicle; *ii*) generate the OpenDrive file allowing reproducing the SUMO road network in a 3D visualisation environment.
Once the communication is established via TraCI4MATLAB, SUMO and MATLAB/Simulink can share information about the mixed traffic flow conditions. Specifically, at each simulation step, fixed at $\Delta t = 0.1$ $[s]$, CAVs (running on MATLAB/Simulink platform) receive information about the surrounding environment by SUMO (such as position and speed of all the CHVs within the mixed traffic flow). Then, a control strategy can be computed and imposed on CAVs that move accordingly. Finally, SUMO updates the global traffic information that will be available for CAVs at the next simulation step.

4.3 Modeling

In this section, a detailed description of each component of MiTraS simulation environment is provided.
Above all, the Ego-Vehicle model is given. It is worth noting that it is built in a modular framework allowing to choose between two types of propulsion and relative model of consumption, Internal Combustion Engine (ICE) or Electric Motor (EM), and different configurations for wheels (bicycle or four wheels model).

4.3.1 Vehicle Model

The motion of the Ego-Vehicle is described through dynamics equations which refer to a 3-Degree-of-Freedom (DoF), rear-drive and front steering vehicle model. Under the assumption that the vehicle moves like a rigid body, the motion can be described by the following non-linear longitudinal, lateral and yaw dynamics [60]:

$$\ddot{x} = \dot{y}\dot{\psi} + \frac{F_{x_{f,l}} + F_{x_{f,r}} + F_{x_{r,l}} + F_{x_{r,r}}}{m}, \tag{4.1a}$$

$$\ddot{y} = -\dot{x}\dot{\psi} + \frac{F_{y_{f,l}} + F_{y_{f,r}} + F_{y_{r,l}} + F_{y_{r,r}}}{m}, \tag{4.1b}$$

$$\ddot{\psi} = \frac{\ell_f(F_{y_{f,l}} + F_{y_{f,r}}) - \ell_r(F_{y_{r,l}} + F_{y_{r,r}}) + \ell_c(-F_{x_{f,l}} + F_{x_{f,r}} - F_{x_{r,l}} + F_{x_{r,r}})}{I_z}, \tag{4.1c}$$

where ψ $[rad]$ is the yaw angle while $\dot{\psi}$ $[rad/s]$ is the yaw-rate; $\dot{x}$ $[m/s]$ and $\dot{y}$ $[m/s]$ are the vehicle longitudinal and lateral speed respectively; m $[kg]$ is the vehicle mass; $\ell_{f\ [m]}$ and ℓ_f $[m]$ are the distances of front and real wheels w.r.t. the centre of gravity; I_z $[m \cdot N \cdot s]$ is the vehicle body inertia moment about the vehicle-fixed z-axis; $\ell_{c\ [m]}$ is the distance of vehicle longitudinal axis from the wheels; $F_{y_{f,l}}$ $[N]$ and $F_{y_{f,r}}$ $[N]$ are the lateral forces acting on the front-left and front-right vehicle axle, respectively; $F_{y_{r,l}}$ $[N]$ and $F_{y_{r,r}}$ $[N]$ are the lateral forces acting on the rear-left and rear-right vehicle axle, respectively; $F_{x_{f,l}}$ $[N]$ and $F_{x_{f,r}}$ $[N]$ are the longitudinal forces acting on the front-left and front-right vehicle axle, respectively; $F_{x_{r,l}}$ $[N]$ and $F_{x_{r,r}}$ $[N]$ are the longitudinal forces acting on the rear-left and rear-right vehicle axle, respectively.
All the these forces are expressed as function of the wheel steering angle. Specifically, using, for sake of conciseness, the symbol $\star \in \{f, r\}$ to denote the variables related to front and rear axles, and the symbol $\bullet \in \{r, l\}$ to denote the variables related to right and left sides of vehicle, they are computed as:

$$F_{y_{\star,\bullet}} = F_{l_{\star,\bullet}} \sin\delta_\star + F_{c_{\star,\bullet}} \cos\delta_\star, \tag{4.2a}$$

$$F_{x_{\star,\bullet}} = F_{l_{\star,\bullet}} \cos\delta_\star - F_{c_{\star,\bullet}} \sin\delta_\star, \tag{4.2b}$$

where $F_{l_{\star,\bullet}}$ $[N]$ is the longitudinal tire forces; $F_{c_{\star,\bullet}}$ $[N]$ the lateral tire forces; $\delta_\star$ $[rad]$ is the wheel steering angle. For forward driving, the guiding wheels are the front wheels and, consequently, $\delta_{r,\bullet}$ are equal to 0. The lateral and longitudinal tire forces for each tire are non-linear functions given as

$$F_{c_{\star,\bullet}} = f_c(\alpha_{\star,\bullet}, s_{\star,\bullet}, \mu_{\star,\bullet}, F_{z_{\star,\bullet}}), \tag{4.3a}$$

$$F_{l_{\star,\bullet}} = f_l(\alpha_{\star,\bullet}, s_{\star,\bullet}, \mu_{\star,\bullet}, F_{z_{\star,\bullet}}), \tag{4.3b}$$

being $\alpha_{\star,\bullet}$ the tire slip angles; $s_{\star,\bullet}$ the tire slip ratios; $\mu_{\star,\bullet}$ the road friction coefficients; $F_{z_{\star,\bullet}}$ $[N]$ the tire vertical forces.
The slip ratios $s_{\star,\bullet}$ are defined as follows:

$$s_{\star,\bullet} = \begin{cases} \frac{r_w \omega_{\star,\bullet}}{v_{l_{\star,\bullet}}} - 1, & \text{if } v_{l_{\star,\bullet}} > r_w \omega_{\star,\bullet}, v_{l_{\star,\bullet}} \neq \text{for braking}, \\ 1 - \frac{v_{l_{\star,\bullet}}}{r_w \omega_{\star,\bullet}}, & \text{if } v_{l_{\star,\bullet}} < r_w \omega_{\star,\bullet}, \omega_{\star,\bullet} \neq \text{for driving}, \end{cases} \tag{4.4}$$

where r_w $[m]$ is the wheel radius and $\omega_{\star,\bullet}$ $[rad/s]$ is the angular speed.
The slip angles represent the angle between the wheel velocity and the direction of the wheel itself:

$$\alpha_{\star,\bullet} = tan^{-1} \frac{v_{c_{\star,\bullet}}}{v_{l_{\star,\bullet}}}, \tag{4.5}$$

where $v_{c_{\star,\bullet}}$ $[m/s]$ and $v_{l_{\star,\bullet}}$ $[m/s]$ are the lateral and longitudinal wheel velocities, respectively, which are expressed as:

$$v_{c_{\star,\bullet}} = v_{y_{\star,\bullet}} \cos \delta_\star - v_{x_{\star,\bullet}} \sin \delta_\star, \tag{4.6a}$$

$$v_{l_{\star,\bullet}} = v_{y_{\star,\bullet}} \sin \delta_\star + v_{x_{\star,\bullet}} \cos \delta_\star, \tag{4.6b}$$

where

$$v_{y_{f,l}} = \dot{y} + \ell_f \dot{\psi} \quad v_{x_{f,l}} = \dot{x} - \ell_c \dot{\psi}, \tag{4.7a}$$

$$v_{y_{f,r}} = \dot{y} + \ell_f \dot{\psi} \quad v_{x_{f,r}} = \dot{x} + \ell_c \dot{\psi}, \tag{4.7b}$$

$$v_{y_{r,l}} = \dot{y} - \ell_r \dot{\psi} \quad v_{x_{r,l}} = \dot{x} - \ell_c \dot{\psi}, \tag{4.7c}$$

$$v_{y_{r,r}} = \dot{y} - \ell_r \dot{\psi} \quad v_{x_{r,r}} = \dot{x} + \ell_c \dot{\psi}. \tag{4.7d}$$

Resistant and inertial forces generate a load transfer phenomenon which affects the tires vertical forces $F_{z_{\star,\bullet}}$ and, as a consequence, their longitudinal and lateral stiffness. To closely estimate vertical loads, roll motion has to be considered. The body roll angle φ $[rad]$, assumed to be small, is calculated by dividing the moment about the roll axis by the apparent roll stiffness which is reduced with the term $mgh^{'}$ due to the additional moment $mgh^{'}\varphi$:

$$\varphi = \frac{-m\ddot{y}h^{'}}{c_{\varphi,f} + c_{\varphi,r} - mgh^{'}} \tag{4.8}$$

where $h^{'}$ $[m]$ is the distance from the centre of gravity to the roll axis; $c_{\varphi,\star}$ $[N/rad]$ are the roll stiffness of front and rear part; g $[m/s^2]$ is the gravitational acceleration. The total moment about the roll axis is distributed over the front and rear axles in proportion to the front and rear roll stiffness. The load transfer from the inner to the outer wheels that occurs at each axle in a steady-state cornering motion with centripetal acceleration $\ddot{y}$ is computed according to the following formula:

$$\Delta F_{z_f} = \frac{m\ddot{y}}{2\ell_c}\left(\frac{\ell_f}{\ell}h_\star + \frac{c_{\varphi,f}}{c_{\varphi,f}+c_{\varphi,r}-mgh'}h'\right), \tag{4.9a}$$

where $h_\star$ $[m]$ are the heights of the front and rear roll centres.
Finally, the tire vertical forces $F_{z_{\star,\bullet}}$ are computed as [60]:

$$F_{z_{f,l}} = \frac{1}{2}\Big[\frac{mg\ell_r}{\ell} + \frac{1}{2}\rho_{air}S_aC_{z_f}\dot{x}^2 - \frac{mh\ddot{x}}{\ell}\Big] + \Delta F_{z_f}, \tag{4.10a}$$

$$F_{z_{f,r}} = \frac{1}{2}\Big[\frac{mg\ell_r}{\ell} + \frac{1}{2}\rho_{air}S_aC_{z_f}\dot{x}^2 - \frac{mh\ddot{x}}{\ell}\Big] - \Delta F_{z_f} \tag{4.10b}$$

$$F_{z_{r,l}} = \frac{1}{2}\Big[\frac{mg\ell_f}{\ell} + \frac{1}{2}\rho_{air}S_aC_{z_r}\dot{x}^2 - \frac{mh\ddot{x}}{\ell}\Big] + \Delta F_{z_r}, \tag{4.10c}$$

$$F_{z_{r,r}} = \frac{1}{2}\Big[\frac{mg\ell_f}{\ell} + \frac{1}{2}\rho_{air}S_aC_{z_r}\dot{x}^2 - \frac{mh\ddot{x}}{\ell}\Big] - \Delta F_{z_r}, \tag{4.10d}$$

being $\ell = \ell_f + \ell_r$ $[m]$ the length of the wheelbase; h $[m]$ is the height of the vehicle; ρ_{air} $[kg/m^3]$ is the air density; S_a $[m/s^2]$ is the cross sectional area; $C_{z_\star}$ are the front/rear lift coefficient.
Regarding the tire-road friction coefficient in (4.3), the model for tire tractive and cornering forces is described thorough the Magic Formula 5.2 of Pacejka [60] to determine the longitudinal force arising from this interaction. For sake of simplicity, the longitudinal and lateral forces are computed in a decoupled way. Accordingly, in the purely longitudinal case, the longitudinal forces are

$$F_{x_{\star,\bullet}} = D_x sin\{C_x atan[B_x s_{\star,\bullet} - E_x(B_x s_{\star,\bullet} - atan(B_x s_{\star,\bullet}))]\} \tag{4.11}$$

while in the purely sideslip case, the lateral forces are

$$F_{y_{\star,\bullet}} = D_y sin\{C_y atan[B_y \alpha_{\star,\bullet} - E_y(B_y \alpha_{\star,\bullet} - atan(B_y \alpha_{\star,\bullet}))]\} \tag{4.12}$$

where $B_\star$, $C_\star$, D_{star}, $E_\star$ represent the stiffness, shape, peak and curvature coefficients, respectively. These factors are described as the function of the tire vertical load, tire slip rate, and tire slip angle.

4.3.2 Consumption Models

In the following, the embedded models used to estimate both fuel and energy consumption of the Ego-Vehicle are described.

4.3.2.1 Fuel Consumption Model

The power-based model Virginia Tech Comprehensive Power-Based Fuel Consumption Model (VT-CPFM)-2 proposed in [144] is used to compute the instantaneous fuel consumption $FC(t)$ $[l/s]$ of vehicle in an endothermic engine configuration:

$$FC(t) = \begin{cases} \beta_0 \omega_e(t) + \beta_1 P(t) + \beta_2 P(t)^2 & \text{if } P(t) \geq 0 \ , \\ \beta_0 \omega_{idle} & \text{if } P(t) < 0, \end{cases} \tag{4.13}$$

where $P(t)$ $[kW]$ is the instantaneous vehicle power; $\omega_e(t)$ $[rpm]$ is the engine speed of the vehicle at time t; ω_{idle} $[rpm]$ is the engine idling speed; β_0, β_1 and β_2 are vehicle-specific model constants to be calibrated with the VT-CPFM calibration tool.
According to [145], the power required by a vehicle to advance is computed as follows:

$$P(t) = \Big(\frac{R(t) + ma(t)\big(1.04 + 0.0025\xi(t)^2\big)}{1000\eta_d}\Big) \cdot v(t), \tag{4.14}$$

where $R(t)$ $[N]$ is the total resistance force; $a(t)$ $[m/s^2]$ is the vehicle longitudinal acceleration at time t; $\xi(t)$ is the gear ratio at time t defined as $\tau_{gb}(t)/\tau_{diff}$, being $\tau_{gb}(t)$ and τ_{diff} the gear ratio and differential ratio, respectively; η_d is the driveline efficiency; $v(t)$ $[m/s]$ is the vehicle longitudinal speed at time t.
The total resistance force $R(t)$ is computed as the sum of the aerodynamic, grade and rolling resistance forces:

$$\begin{aligned} R(t) =& \frac{1}{2}\rho_{air} C_d (1-\phi) C_h(t) A_f v(t)^2 + mgsin(\theta) \\ &+ mgcos(\theta)\frac{C_r}{1000}\big(c_1 v(t) + c_2\big), \end{aligned} \tag{4.15}$$

where C_D is the aerodynamic drag coefficient; A_f $[m^2]$ is the vehicle frontal area; θ $[rad]$ is the road grade; $C_r(t)$, $c_1(t)$ and $c_2(t)$ are the

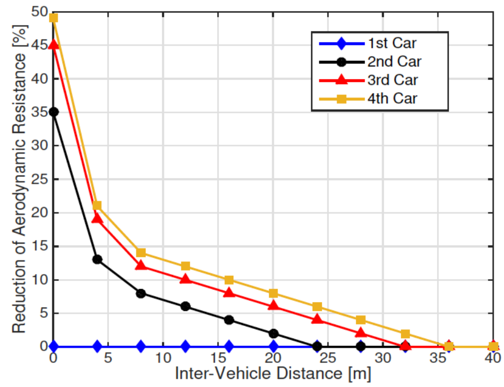

Figure 4.2: Air-Drag Reduction of Passenger Cars [2]

rolling resistance parameters that vary as a function of the road surface type, road condition, and vehicle tire type; $C_h(t)$ is a correction factor (unitless) due to the altitude of the road where vehicle moves computed as $C_h(t) = 1 - 0.085H(t)$ where $H(t)$ $[km]$ is the road altitude [144]; ϕ is the air-drag reduction coefficient due to the platooning effects [2] (see Figure 4.2).Note that, platooning effect (or slipstream effect) allows to reduce consumption by reducing the air friction at the front as well as disrupting the turbulent flow at the tail (Fig. 4.3). If vehicles travel in a platoon, also the platoon leader can profits from positive aerodynamic effects in presence of an ahead vehicle. Obviously, vehicles at the centre of the platoon have larger benefits than head and tail vehicles. The air-drag reduction represents one of the main advantages of platooning [3]. Given the instantaneous $FC(t)$ as in (4.14), the average fuel consumption for a given traveled route FC_t $[l/km]$ is computed as

$$FC_t = \frac{1}{d_t} \cdot \int_0^t FC(t)\, dt, \tag{4.16}$$

where d_t $[km]$ is the distance travelled.

4.3.2.2 Power-Based Energy Consumption Estimation Model

To estimate the energy consumption of the vehicle, the Comprehensive Power-based EV Energy consumption Mode (CPEM) [146] is embedded within the proposed Integrated Simulation Environment. It requires the

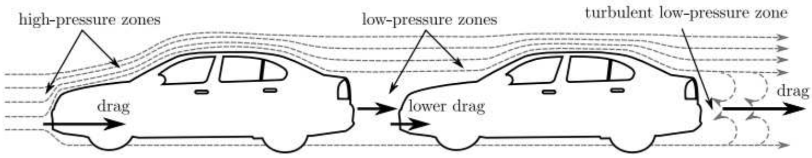

Figure 4.3: The slipstream effect [3]

instantaneous speed of the vehicle and its characteristics as inputs, while the outputs are the instantaneous power consumed $P_t(t)$ $[W]$ and the total energy consumption (EC) $[kWh/km]$ for a specific driving cycle.
To derive EC, it is firstly required to compute the electric power at wheels $P_w(t)$ $[W]$ as:

$$P_w(t) = \Big(ma(t) + R(t)\Big)v(t). \tag{4.17}$$

The electric motor power loss P_{loss} $[W]$ referring to iron loss, copper loss and line loss inside the motor can be computed as follows [147]:

$$P_{loss}(t) = \frac{r_{arm}\, r_w^2}{K^2}\Big(ma(t) + R(t)\Big)^2, \tag{4.18}$$

where r_{arm} $[\Omega]$ is the resistance of the motor armature; $K = K_a \cdot \phi_d \cdot I_m$, being K_a a constant of the armature, ϕ_d (in weber) the magnetic flux and I_m $[A]$ the current of the motor.
Since electric vehicles are equipped with regenerative braking system, the power required at electric motor $P_{em,net}(t)$ $[W]$ can be expressed as

$$P_{em,net}(t) = \begin{cases} \frac{\big(P_w(t)+P_{loss}(t)\big)}{\eta_b}, & \text{if } P_w(t) \geq 0 \\ \big(P_w(t) + P_{loss}(t)\big) \cdot \eta_b \cdot \eta_{rb}, & \text{if } P_w(t) < 0 \end{cases}$$

where η_b is the battery efficiency, while $\eta_{rb}(t)$ is the regenerative braking energy efficiency computed as:

$$\eta_{rb_j}(t) = \begin{cases} \left[e^{\frac{0.0411}{|a(t)|}}\right]^{-1} & if\ a(t) < 0, \\ 0 & if\ a(t) \geq 0. \end{cases} \tag{4.19}$$

Hence, considering also the electric power consumed by the auxiliary systems, i.e. $P_{aux} = 700$ $[W]$, the instantaneous total power required at battery $P_{bat}(t)$ $[W]$ can be estimated as

$$P_{bat}(t) = P_{em,net}(t) + P_{aux}. \tag{4.20}$$

Finally, the average energy consumption EC $[kW/h\ km]$ can be computed as

$$EC = \frac{1}{3600000} \cdot \frac{1}{d_t} \cdot \int_0^t P_{bat}(\tau)\ d\tau. \tag{4.21}$$

Battery Pack Model The battery pack of the vehicle is modelled via the equivalent simplified electric circuit [4] shown in Figure 4.4.

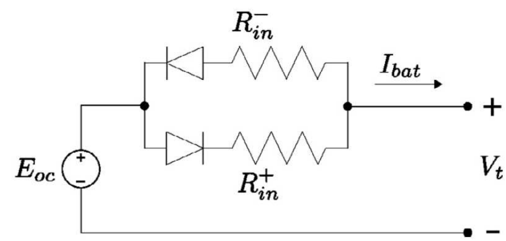

Figure 4.4: Battery Model [4]

It consists of an internal voltage source E_{oc} $[V]$, two ideal diodes, and two inner resistances R_{in}^+ $[\Omega]$ and R_{in}^- $[\Omega]$ which represent the battery internal discharging and charging resistances. The value of these latter parameters depend on the current value of the battery State Of Charge (SOC) and are implemented as look-up tables [4]. The voltage at the terminal of the battery is computed as:

$$V_t(t) = \begin{cases} E_{oc} - R_{in}^+ I_{bat}(t) & if\ discharging, \\ E_{oc} - R_{in}^- I_{bat}(t) & if\ charging. \end{cases} \tag{4.22}$$

The power required at the battery, the current $I_{bat}(t)$ $[A]$ can be derived as

$$I_{bat}(t) = \begin{cases} \frac{E_{oc} - \sqrt{E_{oc}^2 - 4R_{in}^+ P_{bat}(t)}}{2R_{in}^-} & if\ discharging \\ \frac{E_{oc} - \sqrt{E_{oc}^2 - 4R_{in}^- P_{bat}(t)}}{2R_{in}^+} & if\ charging. \end{cases} \tag{4.23}$$

The battery State of Charge can be, hence, computed as

$$SOC(t) = \begin{cases} -\frac{1}{C_{bat}} \int_0^t I_{bat}(\tau) d\tau & if\ discharging \\ -\frac{\eta_{bat}}{C_{bat}} \int_0^t I_{bat}(\tau) d\tau & if\ charging. \end{cases} \tag{4.24}$$

where C_{bat} $[Ah]$ is the battery capacity while η_{bat} is the recharging efficiency.

CHAPTER 5

Development and Testing of a Green Light Optimal Speed Advisory Service Under Different Working Conditions

The Green Light Optimal Speed Advisory (GLOSA) is a C-ITS service that reduces the energy consumption and travel time associated with a vehicle trip by providing an optimal speed profile to avoid unnecessary stops at an intersection exploiting TLSs information. It is expected that GLOSA solutions will be widely deployed on transportation networks, thanks to the rapid spread of increasingly effective and pervasive communication technologies. Thus, appropriate methodologies and tools should be adopted to test sustainability objectives and evaluate the effects of such systems on the performance of traffic networks. In this perspective, this chapter focuses on developing a GLOSA service and its assessment via an enhanced testing approach exploiting the MiTraS Integrated Simulation Environment. The proposed approach can be used to cover several aspects which, in the existing technical literature, are: *i*) not considered (traffic signal phase condition); *ii*) rarely considered (electric engine); *iii*) considered in a non-integrated way (traffic condition, TLSs cycle duration, communication distance, and minimum speed). Indeed, the considered factors pertain to different subsystems of the mobility environment (network and vehicles). The proposed testing framework allows an equally detailed simulation of all, thus enhancing the accuracy of the results. To show the validity of the proposed approach, one controlled vehicle, equipped with a GLOSA system, travelling along a single route through a city centre including many TLSs, is considered. The simulation analysis deals with different levels of considered factors, assessed through Key Performance Indexes (KPIs) related to mobility and environmental indicators. Numerical results confirm that the proposed Integrated Simulation Environment can give valuable insights and suggestions to design a GLOSA service to enhance mobility and environmental performance. They also show that the factors in question affect system performance differently.

5.1 Green Light Optimal Speed Advisory System

The development of C-ITS aims to enhance the performance of transportation systems in terms of safety, efficiency, and environmental footprint [148] by exploiting V2V and V2I wireless communication technologies.
In particular, the GLOSA service is supposed to significantly reduce both consumption and travel time by providing, based on information dispatched by TLS), an optimal speed profile to cross the intersection, avoiding, as much as possible, unnecessary stops [149]. TLSs, equipped with RSUs, share via Infrastructure-to-Vehicle (I2V) wireless communication protocols (DSRC or C-V2X), the MAP and Signal Phase and Timing Message (SPaT) message data package (see Sec. 2.4) to any Connected and Automated/Autonomous Vehicle (CAV) and Connected Vehicle (CV) within their communication range.
Although the technical literature has widely studied GLOSA systems, their assessment has been frequently carried out under partially realistic conditions [150]. Assessment frameworks often focus on one factor (e.g., traffic environment or longitudinal vehicle dynamics) with a high level of detail, while others are neglected or modelled in a simplified way. Thus,

an open challenge in testing such systems is to develop and exploit an integrated modelling tool, able to simulate, with a high level of detail, all the following factors: *i*) traffic environment; *ii*) communications among TLSs and vehicles: *iii*) vehicle dynamics; *iv*) control strategy for CAVs. It is worth noting that with this approach, the number and type of factors considered in the same framework could be increased and detailed each time as needed.
Within this framework, the aims of this chapter are to

1. develop a GLOSA system aiming at reducing both travel time and *stop&go* phenomena at intersection;

2. enhance the testing approach of C-ITS systems by exploiting an Integrated Simulation Environment proposed in Chapter 4, which allows to model in detail the following components: the vehicle dynamics, the traffic environment and the control logic. In so doing, it is thereby possible to overcome the shortcomings and limitations in existing testing approaches arising from the over-simplified modelling of all components of the traffic environment [151];

3. investigate the impact, on both mobility and environmental performance of GLOSA services, of factors that are often not considered (traffic signal phase condition), rarely considered (electric engine), or one-to-one considered (traffic condition, TLS cycle duration, communication distance, and minimum speed); in so doing, it is possible to correctly identify the critical factors for a proper assessment of the considered C-ITS system;

4. compare outputs of a simple consumption model - the one embedded within the exploited micro-simulator software (SUMO) - with those of a detailed model to highlight how the use of the latter is crucial to evaluate the energy performance of a C-ITS control system correctly.

5.2 Related Works on GLOSA System

GLOSA systems have gained considerable interest from different research domains, such as computer science, civil engineering, and transportation

Table 5.1: Comparison of GLOSA research works

Paper analysed	**Testing objectives [Effects on Traffic Flow, Vehicle performances, both]**	**Traffic representation [No Traffic, MicroSimulator (e.g. SUMO, VISSIM), ...]**	**Energy consumption computation [Energy consumption model, Vehicle Dynamics model]**	**Type of Engine [Traditional, Electric]**	**Technical notes [e.g. varied traffic density and penetration rate of GLOSA, varied communication range, varied communication range and gear]**
[152]	vehicle performances	no traffic	CMEM	gasoline	effects of link length and communication range
[153]	both	VISSIM	PHEM	gasoline and Diesel	effects of communication range and gear choice
[154]	effects on traffic	SUMO	energy-related consumption model	gasoline	effects of penetration rate of GLOSA-equipped vehicles, traffic demand and communication range
[155]	both	SUMO	HBEFA	gasoline	effects of communication range
[156]	vehicle performances	no traffic	vehicle longitudinal nonlinear dynamics	gasoline VT-Micro	-
[157]	vehicle performance	no traffic	vehicle longitudinal nonlinear dynamics	gasoline	effects of following a GLOSA-equipped vehicle, different speed limit and weather conditions
[158]	traffic flow	SUMO	EMIT	gasoline	effects of penetration rate of GLOSA-equipped vehicles, traffic demand and adaptive TLS
[159]	traffic flow	VISSIM	CMEM	gasoline	effects of penetration rate of GLOSA-equipped vehicles
[160]	vehicle performances	no traffic	speed-based model	gasoline	multi-segment approach, GLOSA works well with fixed-time TLS w.r.t. actuated TLS
[161]	vehicle performances	no Traffic	VT-Micro model	gasoline	-
[162]	vehicle performances	driving simulator without traffic	-	gasoline	effects of communication distance
[163]	both	VISSIM	VERSIT+ model	gasoline and diesel	effects of traffic demand, GLOSA works well with fixed-length cycle TLS
[164]	traffic flow	custom micro-simulator	-	-	effects of MPC-based traffic control
[165]	traffic flow	Paramics	vehicle longitudinal nonlinear dynamics engine torque-speed-based model	gasoline gasoline	effects of CAVs equipped with GLOSA system in mixed traffic flow penetration rate of GLOSA-equipped vehicles
[166]	vehicle Performances	Aimsum	vehicle longitudinal nonlinear dynamics	electric	multiple signalized intersections penetration rate of GLOSA-equipped vehicles
[167]	platoon performances	custom micro-simulator	VT-Micro emissions model	gasoline	effects of traffic demand
[168]	traffic flow	VISSIM	-	-	effects of intersection queues
[169]	traffic flow	custom micro-simulator	custom power-based	gasoline	effects of TLS signal phase and traffic demand
[150]	traffic flow	SUMO	HBEFA	gasoline	comparison of different GLOSA algorithms
[170]	traffic Flow	custom micro-simulator	custom power-based	gasoline	effects of TLS signal phase, traffic demand, communication range and penetration rate of GLOSA-equipped vehicles
[171]	traffic flow	SUMO	HBEFA	gasoline	effects of traffic demand, CAVs penetration rate and multi-vehicle coordination
[172]	vehicle Performance	no traffic	vehicle longitudinal nonlinear dynamics	diesel	effects of information availability about the state of the TLS.
[173]	traffic flow	VISSIM	-	-	effects of traffic demand
[174]	vehicle performances	no traffic	vehicle longitudinal nonlinear dynamics power-based energy model	electric	effects of segment length, segment slope, TLS period time and green duration
[175]	vehicle performances	real-world tests	vehicle longitudinal nonlinear dynamics	gasoline	

research. Indeed, an extensive technical literature exists that seeks to evaluate the effects on system performance of different factors, such as communication distance and penetration rate of CAVs [150].
The first attempts focused on the effect of control strategies on controlled vehicles energy consumption performance, neglecting all traffic factors. For instance, [152] evaluated the effectiveness of three velocity planning algorithms aiming at minimising the acceleration rates of a vehicle travelling along an empty 10-intersection signalised corridor. Results of stochastic simulations, considering edges length and communication distance as uniformly distributed random variables, showed a 12-14% reduction in fuel consumption and pollutant emissions, computed exploiting the CPEM [176], compared to no control scenario.
Subsequently, some authors focused on the impact of communication distance and traffic demand. The impact of gear choice and communication distance on fuel consumption were investigated in [153], who found that a sub-optimal gear choice reduces the benefits of the GLOSA system, while a communication distance greater than 600 [m] has no further advantage. Along similar lines, [154] exploited SUMO and an energy-related fuel consumption model [177] to show that high penetration rates of GLOSA-equipped vehicles within traffic flows reduce stop time by 80% and fuel consumption by up to 7%. The same authors also show that the optimal communication range is close to 350 [m]. Similar values of the optimal communication distances, 300 [m] and 400 [m] for urban and rural areas, respectively, were found in [162] in the case of empty roads. The need to share and exploit traffic and/or TLS data further ahead of an intersection was clearly stated in [158], showing that the system's performance degrades under certain traffic conditions. A driving simulator investigated the effect of several traffic demand levels and two different pre-timed signal phases for TLS, and different communication distances [169, 170]. Finally, [168] proposed a GLOSA strategy accounting also for the dissipation time of queues. Simulations, performed by leveraging the Car2X interface of VISSIM, showed a reduction in waiting time, queue length, and the number of stops compared to no GLOSA, even without considering queue discharge time.
Since enabling GLOSA for non-adaptive TLSs is trivial, as they run

their static program in an endless loop, some works considered fully-adaptive or semi-adaptive TLSs. For instance, results in [163] proved that such systems work well with fixed-length cycle TLS. At the same time, adaptive-coordinated TLS can increase conflict in traffic flow due to the low accuracy of the information obtained in the SPaT message. To overcome these issues, [159] suggested exploiting additional information (e.g., time history of TLS) for adaptive-coordinated TLSs, while [164] recommended sharing the SPaT message far enough in advance from the intersection location.

More recently, a GLOSA system that ideally suits CAVs was proposed in [167]: the results proved the ability to reduce both delay time and fuel consumption by 30-50% and 15-20%, respectively. Along the same lines, [171] investigated the impact of the CAVs penetration rate within traffic flow, resulting in an increase in pollutant emissions of V2X unequipped vehicles for low penetration rates. The case of 100% of CAVs equipped with GLOSA system was analysed by [173]: results of simulations, performed for two different levels of traffic demand, indicated a reduction in average delays of around 83.84% and 86.46% for the traffic conditions considered, showing that traffic density significantly affects GLOSA performance.

All the above works exploit point-mass kinematic models for vehicle motion and simplified models for energy consumption estimation. [156] first highlighted the need for more detailed models. They adopted a non-linear dynamic model to emulate the behaviour of a single-vehicle travelling along a 1-TLS road; the VT-Micro model [178]. The same approach was used in [157] to investigate the effects of different speed limits and weather conditions, as well as the benefit for vehicles following a GLOSA-equipped one. [166] investigated the effectiveness of a multi-segment GLOSA system for electric vehicles, assuming no losses in transmission, no slip at the wheels, a constant road slope, and constant traffic demand. The results revealed that, by increasing the penetration rate of GLOSA-equipped vehicles up to 100%, it is possible to reduce energy consumption and travel time by 28.5% and 3.8%, respectively. Similarly, [165] evaluated the influence of such a system in mixed traffic conditions, considering three different traffic demand levels and seven different penetration rate values of GLOSA-equipped vehicles. Their results revealed that, even at relatively low penetration levels, the GLOSA system improves the energy efficiency of non-equipped vehicles, although travel time slightly increases. [172] evaluated the impact of TLS information availability on fuel consumption and emissions for a Euro 5 diesel vehicle, modelled by non-linear longitudinal dynamics, travelling on a 1km-long route with two traffic lights in between. The results of three different information scenarios proved that TLS information is crucial for energy saving in urban conditions, promoting 7.5-12% and 13-32% reductions in, respectively, fuel consumption and NOx emissions. A non-linear longitudinal dynamics and a transmission model with a standard motor efficiency map and a four-gear transmission system [174] allowed an EV with enhanced simulation results to be modelled. The control system assessment was carried out by taking into account some factors of the urban route (segment length, segment slope, TLS period time, and green duration) but neglecting the presence of surrounding traffic. More recently, [175] evaluated the energy-saving performance of the GLOSA system by considering queuing effects and driving errors both in simulations and real-vehicle tests. However, the impact of factors such as communication distance, link length, and traffic demand was not investigated since they were assumed to have fixed values. All the above works took into account only the longitudinal dynamics of vehicles, neglecting lateral dynamics. Moreover, they usually assumed no losses in vehicle transmission, simplified power-train model, no slip at the wheels, and constant road slope, resulting in oversimplified vehicle behaviour and hence improper performance evaluation. Tab. 5.1 provides an overview of the above works showing explicitly: *i*) testing objectives; *ii*) traffic environment modelling; *iii*) consumption model adopted; *iv*) engine type; *v*) technical notes. Two important aspects, which are strictly related to the motivations for this paper, are highlighted in Tab. 5.1: *i*) the technical literature focusing on vehicle technological development does not usually take into account some critical factors of the road traffic environment (e.g., traffic conditions); *ii*) the technical literature usually focuses on evaluating traditional engine types (petrol or diesel), while very few works [166, 174] consider electric engines, which, as will be shown below, may require a slight change in the C-ITS development process.

The proposed testing approach goes beyond the existing technical literature by exploiting an Integrated Simulation Environment, based on the combined use of a set of tools, enabling the test of factors belonging to different domains of engineering simultaneously, thus resulting in a holistic quantification, within the same simulation scenario, of the effects of different factors believed to affect the performance of GLOSA systems. This holistic approach also applies to other in-vehicle technologies within similar intra-domain evaluation needs [9].

5.3 GLOSA Algorithm

The proposed GLOSA algorithm, reported in the Algorithm 1 box, aims to minimise travel time spent at each TLS-controlled segment i by computing a reference speed that avoids unnecessary stops and reduces *stop&go* phenomena, which negatively affect vehicle energy performance. Very broadly, when in the communication range D_{com} $[m]$ of a TLS i, the Ego-Vehicle receives the SPaT and MAP messages and, based on both the latter and its position, the algorithm checks whether or not the TLS is relevant (the next one on the Ego-Vehicle's route). Then, given the actual speed and acceleration, the algorithm computes, by exploiting basic rules of motion $d(t) = v(t) \cdot t + 0.5a(t) \cdot t^2$, the time required to reach the TLS:

$$\Delta t_{tls,0} = \begin{cases} \dfrac{d_i(t)}{v(t)} & \text{if } a(t) = 0\ , \\ -\dfrac{v(t)}{a(t)} + \sqrt{\dfrac{v(t)^2}{a(t)} + \dfrac{2d_i(t)}{a(t)}} & \text{if } a(t) \neq 0, \end{cases} \tag{5.1}$$

where $d_i(t)$ $[m]$ is the distance from the i-th TLS at time t; $v(t)$ $[m/s]$ is the speed of the Ego-Vehicle at time t; and $a(t)$ $[m/s^2]$ is the acceleration of the Ego-Vehicle at time t.

The algorithm then checks the i-th TLS phase at time $t + \Delta t_{tls,0}$: if it is green, then the Ego-Vehicle continues its trip trying to maintain the current vehicle behaviour. Otherwise, if the phase is red or yellow, it computes a reference speed profile which allows the i-th TLS to be passed while minimising travel time.

Note that, for comfort and safety reasons [179], acceleration can assume values in the range $[a_{min}, a_{max}]$, where $a_{min} = -3.5$ $[m/s^2]$ is the maximum deceleration and $a_{max} = 2.5$ $[m/s^2]$ is the maximum acceleration.

Algorithm 1: GLOSA Algorithm executed when the Ego-Vehicle enters the communication range of upstream TLS i

---

Find the next TLS upstream
Calculate time to reach the TLS $\Delta t_{tls,0}$ with current speed and acceleration
Check phase at time $t + \Delta t_{tls,0}$
if *Green* **then**
  Calculate remaining time to green phase $\Delta t_{tls,g}$
  Calculate reference speed for $t + \Delta t_{tls}(V_r) : V_r \in [V_{min}, V_{max}]$ & $\Delta t_{tls}(V_r) \geq \Delta t_{tls,g}$
else
  Calculate time to next green phase $\Delta t_{tls,ng}$
  Calculate reference speed for $t + \Delta t_{tls}(V_r) : V_r \in [V_{min}, V_{max}]$ & $\Delta t_{tls}(V_r) \geq \Delta t_{tls,ng}$
end

Finally, the reference speed V_r $[m/s]$ is chosen within the range $[V_{min}, V_{max}]$, where V_{max} $[m/s]$ is the maximum allowable speed on the road segment controlled by TLS i. It is computed as follows:

$$\begin{aligned}
&\textit{minimise} \quad && f(v) \\
&\textit{subject to} \quad && V_{min} \leq V_r \leq V_{max} \\
& && a_{min} \leq a_r \leq a_{max} \\
& && phase_i\Big(t + \Delta t_{tls}(V_r)\Big) = GREEN,
\end{aligned} \tag{5.2}$$

where $f(v) = d_i(t)/V_r$ is the objective function to minimise; $a_r(t)$ $[m/s^2]$ is the acceleration to reach the reference speed V_r.

5.4 Testing Methodology

The Integrated Simulation Environment proposed in Chapter 4 is used to test the GLOSA service. The proposed testing methodology is used in a traffic scenario with: a single controlled CAV, named Ego-Vehicle, embedding a single-segment GLOSA (S-GLOSA) algorithm, which travels along an urban road corridor composed of M edges and N signalised intersections regulated by fixed-cycle TLSs, with $M > N$. The Ego-Vehicle

is equipped with IMU and GPS to measure its state, with on-board ranging sensors (radar and camera) to measure its relative position and speed to a vehicle ahead and with an OBU, configured as a receiving and transmitting host, enabling the communication with TLSs. Furthermore, each TLS i ($i = 1, ..., N$) is equipped with RSU and shares both MAP and SPaT messages within its communication range D_{com}. It is worth noting that the Ego-Vehicle is the only one equipped with the technologies mentioned above, while other vehicles are assumed to be human-driven and not connected.
The considered urban scene is complex enough to challenge the proposed simulation model, evaluate its suitability, and investigate its ability to test the impact of several different factors on the performance of the control algorithm. To achieve this goal, the complete set approach [180] is exploited so to assess the impact of the following factors: *i*) the minimum speed V_{min} $[m/s]$ that the GLOSA algorithm can provide; *ii*) the communication range D_{com} $[m]$ of all TLSs within the network; *iii*) the cycle duration C $[s]$ of TLSs within the network; *iv*) the phase condition (PC) $[s]$, i.e., the relative time instant when the Ego-Vehicle enters the network in the time framework of the TLS cycle; *v*) traffic conditions (TC), defined based on vehicle density $[veh/km]$ within the testing area; *vi*) engine type configuration (endothermic and electric).
Ego-Vehicle parameters, both generic and specific for each engine type, are listed in Tab. 5.2. Note that, β_0, β_1 and β_2 are vehicle-specific model constants calibrated with the VT-CPFM calibration tool assuming the Ego-Vehicle is a generic EURO 4 car [181]

5.4.1 Testing Scenario

The simulation network used for the proposed modelling framework is extracted from the city centre of Trento (Italy), and is depicted in Fig. 5.1. The Ego-Vehicle enters the network in section A (red point), located along *via Torre Vanga* at coordinates ($46.069\,929°N$, $11.118\,326°E$), while the route ends in section B (magenta point), located along *via del Brennero* at coordinates ($46.078\,166°N$, $11.123\,064°E$). The road corridor in question is a one-way road of length 1.186 $[km]$ with $M = 8$ edges (or segments) and $N = 6$ signalised intersections. The layout of the road corridor, depicted in Fig. 5.1b, consists of six two-lane edges and a three-lane edge between the 3^{rd} and 4^{th} TLS, having different lengths that vary

Table 5.2: Ego-Vehicle Model Parameters

Parameter	Description	Value	VehType
m	vehicle mass	1235 $[kg]$	both
C_d	aerodynamic drag coefficient	0.28	both
A_f	frontal area	2.118 $[m^2]$	both
C_r	rolling resistance w.r.t. surface type	1.75	both
c_1	rolling resistance w.r.t. road condition	0.0328 $[s/m]$	both
c_2	rolling resistance w.r.t. tire type	4.575	both
η_d	driveline efficiency	0.92	both
ω_{idle}	engine idling speed	800 $[rpm]$	ICE
β_0	model consumption constant	$2.0708e^{-7}$	ICE
β_1	model consumption constant	$3.7409e^{-5}$	ICE
β_2	model consumption constant	$1e^{-6}$	ICE
τ_1	first gear ratio	3.630	ICE
τ_2	second gear ratio	2.052	ICE
τ_3	third gear ratio	1.380	ICE
τ_4	fourth gear ratio	1.048	ICE
τ_5	fifth gear ratio	0.842	ICE
τ_{diff}	differential gear ratio	0.245	ICE
η_{em}	electric motor efficiency	0.91	EV
$\eta_{battery}$	Electric battery efficiency	0.90	EV
P_{aux}	auxiliary power losses	0.7 $[kW]$	EV

from 95 to 250 $[m]$. The legal speed limit of all the edges is 50 $[km/h]$. Fig. 5.1c shows the elevation profile of the considered route. Fixed-cycle TLSs (yellow points) with an inter-distance varying from 120 to 250 $[m]$ regulate the signalised intersections within the network.

5.4.2 Traffic Conditions

The performance of the proposed GLOSA algorithm explained in Section 5.3 are tested un under four different traffic conditions, defined according to Macroscopic Fundamental Diagram (MFD) theory [182]. This latter allows traffic behaviour to be modelled dynamically in urban areas at an aggregate level, thus providing an effective tool to estimate the traffic conditions of a whole network area through space-mean flow, density, and speed. To this end, 16 loop-detectors are located on the most important

Figure 5.1: Simulation Network: (**a**) SUMO network capture; (**b**) corridor layout; (**c**) altitude profile.

edges, providing 5-min vehicle counts and occupancy measurements to estimate the MFD-based flow-density relationship for the network area considered (see [183] and references therein). The estimated MFD is used to recognise traffic congestion level in each experiment under the three conditions shown in Fig. 5.2: *i*) *Free Flow (FF)*, with low densities and flows; *ii*) *Under-Saturation Flow (U-Sat)*, with low densities but high values of flows; *iii*) *Saturation Flow (Sat)*, with both high densities and flows. The fourth and last traffic condition concerns the case of *Empty Network* (*E*) (there are no other vehicles except the Ego-Vehicle), and it is not reported in Fig. 5.2. In so doing, it is possible to cover all the traffic condition cases that a vehicle could encounter while driving

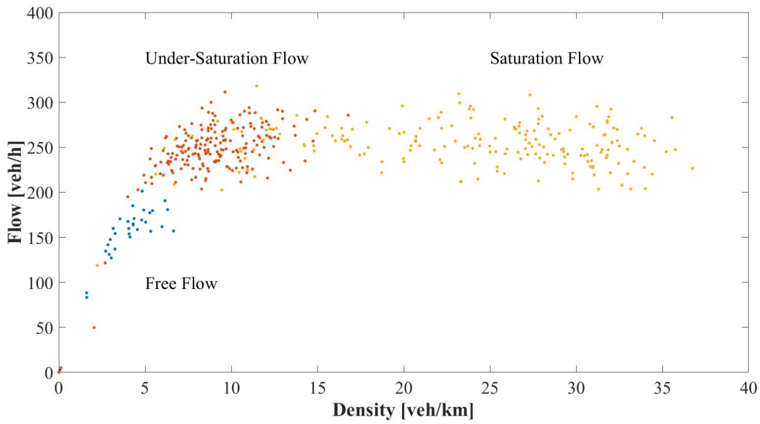

Figure 5.2: Average flow vs. average density from all the detectors in the appraised network area.

along an urban road.
Note that, in *Free Flow* and *Under-Saturation Flow* conditions, a pre-loading time for the network of 575 or 600 [s] (based on TLS cycle duration) allows steady-state conditions to be reached in traffic simulation. For *Saturation Flow* conditions, the pre-load time is 3600 [s].

5.4.3 TLS Cycle Duration

Three different configurations of TLS cycle duration are considered, one with the optimal value and the others, respectively, with values smaller and greater than the optimal one.
The optimal signal parameters are computed according to the method proposed in [184], which allows cycle duration and green times to be obtained for each TLS i, assuming that the phase matrix is known to minimise the time delay for vehicles.
The cycle duration C_i [s] of the generic i-th TLS is computed by Eq. (5.3):

$$C_i = \frac{1.5 \cdot \sum_{p=1}^{n} l_{p,i} + 5}{1 - \sum_{p=1}^{n} \cdot \frac{q_{p,i}}{S_{p,i}}} \tag{5.3}$$

where $q_{p,i}$ [veh/h] is the flow entering the intersection for each phase p; $S_{p,i}$ [veh/h] is the saturation flow for each phase p; and $l_{p,i}$ [s] is the delay for each phase p.

Note that each phase p is represented by a single traffic current, the one with the highest value of the flow ratio $\frac{q_i}{S_i}$.
Having defined optimal cycle duration, the effective green $G_{p,i}$ $[s]$ for each phase p of the i-th TLS is computed as follows:

$$G_{p,i} = \frac{\frac{q_{p,i}}{S_{p,i}}}{\sum_{p=1}^{n} \cdot \frac{q_{p,i}}{S_{p,i}}} \cdot (C_i - \sum_{p=1}^{n} l_p) \tag{5.4}$$

The design is performed for all N TLS within the network w.r.t. *free flow* and *under-saturation traffic flow* conditions. Based on our results, the optimal cycle duration is 60 $[s]$; thus, 45 $[s]$ and 75 $[s]$ are tentative duration values that should increase the delay at intersection w.r.t. the optimal value. Finally, the duration of effective green w.r.t. the whole cycle duration is derived for all TLSs within the network for each cycle configuration considered. Note that, given a cycle configuration (e.g. a cycle time of 60 $[s]$), the duration of the adequate green time differs from one TLS to the other since, based on (5.4) according to [184], it depends on the number of different phases that varies according to the number of manoeuvres allowed at the intersection.

5.4.3.1 Communication Distance

The impact of communication distance, assuming there is no packet loss or access delay (the OBU immediately receives all data shared by each RSU), is investigated. Different wireless communication technologies directly are not explicitly modelled and tested, but the range value of 100 $[m]$ is used to emulate short-range wireless communication technologies, while 500 $[m]$ mimics long range ones.

5.4.4 Minimum Speed

The minimum speed that the control algorithm can provide is a critical factor for the functioning of the GLOSA system. While it allows the control algorithm to compute a speed profile to cross an intersection easily, it could produce unnecessary *stop&go* or *slow&go* phenomena that negatively affect both traffic conditions, and energy consumption [185]. For this purpose, the minimum speed is usually set at 6 $[m/s]$ [154].

The following four different values as minimum allowable speed for the algorithm are considered [4.00, 5.50, 7.00, 8.50] [m/s].

5.4.5 Traffic Signal Phase Condition

In addition to the TLS cycle duration, the impact of the TLS phase that the Ego-Vehicle encounters along its route is evaluated. To this end, different time instants in which the Ego-Vehicle enters the network are defined. Specifically, the cycle time of the first TLS along the route is divided into four intervals (equally spaced over time), and the Ego-Vehicle enters the network at the beginning of each of them. Any of the four intervals are identified as *insertion time*. In practice, different initial conditions are explored by randomly varying the insertion time w.r.t. the arrival time of the vehicle at the traffic signals.

5.5 Numerical Analysis

To test the suitability of the proposed modelling framework, 4800 simulations (2400 per engine type) are carried out. All the factors described in Section 5.4 are varied with a complete-set approach. It is worth noting that although one scene (i.e., one simulation network and one route travelled by the Ego-Vehicle) is considered, several different scenarios by varying all the considered traffic factors are investigated. Indeed, the supposed route consists of eight heterogeneous segments (with varying numbers of lanes and different lengths) and six TLSs (with varying numbers of controlled lanes and different effective green duration also in the case of the same cycle time duration). Thus, traffic conditions encountered by the Ego-Vehicle along the route vary from simulation to simulation, covering many different scenarios and providing generalisable results.

To compare performances achievable with and without the control algorithm, as well as under different traffic conditions, we consider the following KPIs: *i*) travel time (TT) [s]; *ii*) stop time (ST) [s], the time the Ego-Vehicle has a speed lower than 0.1 [m/s]; *iii*) fuel (FC) [l/km] and energy (EC) [kWh/km] consumption, computed by both SUMO and external consumption models. The relationship among the KPIs and

the considered traffic factors is investigated both qualitatively and quantitatively employing different methods, namely boxplot and multiway (n-way) analysis of variance (ANOVA) [186]. Boxplots are used to gain greater insight into the statistical distribution of analysed points. On each box, the central mark indicates the median, and the bottom and top edges of the box indicate the 25^{th} and 75^{th} percentiles, respectively. The whiskers extend to the most extreme data points not considered outliers, while the outliers are plotted individually using the '+' symbol. The n-way ANOVA returns a vector of p-values, one per term, for testing the effects of multiple factors on the mean of the output vector. The p-values represent the probability that the F-statistic can take a value larger than a computed test-statistic value. The F-statistic, calculated as $F = \frac{Mean\ Sq.}{Errors}$, is the ratio of the mean squared errors and assesses the significance of the terms or components in the model. A small p-value for a factor indicates that at least one group mean significantly differs from the others; that is, there is a significant effect due to that factor. Here, it is assumed that a result is significant if the p-value is lower than 0.01 (according to common practise 0.05 or 0.01). Note that a factor's significance is related to its contribution to the variation compared to errors; hence, a factor is significant if its contribution is high.
Statistical distributions, when necessary, are compared with each other by using:i) a two-sample t-test [187]; ii) Kruskal Wallis test [188]. The two-sample t-test returns a test decision for the null hypothesis that the data in the two samples comes from independent random samples drawn from normal distributions with equal means and unknown unequal variances. The alternative hypothesis is that the data comes from populations with unequal means. The Kruskal-Wallis test is a non-parametric version of classical one-way ANOVA. It compares the medians of two samples to determine whether they come from the same population (or, equivalently, from different populations with the same distribution).

5.5.1 Consumption-Related Results

5.5.1.1 Validation of Consumption Computing Methods

The consumption results are obtained using the consumption models presented in Sec. 4.3.2.1 and Sec. 4.3.2.2. First, the distribution of both fuel and energy consumption among different simulations are analysed,

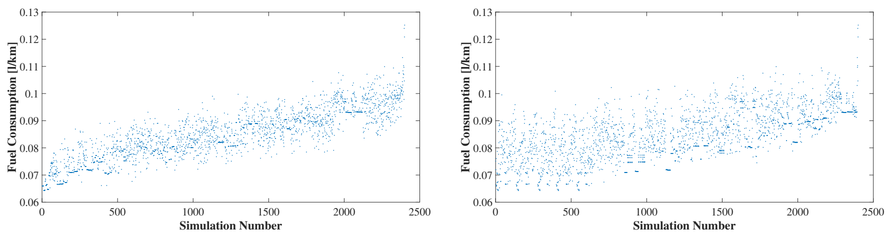

(a) (b)

Figure 5.3: Distribution of fuel consumption among simulations sorted w.r.t.: (a) travel time [s]; (b) stop time [s].

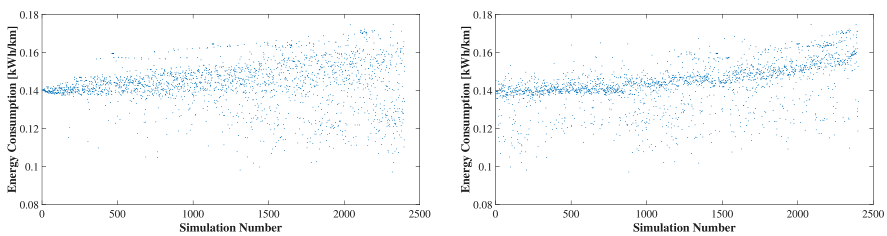

(a) (b)

Figure 5.4: Distribution of energy consumption among simulations sorted w.r.t.: (a) travel time [s]; (b) stop time [s].

sorted w.r.t. TT (Fig. 5.3a and Fig. 5.4a respectively) and ST (Fig. 5.3b and Fig. 5.4b respectively). The two distributions are different: for the endothermic engine, the mean values are 0.10 and 0.08 [l/km], while for the electric engine, they are 0.05 and 0.14 [kWh/km]. It is worth noting that the first values refer to SUMO consumption models, while the second to the external ones; in both cases, the means were verified to be significantly different based on a two-sample t-test. Moreover, standard deviations have quite different patterns, with 0.022 and 0.009 for the endothermic engine and 0.006 and 0.012 for the electric one; again, the first values refer to SUMO consumption models, while the second values refer to the second to the external ones. Consumption outcomes are compare with the ones suggested by the technical literature for passenger cars: for Euro4 vehicles with endothermic engines, the mean fuel consumption is in the range [8-10] [$l/100km$] as in [189],

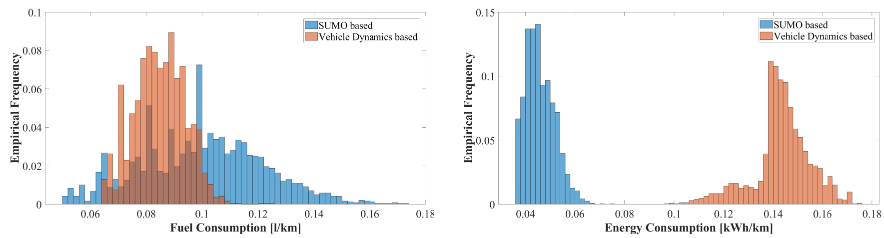

(a) (b)

Figure 5.5: Comparison of the distribution of consumption outputs between external models and SUMO built-in models. Histogram of: (a) fuel consumption [l/km]; (b) energy consumption [kWh/km].

while for electric vehicles the energy consumption is in the range [0.1-0.3] [kWh/km] as in [190]. Hence, results indicate that the considered external models estimate energy consumption quite well.

Finally, the results of consumption models embedded in the Integrated Simulation Environment are compared with the ones achievable with SUMO built-in models (see [191] and [192] for endothermic and electric models, respectively). Distribution for the endothermic engine case (Fig. 5.5a) shows that the SUMO model provides slightly overestimated values w.r.t. the external model; a greater variance means that it is more sensitive to variations in traffic conditions. By contrast, distribution for the electric engine case (Fig. 5.5b) shows that the SUMO model strongly underestimates energy consumption, w.r.t. a more detailed model, providing unrealistic values. A similar result is also shown in [193], linking the underestimated results to the design of an energy model and its validation process. In conclusion, results show that using an Integrated Simulation Environment to emulate highly detailed vehicle dynamics and correctly estimate consumption can play a crucial role in developing efficient automated/autonomous vehicle systems. Indeed, since the consumption performance of a vehicle depends on several parameters such as mass, power, and battery capacity [190], the use of a simulation environment embedding detailed models appears to be crucial for obtaining accurate findings.

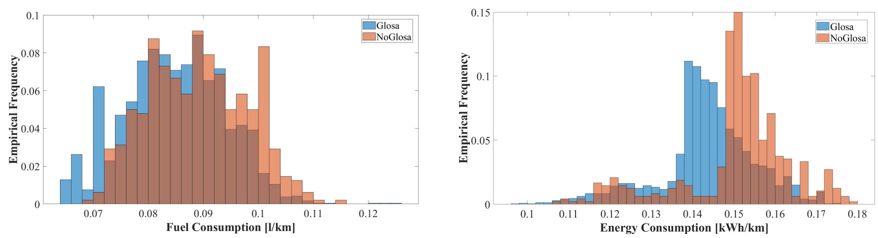

(a) (b)

Figure 5.6: Comparison of the distribution of consumption outputs between GLOSA and no GLOSA cases. Histogram of: (a) fuel consumption $[l/km]$; (b) energy consumption $[kWh/km]$.

5.5.1.2 Analysis of S-GLOSA Improvement

To prove the suitability of the proposed modelling framework to assess the effects of GLOSA in enhancing vehicle consumption, the consumption performance of the proposed GLOSA algorithm w.r.t. the no GLOSA case, labelled as noGLOSA in Fig. 5.6 is compared. Both the GLOSA and noGLOSA cases adopt the same modelling framework. The shapes of consumption distributions are pretty similar, while the means are significantly different (verified through a two-sample t-test). For both endothermic and electric engine cases, the S-GLOSA algorithm allows consumption to be reduced by about 5% (4.98%) for the endothermic case and 4.72% for the electric. Thus, our results confirm that the spread of information about TLS operations improves consumption efficiency even by using a simple control strategy.

5.5.1.3 Effects of Different Conditions on System Performance - Endothermic Engine

The effect of the considered traffic variables on GLOSA system performance in terms of fuel consumption is disclosed in this section. Boxplots in Fig. 5.7 show the relationship between fuel consumption and each factor. The findings show that fuel consumption is strongly dependent on TLS cycle duration (Fig. 5.7a), traffic conditions (Fig. 5.7b) and phase condition (see Fig. 5.7c). Specifically, the higher the traffic congestion and TLS cycle duration, the higher the FC is likely to be. Furthermore,

there is a low dependency on communication distance (Fig. 5.7d) and no dependency on minimum speed (Fig. 5.7e).
To quantify the impact of each factor on the consumption performance of the considered control system, an n-way ANOVA analysis is performed. The results reported in Tab. 5.3 are in line with those in Fig. 5.7: all but one of the variables (minimum speed) have a significant effect on the considered output. The analysis of the residuals validates the findings; it includes: *i*) a run sequence plot of the residuals; *ii*) a normal probability plot of the residuals (a t-test confirmed the normality assumption); *iii*) a scatter plot of the predicted values against the residuals (where no pattern was evidenced). Results of ANOVA analysis in Tab. 5.3 reveal that the minimum speed is not a significant factor since its p-value is higher than 0.01. Accordingly, by considering only the effect of the significant factors, it is possible to derive the following linear model to estimate the fuel consumption:

$$FC_{lm} = \alpha_C \cdot C + \alpha_{TC} \cdot TC + \alpha_{PC} \cdot PC + \alpha_{D_{com}} \cdot D_{com}, \qquad (5.5)$$

where $\alpha_C = 0.3828$, $\alpha_{TC} = 0.3676$, $\alpha_{PC} = -0.3592$ and $\alpha_{D_{com}} = -0.1168$ are standardised regression coefficients of the model related to cycle duration, traffic condition, phase condition and communication distance, respectively.

5.5.1.4 Effects of Different Conditions on System Performance - Electric Engine

Here the suitability of the proposed modelling framework to simulate the effect of traffic variables on GLOSA system performance in terms of

Table 5.3: ANOVA results for the endothermic engine

Source	**Sum Sq.**	**Degrees of Freedom**	**Mean Sq.**	**F**	**Prob >F**
Cycle duration	0.03056	2	0.01528	344.89	0
Traffic condition	0.03125	3	0.01042	235.12	0
Phase condition	0.03208	3	0.01069	241.37	0
Communication distance	0.00277	1	0.00277	62.41	0
Minimum speed	0.00011	3	0.00004	0.85	0.464
Error	0.10576	2387	0.00004	[ ]	[ ]
Total	0.20254	2399	[ ]	[ ]	[ ]

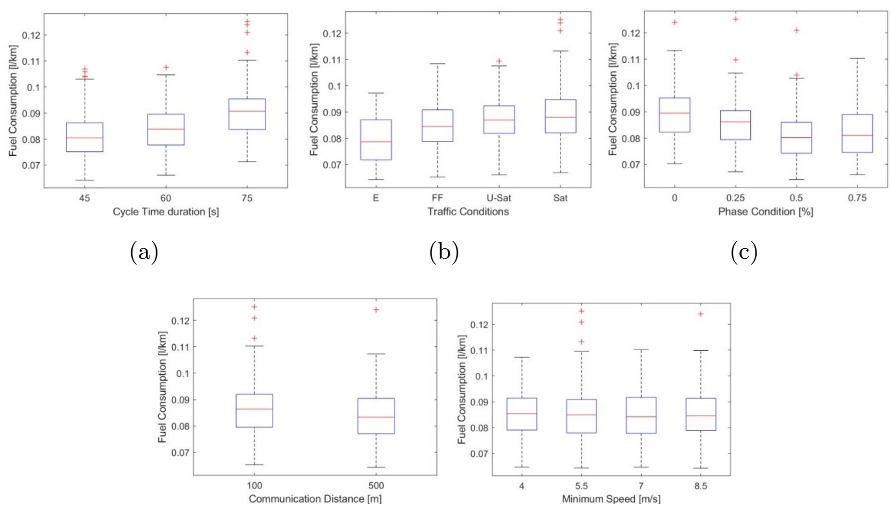

(a) (b) (c)

(d) (e)

Figure 5.7: Input-output relationship for endothermic engine. Boxplot of FC w.r.t.: (a) TLS cycle duration [s]; (b) traffic condition; (c) phase condition [s]; (d) communication distance [m]; (e) minimum speed [m/s].

energy consumption is evaluated. The boxplots in Fig. 5.8 investigate the relationship between energy consumption and each input variable. Results show that energy consumption increases as cycle duration (Fig. 5.8a) and minimum speed (Fig. 5.8e) increase, while it decreases as traffic congestion (Fig. 5.8b) and communication distance (Fig. 5.8d) increase. Finally, it is possible to note a low dependency of energy consumption on the TLS phase condition (Fig. 5.8c).

Note that the reduction in energy consumption as traffic congestion increases is not a poor outcome since it concerns: *i*) the specific operation of electric vehicles, whose travel range is a decreasing function of speed; *ii*) the presence of a regenerative braking system. As for the endothermic case in Sec. 5.5.1.3, an n-way ANOVA analysis is performed to quantify the impact of each factor on consumption performance, as well as a residual analysis to validate results as follows: *i*) a run sequence plot of the residuals; *ii*) a normal probability plot of the residuals (normality also confirmed with t-test); *iii*) a scatter plot of the predicted values against the residuals (without patterns). The results, listed in Tab. 5.3,

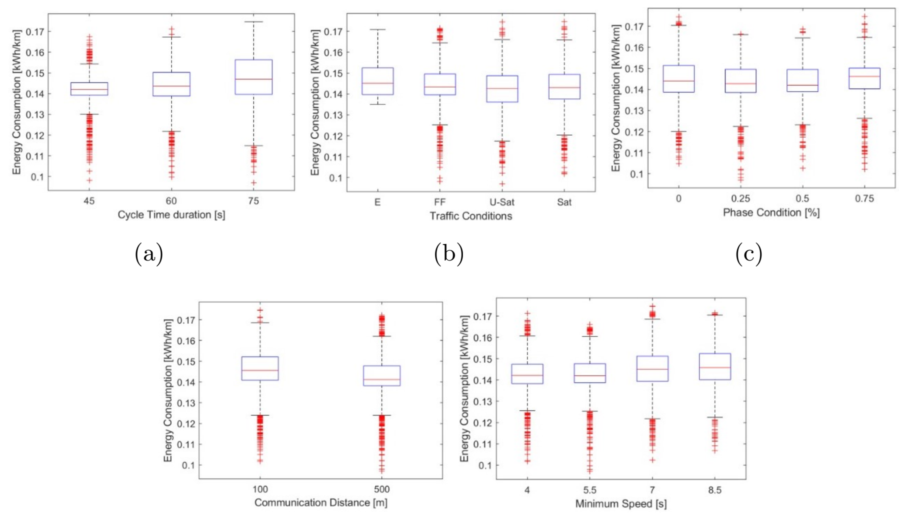

(a) (b) (c)

(d) (e)

Figure 5.8: Input-output relationship for electric engine. Boxplot of EC w.r.t.: (a) TLS cycle duration [s]; (b) traffic condition; (c) phase condition [s]; (d) communication distance [m]; (e) minimum speed [m/s].

are in line with those in Fig. 5.8: all variables have a significant effect on output, i.e. a p-value lower than 0.01.
Finally, the following linear model is obtained to quantify the effect of input variables on the energy consumption output:

$$EC_{lm} = \beta_C \cdot C + \beta_{TC} \cdot TC + \beta_{PC} \cdot PC + \beta_{D_{com}} \cdot D_{com} + \beta_{V_{min}} \cdot V_{min}, \quad (5.6)$$

where $\beta_C = 0.1990$, $\beta_{TC} = -0.1790$, $\beta_{PC} = 0.0107$, $\beta_{D_{com}} = -0.1451$ and $\beta_{V_{min}} = 0.1307$ are standardised regression coefficients of the model related to cycle duration, traffic condition, phase condition, communication distance and minimum speed, respectively.

5.5.2 Mobility-Related Results

The suitability of the modelling framework to assess the performances of the proposed S-GLOSA algorithm in terms of TT and ST is here analysed. Unlike consumption KPIs reported in Section 5.5.1, these are independent of engine type. Hence, statistical analysis is performed on the whole set of simulations to maximise the significance of statistical indicators.

5.5.2.1 Analysis of S-GLOSA Improvement

Here the performance in terms of TT and ST of the proposed control algorithm w.r.t. the no GLOSA case, which is labelled as noGLOSA in Fig. 5.9, are evaluated. Although the shapes of the distributions of both factors are quite similar for GLOSA and no GLOSA, the statistical distribution of the different samples is verified to be significantly different by means of a Kruskal Wallis test; in particular the presence of the control algorithm allows statistically significant reductions of about 5% and 13% in TT (Fig. 5.9a) and ST (Fig. 5.9b), respectively. The results confirm that, by exploiting information about TLS operations, it is possible to reduce both TT and ST even in the presence of a very simple control logic.

5.5.2.2 Effects of Different Conditions on System Performance

Here is evaluated the effect of the traffic factors considered (inputs) on the GLOSA system in terms of TT and ST (outputs). First, the relationship among these variables is investigated by using boxplots. Results for TT show that it is strongly dependent on TLS cycle duration (Fig. 5.10a), traffic congestion (Fig. 5.10b) and phase condition (Fig. 5.10c). Specifically, the higher the TLS cycle duration and traffic congestion, the higher the TT is likely to be. Furthermore, there is no dependence on either communication distance (Fig. 5.10d) or minimum speed (Fig. 5.10e).

Table 5.4: ANOVA results for electric engine

Source	**Sum Sq.**	**Degrees of Freedom**	**Mean Sq.**	**F**	**Prob >F**
Cycle duration	0.0135	2	0.0068	56.29	0
Traffic conditions	0.0138	3	0.0046	38.40	0
Phase condition	0.0017	3	0.0006	4.74	0.0027
Communication distance	0.0069	1	0.0069	57.32	0
Minimum speed	0.0063	3	0.0021	17.57	0
Error	0.2863	2387	0.0001	[ ]	[ ]
Total	0.3287	2399	[ ]	[ ]	[ ]

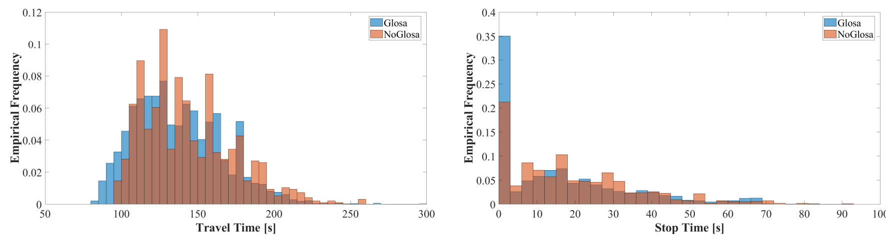

(a) (b)

Figure 5.9: Comparison of mobility indexed distribution between GLOSA and no GLOSA cases. Histogram of: (a) travel time $[s]$; (b) stop time $[s]$.

By contrast, ST strongly increases as both cycle duration (Fig. 5.11a) and minimum speed increase (Fig. 5.10e). At the same time, it slightly decreases as both phase condition and communication distance increase. In this case, no dependence on traffic conditions (Fig. 5.10b) exists.
To quantify the impact of each variable on both TT and ST, an n-way ANOVA analysis is performed and, then, the results are validated by performing an analysis on the residuals including: *i*) a run sequence plot of the residuals; *ii*) a normal probability plot of the residuals (normality also confirmed with t-test), and *iii*) a scatter plot of the predicted values against the residuals (without evidence of patterns). ANOVA analysis for TT in Tab. 5.5, consistent with Fig. 5.10, reveals that communication distance and minimum speed are not significant factors since they have a p-value higher than 0.01. Similarly, the ANOVA analysis for ST in Tab. 5.6, following Fig. 5.11, reveals that all the input factors except traffic conditions are significant. Thus, the following linear models are proposed to estimate the effect of each significant input factor on travel time and stopping time outputs, respectively

$$TT_{lm} = \gamma_C \cdot C + \gamma_{TC} \cdot TC + \gamma_{PC} \cdot PC, \tag{5.7a}$$
$$ST_{lm} = \rho_C \cdot C + \rho_{IT} \cdot IT + \rho_{D_{com}} \cdot D_{com} + \rho_{V_{min}} \cdot V_{min}, \tag{5.7b}$$

where $\gamma_C = 0.3705$, $\gamma_{TC} = 0.3060$ and $\gamma_{PC} = -0.26857$ are standardised regression coefficients that relate the TT model to cycle duration, traffic condition and phase condition, respectively; Similarly, $\rho_C = 0.4058$, $\rho_{IT} = -0.1839$, $\rho_{D_{com}} = -0.1942$ and $\rho_{V_{min}} = 0.2182$ are standardised

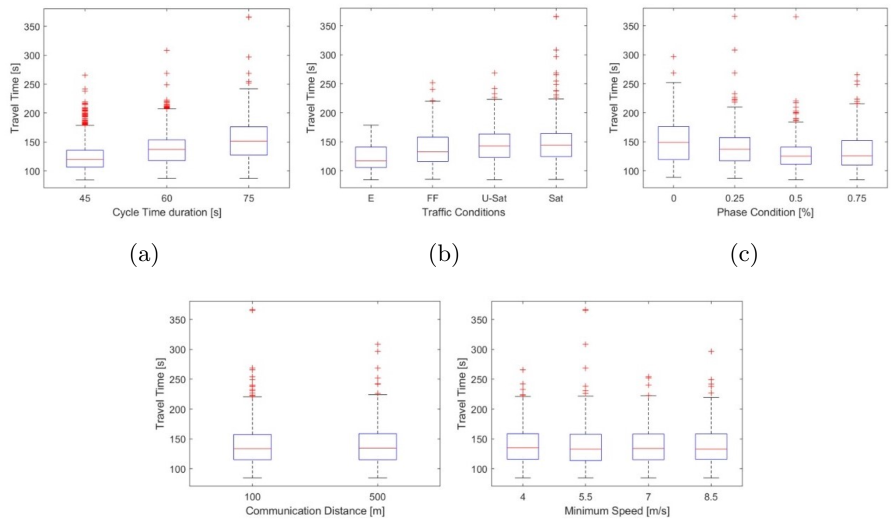

(a) (b) (c)

(d) (e)

Figure 5.10: Boxplot of input-output relationship for TT w.r.t.: (a) TLS cycle duration [s]; (b) traffic condition; (c) phase condition [s]; (d) communication distance [m]; (e) minimum speed [m/s].

regression coefficients that relate the ST model to cycle duration, phase condition, communication distance and minimum speed, respectively.

5.6 Significance of Results

The results in Section 5.5 yield exciting insights on some different aspects of testing and validation of GLOSA services.

Table 5.5: ANOVA results for travel time

Source	**Sum Sq.**	**Degrees of Freedom**	**Mean Sq.**	**F**	**Prob >F**
Cycle duration	5733766	2	286883	502.89	0
Traffic condition	442993	3	147664	258.85	0
Phase condition	401226	3	133742	234.44	0
Communication distance	152.4	1	152.4	0.27	0.6053
Minimum speed	1607.3	3	535.8	0.94	0.4207
Error	2730858	4787	570.5	[ ]	[ ]
Total	4132169	4799	[ ]	[ ]	[ ]

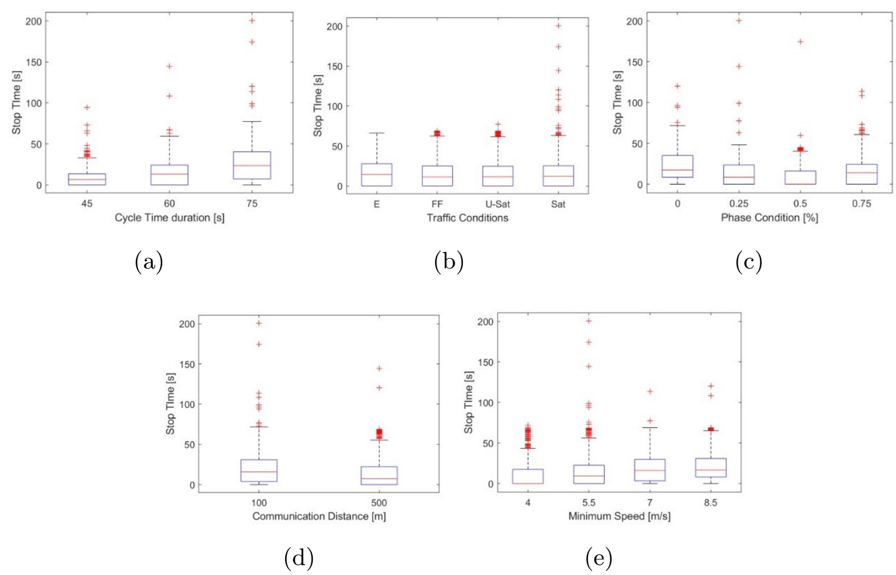

Figure 5.11: Boxplot of input-output relationship for ST w.r.t.: (a) TLS cycle duration $[s]$; (b) traffic condition; (c) phase condition $[s]$; (d) communication distance $[m]$; (e) minimum speed $[m/s]$.

First of all, the comparison among consumption models in Section 5.5.1.2 proves that microscopic simulations tools do not provide realistic outputs. Hence, they could lead to incorrect assessments of the impact of technology. Moreover, the development of GLOSA systems and, more generally, of C-ITS ones should explicitly take account of engine type functioning since EVs have a different behaviour w.r.t. traditional endothermic ones. Indeed, the results in Tab. 5.7 show that the power consumption in the electric engine case, unlike the endothermic one, can not be correctly predicted via a linear model on mean values. Indeed, the adjusted R^2 (Adj-Rsq in Tab. 5.7) clearly show fitting performance differences in the two models. Consistently, the $F - test$ (see F in Tab. 5.7) shows different statistical significance. The two linear models also differ in terms of components (Tab. 5.3 and Tab. 5.4), since both depend on TLS cycle duration and communication distance in the same way (positively and negatively, respectively), while the opposite holds for both phase condition and traffic conditions. Lastly, the EC_{lm} model depends also on minimum speed. Note that positive dependence (positive standardised coefficient) means that the consumption increases as the value of the considered variable increases, while negative dependence (negative standardised coefficient) implies the opposite.

As regards the FC_{lm} prediction model for the endothermic engine case, the dependence of consumption on traffic condition and communication distance is well-known in the technical literature. While the former is not strictly related to GLOSA functioning since it is an exogenous variable, the latter allows computation, as its value increases, a smoother reference speed profile for the vehicle, thereby reducing FC. By contrast, dependence on phase condition requires a broad explanation as the testing scenario strongly influences it. The negative sign of the corresponding standardised model coefficient is related to the transition to different phases: the probability of having a red stage at the intersection increases if the Ego-Vehicle enters the network at the early stage of the TLS_i $i = 1$ cycle since, in our case, the succession of the three phases is *Red* from 0% to 50% of C, *Green* from 50% to 95% of C, and *yellow* from 95% to 100% of C. The last result concerns the dependence on TLS cycle duration, which shows that FC increases as the latter variable increases. Indeed, shorter values of cycle duration result in a succession of shorter but more frequent green windows. Consequently, the control algorithm can compute a smoother reference speed profile, a mechanism very similar to what is expected concerning the communication distance.

Regarding the EC_{lm} prediction model for the electric engine case, the increase in communication distance allows EC to be improved, while the increase in minimum speed reduces the set of possible optimal reference speeds, leading to increased energy consumption. Unlike the endothermic engine case, the increase in traffic congestion improves EC, while the

Table 5.6: ANOVA results for stop time

Source	**Sum Sq.**	**Degrees of Freedom**	**Mean Sq.**	**F**	**Prob >F**
Cycle duration	264503	2	132251	502.89	0
Traffic condition	993.8	3	331.3	258.85	0.2094
Phase condition	12389.4	3	41283	234.44	0
Communication distance	57937	1	57937	0.27	0
Minimum speed	76071	3	25357	0.94	0
Error	1049128	4789	219.2	[ ]	[ ]
Total	1577966	4799	[ ]	[ ]	[ ]

dependence on the phase condition, albeit significant (Tab. 5.4), becomes negligible. These different behaviours w.r.t. the endothermic engine, are related to substantial differences in the engine functioning. For EVs, energy consumption is approximately zero when the vehicle speed is zero. On the other hand, the presence of a regenerative braking system mitigates the impact of *stop&go* phenomena.
Regarding mobility KPIs, parameters of both the TT_{lm} and ST_{lm} prediction model are very consistent with each other, while they prove to be more consistent for the endothermic engine case w.r.t. the electric engine one. Indeed, although there are some differences in significance and absolute values of coefficients, their signs (the causal relationships they describe) are the same for all the considered parameters. Specifically, travel time model coefficients have roughly the same values as those of the endothermic engine (dependence ranging from about 0.37 to 0.31 and from about -0.36 to -0.27 for traffic condition and phase condition, respectively), except for the dependence on communication distance which becomes non-significant. The ST_{lm} maintains a similar structure and reasonable dependence on the input variables, and hence the same considerations for the signs of TT_{lm} coefficients still hold. However, dependence on traffic conditions becomes non-significant. In contrast, dependence on both minimum speed and communication distance, which is not significant in the previous case, becomes significant for the ST_{lm}. Finally, obtained results are compared with those of the related technical literature. The findings confirm that system performance improves as the communication distance increases (see [153, 150, 152, 170]). Again, in line with other studies [167], it is possible to note that traffic conditions negatively affect fuel consumption. Instead, other studies considering

Table 5.7: Comparison of linear regression models for consumption and mobility KPIs.

Model	**Coefficient**					**RMSE**	**AdjRsq**	**F**	**p**
	C	**TC**	**PC**	D_{com}	V_{min}				
FC_{lm}	0.3828	0.3676	-0.3592	-0.1168	-	0.00698	0.423	441	0
EC_{lm}	0.1990	-0.1790	0.0107	-0.1451	0.1307	0.01105	0.108	73.8	0
TT_{lm}	0.3705	0.3060	-0.2685	-	-	24.4874	0.304	698	0
ST_{lm}	0.4058	-	-0.1839	-0.1942	0.2182	15.3517	0.283	475	0

electric vehicles do not account for different traffic demand levels. Hence, here are quantified for the first time this kind of dependence, evidencing that results could be counterintuitive. Regarding the effectiveness of the GLOSA system in reducing fuel consumption, obtained results indicate fuel savings of up to 4.98% w.r.t. NoGLOSA case. This reduction is lower than the $10-16\%$ of fuel save obtained by [167, 162, 152, 157], while it is in line with that found by [170]. It is worth noting that fuel consumption is strongly affected by vehicle dynamics, testing conditions, and, above all, the control strategy. The control strategy used in this chapter does not aim explicitly to reduce consumption, while those mentioned above were developed to achieve such an environmental goal. For the electric case, we obtain an energy reduction of about 4.72% w.r.t. NoGLOSA, but a clear comparison can not be made due to the different outcomes of the other works. Indeed, [166] proposed a Multi-segment GLOSA, obtaining a significant energy reduction for penetration rate of GLOSA-equipped vehicles higher than 20%. On the other hand, the control algorithm proposed by [174] was developed to achieve the environmental goal explicitly, and it thus allowed energy consumption to be reduced by up to 35%. Concerning mobility indicators, findings are in line with the ones of technical literature regarding the negative impact of congested traffic conditions as shown in [167, 152, 162, 163], while contrasting with them regarding non-dependence on communication distance. This outcome could be related to the urban network used as an exemplary scenario since, for instance, the distance between TLSs does not vary in a wide range ($[120-250]$ $[m]$) and hence the positive effect of large communication distances on mobility performance is null. The reduction in travel time and stop time of about 5% and 12%, respectively, are comparable to results obtained by [163, 167]. By contrast, a lower travel time reduction of about 1.06% was found in [152], while in [162] the control system led to small increases in travel times. Once again, differing objectives of the control logic tested in the above works may account for differences in the results.

5.7 Concluding Remark

This chapter discusses the development of a GLOSA system and the benefits deriving from the use of an Integrated Simulation Environment to assess C-ITS services. The proposed GLOSA algorithm can avoid unnecessary stops and *stop&go* phenomena at an intersection by leveraging SPaT data shared by each TLS within the network (in a single-segment approach) to compute an optimal reference speed aiming to minimising the travel time. Under the assumption of controlling a single GLOSA-equipped vehicle, the capabilities of the algorithm are evaluated in a challenging use case with real-world characteristics (the city centre of Trento, Italy). The surrounding traffic environment conditions affect both the effectiveness and efficiency of the control strategy. For instance, the vehicle may not reach the desired speed and fail to pass the intersection on green due to car-following constraints. A novel simulation approach is used to bring out the main factors determining significant impacts of GLOSA solutions. To this end, the evaluation assessment is performed by exploiting the proposed Integrated Simulation Environment MiTraS, assuming two possible engine configurations for the Ego-Vehicle (endothermic engine and electric engine). To deal with the stochastic nature of the traffic flow, 4800 simulations are carried out (2400 per engine type), varying, in a $complete - set$ approach, the following variables: i) infrastructure variables (TLS cycle duration and communication distance); ii) exogenous variables (traffic conditions and phase condition); iii) vehicle variable (engine type); iv) algorithm variable (minimum allowed speed). Moreover, the case without information about the state of TLSs (noGLOSA) was used as a baseline scenario.

First, both MiTraS-embedded and SUMO built-in consumption model outputs are validated w.r.t. the technical literature; reasonable results are obtained for MiTraS-embedded models. Instead, the SUMO models returned inconsistent outcomes as the electric model strongly underestimates consumption while the endothermic model slightly overestimated. The findings show that the chosen testing tool could affect the effectiveness and efficiency of the assessment process. Therefore, an integrated testing platform, with appropriate modelling and simulation for each component, drastically improves the evaluation process of automated/autonomous vehicle technologies, also w.r.t eco-driving.

Concerning the specific case tested, results confirm that, even exploiting TLS information with a simple S-GLOSA control algorithm, is possible to improve both mobility and energy performance of the assisted vehicle. Specifically, results show a consumption reduction of about 5% for both

endothermic and electric engine cases and a reduction of about 5% and 13% in TT and ST, respectively.
Finally, the proposed evaluation framework gathers valuable data for assessing the effects of several variables on the control strategy via n-way ANOVA analysis, which allows statistically relevant variables to be quantitatively determined. Different results for endothermic and electric engines are obtained from an energy perspective. More specifically, fuel consumption is strongly affected by cycle duration, traffic conditions, and signal phases, while there is a very low dependence on communication distance and no dependence on minimum speed. By contrast, energy consumption is weakly influenced by cycle duration, traffic condition, communication distance, and minimum speed, while there is no dependence on phase conditions. The differences in dependence on the considered variables could be related to the specific operation of each engine type and the presence of a regenerative braking system for electric engines. From a mobility perspective, the results show a strong dependence on cycle duration and phase conditions for both TT and ST. Moreover, while TT was also affected by traffic conditions, communication distance and minimum speed affected ST. In principle, the results show that both communication distance and minimum speed are not critical factors for the effectiveness of the GLOSA service in urban areas, as opposed to exogenous variables. In particular, the proposed modelling framework shows that TLS cycle duration strongly affected the performance of the control algorithm since lower values allow a readily available green phase to be found to pass the intersection, thereby avoiding *stop&go* phenomena. This is a major outcome since the setting of TLS does not usually take into account the penetration rate of connected and automated vehicles. A further exciting result for practitioners of vehicle development is that the optimisation of endothermic engine consumption agrees with the optimisation of mobility-related quantities (e.g., TT). At the same time, this assumption no longer holds for the case of electric engines.

CHAPTER **6**

Combined Energy-Oriented Path Following and Collision Avoidance Approach for Autonomous Electric Vehicles via Nonlinear Model Predictive Control

This chapter addresses the problem of computing an eco-driving speed profile for an autonomous electric vehicle travelling along curved roads while ensuring path following/car following functionalities w.r.t. possible preceding vehicles ahead. A double-layer control architecture combining the classical Adaptive Cruise Control with a Nonlinear Model Predictive Control is proposed to solve it. This latter is designed to drive the autonomous vehicle along a predefined path while guaranteeing the maintenance of a safe distance to a predecessor vehicle ahead and ensuring energy-saving consumption. The appraised control-oriented design model is non-linear, and the energy consumption one explicitly accounts for the cornering effects. Numerical results confirm the effectiveness of the proposed control architecture and disclose its ability to guarantee energy saving.

6.1 Multiple-Objective Control Problem

Eco-driving strategies have recently gained significant attention to deal with the environmental open challenge [194, 195]. Indeed, they aim to compute, based on the surrounding environmental conditions, an energy-saving oriented optimal driving profile to follow to improve the ecological performance [196]. Within this framework, the technical literature proposed several optimal control techniques. For instance, the Optimal Control Problem (OPC) approach was suggested in [197] with the aim at computing, based on both route and traffic information, an optimal speed profile able to reduce vehicle consumption. Similarly, authors in [198] developed a central cloud-based controller that, solving the optimisation problem via Dynamic Programming (DP) algorithm, exploits vehicle and fuel consumption models to determine the optimal speed trajectory to be tracked. Leveraging, instead, the ability of MPC in predicting and optimising the future behaviour of the vehicle also in presence of constraints, [199] exploits this control technique for computing an energy-oriented speed profile that also takes into account the consumption map of the appraised electric vehicle. Again, MPC was proposed in [200] to adapt the jerk profile to road condition variations for energy-saving purposes. More recently, to also takes into account the vehicle consumption at hilly road, by leveraging a nonlinear model for the vehicle dynamics, [201] and [202] proposed an energy-oriented NMPC for autonomous electric vehicles and hybrid vehicles, respectively. However, in addition to the energy-saving problem, in real traffic scenarios, vehicles have also to accomplish different driving tasks at the same time such as, for example, avoiding collisions with obstacles while tracking a path along a curvy road. In this context, the MPC approach has been widely used for solving the trajectory tracking control problem [203] or collision avoidance requirement [204]. Few authors proposed an integrated solution to solve both the issues mentioned above simultaneously. For example, authors in [205] proposed an integrated MPC controller able to ensure both lateral stability and collision avoidance. Note that the controller is synthesised considering a linear model of the vehicle to be controlled. With the aim at guaranteeing both the energy-saving objective and the path tracking control problem, [206] proposed a dual control objective Nonlinear Model Predictive Control (NMPC) which embeds a power-related term in the cost function to be optimised. However, the collision avoidance requirement is not addressed, and the vehicle consumption model does not account for the cornering effect, which is very relevant in curvy road [8].

Based on the above facts, this chapter addresses the problem of computing an eco-driving speed profile for an autonomous electric vehicle travelling along curved roads while ensuring path following/car following functionalities w.r.t. possible preceding vehicles ahead. A double-layer control architecture that combines the classical ACC with the multi-objective NMPC approach is proposed to solve this problem. The first layer, i.e., the ACC controller, is designed for car-following purposes and computes a collision-free acceleration profile to be imposed on the vehicle. Based on this latter and a desired lateral trajectory profile, the second layer, i.e. the NMPC controller, imposes an optimal energy-oriented acceleration and steering angle control actions so to drive the electric vehicle along a predefined path while maintaining a safe distance w.r.t. a predecessor vehicle ahead and ensuring energy-saving consumption. A non-linear longitudinal-lateral model for the vehicle to be controlled and an energy consumption model explicitly accounting for cornering effects are exploited for the control design.

6.2 Combined Energy-Oriented Path Following and Collision Avoidance Approach

Consider an autonomous electric vehicle, named Ego-Vehicle, travelling along a curved road in the presence of ahead vehicles. It is equipped with on-board sensors (e.g., GPS receiver and IMU) measuring its absolute position/speed and on-board ranging sensors (camera, radar, and lidar) measuring its relative position and speed w.r.t. ahead vehicles.

The aim is to develop a novel control architecture able to guarantee multiple control objectives: *i*) energy consumption reduction; *ii*) path-following in a curved road; *iii*) car-following functionality, i.e., collision avoidance w.r.t. preceding vehicle.

6.2.1 Nonlinear Ego-Vehicle Dynamics

The motion of the Ego-Vehicle is described via the bicycle model [207, 208], which is derived on the basis of the following assumptions: *i*) the forces act along the centre line at the front and rear axles; *ii*) roll and pitch motions are neglected (i.e., no load transfer due to roll and pitch motions); *iii*) the vehicle mass is entirely in its rigid base.
Accordingly, the motion of the Ego-Vehicle can be described by the following non-linear dynamical system [209, 9]:

$$\begin{aligned}
\dot{\psi}(t) &= r(t),\\
\dot{r}(t) &= \frac{-2C_f l_f - 2C_r l_r}{I_z v_x(t)} v_y(t) + \frac{-2C_f l_f^2 + 2C_r l_r^2}{I_z v_x(t)} r(t) + \frac{2C_f l_f}{I_z}\delta(t),\\
\dot{v}_y(t) &= -\frac{2C_f + 2C_r}{m\dot{x}(t)} v_y(t) - v_x(t) - \frac{2C_f l_f - 2C_r l_r}{m v_x(t)} \dot{r}(t) + \frac{2C_f}{m}\delta(t),\\
\dot{v}_x(t) &= v_y(t) r(t) + a_x(t),\\
\dot{a}_x(t) &= \frac{1}{\tau_d}(a_c(t) - a_x(t)),
\end{aligned} \tag{6.1}$$

where $\psi(t)$ $[rad]$ is the yaw angle while $r(t)$ $[rad/s]$ is the yaw-rate; $v_x(t)$ $[m/s]$ and $v_y(t)$ $[m/s]$ are the longitudinal and lateral speed of the Ego-Vehicle, respectively; $\dot{v}_x(t)$ $[m/s^2]$ and $\dot{v}_y(t)$ $[m/s^2]$ are the longitudinal and lateral acceleration, respectively; $\dot{a}_x(t)$ $[m/s^3]$ is the jerk; $m = 2000$ $[kg]$ is the vehicle mass; $l_f = 1.4$ $[m]$ and $l_r = 1.6$ $[m]$ are the distances of front and real wheels w.r.t. the centre of gravity; $I_z = 4000$ $[kg/m^2]$ is the vehicle body inertia moment about the vehicle-fixed z-axis; $C_f = 12000$ $[N/rad]$ and $C_r = 11000$ $[N/rad]$ are the front and rear corner stiffness; $\tau_d = 0.5$ $[s]$ is the driveline time constant; $\delta(t)$ $[rad]$ is the wheel steering angle control input; $a_c(t)$ $[m/s^2]$ is the longitudinal acceleration control input.
By exploiting a more compact notation, the non-linear vehicle dynamics in Eq. (6.1) can be rewritten as:

$$\dot{\zeta}(t) = f(\zeta(t), u(t)), \tag{6.2}$$

where $\zeta = [\psi, r, v_y, v_x, a_x] \in \mathbb{R}^{5\times1}$ is the state variable vector; $u = [a_c, \delta] \in \mathbb{R}^{2\times1}$ is the input vector; f is the nonlinear dynamical field.

6.3 Control Design

This section details the design of the proposed double-layer control architecture that drives the Ego-Vehicle along a predefined path, avoiding collisions with ahead vehicles while ensuring its energy saving.

6.3.1 ACC Controller Design

The goal of the collision-free longitudinal control problem is to compute a proper longitudinal acceleration profile, say $a_{des}(t)$, such that:

$$\lim_{t\to\infty} \|\Delta d(t) - d_{safe}(t)\| = 0, \tag{6.3a}$$

$$\lim_{t\to\infty} \|\Delta v(t)\| = 0, \tag{6.3b}$$

where $\Delta d(t)$ $[m]$ and $\Delta v(t)$ $[m/s]$ are the relative distance and speed between the Ego-Vehicle and its predecessor, measured via on-board ranging sensors; $d_{safe}(t) = d_{min} + h_{gap} \cdot v_x(t)$ is the safety inter-vehicle distance in $[m]$, being d_{min} $[m]$ and h_{gap} $[s]$ the standstill distance and the minimum time gap, respectively.
To achieve the control goal in (6.3) following ACC control strategy [210, 211] is considered:

$$a_{des} = \begin{cases} min\{K_v e_v(t); [K_p e_d(t) + K_w \Delta v(t)]\} & \text{if } e_d \leq 0 \text{ ,} \\ K_w \Delta v(t) - K_p e_d(t) & \text{if } e_d > 0, \end{cases} \tag{6.4}$$

where $e_v(t) = v_{set}(t) - v_x(t)$, being v_{set} $[m/s]$ the ACC speed set-point while $e_d(t) = d_{safe}(t) - \Delta d(t)$; K_v and K_p and K_w are the control gains.

6.3.2 NMPC Controller

Here is described in detail the design of a NMPC control strategy able to drive the Ego-Vehicle along a predefined path via the acceleration $a_c(t)$ and the steering $\delta(t)$ control inputs. The aim of the proposed NMPC controller is threefold: *i*) ensuring lateral vehicle stability while following a predefined path; *ii*) tracking the reference acceleration trajectory a_{des} computed by the ACC controller; *iii*) guaranteeing energy saving.

To ensure lateral stability, the following dynamics for the lateral tracking error is introduced:

$$\dot{e}_1 = v_x(t)(r(t) - r_{des}(t)) + v_y(t), \tag{6.5a}$$

$$\dot{e}_2 = r(t) - r_{des}(t), \tag{6.5b}$$

where $r_{des}(t)$ $[rad/s]$ is the desired yaw rate computed as $r_{des}(t) = v_x(t) \cdot k(s(t))$.

To design the NMPC so to take into account both the lateral-stability control problem and the collision avoidance one, the control-oriented model is derived by embedding the vehicle dynamics in (6.1) with the lateral tracking error dynamics in (6.5) as

$$\dot{\bar{\zeta}}(t) = f\Big(\bar{\zeta}(t), u(t)\Big), \tag{6.6a}$$

$$\eta(t) = h\Big((\bar{\zeta}(t)\Big), \tag{6.6b}$$

where $\bar{\zeta} = [\psi, r, v_y, v_x, a_x, e_1, e_2] \in \mathbb{R}^{7\times 1}$ is the enlarged state variable vector while the the output map h is given as

$$h(\bar{\zeta}(t)) = \begin{bmatrix} 0 & 0 & 0 & 0 & 0 & 0 & 0 \\ 0 & 0 & 0 & 0 & 0 & 0 & 0 \\ 0 & 0 & 0 & 0 & 0 & 0 & 0 \\ 0 & 0 & 0 & 1 & 0 & 0 & 0 \\ 0 & 0 & 0 & 0 & 1 & 0 & 0 \\ 0 & 0 & 0 & 0 & 0 & 1 & 0 \\ 0 & 0 & 0 & 0 & 0 & 0 & 1 \end{bmatrix} \bar{\zeta}(t). \tag{6.7}$$

Now, to achieve the three control objectives as mentioned earlier, the control input $u(t)$ in (6.6) is computed by solving the following multiple-objective nonlinear constrained optimisation problem:

$$\min_u J = \int_t^{t+T} L\Big(\bar{\zeta}(\tau,t), \bar{\zeta}^*(\tau,t), u^*(\tau,t)\Big) d\tau \tag{6.8}$$

subject to:

$$\begin{aligned}
&\dot{\bar{\zeta}}(t) = f\Big(\bar{\zeta}(t), u(t)\Big))\\
&v_{x,\min} \leq v_x(\tau, t) \leq v_{x,\max}\\
&a_{x,\min} \leq a_x(\tau, t) \leq a_{x,\max}\\
&\delta_{\min} \leq \delta(\tau, t) \leq \delta_{\max}\\
&\Big(ma_x(\tau, t)\Big)^2 + \Big(mv_x(\tau, t)^2 k(s(t))\Big)^2 \leq (m\mu_r g)^2
\end{aligned}$$

where T $[s]$ is the prediction horizon duration; $\bar{\zeta}^*(\tau|t)$ and $u^*(\tau|t)$ are the prediction of the Ego-Vehicle state and the control input trajectories, respectively, along the τ-axis starting from $\bar{\zeta}(t)$ as the initial state at $\tau = t$ over the prediction horizon T; $v_{x,\min}$ $[m/s]$ and $v_{x,\max}$ $[m/s]$ are the minimum and maximum speed that Ego-Vehicle can reach; $a_{c,\min}$ $[m/s^2]$ and $a_{c,\max}$ $[m/s^2]$ are the minimum and maximum longitudinal acceleration; $\delta_{\min}$ $[rad]$ and $\delta_{\max}$ $[rad]$ are the minimum and maximum steering angle; μ_r is the friction coefficient of the road, fixed at 1 for sake of simplicity. Note that the last constraint is related to the maximum acceleration during cornering for safety reason, i.e. it allows avoiding the vehicle to slip on curved road stretch. The term L within J is designed as follows:

$$\begin{aligned}
L =& \Big(\frac{w_1}{s_{f,1}}(v_x(t) - v_{des}(t))\Big)^2 + \Big(\frac{w_2}{s_{f,2}}(a_c(t) - a_{des}(t))\Big)^2\\
&+ \Big(\frac{w_3}{s_{f,3}}(e_1(t))\Big)^2 + \Big(\frac{w_4}{s_{f,4}}(e_2(t))\Big)^2 + \Big(\frac{w_5}{s_{f,5}}(P_{bat}(t))\Big)^2,
\end{aligned} \tag{6.9}$$

where w_i ($\forall i = 1, ..., 5$) are positive weights; $s_{f,i}$ ($\forall i = 1, ..., 5$) are positive scale factor to homogenise the magnitude of the considered variables; $v_{des}(t)$ is the reference speed computed by the desired acceleration $a_{des}(t)$. It is worth noting that each term of the cost function is related to a specific aim of the control problem, namely: *i*) the first and the second terms ensure that Ego-Vehicle tracks the desired acceleration and speed profile defined by the ACC control strategy in (6.3); *ii*) the third and fourth terms ensure that Ego-Vehicle follows the desired path; *iii*) the last one ensures the minimisation of the instantaneous power consumption. The computation of the instantaneous power consumption $P_{bat}(t)$ $[W]$ for control purposes will be described in detail in the following subsection.

6.3.2.1 Energy Consumption Model for Control Purpose

The estimate of electric Ego-Vehicle energy consumption is performed through a modified version of the CPEM (see Sec. 4.3.2.2 for the detailed description of the model). Firstly, the required electric power at wheels $P_w(t)$ $[W]$ is computed as:

$$P_w(t) = \Big(ma_x(t) + R_g(t) + R_a(t) + R_r(t) + R_c(t) \Big) v_x(t), \qquad (6.10)$$

where $a_x(t)$ $[m/s^2]$ is the vehicle acceleration; $R_g(t) = mgsin\theta(t)$ $[N]$ is the grade resistance, being $g = 9.81$ $[m/s^2]$ the gravitational acceleration and θ $[rad]$ the road grade; $R_a(t) = 0.5\rho_{air} A_f C_D v_x(t)^2$ $[N]$ is the aerodynamic drag resistance, being $\rho_{air} = 1.21$ $[kg/m^3]$ the air density, $A_f = 2.00$ $[m^2]$ the frontal area of the Ego-Vehicle and $C_D = 0.30$ the air-drag resistance coefficient; $R_r(t) = mg\cos\theta(t)(C_r/1000)(c_1 v(t) + c_2)$ $[N]$ is the rolling resistance, being $C_r = 1.75$, $c_1 = 0.0328$ and $c_2 = 4.575$ the rolling resistance parameters that vary as a function of the road surface type, road condition, and vehicle tire type; $R_c(t) = ml_r v_x^2 (k(s(t)))^2$ is the cornering effect in longitudinal direction [212], being $k(s(t))$ $[1/m]$ the curvature at the trajectory point $s(t)$.
Then, $P_{em}(t)$ $[W]$ and $P_{bat}(t)$ $[W]$ are computed in a similar way to what described in Sec. 4.3.2.2. More specifically, starting from Sec. 4.3.2.2, $P_{em,net}(t)$ is calculated in a simplified way by assuming a constant electric motor power loss $P_{loss} = 1/\eta_d$ $[W]$ as

$$P_{em,net}(t) = \begin{cases} \frac{P_w(t)}{\eta \cdot \eta_b}, & \text{if } P_w(t) \geq 0 \\ P_w(t) \cdot \eta \cdot \eta_b \cdot \eta_b, & \text{if } P_w(t) < 0 \end{cases}$$

where $\eta_{rb}(t)$ is the regenerative braking energy efficiency computed as Eq. (4.19).
Finally, assuming $P_{aux} = 700$ $[W]$, the instantaneous total power required at battery $P_{bat}(t)$ $[W]$ is estimated as in Eq. (4.20).

6.4 Numerical Analysis

In this section, the effectiveness of the proposed control strategy in improving the energy performance of the Ego-Vehicle while guaranteeing, at the same time, the path tracking on the curved road and collision

Table 6.1: Ego-Vehicle Controllers Parameters.

Parameter	**Description**	**Value**
δ_{min}	min steering wheel	$-65°$
δ_{max}	max steering wheel	$+65°$
$a_{x,min}$	min acceleration	-3 $[m/s^2]$
$a_{x,max}$	max acceleration	$+2$ $[m/s^2]$
d_{min}	standstill distance	5 $[m]$
h_{gap}	time gap	1.0 $[s]$
v_{set}	ACC speed set-point	15 $[m/s]$
K_v	ACC control gain	0.5 $[1/s]$
K_p	ACC control gain	0.2 $[1/s^2]$
K_w	ACC control gain	0.4 $[1/s]$
$s_{f,i}$	scale factors	[15,5,0.5,0.5,40]

Table 6.2: Cost function weights for each considered operating configuration.

Parameters	**Operating Configuration**			
	Baseline	**1**	**2**	**3**
w_1	1	1	1	1
w_2	0.3	0.3	0.3	0.3
w_3	1	1	1	1
w_4	1	1	1	1
w_5	0	0.05	0.1	0.15

avoidance w.r.t. ahead vehicles is evaluated. To this end, the numerical analysis, carried out via the MiTraS platform, is carried out for an exemplary road scenario where three vehicles are driving along a curved road (Fig. 6.1). More specifically, the considered stretch is a three-lane curvy road (one curve to the right and one to the left) with a total length of about 600 $[m]$. As an exemplary driving scenario, each vehicle is assumed to follow a specific path, namely: *i*) Car 1 (the yellow one in Fig. 6.2) travels along the middle lane at a constant low speed of 10.00 $[m/s]$; *ii*) Car 2 (the orange one in Fig. 6.2), starting at 85 $[m]$ far away from Car 1, initially travels along the middle lane with a constant speed of 13.90 $[m/s]$, then it performs a lane change manoeuvre and

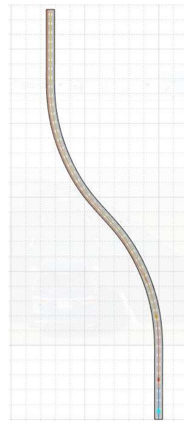

Figure 6.1: Cured Road for the appraised simulation scenario.

moves into the left one; *iii*) the Ego-Vehicle (the blue one in Fig. 6.2) drives along the middle lane, starting at 40 $[m]$ far away from Car 2, with a desired speed of 15 $[m/s]$. It is worth noting that the dynamical conditions in this simulation scenario are chosen such that collisions would occur if Ego-Vehicle would make no action.

Moreover, different configurations for the proposed NMPC controller are taken into account, i.e., different weights for terms within the cost function in (6.9), choosing the case without the power term (or weighted 0) as baseline configuration. The control gains values for both the ACC control and scale factors for NMPC controller are summarised in Tab. 6.1, while the weights of the cost function-terms for each operating configuration of NMPC controller are listed in Tab. 6.2.

To quantify and compare the energy, tracking, and collision avoidance performances of the proposed controller with respect to the baseline configuration, the following simulation outputs are taken into account: *i*) speed profile $[m/s]$; *ii*) inter-vehicle distance $[m]$; *iii*) lateral distance error $[m]$, i.e., the distance between the Ego-Vehicle centre of gravity and the reference path; *iv*) yaw error $[rad]$, i.e., the angular deviation of the yaw of the Ego-Vehicle w.r.t. reference yaw; *v*) average Energy Consumption $[kWh/km]$.

Figure 6.2: 3-D snapshot of all three vehicles within the simulation scenario.

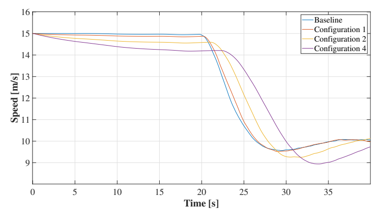

(a)

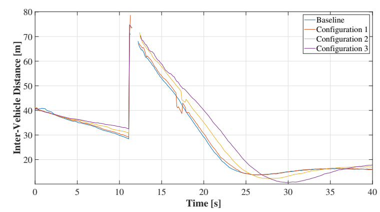

(b)

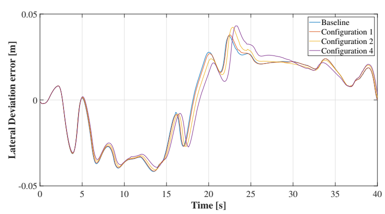

(c)

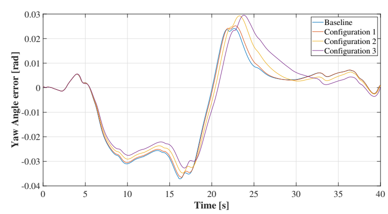

(d)

Figure 6.3: Ego-Vehicle motion under the action of the proposed double-layer control architecture. Time history of: a) Ego-vehicle speed; b) inter-vehicle distance w.r.t. the preceding; c) lateral deviation error; d) yaw error.

6.4.1 Car-Following and Path-Following Results

Results of numerical analysis displayed in Fig. 6.3 disclose the effectiveness of the proposed control architecture (see Sec. 6.3) in guaranteeing the tracking of the ahead vehicle in following the curved path while avoiding collisions. More specifically, both the lateral error in Fig. 6.3(c) and yaw error in Fig. 6.3(d) assume small values, involving a good path following

Table 6.3: Energy consumption results for each operating condition and energy reduction w.r.t. baseline scenario.

	Baseline	**1**	**2**	**3**
EC [kWh/km]	0.0970	0.0958	0.0957	0.0954
Reduction [%]	-	1.19	1.38	1.63

performance for all considered operating configurations of the NMPC controller. At the same time, the inter-vehicle distance (Fig. 6.3(b)) and speed (Fig. 6.3(a)) profiles prove that the proposed controller allows the Ego-Vehicle to adapt its motion based on the behaviour of its ahead vehicle. Despite the different appraised operating configurations for the control action tuning, the proposed double-layer control architecture always guarantees safety requirements. Globally, Fig. 6.3 proves how the control strategy can satisfy both car-following and path-following purposes at the same time.

6.4.2 Energy Consumption Results

The different weighting configurations of the NMPC controller stronger affect the energy consumption results. Indeed, by embedding a power-related term with the cost function, it is possible to smooth the behaviour of the Ego-Vehicle (as showed in Fig. 6.38a)) which results in a reduction of energy consumption. As shown in Tab. 6.3, all the power-related operating configurations have improved energy performance w.r.t. the baseline scenario. It is worth noting that, by increasing the weight of the power-related term, it is possible to obtain an energy-saving up to $+1.63\%$ (condition 3). On the other hand, this implies a smoother behaviour of the Ego-Vehicle during driving operations, i.e., in operating scenario 3 it has a smoother speed profile w.r.t. the other ones (Fig. 6.3(a)). Overall, operating configuration 2 seems to provide the best trade-off w.r.t. the other configurations since it allows reducing the energy consumption up to -1.36% while guaranteeing good tracking performance.

6.5 Concluding Remarks

In this chapter, the problem of computing an eco-driving speed profile for an autonomous electric vehicle travelling along curvy roads while ensuring both path-following and car-following functionalities w.r.t. possible preceding vehicles ahead has been addressed. To solve this problem, a double-layer control architecture that combines the classical ACC controller for guaranteeing car-following functionality with a NMPC for optimising the Ego-Vehicle trajectory from an energy-saving point of view while ensuring lateral stability has been proposed. Numerical analysis, carried out exploiting MiTraS platform, has been performed to evaluate the effectiveness of the proposed control strategy. Results have confirmed how the combined use of classical ACC controller and NMPC one allows accomplishing different control goals at the same time and, in particular, to improve the energy-saving performances

CHAPTER 7

Decentralized Cooperative Crossing at Unsignalized Intersections via Vehicle-to-Vehicle Communication in Mixed Traffic Flows

CAVs will share the road environment with human drivers until their full market deployment achievement. In this context, this chapter deals with the open challenge of decentralised crossing at unsignalized road intersections for mixed traffic flows composed of connected CHVs and CAVs. To this end, a cooperative fully-distributed control protocol for CAVs, augmenting the classical ACC control action with an additional networked protocol exploiting V2V, is proposed. This further collaborative action automatically adapts the CAVs motion at road intersections to avoid collisions and reduce both waiting time and stop-time at intersections. The analysis for an exemplary two-lane four-way unsignalised intersection considers different traffic demands and CAVs penetration rates.

Moreover, variable delays in information delivery due to the wireless communication network have also been explicitly accounted for control design and validation process. The extensive simulation analysis confirms how the presence of CAVs, equipped with the proposed control algorithm, strongly improves both the safety and efficiency of the intersection.

7.1 Cooperative Crossing at Intersection in Mixed Traffic

Road traffic environment will achieve a significant market deployment of CAVs in 20/25 years [213]; as a consequence, road traffic will be composed of a mix of CAVs and human-driven vehicles for a relatively long time. The interaction among them will be unavoidable and will create complex traffic scenarios. Hence it is crucial to make up for the lack of studies related to mixed traffic, which will likely be the prevalent traffic condition in the very next future [214]. In this technological framework, most researchers focus on designing cooperative control strategies for CAVs to mitigate traffic congestion in extra-urban traffic environments by exploiting information shared by CAVs and CHVs vehicles through wireless communication technologies [215, 216, 217]. All these works assume that human-driven vehicles are equipped with V2X communication devices and share information with the other road actors by exploiting the IoT paradigm [218]. Indeed, with the increasing numbers of heterogeneous devices connected to the IoT, connected vehicles represent a significant portion of these devices [219, 214], and it is estimated that the number of connected vehicles on the road will be more than 250 million [220]. In addition, it is also crucial to highlight that, given the relatively low cost of V2X devices compared with driving automation systems (e.g., ACC), it is desirable to exploit the benefits of V2X without being restricted by the penetration rate of automation (see, e.g., [215] and references therein). Indeed, equipping conventional vehicles with V2X capability is not tricky as equipping it with automated features and, along this line, nowadays, different solutions, such as the smartphone-based system one, have been proposed [221]. Therefore, based on the facts mentioned above, it is reasonable to assume human-driven vehicles to be connected in the very next future.

In this mixed traffic environment, the urban intersection crossing is an open challenge due to, for instance, complex traffic conditions and occlusions in line of sight [222].
The technical literature proposes different urban road junction management systems for signalised and unsignalised intersections. In signalised intersections-based approaches, TLSs separate conflicting traffic movements to improve road safety even in mixed traffic [223, 224]. CAVs can play an active role in enhancing the efficiency of the intersection. By leveraging the V2I communication paradigm, TLSs can exploit information shared by connected vehicles to adapt signal timing and phases to improve the efficiency of the intersection. Several studies have shown that CAVs can help road intersection management (see [223] and references therein). Indeed, based on signals and vehicles data, they can adequately adapt and optimise their motion so to achieve specific objectives, such as the minimisation of the fuel consumption [225], the reduction of the travel times, and the increasing of the traffic safety [226]. However, TLS-based approaches do not eliminate all traffic conflicts among vehicles, hence increasing crossing time-delay [227] and intersection capacity is not exploited at all [224]. Moreover, it is not feasible to make all urban intersections regulated by TLSs and equipped by RSU.
Unsignalised intersections represent the most common intersection type in urban areas, and existing technical literature their crossing management assume the presence of only fully autonomous vehicles [5, 6, 7]. Cooperative unsignalised intersection crossing for mixed traffic is still an unexplored research challenge rarely addressed [7]. A recent attempt along this direction is given in [13], where a cooperative control strategy for CAVs is proposed by regulating their motion based on both the onboard ranging sensors and V2V communication data to cross a four-way intersection safely. Based on the information shared by the oncoming vehicle at a T-intersection, a finite state machine determining the optimal driving profile to be imposed to the CAV to avoid collisions is proposed in [228]. However, both the works above do not consider realistic traffic flow conditions, considering few vehicles approaching the intersection. Finally, [229] proposes a decentralised control strategy for CAVs aimed at optimising the acceleration profile of vehicles and minimising both energy consumption and intersection throughput. However, each CAV is modelled via a second-order linear system, and the conflicting intersection

area is partially controlled, i.e., vehicles on the main road have priority to cross w.r.t. vehicles on the minor one.

Alternative attempts to solve this problem consider only partially-automated vehicles, rather than CAVs, i.e. cars equipped with ADAS, but not replacing, the drivers in complex traffic situations [230]. Along this line, most of the attempts focus on the development of Cooperative Collision Warning Systems [231], which provide warnings to drivers based on information coming from V2V or roadside units, and Intersection Advanced Driver Assistant Systems (I-ADAS), which solely exploit on-board ranging sensors to help drivers during the crossing [232].

Based on the above considerations, this chapter deals with the open challenge of the safe crossing of an unsignalised intersection under mixed traffic flow conditions without exploiting a centralised signalling system (e.g., a physical TLS or virtual one communicating via V2I). Moreover, although all vehicles are connected, only CAVs are equipped with on-board control algorithms adapting their motion to the surrounding environment. A cooperative fully-distributed control strategy for CAVs is proposed to deal with such a problem. By leveraging on-board sensors and information shared by all the connected vehicles via V2V, the control strategy guarantees a safe intersection crossing, manages unfavourable traffic situations to slowing-down phenomena, and improves the intersection throughput. Indeed, by controlling some portion of the traffic flow, it is possible to regulate the intersection crossing, without requiring a central arbiter or an orchestrating infrastructure communicating with vehicles via V2I, since the behaviour of human-driven vehicles is strongly affected by the presence of CAVs, even if they do not adequately coordinate their motion with other road users [233, 234].

The novel proposed cooperative control strategy augments the classical ACC [210], computed the on basis of on-board proximity sensor measurements, with an additional networked control action that exploit the shared information for the cooperative evaluation of the Time-to-Intersection (TTI) of all incoming vehicles within the communication range. This further action allows avoiding collisions at the intersection with vehicles beyond the CAVs line of sight. Moreover, wireless V2V networks are not ideal and, hence, are affected by unavoidable technological impairments; therefore, information is affected by time-varying delay whose current value depends on the actual network condition. To this end, the control strategy is designed in the presence of time-varying communication delays affecting each communication link of the vehicular network [71, 52]. It is worth noting that the proposed approach is feasible since, in the very next future, road networks will also be equipped with intelligent systems (e.g., intelligent cameras, loop detectors, RSU) to collect and share some helpful information [220] with connected vehicles [235, 236]. In so doing, each CAV can share information with different sources (via V2X communication) and, combining them, obtain a complete representation of the surrounding road environment. Finally, the effectiveness of the proposed control strategy is tested by exploiting the proposed Integrated Simulation Environment MiTraS (see Chapter 4) under different under different mixed traffic flows conditions (e.g. different CAVs penetration rates) so to investigate how and if the safety of crossing, as well as mobility performance, can be preserved and improved. To summarise, the main contributions w.r.t. the technical literature are:

- The open challenge of fully-decentralised safe crossing at an unsignalised intersection for mixed traffic flow conditions, i.e. composed by both CHVs and CAVs, is addressed, and a viable solution is proposed;

- A novel cooperative fully-distributed control protocol is proposed for the CAVs that, combining information from V2V communication and on-board ranging sensors, can safely drive them through the unsignalised intersection, avoiding collisions and intersection deadlock. The proposed control protocol augments only at crossing any state-of-the-art ACC controller, hence behaving as an additional networked control action, based on the cooperative evaluation of the TTI (i.e., arrival time to the intersection entrance or border) of all incoming vehicles. Once the intersection is crossed, only the classical ACC drives the CAVs. Furthermore, since it is based on information shared via V2V, the networked action explicitly accounts for the presence of different time-varying delays affecting each of the communication links between vehicles.

- The analysis, performed exploiting the novel Integrated Simulation Environment MiTraS, is carried out under mixed traffic flows conditions considering different CAVs penetration rates, different traffic demand, and heterogeneity of the CAVs.

7.2 Unsignalised Intersection Crossing

The crossing coordination problem at n urban unsignalised intersection is related to the proper scheduling of the vehicles approaching it [237]. Therefore, a mixed traffic flow composed of N human-driven vehicles and M fully autonomous vehicles incoming an unsignalised urban intersection is considered. Both CHVs and CAVs vehicles are assumed to be equipped with on-board sensors (e.g., GPS and IMU to measure their absolute position and speed). The CAVs are also equipped with ranging sensors (camera and radar) measuring relative position and velocity with respect to surrounding vehicles within their line of sight and an OBU, where online autonomous driving control algorithms run. Furthermore, all vehicles are connected, i.e., they share their state information in a broadcast way via the V2V communication paradigm with all the other vehicles within the communication range. Note that, while CHVs exploit the state information shared among vehicles for improving info-mobility services [114], CAVs can combine them with the local measurements obtained from on-board ranging sensors to adapt their motion to conflicting vehicles autonomously.
The exemplary unsignalised intersection is a typical two-lane (one for each direction) four-way intersection (also named four-branches), with both four entrances and four exits as in Fig. 7.1 (a). These kinds of junctions, where drivers usually have to negotiate the crossing since no rules of priority are provided, are prevalent in the urban and rural environment. Assume that overtaking manoeuvre is not allowed along road edges. Moreover, assuming that vehicles can perform all the turning manoeuvres at intersection entrance (i.e. turn left, go straight, turn right), 12 movements can be performed at the intersection, generating 32 possible conflict points: 16 crossing, 8 merging and 8 diverging, as depicted in Fig. 7.1 (b). Accordingly, the *Conflicting Area (CA)*, i.e., the area in which collisions could occur, is formed by both overlapping zone and safe zones of each road edge [238]. In contrast, the larger circular zone around the CA (say r_{cz} its radius) is the *Cooperative Zone (CZ)*, i.e., the intersection zone where vehicles share information via V2V. Note that such intersection configuration involves the presence of traffic disturbance due to both the presence of high conflicts among approaching vehicles and the possibility to perform curved trajectories. As evidence of this,

the Highway Capacity Manual explicitly takes into account turning manoeuvres as a reduction factor in calculating the capacity of intersections [239].
The aim is to disclose how and if, taking advantage of information beyond the vehicle line of sight via connectivity in the CZ, the road safety in mixed traffic conditions can be increased, avoiding collisions and dangerous driving manoeuvres in the CA. Note that most of the works in the technical field usually assume the 100% penetration rate of CAVs for unsignalised intersection, neglecting possible interactions among autonomous and human-driven cars [7]. To achieve this goal, a novel TTI-based consensus protocol for CAVs that adds to the classical ACC algorithm a further collaborative action based on shared information is designed with the aim of:

- guaranteeing a safe intersection crossing by ensuring that each CAV maintains a safe distance to all the vehicles approaching the collision area;
- adapting the speed of each CAV to avoid sudden hard braking manoeuvres, avoid unnecessary standstill, reduce waiting time, and reduce slowing-down phenomena occurrence;
- eliminating the need for a centralised traffic controller (hence reducing infrastructure costs).

7.2.1 CHV Dynamics

The longitudinal behaviour of i-th CHV ($i = 1, \ldots, N$) is modelled according to the classical car-following approach proposed in [240], under the assumption that humans can detect by vision the distance from the vehicle ahead and safely drive to keep a desired distance gap from it. The gap-distance between the i-th CHV and its vehicle ahead can be described in terms of distances from the entrance of CA as:

$$g_i(t) = d_i(t) - d_{i-1}(t) - l_{i-1} - g_{i_{min}}, \tag{7.1}$$

where $d_i(t)$ $[m]$ and $d_{i-1}(t)$ $[m]$ are the the euclidean distance from the entrance (border) of the CA of the generic CHV i and its vehicle ahead $(i-1)$, respectively (where the vehicle $(i-1)$ can be, without loss of

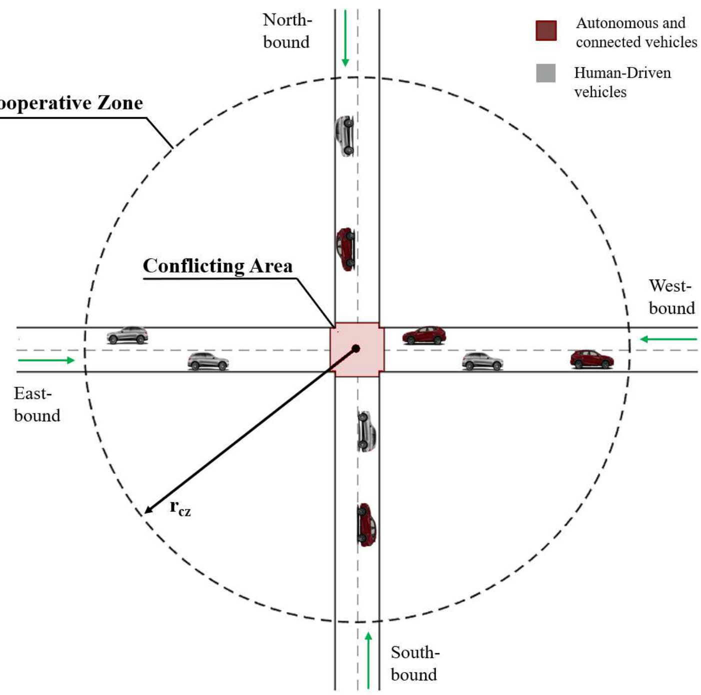

(a)

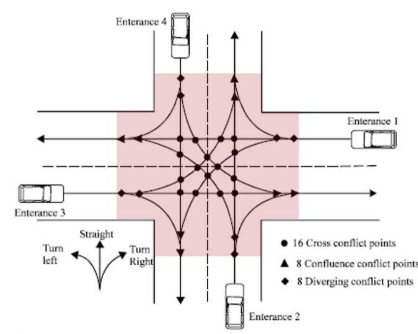

(b)

Figure 7.1: Unsignalised Intersection Crossing Problem: a) example of Two-lane four-way unsignalised intersection; b) conflict points for the two-lane four-way intersection. The dashed circle is the Cooperative Zone (CZ), while the red zone is the Conflicting Area (CA).

generality, CHV or CAV); l_{i-1} $[m]$ is the length of the $i-1$ vehicle ahead; $g_{i_{min}}$ $[m]$ is the minimum gap that the i-th vehicle intends to keep from the vehicle ahead. The safe speed for the i-th vehicle can be then expressed as:

$$v_{i_{safe}}(t) = -\tau_i \cdot b_i + \sqrt{(\tau_i \cdot b_i)^2 + v_{i-1}(t-\tau_i)^2 + 2 \cdot b_i \cdot g_i(t-\tau_i)} \quad (7.2)$$

where τ_i $[s]$ is the reaction time of the i-th driver [241, 242]; b_i $[m/s^2]$ is the maximum deceleration of the i-th vehicle, while $v_{i-1}(t-\tau_i)$ $[m/s]$ is the speed of the vehicle ahead at time $t-\tau_i$.
Since vehicles must respect the legal requirements related to the maximum speed limits at a given intersection, letting v_{max} $[m/s]$ the maximum allowable speed on the current road edge, the reference, or desired, speed for the human driver i is:

$$v_{i_{des}}(t) = \min\{v_{i_{safe}}(t); (v_i(t-\tau_i) + a_{i_{max}}); v_{max}\} \quad (7.3)$$

being $a_{i_{max}}$ $[m/s^2]$ the maximum acceleration according to the mechanical features.
Since a human driver is not able to perfectly track its desired reference speed profile due to driving imperfection, the actual speed profile of the human-driven vehicle i can be modelled as:

$$v_i(t) = \max\{0; (v_{i_{des}}(t) - \eta)\}, \quad (7.4)$$

where η is a random variable with uniform discrete distribution within $[0, \bar{\eta}]$, being $\bar{\eta} = a_{i_{max}} \cdot \epsilon$ and $\epsilon \in [0,1]$. Here it is assumed $\epsilon = 0.5$ for all CHVs according to [240]. Note that the information shared by the CHVs over the wireless V2V communication network are the current distance to the CA entrance and velocity, i.e. $\tilde{x}_i(t) = [d_i(t) \;\; v_i(t)]^\top$, $i = 1, \ldots, N$. Finally, the model already implemented into the SUMO platform is used for the lateral dynamics [243].

7.2.2 CAV Dynamics

The behaviour of each CAV k ($k = N+1, \ldots, N+M$), is derived according to [13] from the classical bicycle model [244, 208] as the following non-linear longitudinal, lateral and yaw dynamics:

$$\dot{\psi}_k = r_k, \tag{7.5a}$$

$$\ddot{y}_k = -v_k r_k + \frac{F_{k,l,f}\sin\delta_{k,f} + F_{k,c,r}\cos\delta_{k,f} + F_{k,l,r}}{m_k}, \tag{7.5b}$$

$$\ddot{x}_k = \dot{y}_k r_k + \frac{F_{k,l,f}\cos\delta_{k,f} - F_{k,l,r}\sin\delta_{k,f} + F_{k,l,r}}{m_k}, \tag{7.5c}$$

$$\dot{r}_k = \frac{\ell_{k,f}(F_{k,l,f}\sin\delta_{k,f} + F_{k,c,f}\cos\delta_{k,f}) - \ell_{k,r}F_{k,c,r}}{I_{k,z}}. \tag{7.5d}$$

where ψ_k $[rad]$ and r_k $[rad/s]$ are the yaw-angle and the yaw-rate of the k-th vehicle, respectively; $x_k(t)$ and $y_k(t)$ are the k-th vehicle longitudinal and lateral position, respectively; v_k $[m/s]$ and $\dot{y}_k$ $[m/s]$ are the k-th vehicle longitudinal and lateral speed, respectively; m_k $[kg]$ is the k-th vehicle mass; $\ell_{k,f}$ $[m]$ and $\ell_{k,r}$ $[m]$ are the distances of front and rear wheels w.r.t. the centre of gravity; $I_{k,z}$ $[kg/m^2]$ is the k-th vehicle body inertia moment about the vehicle-fixed z-axis; $F_{k,l,r}$ $[N]$ and $F_{k,c,r}$ $[N]$ are the longitudinal and lateral forces acting on the rear tire; $F_{k,l,f}$ $[N]$ and $F_{k,c,f}$ $[N]$ are the longitudinal and lateral forces acting on the front tire; $\delta_{k,f}$ $[rad]$ is the front wheel steering angle. Note that in the case of forward driving $\delta_{k,r}$ $[rad]$ is equal to 0, since the guiding wheel is the front wheel. Assuming a linear tire model [244], the lateral front and rear tire forces $F_{k,c,r}$ and $F_{k,c,f}$ are proportional to the tire slip angles, say $\alpha_{k,r}(t)$ $[rad]$ and $\alpha_{k,f}(t)$ $[rad]$ as:

$$F_{k,c,f}(t) = -C_{k,y,f}\alpha_{k,f}(t),$$
$$F_{k,c,r}(t) = -C_{k,y,r}\alpha_{k,r}(t),$$

where $C_{k,y,f}$ $[N/rad]$ and $C_{k,y,r}$ $[N/rad]$ are the front and rear corner stiffness of the k-th vehicle, respectively, that are computed on the basis of the steering angle $\delta_{k,f}$ as:

$$\alpha_{k,f}(t) = \arctan\left(\frac{\dot{y}_k(t) + r_k(t)\ell_{k,f}}{\dot{x}_k(t)}\right) + \delta_{k,f}(t),$$
$$\alpha_{k,r}(t) = \arctan\left(\frac{\dot{y}_k(t) - r_k(t)\ell_{k,r}}{\dot{x}_k(t)}\right).$$

The steering angle $\delta_{k,f}(t)$ has to be commanded to guarantee that the k-th CAV follows the desired path.
The longitudinal forces $F_{k,l,f}$, $F_{k,l,r}$, acting respectively on the front and rear tire, are instead computed based on the desired acceleration profile that has to be imposed to the k-th CAV for controlling its longitudinal motion. Specifically, introducing the notation $\star \in \{f, r\}$ to denote the variables related to the front and rear part of the vehicle, the longitudinal forces are computed according to the following linear dynamical system [52]:

$$F_{k,l,\star}(t) = \frac{m_{k,\star}}{\varphi s + 1} u_k(t) \tag{7.8}$$

where φ is the drivetrain constant, assumed to be equal to 0.5 $[s]$; $m_{k,\star}$ $[kg]$ is the vehicle mass on rear or front side; $u_k(t)$ $[m/s^2]$ is the desired longitudinal acceleration profile to be imposed so to adapt the motion of the k vehicle w.r.t. the presence of conflicting vehicles.
Now, by taking into account (7.8) and (7.5), the non-linear vehicle dynamics for the k-th vehicle can be recast as:

$$\dot{\zeta}_k(t) = \mathcal{F}(\zeta_k(t), \bar{u}_k(t)), \tag{7.9a}$$

$$\eta_k(t) = h(\zeta_k(t)), \tag{7.9b}$$

where $\zeta_k = [\psi_k, x_k, v_k, y_k, \dot{y}_k, r_k, F_{k,l,f}, F_{k,l,r}]^\top$ and $\bar{u}_k(t) = [u_k(t), \delta_{k,f}(t)]$ are the state variable vector and the control input vector, respectively; the output map $h(\zeta_k(t))$ is such that the output vector is $\eta_k = [\psi_k, d_k, v_k, \dot{y}_k, r_k]^\top$, where $d_k(t)$ (computed on the basis of $x_k(t)$ and $y_k(t)$) is the euclidean distance of CAV k w.r.t. to the border (entrance) of the CA. The information embedded into the output vector η_k is shared among the CAVs over the V2V communication network.

7.3 Cooperative Distributed Control Protocol for CAV in a Mixed-Traffic Flow

Here the design of the control actions $u_k(t)$ and $\delta_{k,f}(t)$, able to steer the longitudinal and the lateral dynamics in (7.9) of the CAVs approaching the CA, is described.

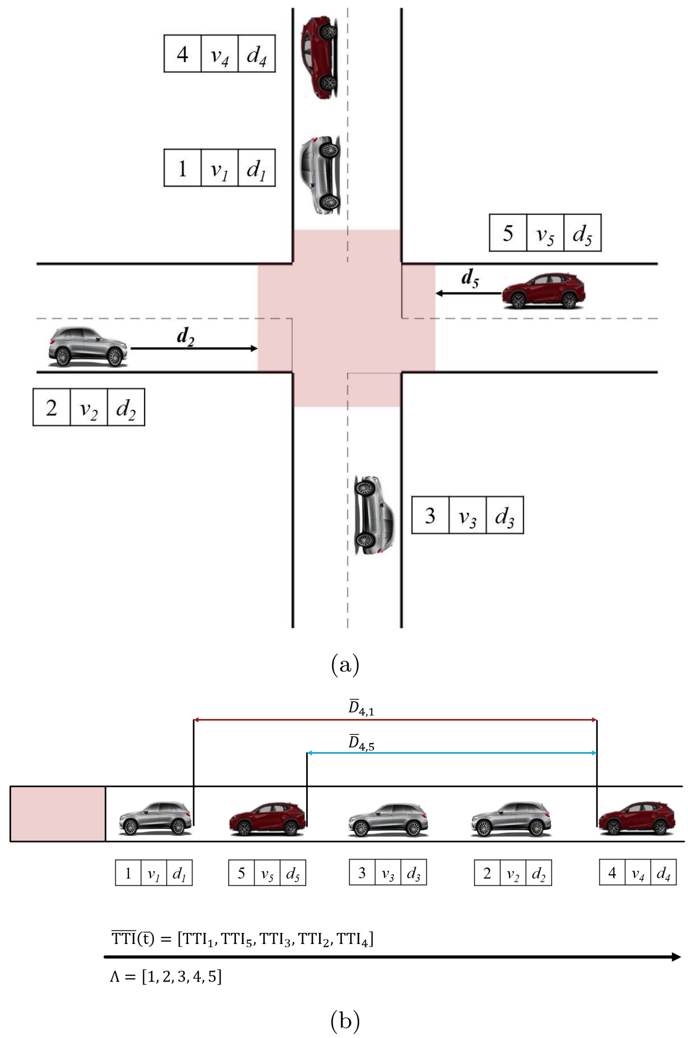

Figure 7.2: Definition of the intersection crossing sequence leveraging the Virtual Platoon control concept: a) example of a mixed traffic flow composed by $M = 2$ autonomous vehicles and $N = 3$ human-driven vehicles approaching the intersection; b) virtual crossing sequence definition on the basis of the TTI of each incoming vehicle.

7.3.1 Cooperative Time-to-Intersection-Based Longitudinal Controller

The cooperative coordination problem in mixed traffic at the intersection stated in Sec. 7.2 is here solved by taking advantage from the *Virtual*

Platoon control concept (see [245] and reference therein). The idea is to form a virtual platoon by considering the virtual gap-distance between vehicles driving on different lanes by a cooperative longitudinal controller individually driving the automated vehicles in a fully-distributed fashion. This approach leaves the task of $gap - making$ (i.e., to ensure the safe crossing of a vehicle with higher priority) solely in the hands of the longitudinal control system.

This control approach is here extended to mixed-traffic flows via the V2V cooperative estimation of the TTI: by leveraging the arrival time at intersection information of each vehicle, the crossing sequence is mapped at each time instant into a position within a virtual formation, where all vehicles (CHVs and CAVs) are sorted in ascending order of TTI, say $TTI_j(t)$, $j = 1, \dots, N + M$, see Fig. 7.2. Hence, at each instant, the position within the virtual formation defines the current intersection crossing sequence for all the $M + N$ approaching the CA. The vehicle with the smallest TTI goes first, the one with the second smallest TTI crosses as second, and so on. Note that, in the particular case when two or more vehicles have the same TTI, their index within the virtual platoon is defined by comparing their distance w.r.t. the CA entrance, i.e., the one having the shortest distance crosses first. Side and rear-end collisions are hence avoided by the networked control action that adapts the longitudinal acceleration of each CAV to preserve the order of the virtual formation and reach and maintain a prefixed inter-vehicular gap-distance to the other vehicles.

Following this approach, each incoming CAV is driven by the classical ACC augmented with the additional networked control protocol leveraging V2V information as:

$$u_k(t) = u_{k_{ACC}}(t) + u_{k_{net}}(t), \tag{7.10}$$

where $u_{k_{ACC}}$ $[m/s^2]$ is the classical ACC driving command depending from the distance and speed of the preceding vehicle, evaluated on-board by proximity sensors (e.g., radar, lidar), while $u_{k_{net}}$ $[m/s^2]$ is the networked control action that weights the information shared over the wireless V2V network. Since the networked action $u_{k_{net}}$ augments any state-of-the-art ACC controller, the one proposed by [210] is considered. Note that, since the ACC controller weights the measured distance between a specific vehicle and the nearest point of the ones that are in its

Algorithm 2: On-board computation of the minimum gap $\overline{D}_{k,j}$ for the k-th CAV approaching the CA (see (7.13)).

Data: $d_j(t)$, $v_j(t)$ ($\forall\, j = 1, \cdots, N+M$)
Result: $\overline{D}_{k,j}$ ($\forall j \neq k$)
Declarations
Let D^{st} a fixed gap distance between consecutive vehicles in the virtual platoon at standstill.
Let l_ν the length of the ν-th vehicle in the virtual platoon.
Let v_{p_p} and v_{p_ρ} the vehicle priority index associated to the CAV k and to the generic vehicle j, corresponding to their position within the virtual platoon, respectively.
Initialisation
$\Lambda \leftarrow$ initialise a vector with size $(N+M)$
Procedure
At each time instant $\bar{t}$:
while $d_k < r_{cz}$ **do**
    Compute $TTT_j(\bar{t})$ $\forall j$ as in (7.14)
    $TTI(\bar{t}) = [TTI_1(\bar{t}), \ldots, TTI_j(\bar{t}), \ldots, TTI_{N+M}(\bar{t})] \leftarrow$ Built the TTI vector
    $\overline{TTI}(\bar{t}) = [\overline{TTI}_1(\bar{t}), \ldots, \overline{TTI}_\rho(\bar{t}), \ldots, \overline{TTI}_{N+M}(\bar{t})] \leftarrow$ Sort $TTI(\bar{t})$ in increasing order
    $v_{p_\rho} \leftarrow$ Assign to each vehicle its priority crossing index (i.e. the ρ-th position within the virtual platoon) depending on $\overline{TTI}_\rho(\bar{t})$
    $\Lambda = [v_{p_1}, \ldots, v_{p_\rho}, \ldots, v_{p_{N+M}}] \leftarrow$ Build the crossing index vector
    $vp_p \leftarrow$ Find the priority crossing index of CAV k
    for $v_{p_\rho} = 1 : length(\Lambda)$ & $v_{p_\rho} \neq v_{p_p}$ **do**
        if $v_{p_p} > v_{p_\rho}$ **then**

$$\overline{D}_{k,j} = D^{st} \cdot (v_{p_p} - v_{p_\rho}) + \sum_{\nu = v_{p_p} - 1}^{v_{p_p} - v_{p_\rho} - 1} l_\nu;$$

        else

$$\overline{D}_{k,j} = D^{st} \cdot (v_{p_p} - v_{p_\rho}) - \sum_{\nu = v_{p_p}}^{v_{p_\rho} - 1} l_\nu$$

        end
    end
end

line of sight [246], it plays a crucial role in preventing vehicles collisions in the narrow space at the conflicting area when they perform conflicting left/right turning manoeuvre [232, 247].

Instead, the networked control protocol $u_{k_{net}}$ is composed of two different actions; one is distance-based, i.e., imposes the prescribed inter-spacing policy, while the other one is velocity-based, i.e., aims to impose a desired speed profile, as:

$$u_{k_{net}}(t) = u^d_{k_{net}}(t) + u^v_{k_{net}}(t). \tag{7.11}$$

Note that the proposed cooperative control strategy is active within the CZ, so that all inside vehicles approaching the intersection will take part in the current crossing. In contrast, vehicles outside will be considered in subsequent passing.

The two actions mentioned above are designed as follows.

Cooperative gap-regulation action. The first control action in (7.11) is designed as:

$$u^d_{k_{net}}(t) = \frac{1}{\Delta_k} \sum_{\substack{j=1,\\ j\neq k}}^{N+M} \alpha_{kj} K_{kj} (d_k(t-\tau_{kj}(t)) - d_j(t-\tau_{kj}(t)) - D_{k,j}), \tag{7.12}$$

where d_k $[m]$ and d_j $[m]$ are the euclidean distances w.r.t. the CA entrance (border) of the k-th CAV and the j-th vehicle, respectively (being $j = 1, \dots N + M, j \neq k$); $D_{k,j}$ is the desired gap between the CAV k and the vehicle j; K_{kj} are positive control gains; α_{kj} models the presence/absence of communication links among the CAV k and vehicle j, while Δ_k is the number of vehicles j communicating with the CAV k according to the communication topology (see Sec. 3.1.2 for more detail); $\tau_{kj}(t)$ $[s]$ is the time-varying communication delay affecting the communication link between the CAV k and vehicle j.

The inter-vehicle spacing policy [73] in the virtual formation $D_{k,j}$ (between the k-th CAV and the j-th vehicle $j = 1, \dots, N + M$ with $j \neq k$) is computed at each time instant as:

$$D_{k,j} = \overline{D}_{k,j} + h_k v_k(t), \tag{7.13}$$

where h_k $[s]$ is the time gap and $v_k(t)$ is the current speed of the CAV k, while $\overline{D}_{k,j}$ $[m]$ is the minimum gap distance between the CAV k and vehicle j, depending on their relative TTI.

Specifically, each CAV estimates its TTI on the basis of on-board sensor measurements as well as the ones of all the other vehicles approaching the CA based on V2V information as:

$$TTI_j(t) = \begin{cases} \dfrac{d_j(t)}{v_{th}} & \text{if } v_j(t) < v_{th} \ , \\ \dfrac{d_j(t)}{v_j(t)} & \text{otherwise,} \end{cases} \tag{7.14}$$

where $j = 1, \cdots, N+M$; v_{th} $[m/s]$ is a fixed speed threshold that allows to compute the TTI also when vehicles are at standstill (by default set to 0.1 $[m/s]$) [248].

At each time instant, based on the current value assumed by TTI_j $(\forall j)$, a priority crossing index (corresponding to the actual position within the virtual platoon) is associated with each vehicle approaching the CA according to a FAFP strategy (First Arrive First Pass [237]). Then, all indexes are embedded within the crossing index vector Λ and the minimum gap-distance $\overline{D}_{k,j}$ is computed according to Algorithm 2.

Cooperative speed-regulation action. The second control action in (7.11) aims to avoid intersection deadlocks and slowing-down phenomena. Specifically, this control action adapts the longitudinal speed of the k-th CAV to the desired one ensuring collision-free access according to the FAFP strategy based on the cooperative estimation of the TTI of all vehicles approaching the CA, as:

$$u^v_{k_{net}}(t) = \frac{1}{\Delta_k} \sum_{\substack{j=1 \\ j \neq k}}^{N+M} \beta_{kj} \alpha_{kj} (v_k(t - \tau_{kj}(t)) - v_{kj}{}^{\star}(t - \tau_{kj}(t)), \tag{7.15}$$

where β_{kj} is a positive constant control gain, v_k $[m/s]$ is the speed of the CAV k and $v_{kj}{}^{\star}$ $[m/s]$ is the desired reference speed computed as the non-linear smooth function of the differences between the TTI of the CAV k and of the vehicle j depicted in Fig. 7.3, i.e.:

$$v_{kj}{}^{\star}(t) = f(\Delta_{TTI_{kj}}(t))$$

being $\Delta_{TTI_{kj}}(t) = TTI_k(t) - TTI_j(t)$ $(j = 1, \ldots, N+M;\ j \neq k)$. More specifically, the function $v_{kj}{}^{\star}$ assumes its minimum zero value for $\Delta_{TTI_{kj}} \in [-\epsilon_{kj}, +\epsilon_{kj}]$, the cut-off value V_R $[m/s]$ for $\Delta_{TTI_{kj}}(t) = R_{dx}$ $[s]$ and $\Delta_{TTI_{kj}}(t) = R_{sx}$ $[s]$, while it tends asymptotically to a maximum value V_M $[m/s]$ as $\Delta_{TTI_{kj}}(t) \to \pm\infty$. In so doing, the CAV k reduces

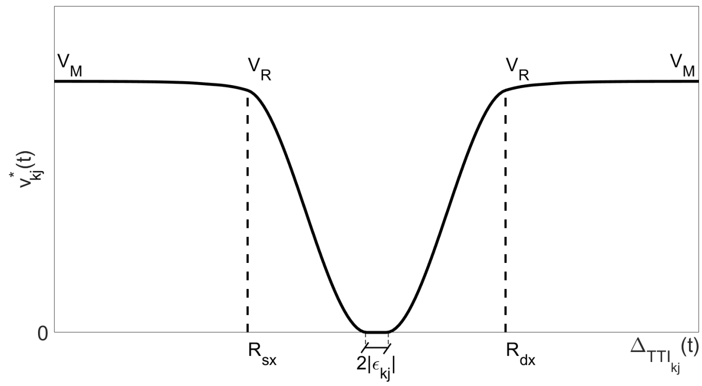

Figure 7.3: Desired reference speed $v_{kj}{}^{\star}(t)$ (see Eq. (7.15)) computed as a function of the difference $\Delta_{TTI_{kj}}$ between the Time-to-Intersection of the CAV k and of the vehicle j.

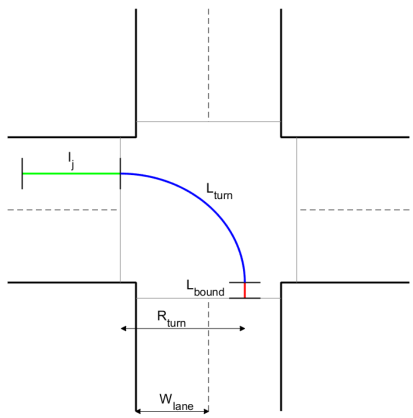

Figure 7.4: Example of the left-turning manoeuvre allowing to compute the value assumed by of R_{dx} and R_{sx} in Fig. 7.3

its longitudinal speed if there exists a conflicting vehicle j, while it autonomously increases its longitudinal speed with respect to the neighbouring vehicle j, until its maximum value V_M, if safety conditions are fulfilled.

Zero-speed range can be computed as $\epsilon_{kj} = (l_k + l_j)/(2 \cdot V_M)$, being l_k $[m]$ and l_j $[m]$ the length of vehicles k and j, respectively. Furthermore, following the approach in [238] the values R_{dx} and R_{sx}, at witch the cut-off velocity V_R is commanded to the CAV, are set on the basis of the time required by a generic vehicle j to perform a turn-left manoeuvre, accelerating from standstill to a minimum crossing speed. Specifically, computing the length of this trajectory (see Fig. 7.4) as:

$$L_{\text{left-turn}} = L_{\text{bound}} + L_{\text{turn}} + l_j,$$

where L_{bound} $[m]$ is the length of a safe bound to the intersection (set as 0.7 $[m]$); L_{turn} $[m]$ is the arc-length of the left-turn path with radius $R_{turn} = 3/2 \cdot W_{\text{lane}} + L_{\text{bound}}$, being W_{lane} the width of each lane $[m]$; l_j $[m]$ is the length of the vehicle. The time required to perform the left-turn manoeuvre is [238]:

$$T_{\text{left-turn}} = |R_{dx}| = |R_{sx}| = T_{\min} + T_F, \tag{7.16}$$

where $T_{\min}$ $[m/s]$ is the time needed to reach the minimum crossing speed $v_{\min}$ $[m/s]$ and T_{F} $[m/s]$ is the time needed to complete the left-turning manoeuvre at the constant minimum speed. It follows that, for example, setting $l_j = 4.0$ $[m]$, the width of each lane as 3.25 $[m]$, a minimum crossing speed of $v_{\min} = 4.5$ $[m/s]$ and a constant-comfortable acceleration rates of 2 $[m/s^2]$, the value of $T_{\min}$ is equal to 2.2 $[s]$, while the value of T_{F} is equal to 2.3 $[s]$, and therefore $R_{dx} = R_{sx} = 4.5$ $[s]$.

Remark 1. *Note that, in the appraised driving scenario, the specific path each vehicle has to follow is unknown to other vehicles within the cooperation zone until this vehicle itself starts crossing the intersection. Therefore, for safety reasons and without loss of generality, each CAV k ($k = N+1, \cdots, N+M$) has to assume that all the communicating vehicles j ($j = 1, \cdots, N+M$ with $j \neq k$) approaching the intersection are a foe. Consequently, the control algorithm driving each CAV k has to take into account the position and speed information of each communicating vehicle j. Once the vehicle j enters the CA, following a path that does not conflict with any CAV k within the CZ, its information is neglected in the computation of control action for the k-th CAV.*

7.3.2 Lateral Control

Given the vehicle dynamics in (7.9), the automatic control of the lateral behaviour of the k-th CAV, is achieved by commanding the front steering wheel angle as in [249]:

$$\delta_{k,f}(t) = (\psi_k(t) - \psi_k^\star(t)) + \arctan \frac{K_k^e e_k(t)}{K + v_k(t)} + K_k^r(r_k(t) - r_k^\star(t)), \tag{7.17}$$

where $\psi_k(t)$ $[rad]$ and $r_k(t)$ $[rad/s]$ are the yaw angle and the yaw rate of the CAV k, respectively; $\psi_k^\star(t)$ $[rad]$ and $r_k^\star(t)$ $[rad/s]$ are the reference yaw angle and yaw rate to be tracked, respectively; e_k is the cross-track error [250]; K_k^e, K, K_k^r are control gains to be tuned (see [249] and references therein for further details, also about the controller stability analysis).

7.4 Numerical Analysis

The assessment of the proposed approach is performed for an exemplar case study considering different mixed traffic flows conditions leveraging MiTraS platform described in Chapter 4. Since each road edges have the same crossing priority, based on the surrounding traffic conditions, each CHV has a twofold behaviour: under high traffic demand condition, it follows the right-before-left passing policy; otherwise, it follows the first-in-first-out policy. Regarding the CAVs, they always follow the proposed scheduling passing order (according to the Algorithm 2).
Mobility and safety transportation performances indexes are used to quantify the performance of the proposed control strategy. Specifically, for mobility the following indexes [251] are used: *i*) average travel time $[s]$; *ii*) intersection throughput; *iii*) average speed $[m/s]$; *iv*) number of stops; *v*) average waiting time $[s]$; *vi*) total waiting time $[s]$. As for safety the following are considered [252]: *i*) Time-to-Collisions $[s]$; *ii*) number of near-crash conditions; *iii*) number of collisions. Finally, the vehicles

Table 7.1: Dynamic Parameters for each CAV vehicle type

	Parameters									
Vehicle Type	m_k $[kg]$	ℓ_k $[m]$	I_{zk} $[m \cdot N \cdot s^2]$	$\ell_{k,f}$ $[m]$	$\ell_{k,r}$ $[m]$	$C_{k,y,f}$ $[N/rad]$	$C_{k,y,r}$ $[N/rad]$	$\delta_{k,f,max}$ $[°]$	$a_{k,max}$ $[m/s^2]$	$a_{k,min}$ $[m/s^2]$
1	1575	4.0	2875	1.10	1.30	19000	33000	± 45°	2.5	-4.5
2	1600	4.5	2454	1.22	1.44	40000	35000	± 45°	2.5	-4.5
3	2000	4.9	4000	1.40	1.60	12000	11000	± 45°	2.5	-4.5

acceleration $[m/s^2]$ is used to evaluate both mobility and safety impacts of the proposed control strategy.

7.4.1 Case Study

Consider a four branches unsignalised intersection, as formerly described in Sec. 7.2 and depicted in Fig. 7.1, where the CZ has a radius $r_{cz} = 40$ $[m]$ [253] according to the features of the V2V communication equipment. The vehicles, entering randomly at 100 $[m]$ far from the CA, move along the road edges with a maximum allowable speed of 10 $[m/s]$ and perform all turning manoeuvres at the intersection. Here 5 symmetric traffic demand distribution within $[300, 500]$ $veh/h/ln$ with variable CAVs penetration rate within $[0, 60]\%$ are considered. Demand distribution, turning movement percentage and CAVs penetration rate are summarised in Tab. 7.2, while heterogeneous CAVs specific parameters are listed in Tab. 7.1. Moreover, since the behaviour of the CHVs is unpredictable, the simulations have been performed for each traffic scenario under two different driving conditions: A) *Deterministic Desired Driving Speed* -

Table 7.2: Demand Patterns

Scenario	**Flow** (veh/h/ln)	**Left-turn** (%)	**Right-turn** (%)	**CAV** (%)
1	300	15	25	0,20,40,60
2	350	15	25	0,20,40,60
3	400	15	25	0,20,40,60
4	450	15	25	0,20,40,60
5	500	15	25	0,20,40,60

Table 7.3: CAV Controllers Parameters ($\forall k = N+1, \dots, N+M$)

Parameter	**Description**	**Value**	**Parameter**	**Description**	**Value**
D^{st}	min gap distance	2 $[m]$	K_{kj}	networked control gain	0.11 $[1/s^2]$
h_k	min time gap	1.0 $[s]$	β_{kj}	networked control gain	0.5 $[1/s]$
$v_{k,set}$	ACC speed set-point	10 $[m/s]$	$K_{k,soft}$	lateral control gain	1 $[m/s]$
K_v	ACC control gain	0.5 $[1/s]$	$K_{k,d,yaw}$	lateral control gain	0.2 $[rad \cdot s]$
$\tilde{K}_{k,e}$	ACC control gain	0.2 $[1/s]$	$K_{k,e}$	lateral control gain	2.5 $[1/s]$
$\tilde{K}_{k,d}$	ACC control gain	0.4 $[1/s^2]$	$d_k(0)$	initial distance	100 $[m]$
$\tilde{K}_{k,v}$	ACC control gain	0.2 $[1/s]$			

all CHVs have the same desired driving speed $v_{i_{des}}(t) = 10$ $[m/s]$; $B)$ *Stochastic Desired Driving Speed* - each CHVs has a different desired driving speed $v_{i_{des}}(t)$, which is modelled as a stochastic variable with normal distribution, i.e. $v_{i_{des}}(t) \in [8, 12]$ $[m/s]$.
Control parameters, as well as initial conditions for each of the CAV, are summarised in Tab. 7.3. The heterogeneous time-varying delays affecting each of the V2V communication link are emulated as stochastic variables with a uniform discrete distribution within typical delay ranges exhibited by vehicular networks in normal operating conditions, i.e. $\tau_{kj}(t) \in [0, \tau^\star]$, being $\tau^\star = 10^{-2}$ $[s]$ as in [142].

7.4.2 Mobility Performance

Results related to mobility performance are reported Tab. 7.4 and disclose how traffic mobility conditions improve as the number of CAVs increases. Indeed, their driving behaviour allows to increase the throughput up to +7.39% in the scenario A-5 with a 60% of CAVs compared to the same scenario with 0% of CAVs. As expected, the average speed follows the same growing trend with a simultaneous variance reduction (see also Figure 7.6). The Average Travel Time decreases, except for a few scenarios characterised by a very low traffic demand. In these cases, the simultaneous presence of a few vehicles within the CA does not affect the vehicular outflow. Indeed, the benefits of the proposed approach w.r.t. mobility are obviously more evident as traffic demand grows as also shown in Fig. 7.5-Fig. 7.6, and in Fig. 7.8-Fig. 7.9-Fig. 7.10-Fig. 7.11, where it is disclosed how the cooperative control prevents CAVs from performing sudden deceleration manoeuvres. Furthermore, results in Tab. 7.4 show that, even in those cases when the number of vehicles that stop at the beginning of the intersection tends to increase, the Total Waiting Time decreases in all the appraised traffic scenarios.
In what follows, the results related to the two different human driving conditions mentioned above, namely *A) Deterministic Desired Driving Speed* and *B) Stochastic Desired Driving Speed* are analysed.
A) Deterministic Desired Driving Speed. The scenario $A-1$, characterised by the lower traffic demand, does not benefit from the proposed control strategy (see the result in Tab.7.4) since the level of interaction among vehicles is low and, accordingly, does not affect the intersection crossing manoeuvre. However, the presence of CAVs still reduces the Waiting

Table 7.4: Mobility Performance

Scenario	**Mobility Indicator**	**CAV Penetration Rate (%)**				**Difference (%)**		
		0	**20**	**40**	**60**	**0-20**	**0-40**	**0-60**
A-I	Average Travel Time $[s]$	10.72	10.56	10.62	10.78	-1.49	-0.96	0.52
	Throughput	345	348	348	348	0.87	0.87	0.87
	Average Speed $[m/s^2]$	8.01	8.13	8.09	7.98	1.51	0.97	-0.37
	Number of Stop	173	195	180	177	13	4.35	2.61
	Average Waiting Time $[s]$	0.76	0.56	0.35	0.27	-26.20	-53.66	-64.47
	Total Waiting Time $[s]$	186.00	193.50	121.50	94.50	4.03	-34.68	-49.19
A-II	Average Travel Time $[s]$	11.43	11.24	11.03	10.44	-1.67	-3.57	-8.70
	Throughput	393	393	397	400	0.00	1.53	2.29
	Average Speed $[m/s^2]$	7.51	7.64	7.79	7.85	1.70	3.70	4.45
	Number of Stop	197	225	171	168	14.50	-12.98	-14.50
	Average Waiting Time $[s]$	0.88	0.66	0.43	0.25	-25.19	-62.81	-71.59
	Total Waiting Time $[s]$	216.90	260.70	126.90	112.20	20.19	-40.25	-48.27
A-III	Average Travel Time $[s]$	11.26	10.96	11.14	10.48	-2.64	-1.09	-6.91
	Throughput	426	441	447	451	3.52	4.93	6.34
	Average Speed $[m/s^2]$	7.63	7.84	7.71	7.85	2.71	1.10	2.84
	Number of Stop	256	249	264	225	-2.58	3.29	-11.97
	Average Waiting Time $[s]$	0.81	0.72	0.0.36	0.29	-10.83	-55.32	-64.20
	Total Waiting Time $[s]$	324.60	320.70	159.60	149.40	-1.20	-50.83	-53.97
A-IV	Average Travel Time $[s]$	11.88	11.59	11.52	11.48	-2.46	-3.03	-3.38
	Throughput	492	501	507	510	1.83	3.05	3.66
	Average Speed $[m/s^2]$	7.23	7.41	7.46	7.50	2.52	3.12	3.73
	Number of Stop	295	300	318	306	1.63	7.72	3.66
	Average Waiting Time $[s]$	1.98	1.00	0.67	0.48	-49.37	-66.08	-75.70
	Total Waiting Time $[s]$	557.10	493.80	320.40	296.40	-11.63	-42.49	-46.80
A-V	Average Travel Time $[s]$	12.10	11.73	11.83	11.02	-3.04	-1.85	-8.92
	Throughput	528	561	564	567	6.25	6.82	7.39
	Average Speed $[m/s^2]$	7.10	7.32	7.23	7.30	3.13	1.89	2.82
	Number of Stop	390	438	384	336	12.31	122.61	94.78
	Average Waiting Time $[s]$	2.89	1.06	0.86	0.67	-63.19	-70.27	-76.84
	Total Waiting Time $[s]$	615.90	571.80	418.80	336.60	-7.16	-32.10	-45.35
B-I	Average Travel Time $[s]$	10.72	10.74	10.69	10.41	0.14	-0.31	-2.92
	Throughput	345	348	351	351	0.87	1.74	1.74
	Average Speed $[m/s^2]$	8.02	8.01	8.04	7.89	-0.14	0.31	-1.61
	Number of Stop	135	156	105	87	15.56	-22.22	-35.56
	Average Waiting Time $[s]$	0.37	0.53	0.21	0.19	41.24	-43.55	-48.92
	Total Waiting Time $[s]$	145.80	179.90	74.70	58.80	23.25	-48.77	-59.67
B-II	Average Travel Time $[s]$	11.18	11.25	11.05	10.84	0.63	-1.21	-3.11
	Throughput	387	387	390	396	0.00	0.78	2.33
	Average Speed $[m/s^2]$	7.69	7.64	7.78	7.74	-0.63	1.22	0.64
	Number of Stop	165	171	123	117	3.64	-25.45	-29.09
	Average Waiting Time $[s]$	0.46	0.48	0.33	0.27	5.36	-28.16	-40.74
	Total Waiting Time $[s]$	174.90	188.70	75.60	63.90	7.89	-56.78	-63.46
B-III	Average Travel Time $[s]$	10.86	10.74	10.71	10.96	-1.06	-1.36	0.92
	Throughput	399	405	411	426	1.50	3.01	6.77
	Average Speed $[m/s^2]$	7.92	8.01	8.03	7.73	1.07	1.38	-2.40
	Number of Stop	150	195	174	147	30.00	16.00	-2.00
	Average Waiting Time $[s]$	0.28	0.38	0.20	0.20	35.71	-28.57	-28.57
	Total Waiting Time $[s]$	114.90	149.10	102.90	90.00	24.87	-13.82	-24.62
B-IV	Average Travel Time $[s]$	12.25	11.73	11.33	11.38	-4.26	-7.50	-7.11
	Throughput	495	507	510	516	2.42	3.03	4.24
	Average Speed $[m/s^2]$	7.02	7.33	7.56	7.45	4.45	7.69	2.82
	Number of Stop	261	270	285	246	3.45	9.20	-5.75
	Average Waiting Time $[s]$	0.61	0.85	0.38	0.40	39.05	-38.17	-34.92
	Total Waiting Time $[s]$	286.80	327.90	189.30	197.70	14.33	-34.00	-31.07
B-V	Average Travel Time $[s]$	12.11	12.04	11.72	11.23	-0.56	-3.27	-7.29
	Throughput	531	552	555	555	3.95	4.52	4.52
	Average Speed $[m/s^2]$	7.10	7.14	7.34	7.30	0.56	3.38	2.82
	Number of Stop	300	312	345	303	4.00	15.00	1.00
	Average Waiting Time $[s]$	2.41	1.12	1.07	0.98	-53.51	-55.58	-59.32
	Total Waiting Time $[s]$	672.90	608.70	575.10	528.60	-9.54	-14.53	-21.44

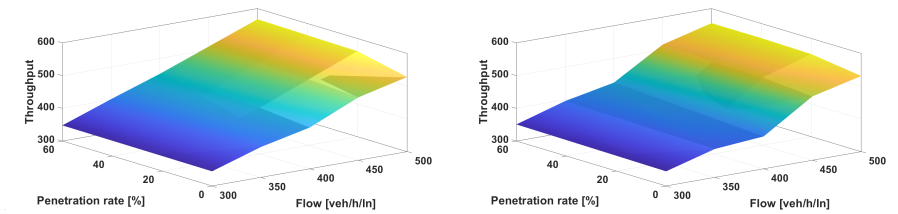

(a) (b)

Figure 7.5: Trend of the Throughput as function of both the traffic demand and CAVs penetration rate for: a) the *Deterministic Desired Driving Speed* scenario; b) the *Stochastic Desired Driving Speed* scenario.

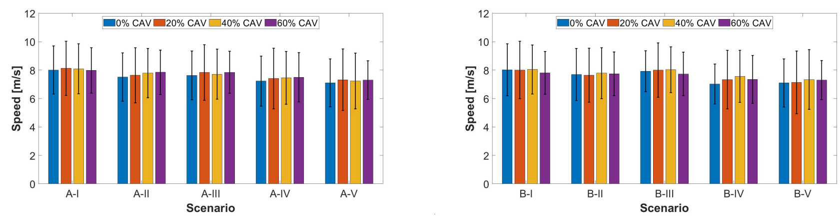

(a) (b)

Figure 7.6: Trend of the Average Speed and the Speed Variance as function of both the traffic demand and CAVs penetration rate for: a) the *Deterministic Desired Driving Speed* scenario; b) the *Stochastic Desired Driving Speed* scenario.

Time, even when the Number of Stop increases. Similar throughput results can be obtained in the scenario $A-2$ (20% of CAVs). Increasing the number of autonomous vehicles in the CZ some improvements arise. Indeed, a rise in the Average Travel Time and the Throughput compared with 0% of CAVs is observed. As the traffic demand grows, the benefit of the proposed control strategy becomes more evident. For instance, by considering scenario $A-III$, where the presence of CAVs is no more negligible, all mobility performances improve (see also Fig. 7.5 (a)). Similar outcomes are obtained in scenarios $A-IV$ and $A-V$, where, except for the number of stops, all mobility indicators raise their value as the number of CAVs boosts. More notably, for the traffic

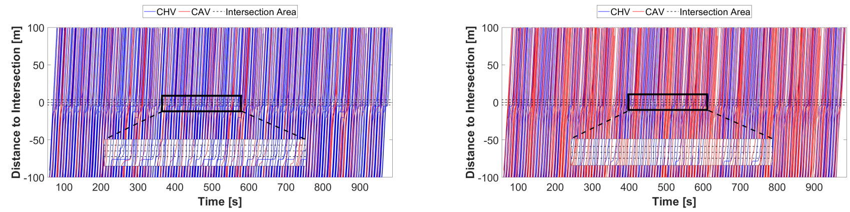

(a) (b)

Figure 7.7: Time histories of the trajectories of both CAVs and CHVs approaching the unsignalized intersection for the scenario A-V considering: (a) 20% of CAVs penetration rate; (b) 60% of CAVs penetration rate.

scenario with the higher traffic demand, i.e., $A-5$, the variation of the CAVs penetration rate from 0% to 60%, allows observing the following improvements: *i*) a percentage increase of 7.39% for the Throughput; *ii*) a percentage decrease of 8.92% for the Average Travel Time; *iii*) a percentage decrease of 45.35% for the Average Waiting Time; *iv*) a reduction of the Average Speed as depicted in Fig. 7.6 (a). Results in Fig. 7.7 show the trajectories of both CAVs and CHVs approaching the appraised unsignalized intersection in the case of traffic demand pattern as in scenario $A-5$ and penetration rate of 20% (Fig. 7.7(a)) and 60% (Fig. 7.7(b)), where the dashed line shows the intersection location from the beginning of each different lane. In contrast, the blue and red lines represent the trajectories of CHVs and CAVs, respectively. Herein, it is possible to observe how the variation of the penetration rate within the mixed traffic flow reduces potential conflicts among vehicles to cross, avoiding a too long waiting-time.
Moreover, comparing results in Fig. 7.7(a) and Fig. 7.7(b), it can be observed how a penetration rate variation from 20% to 60% enhances the road mobility efficiency, allowing the grow of the number of vehicles crossing the intersection. This aspect is also highlighted by the accelerations-related results reported in Fig. 7.8 and Fig. 7.9. More in detail, results in Fig. 7.8, obtained for the exemplary scenario $A-V$, prove how the proposed control strategy can impose a smother driving behaviour to the CAVs compared to CHVs, i.e., CAVs perform the braking manoeuvres with bounded acceleration values ($[-3, 2]$ $[m/s^2]$) while

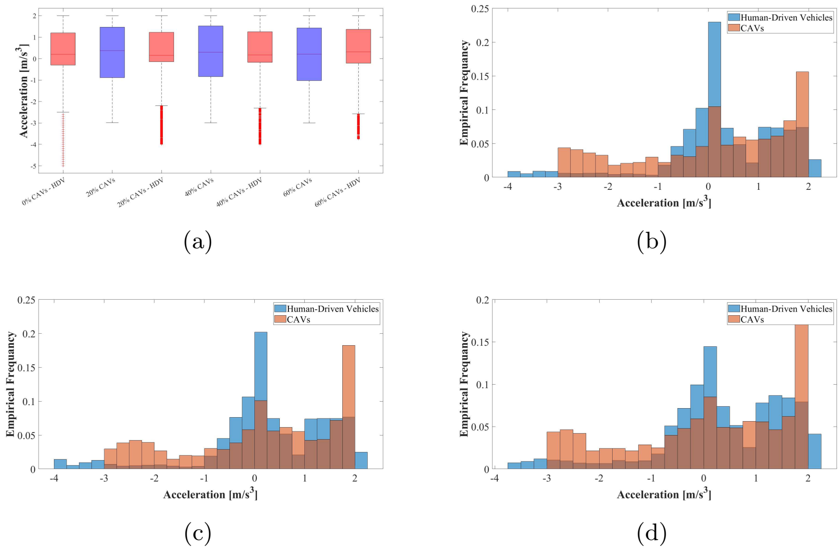

Figure 7.8: Comparison among the CAVs and CHVs accelerations for the scenario A-V: (a) boxplot; (b) histogram of 20% of CAVs penetration rate; (c) histogram of 40% of CAVs penetration rate; (d) histogram of 60% of CAVs penetration rate.

the CHVs reach lower values up to -5 $[m/s^2]$. Indeed, as it is possible to observe in Fig. 7.8(a), the presence of CAVs affects the driving behaviour of CHVs that, hence, have smoother deceleration values. This outcome is also confirmed by outputs in Fig. 7.8(b),(c), and (d) that clearly show the difference in acceleration distribution frequency among CAVs and CHVs. For the sake of completeness, in Fig. 7.9 the acceleration box-plot for the other scenarios under investigation, which disclose similar results to the one presented in Fig. 7.8(a), are also reported.
B): Stochastic Desired Driving Speed. The traffic scenarios $B-I$ and $B-II$ confirm that the benefits of the proposed strategy are minimal in low traffic demand conditions. However, differently from what happens in $A-I$ and $A-II$, all mobility indicators have an improvement as the penetration rate of CAVs increases, especially for CAVs penetration rate greater than 40%. As expected, also in the presence of this human behaviour, for an increase of the traffic demand, the benefits of the proposed control strategy are more significant (see results for $B-II$, $B-III$

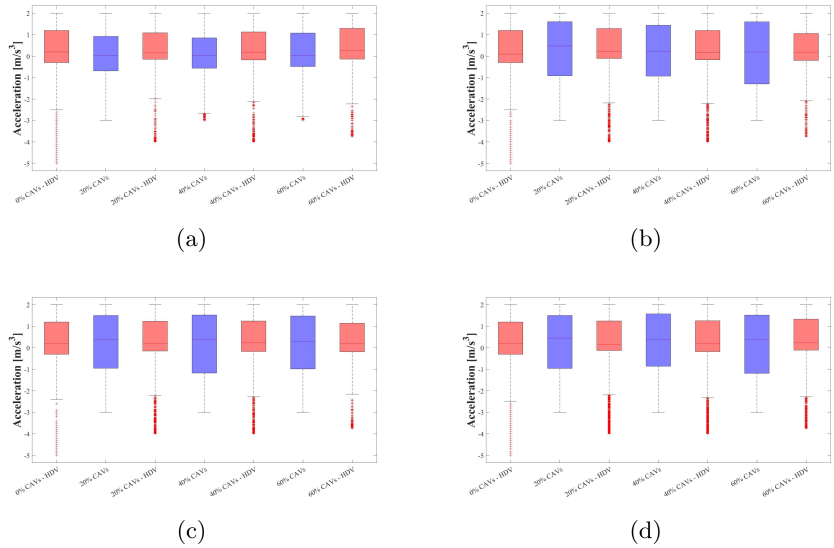

(a) (b) (c) (d)

Figure 7.9: Comparison among the CAVs and CHVs accelerations for the other scenarios under investigation: (a) boxplot for the scenario A-I; (b) boxplot for the scenario A-II; (c) boxplot for the scenario A-III; (d) boxplot for the scenario A-IV.

and $B-V$ in Tab. 7.4). The plot in Fig. 7.5 (b) confirms this latter improvement in terms of Throughput. More notably, for the traffic scenario with the higher demand pattern $B-5$, the variation of the CAVs penetration rate from 0% to 60% allows obtaining the following main performance improvement: *i*) a percentage increase of 4.52% for the Throughput; *ii*) a percentage decrease of 7.29% for the Average Travel Time; *iii*) a percentage decrease of 21.44% for the Average Waiting Time; *iv*) a reduction of the Average Speed (see also Fig. 7.6(b)). The accelerations-related results are reported in Fig. 7.10 and Fig. 7.11. More in detail results in Fig. 7.10, obtained for the exemplary scenario $B-V$, prove how the proposed control strategy can impose a smother driving behaviour to the CAVs w.r.t. CHVs. This aspect is also highlighted by results in Fig. 7.10(b),(c), and (d) that clearly show the difference in acceleration distribution frequency among CAVs and CHVs. For the sake of completeness, in Fig. 7.11 the acceleration box-plot for the other scenarios under investigation are also reported.

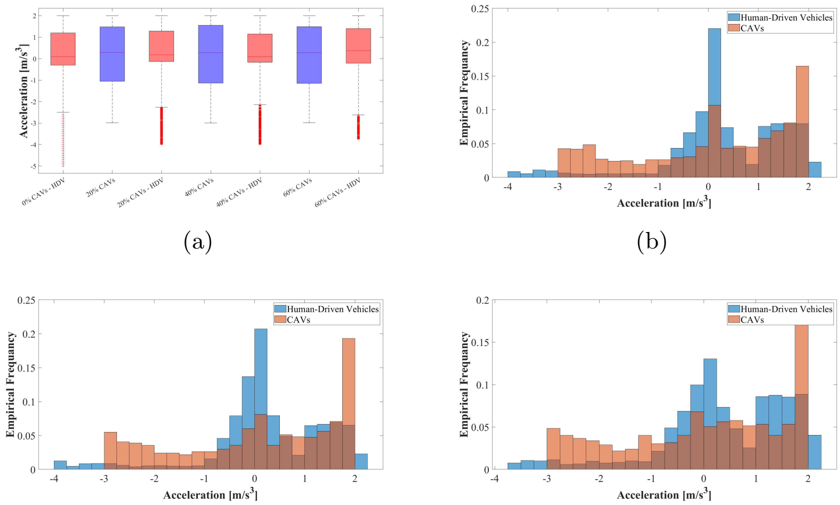

(a) (b) (c) (d)

Figure 7.10: Comparison among the CAVs and CHVs accelerations for the scenario B-V: (a) boxplot; (b) histogram of 20% of CAVs penetration rate; (c) histogram of 40% of CAVs penetration rate; (d) histogram of 60% of CAVs penetration rate.

7.4.3 Safety Performance

Robust safety performance can be evaluated by the results in Tab. 7.5. Indeed, according to [252], the Average TTC is always higher than the

Table 7.5: Safety Performance

Scenario	**Safety Indicator**	**CAV Penetration Rate %**							
		Driving condition A				**Driving condition B**			
		0	**20**	**40**	**60**	**0**	**20**	**40**	**60**
I	Average TTC [s]	> 1.5	> 1.5	> 1.5	> 1.5	> 1.5	> 1.5	> 1.5	> 1.5
	# near-crash conditions	60	87	81	114	57	75	114	141
II	Average TTC [s]	> 1.5	> 1.5	> 1.5	> 1.5	> 1.5	> 1.5	> 1.5	> 1.5
	# near-crash conditions	72	96	138	162	84	108	135	153
III	Average TTC [s]	> 1.5	> 1.5	> 1.5	> 1.5	> 1.5	> 1.5	> 1.5	> 1.5
	# near-crash conditions	108	123	129	126	99	117	126	111
IV	Average TTC [s]	> 1.5	> 1.5	> 1.5	> 1.5	> 1.5	> 1.5	> 1.5	> 1.5
	# near-crash conditions	144	207	258	246	122	234	270	255
V	Average TTC [s]	> 1.5	> 1.5	> 1.5	> 1.5	> 1.5	> 1.5	> 1.5	> 1.5
	# near-crash conditions	168	267	342	330	144	258	339	306

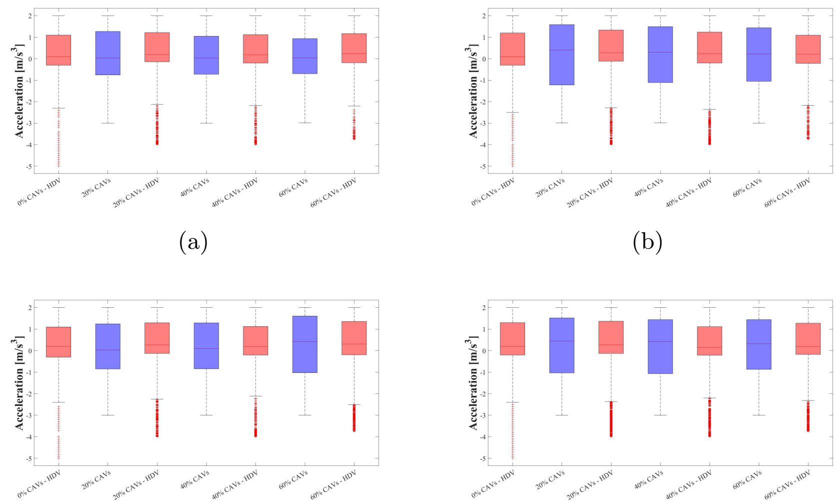

(a) (b)

(c) (d)

Figure 7.11: Comparison among the CAVs and CHVs accelerations for the other scenarios under investigation: (a) boxplot for the scenario B-I; (b) boxplot for the scenario B-II; (c) boxplot for the scenario B-III; (d) boxplot for the scenario B-IV.

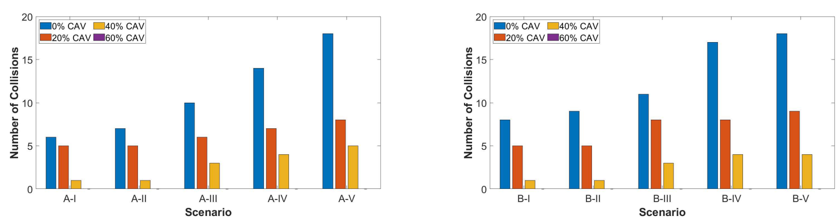

(a) (b)

Figure 7.12: Trend of the Collisions Number as function of both the traffic demand and CAVs penetration rate for: a) the *Deterministic Desired Driving Speed* scenario; b) the *Stochastic Desired Driving Speed* scenario.

minimum desirable TTC threshold of 1.5 $[s]$ in all the appraised traffic scenarios. Moreover, the number of possible collisions is strongly reduced as depicted in Fig. 7.12. Obviously, in the cases of a very crowded CZ, the number of near-crash conditions increases since it is directly related to the Throughput growth (vehicles are moving closer to each other). However, as confirmed by results depicted Fig. 7.7, the strategy can guarantee safety and collision avoidance also in these more challenging cases. At the same time, results in Fig. 7.8-Fig. 7.9-Fig. 7.10-7.11 confirm the ability of the proposed control approach in avoiding hard braking manoeuvres for CAVs by imposing a proper speed profile which positively affects the driving behaviour of the CHVs.

7.5 Concluding Remarks

This chapter has addressed the safe crossing problem of an unsignalised intersection for mixed-traffic flows composed of CHVs and CAVs. To this aim, a novel longitudinal control strategy for CAVs that combines the use of on-board ranging sensors with V2V communications is proposed. The effectiveness of the proposed control strategy has been validated via the MiTraS Integrated Simulation Environment. Simulation analyses are carried out considering different CAVs penetration rates, traffic demand, and heterogeneous vehicles. The obtained results have confirmed how V2V communications can benefit mixed traffic conditions by improving mobility and safety performance indexes at unsignalizeds intersections.

CHAPTER 8

Distributed Robust PID-like Control for Heterogeneous Nonlinear Uncertain Autonomous Vehicles Platoon: Design, Analysis and Cooperative Manoeuvres Evaluation

This chapter addresses the leader-tracking control problem for uncertain heterogeneous nonlinear autonomous vehicles platoon sharing state information through a vehicular communication network and performing cooperative manoeuvres in extra-urban traffic environments. The nonlinear vehicle dynamics are affected by time-varying parameters uncertainties and explicitly consider the air-drag reduction effect arising from the different driving conditions the platoon is involved in. At the same time, the changing of V2V links due to cooperative manoeuvres, are modelled via switching into the communication network topology.

To this aim, a novel robust distributed proportional-integral-derivative (PID)-like control protocol is proposed, which ensures that all vehicles within the platoon robustly track the leader behaviour despite unknown parameters uncertainties and network switching. The stability of the proposed control strategy is analytically proven by leveraging the Lyapunov theory. Sufficient stability conditions are expressed as a set of feasible LMIs whose solution allows the proper tuning of the robust control gains. The effectiveness of the approach is evaluated via the MiTraS Integrated Simulation Environment. The exhaustive simulation analysis, involving the Monte Carlo method, considers different cooperative platooning manoeuvres and confirms the theoretical derivation.

8.1 Tracking Issues in Cooperative Driving Systems

Tracking ability plays a crucial role in platooning applications for: *i*) normal operations, when acceleration and deceleration manoeuvres has to be safely performed to avoid collisions [60]; *ii*) joining/leaving or manoeuvre, where vehicles have to accelerate/decelerate to create a new formation [44].

Several different control approaches focus on leader-tracking or predecessor-tracking in the existing technical literature when all the autonomous vehicles are moving together as a string. In this perspective, the very first attempt is the so-called CACC, which adopts a pre-fixed information flow topology for control design (e.g., P-F). In so doing, the controller aims at providing robustness to the string of vehicles, i.e., it avoids downstream amplification of small perturbations only acting on the leader motion (see e.g., [60]). More recently, some advanced distributed platoon strategies have been proposed by leveraging the framework of multi-agent systems. For instance, distributed Model Predictive Control (MPC) [254], sliding mode [1] approaches have been proposed to tackle the problem of vehicular communication topology variety, while the robustness of the vehicles platoon w.r.t. external disturbances has been instead addressed via H_∞ control protocols (e.g., see [69, 255] and reference therein). Consensus-based approaches have also been proposed in [48, 253, 256] to deal with both topology variety and heterogeneity in the

time-varying communication delays, or in [71] to cope with uncertainties affecting the dynamics of the vehicle.
However, all the works mentioned above assume linear dynamics to describe the vehicle motion and do not consider its nonlinear behaviour, which is supposed to be compensated via some feed-forward control actions. However, in practical implementation, feed-forward approaches suffer from well-known difficulty due to the exact knowledge or the real-time measuring of the various characteristic parameters [19, 92]. It follows that the nonlinearities induced by the vehicle powertrain system (arising, for instance, from the engine, driveline, aerodynamic drag, and so on) need to be taken into account for a more accurate and realistic problem formulation. Consequently, their effect should be considered from the beginning of the control design phase [89, 257].
Control protocols for copying with platoon nonlinearities are usually designed under the restrictive assumption of neglecting uncertainties affecting the dynamics of the vehicle. For instance, authors in [89] proposed a DMPC algorithm for heterogeneous nonlinear vehicles restricting the attention to unidirectional topologies and unknown set points. Instead, a Distributed Sliding Mode Control (DSMC) framework has been presented in [90] for a class of generic topologies. Again, a two-layer distributed and adaptive control architecture was developed in [258] for a heterogeneous platoon of bi-directionally connected vehicles.
Nevertheless, the robustness to uncertain nonlinear dynamics is crucial when deploying cooperative driving applications. Indeed, there are a lot of mismatches between the actual plant and its control-oriented model that inevitably arise due to different environmental conditions, parameter variations, and unmodelled dynamics. This problem has been, very recently, addressed, for example, in [95] where a collision-free optimal robust control for heterogeneous uncertain nonlinear platoon has been proposed for the specific case when vehicles share information via the P-F communication topology. The case of uncertain platoon undergoing bi-directional P-F communication topology has been instead dealt in [259] and in [260] where a back-stepping technique has been proposed for achieving leader-tracking and string stability, respectively.
The presence of unknown parameters has been instead treated in [261]. Still, the investigation restricts its focus to the sole string stability analysis in the presence of unknown constant driving resistance that has been

identified via a neural network. Under the assumption of unknown but constant parameters of the overall vehicle dynamics, a neighbour-based adaptive control law has been proposed in [91], where the estimation of these parameters (e.g., rolling resistance and air drag force coefficients) is also provided and exploited to compensate the nonlinear behaviour via feed-forward control actions. However, in practice, the time-varying nature of the parameters can not be neglected since uncertainties strongly depend on the different driving conditions in which the autonomous vehicles platoon is involved [262, 71]. Along this direction, by modelling the vehicle uncertainties as external disturbances, [263] proposes a robust strategy able to guarantee the longitudinal control of heterogeneous nonlinear vehicle platoon sharing information via a fixed communication topology, i.e., P-F topology or bidirectional one. Conversely, to deal with the problem of both uncertainties and external disturbances, [257] and [264] propose robust control techniques able to guarantee the longitudinal control for heterogeneous nonlinear platoon sharing information via fixed communication topologies. Again, to counteract vehicle uncertainties acting in heterogeneous vehicles platoons sharing information only via the classical L-P-F topology, [265] proposes an additional state-observer that, however, increases the control action computational burden. Besides uncertain nonlinear dynamics, another critical issue within the platooning driving paradigm is related to communication topology among vehicles: it may not be fixed due to communication constraints, environmental disturbances, or platooning manoeuvres (e.g., create, merge and disengage platoons). Hence, there is the need to investigate the performance of vehicle platoon control also under switching topologies, i.e., when some communication links among the vehicles within the platoon are created and/or disrupted (see [266] and references therein for details). This problem has usually been tackled in the technical literature with consensus-based strategies [266, 267] or adaptive controllers [268]. Nevertheless, the proposed solutions have been developed under the main restrictive assumptions that vehicles dynamics are linear and perfectly known, i.e., by neglecting nonlinear behaviours and time-varying parameter uncertainties.

This chapter aims to provide a unified framework for efficiently dealing with nonlinear vehicle dynamics that are affected by time-varying uncertainties and variations in the vehicular network topology. To this end,

a novel distributed proportional-integral-derivative (PID)-like control strategy ensures that all vehicles within the platoon track the leader behaviour despite the unknown uncertainties acting on the vehicle dynamics and simultaneously cope with the time-varying structure of the communication network is proposed. The control strategy weights the vehicles state information via proportional actions that are augmented with an additional integral action on the position state information so as to improve steady-state and robustness performances [71]. Each vehicle is described via a nonlinear dynamical system accounting for the effect of the air-drag reduction due to platooning effect (whose effects are usually neglected into the different control-oriented model proposed into the technical literature about platoons), as well as of time-varying uncertainties ones depending on the different driving conditions in which the platoon is currently involved. In addition, the changing of topologies is modelled via a time-varying communication network.
To analytically prove the ability of the proposed controller in ensuring the above mentioned robust leader-tracking, the closed-loop network stability is disclosed by leveraging Lyapunov theory. Sufficient conditions expressed as a set of feasible LMIs allow the proper tuning of the robust control gains.
The proposed Integrated Simulation Environment MiTraS (see Chapter 4) is exploited to investigate the effectiveness of the proposed control strategy in a realistic traffic environment. The extensive simulation analysis, considering different cooperative driving manoeuvres (e.g., move as a 1-D formation tracking a time-varying speed profile, joining in-the-middle and leaving from-the-middle), confirms the theoretical validation and discloses both the effectiveness and the robustness of the proposed approach. It is worth noting that, since the design of a high-level coordination controller required to perform a successful platoon manoeuvre [46] is beyond the scope, platooning manoeuvres [269] are served to emulate variations in the communication topology.
The main contributions of this work can be summarised as follows:

- a nonlinear vehicle model for the control design is considered, differently from most of the recent works addressing the problem of vehicle uncertainties and/or switching topologies that, instead, leverage linearied model of the vehicle dynamics (e.g., see [19] and references therein). Moreover, the proposed control-oriented model explicitly considers the air-drag reduction coefficient, which is usually neglected in the recent technical literature dealing with heterogeneous nonlinear platoon (see, e.g., [263, 257, 264, 265, 89, 90, 91]). In so doing, the vehicle dynamics also consider the effects of the transient cooperative manoeuvres such as join/ leave in-the-middle;

- the proposed approach, to counteract the effects of model nonlinearities, does not require feed-forward action, which suffers from the well-known issue of knowing real-time measuring of vehicles parameters (as in [89, 90, 91]) or additional state-observer for their compensation (as in [265]);
- the approach deals with the simultaneous presence of uncertainties of parameters that vary in time and in the commutation topologies, which derive from the cooperative manoeuvres carried out by the platoon, differently from the very recent alternative robust protocols proposed in [257, 264].
- the assessment of the control strategy is performed exploiting the Integrated Simulation Environment MiTraS for emulating different realistic traffic scenarios, while, usually, the validation takes place leveraging simplified simulation environments (e.g., see [263, 257, 264]).

8.2 Cooperative Tracking

Consider a heterogeneous platoon composed of N autonomous vehicles plus a leading vehicle, indexed with 0. Assume that vehicles platoon dynamics are nonlinear and uncertain. Each vehicle is equipped with on-board sensors (e.g., IMU, GPS, radars, and camera) measuring its absolute position, speed, acceleration, and relative position and speed w.r.t. the preceding vehicle. Vehicles are also equipped with wireless V2V communication devices that allow them to share their state information with the neighbouring vehicles and receive the reference behaviour signal as imposed by the leader. It is worth noting that different communication topologies may arise any time due to platoon manoeuvres (e.g., join and leave the platoon) that imply the creation

and disruption of virtual couplings links within the vehicular network topology [266].
In this framework, the main aim is to design a distributed robust platoon control strategy ensuring that each vehicle tracks the leader reference behaviour while preserving a pre-fixed inter-vehicle distance, despite the presence of both heterogeneous and uncertain dynamics (mainly governed by aerodynamics drag, rolling resistance, gravitational force [60]) and switching topologies. In so doing, the autonomous vehicles platoon robustly moves as a rigid and cohesive 1-D formation in any driving conditions.

8.2.1 Nonlinear Longitudinal Uncertain Vehicle Dynamics Model for Control Design

The behaviour of each i-th vehicle within the platoon ($i = 1, \ldots, N$) can be described by its nonlinear longitudinal motion as [90, 144]:

$$\begin{aligned}
\dot{p}_i(t) &= v_i(t) \\
\dot{v}_i(t) &= \frac{\xi_i(t)}{r_i(t)m_i(t)} u_{i,\sigma}(t) - gsin(\theta(t)) - g\mu_i(t)cos(\theta(t)) \\
&\quad - \frac{0.5}{m_i(t)} \rho_{air} C_{D,i}(t)(1 - \phi_i(p_i(t), p_{i-1}(t)))C_{h,i}(t)A_{f,i}(t)v_i^2(t),
\end{aligned} \tag{8.1}$$

where $p_i(t)$ $[m] \in \mathbb{R}$ and $v_i(t)$ $[m/s] \in \mathbb{R}$ are the position and the speed of the $i-$th vehicle, respectively; $u_{i,\sigma}(t)$ $[Nm]$ is the switching control input representing the driving/braking torque; $m_i(t)$ $[kg]$ is the mass of the vehicle; $\xi_i(t)$ is the drive-train mechanical efficiency; $r_i(t)$ $[m]$ is the radius of the wheel; $\mu_i(t)$ is the rolling resistance coefficient; ρ_{air} $[kg/m^3]$ is the air density; $C_{D,i}(t)$ is the vehicle air-drag coefficient; $A_{f,i}(t)$ $[m^2]$ is the frontal area of the vehicle; $C_{h,i}(t)$ is a correction factor (unitless) due to the altitude of the road where vehicle moves; $\phi_i(p_i(t), p_{i-1}(t))$ is the air-drag reduction coefficient due to the platooning effects; g $[m/s^2]$ is the gravity acceleration while $\theta(t)$ $[rad]$ is the road-track slope. The air-drag reduction factor $\phi_i(p_i(t), p_{i-1}(t))$ is computed as in [2]. More specifically, as yet illustrated in Fig. 4.2, the reduction is zero for the first vehicle (the leader in this case), increases as the position index of a vehicle within the platoon increases, and, in the end, it assumes

the same value as 4^{th} vehicle for each n^{th} vehicle ($n \geq 4$). Thus, by embedding this factor into the dynamical model of each vehicle i, the variations of $\phi_i(p_i(t), p_{i-1}(t))$ during the different platoon manoeuvres can be explicitly taken into account.
The value of the vehicle parameters strongly depends on the different driving conditions [71] and the change of the operating speed [262]. Here, to take into account this variability,the uncertain parameters are modelled as:

$$
\begin{aligned}
&m_i(t) = \bar{m}_i + \delta m_i(t), \\
&\xi_i(t) = \bar{\xi}_i + \delta \xi_i(t), \\
&r_i(t) = \bar{r}_i + \delta r_i(t), \\
&\mu_i(t) = \bar{\mu}_i + \delta \mu_i(t), \\
&C_{D,i}(t) = \bar{C}_{D,i} + \delta C_{D,i}(t), \\
&C_{h,i}(t) = \bar{C}_{h,i} + \delta C_{h,i}(t), \\
&A_{f,i}(t) = \bar{A}_{f,i} + \delta A_{f,i}(t),
\end{aligned}
\tag{8.2}
$$

where $\bar{m}_i, \bar{\xi}_i, \bar{r}_i, \bar{\mu}_i, \bar{C}_{D,i}, \bar{C}_{h,i}$ and $\bar{A}_{f,i}$ are the nominal values of the vehicle parameters, assumed to be known, while $\delta(\cdot)(t)$ is the corresponding time-varying uncertainty satisfying the following assumption.

Assumption 2. *Time-varying uncertainties are bounded with a known upper-bound [262, 71], i.e.*

$$
\|\delta(\cdot)\| \leq \bar{\delta}(\cdot) < +\infty. \tag{8.3}
$$

▲

Remark 2. *The property of boundedness of the vehicle uncertainties usually holds in the transportation system (e.g., see [262, 257] and references therein).*

Now, naming $f_i(v_i(t)) = -gsin(\theta(t)) - g\mu_i(t)cos(\theta(t)) - \frac{0.5}{m_i}\rho_{air}C_{D,i}(t)(1-\phi_i(p_i(t), p_{i-1}(t)))C_{h,i}(t)A_{f,i}(t)v_i^2(t)$ and $b_i(t) = \frac{\xi_i(t)}{r_i(t)m_i(t)}$, the i-th nonlinear vehicle dynamics in (8.1) can be rewritten as

$$
\begin{aligned}
\dot{p}_i(t) =& v_i(t) \\
\dot{v}_i(t) =& f_i(v_i(t)) + b_i(t)u_{i,\sigma}(t).
\end{aligned}
\tag{8.4}
$$

According to the uncertainties decomposition in (8.2), the i-th vehicle uncertain nonlinear dynamics in (8.4) can be written as

$$\begin{aligned}\dot{p}_i(t) =& v_i(t)\\ \dot{v}_i(t) =& (\bar{f}_i(v_i(t)) + \Delta f_i(v_i(t))) + (\bar{b}_i + \Delta b_i(t))u_{i,\sigma}(t)\end{aligned} \tag{8.5}$$

where

$$\begin{aligned}\bar{f}_i(v_i(t)) =& - gsin(\theta(t)) - g\bar{\mu}_i cos(\theta(t))\\ &- \frac{0.5}{\bar{m}_i}\rho_{air}(1 - \phi_i(p_i(t), p_{i-1}(t)))\bar{C}_{D,i}\bar{C}_{h,i}\bar{A}_{f,i}v_i^2(t),\\ \Delta f_i(v_i(t)) =& - g\delta\mu_i(t)cos(\theta(t)) - 0.5\rho_{air}(1 - \phi_i(p_i(t), p_{i-1}(t)))\Big(\frac{\Delta\Phi_i(t)}{\bar{m}_i + \delta m_i(t)}\\ &- \frac{\bar{C}_{D,i}\bar{C}_{h,i}\bar{A}_{f,i}\delta m_i(t)}{\bar{m}_i(\bar{m}_i + \delta m_i(t))}\Big)v_i^2(t),\\ \bar{b}_i =& \frac{\bar{\xi}_i}{\bar{m}_i\bar{R}_i}\\ \Delta b_i(t) =& \frac{\bar{m}_i\bar{r}_i(\bar{\xi}_i + \delta\xi_i(t)) - \bar{\xi}_i(\bar{m}_i + \delta m_i(t))(\bar{r}_i + \delta r_i(t))}{\bar{m}_i\bar{r}_i(\bar{m}_i + \delta m_i(t))(\bar{r}_i + \delta r_i(t))}\end{aligned} \tag{8.6}$$

with

$$\begin{aligned}\Delta\Phi_i(t) =& \bar{C}_{D,i}\bar{C}_{h,i}\delta A_{f,i}(t) + \bar{C}_{D,i}\delta C_{h,i}(t)\bar{A}_{f,i} + \bar{C}_{D,i}\delta C_{h,i}(t)\delta A_{f,i}(t)\\ &+ \delta C_{D,i}(t)\bar{C}_{h,i}\bar{A}_{f,i} + \delta C_{D,i}(t)\bar{C}_{h,i}\delta A_{f,i}(t)+\\ &\delta C_{D,i}(t)\delta C_{h,i}(t)\bar{A}_{f,i} + \delta C_{D,i}(t)\delta C_{h,i}(t)\delta A_{f,i}(t).\end{aligned} \tag{8.7}$$

Note that, according to (8.3), one has that:

$$\begin{aligned}&\|\Delta\Phi_i(t)\| \leq \Delta\bar{\Phi}_i < +\infty,\\ &\|\Delta f_i(v_i(t))\| \leq \Delta\bar{f}_i < +\infty,\\ &\|\Delta b_i(t)\| \leq \Delta\bar{b}_i < +\infty.\end{aligned} \tag{8.8}$$

By introducing the following state vectors $\zeta_i(t) = [p_i(t), v_i(t)]^\top \in \mathbb{R}^2$, the i-th agent dynamics in (8.5) can be rewritten in a more compact notation as:

$$\dot{\zeta}_i(t) = A\zeta_i(t) + B(\bar{f}_i(v_i(t)) + \Delta f_i(v_i(t))) + B(\bar{b}_i + \Delta b_i(t))u_{i,\sigma}(t), \tag{8.9}$$

being

$$A = \begin{bmatrix}0 & 1\\ 0 & 0\end{bmatrix}, \quad B = \begin{bmatrix}0\\ 1\end{bmatrix}. \tag{8.10}$$

Instead, the following nonlinear system, exploited for generating the desired trajectories to be commanded [270], describes the leader dynamics:

$$\begin{aligned}\dot{p}_0(t) &= v_0(t),\\ \dot{v}_0(t) &= \bar{f}_0(v_0(t)) + \Delta f_0(v_0(t)) + u_0(t),\end{aligned} \tag{8.11}$$

where $p_0(t)$ $[m] \in \mathbb{R}$ and $v_0(t)$ $[m/s] \in \mathbb{R}$ are the position and the speed of the lead vehicle, respectively; u_0 is a reference control input, assumed to be bounded due to physical constraints [270], driving the motion of the leader. It is worth noting that, according to [271, 270, 257], the proper setting of the time-varying reference control input $u_0(t)$ allows emulating different driving conditions. For instance, the case in which the leader has to brake suddenly or reduce its velocity due to the various legal speed limits of the road it travels across.
Again, by introducing the state vectors $\zeta_0(t) = [p_0(t), v_0(t)]^\top \in \mathbb{R}^2$, the leader dynamics in (8.11) can be recast as:

$$\dot{\zeta}_0(t) = A\zeta_0(t) + B(\bar{f}_0(v_0(t)) + \Delta f_0(v_0(t)) + u_0(t)). \tag{8.12}$$

Hence, the problem of robust platooning can be assimilated to the following problem of second-order nonlinear consensus.

Problem 1 (Robust Nonlinear Platooning)**.** *Consider the heterogeneous nonlinear vehicles dynamics as in* (8.9)*. The platooning control problem consists in defining a distributed control protocol $u_{i,\sigma}(t)$ such that each vehicle tracks the reference behaviour imposed by the leader* (8.12) *and keeps a desired inter-vehicle gap-distance from all its neighbors j within the communication range, say d_{ij}, i.e.:*

$$\begin{aligned}&\lim_{t\to\infty} \|v_i(t) - v_0(t)\| = 0,\\ &\lim_{t\to\infty} \|p_i(t) - p_j(t) - d_{ij}\| = 0\end{aligned} \tag{8.13}$$

despite the presence of both unknown time-varying uncertainties acting on the vehicles dynamics ($\forall i = 1, \cdots, N$), and time-varying communication topologies.

8.3 Robust Nonlinear Platooning Control Protocol

To solve Problem 1, the following switching nonlinear cooperative distributed PID-like control strategy, driving the platoon also when links commutations and dynamic changes within the formation occur, is proposed. For each vehicle i, the distributed controller updates its action based on the errors among the state information shared by vehicles via the communication network as

$$\begin{aligned} u_{i,\sigma}(t) = & -\alpha_\sigma \bar{b}_i^{-1} K_{p,\sigma} \sum_{j=0}^{N} a_{ij,\sigma}\Big(p_i(t) - p_j(t) - d_{ij}\Big) \\ & -\alpha_\sigma \bar{b}_i^{-1} K_{i,\sigma} \sum_{j=0}^{N} a_{ij,\sigma} \int_0^t \Big(p_i(\tau) - p_j(\tau) - d_{ij}\Big) d\tau \\ & -\alpha_\sigma \bar{b}_i^{-1} K_{d,\sigma} \sum_{j=0}^{N} a_{ij,\sigma}\Big(v_i(t) - v_j(t)\Big), \end{aligned} \tag{8.14}$$

where $\sigma(t) : [0, \infty) \to \{1, 2, \ldots, m\}$ is the switching signal that determines the actual communication topology among the finite collection of graphs with a common node set $\bar{\mathcal{V}}$ and describes all the possible topologies that can be obtained for all the possible m platoon manoeuvres, i.e., $\Sigma = \{\bar{\mathcal{G}}_1, \bar{\mathcal{G}}_2, \ldots \bar{\mathcal{G}}_m\}$, being $\bar{\mathcal{G}}$ the augmented directed graph; $\alpha_\sigma \in \mathbb{R}_+$ is a tuning parameter; $K_{p,\sigma}$, $K_{d,\sigma}$ are the proportional gains weighting the position and speed information, respectively, while $K_{i,\sigma}$ is the integral gain weighting the integral of the position information; $a_{ij,\sigma}$ models the actual network topology emerging from the presence/absence of the communication link between vehicle i and vehicle j; $\bar{b}_i$, defined as in (8.6), is computed on the basis of the solely nominal value of its own parameters.

Note that, m specifies the finite number of all possible digraphs mimicking V2V connections among vehicles, i.e. $\bar{\mathcal{G}}_\sigma$ ($\sigma = 1, \ldots, m$), while $\sigma(t)$, assumed to be a piecewise constant and right continuous function, determines the index of the active graph at a specific time instant t. For the sake of simplicity, it is assumed that some finite dwell-time separates two consecutive switching instants, such to guarantee the boundedness of the switching frequency and to avoid Zeno behaviour (see [49] and

reference therein for further details).
Before proving the stability of the autonomous platoon under the action of the distributed PID-like control in (8.14), the mathematical representation of the closed-loop platoon dynamical system is derived.

8.3.1 Closed-Loop Vehicular Network

Define the error vector w.r.t. the leading vehicle 0 for the i-th vehicle within the platoon ($i = 1, \cdots, N$) as

$$\tilde{\zeta}_i(t) = \zeta_i(t) - \zeta_0(t) - d^\star = \begin{bmatrix} p_i(t) - p_0(t) - d_{i0} \\ v_i(t) - v_0(t) \end{bmatrix}, \tag{8.15}$$

being $d^\star = [d_{i0}, 0]^\top$, where $d_{i0} \in \mathbb{R}_+$ defines, for each vehicle i, the desired gap-distance distance from the leader. Given the i-th vehicle nonlinear dynamics as in (8.9) and the leader ones as in (8.12), after some algebraic manipulation, the closed-loop error dynamics for the generic vehicle i is derived as

$$\dot{\tilde{\zeta}}_i(t) = \dot{\zeta}_i(t) - \dot{\zeta}_0(t) = A\tilde{\zeta}_i(t) + B\tilde{\Delta}f_i(t) + B(\bar{b}_i + \Delta b_i(t))u_{i,\sigma}(t), \tag{8.16}$$

where $\tilde{\Delta}f_i(t) = ((\bar{f}_i(v_i(t)) - (\bar{f}_0(v_0(t)) + u_0(t)) + (\Delta f_i(v_i(t)) - \Delta f_0(v_0(t))))$.
Introduce the following augmented state vector:

$$\eta_i(t) = \begin{bmatrix} \tilde{\zeta}_i(t) \\ z_i(t) \end{bmatrix} \in \mathbb{R}^{3\times 1} \tag{8.17}$$

with

$$z_i(t) = \int_0^t (p_i(\tau) - p_0(\tau) - d_{i0})d\tau = \tilde{c}^\top \int_0^t \tilde{\zeta}_i(\tau)d\tau, \tag{8.18}$$

being $\tilde{c}^\top = [1 \;\; 0] \in \mathbb{R}^{1\times 2}$.
Accordingly, the control input in (8.24) can be recast as

$$\begin{aligned} u_{i,\sigma}(t) = &- \alpha_\sigma \bar{b}_i^{-1}[K_{p,\sigma} \;\; K_{d,\sigma}] \sum_{j=0}^{N} a_{ij,\sigma}(\tilde{\zeta}_i(t) - \tilde{\zeta}_j(t)) \\ &- \alpha_\sigma \bar{b}_i^{-1} K_{i,\sigma} \sum_{j=0}^{N} a_{ij,\sigma}(z_i(t) - z_j(t)) = \\ = &- \alpha_\sigma \bar{b}_i^{-1} K_\sigma^\top \sum_{j=0}^{N} a_{ij,\sigma}(\eta_i(t) - \eta_j(t)), \end{aligned} \tag{8.19}$$

being $K_\sigma^\top = [K_{p,\sigma} \;\; K_{d,\sigma} \;\; K_{i,\sigma}] \in \mathbb{R}^{1\times 3}$. The i-th closed-loop dynamics (8.16) can be thus recast as follows:

$$\dot{\eta}_i(t) = \bar{A}\eta_i(t) + \bar{B}\tilde{\Delta} f_i(t) + \bar{B}(\bar{b}_i + \Delta b_i(t))u_{i,\sigma}(t), \tag{8.20}$$

being

$$\bar{A} = \begin{bmatrix} A & 0_{2\times 1} \\ \tilde{c}^\top & 0 \end{bmatrix} \in \mathbb{R}^{3\times 3}, \;\; \bar{B} = \begin{bmatrix} B \\ 0 \end{bmatrix} \in \mathbb{R}^{3\times 1}. \tag{8.21}$$

Finally, by defining the global vectors

$$\begin{aligned}
&\eta(t) = \begin{bmatrix} \eta_1(t) \\ \eta_2(t) \\ \cdots \\ \eta_N(t) \end{bmatrix} \in \mathbb{R}^{3N\times 1}, \;\; u_\sigma(t) = \begin{bmatrix} u_{1,\sigma}(t) \\ u_{2,\sigma}(t) \\ \cdots \\ u_{N,\sigma}(t) \end{bmatrix} \in \mathbb{R}^{N\times 1}, \\
&\tilde{\Delta} f(t) = \begin{bmatrix} \tilde{\Delta} f_1(t) \\ \tilde{\Delta} f_2(t) \\ \cdots \\ \tilde{\Delta} f_N(t) \end{bmatrix}, \;\; \underline{b} = diag(\bar{b}_1^{-1}, \bar{b}_2^{-1}, \ldots, \bar{b}_N^{-1}) \in \mathbb{R}^{N\times N}, \\
&\underline{\Delta b}(t) = diag(\Delta b_1(t), \Delta b_2(t), \ldots, \Delta b_N(t)) \in \mathbb{R}^{N\times N},
\end{aligned} \tag{8.22}$$

the nonlinear closed-loop dynamics for the whole platoon can be described as

$$\begin{aligned}
\dot{\eta}(t) = {} & (I_N \otimes \bar{A})\eta(t) + (I_N \otimes \bar{B})\tilde{\Delta} f(t) + (I_N \otimes \bar{B})\underline{b} u_\sigma(t) + \\
& + (I_N \otimes \bar{B})\tilde{\Delta} b(t) u_\sigma(t),
\end{aligned} \tag{8.23}$$

where

$$u_\sigma(t) = -\alpha_\sigma \underline{b}^{-1}(\mathcal{H}_\sigma \otimes K_\sigma^\top)\eta(t), \tag{8.24}$$

with $\mathcal{H}_\sigma = \mathcal{L}_\sigma + \mathcal{P}_\sigma \in \mathbb{R}^{N\times N}$, being $\mathcal{L}_\sigma$ and $\mathcal{P}_\sigma$, $\forall \sigma = 1, \cdots, m$, the Laplacian and the Pinning matrix, respectively, as defined in Section 3.1.2.

8.4 Stability Analysis

Here the robust stability of the closed-loop vehicular dynamics in (8.23) with respect to uncertainties affecting the nonlinear dynamics in the presence of switching among different communication network topologies originated by the occurrence of platoon manoeuvres is analytically assessed. Before deriving the stability proof, some useful lemmas are recalled.

Lemma 4 ([1]). *If $\bar{\mathcal{G}}$ satisfies Assumption 1, then the matrix $\mathcal{H} = \mathcal{L} + \mathcal{P} \in \mathbb{R}^{N\times N}$ is positive definite.*

Lemma 5. *Given a generic matrix $F \in \mathbb{R}^{n\times n}$ and a vector $x \in \mathbb{R}^{n\times 1}$, F and $\frac{1}{2}(F + F^\top)$ both generate the same quadratic form, i.e. the following relation holds:*

$$x^\top F x = \frac{1}{2} x^\top (F + F^\top) x, \tag{8.25}$$

where $\frac{1}{2}(F + F^\top)$ is a symmetric matrix.

Lemma 6 ([70]). *For matrices A, B, C and D with appropriate dimensions, $\otimes$ defines the Kronecker product and satisfies the following properties:*

1. $(A \otimes B)^\top = (A^\top \otimes B^\top)$;
2. $A \otimes (B + C) = (A \otimes B) + (A \otimes C)$;
3. $(A \otimes B)(C \otimes D) = (AC) \otimes (BD)$;
4. $(A \otimes B)^{-1} = (A^{-1} \otimes B^{-1})$ *for any given invertible matrices A and B;*

Lemma 7 ([102]). *For any symmetric matrix $D \in \mathbb{R}^{n\times n}$, i.e. $D = D^\top$ and a vector $x \in \mathbb{R}^{n\times 1}$, the following Rayleigh inequality holds*

$$\lambda_{min}(D)\|x\|^2 \leq x^\top D x \leq \lambda_{max}(D)\|x\|^2 \tag{8.26}$$

being $\lambda_{min}(\cdot)$ and $\lambda_{max}(\cdot)$ are the minimum and the maximum eigenvalues of the matrix, respectively.

Lemma 8 ([70]). *Suppose that Assumption 1 holds. Then, there exist a positive vector $\theta = [\theta_1, \ \theta_2, \ \cdots, \ \theta_N]^\top$ such that*

$$\mathcal{H}\theta = 1_N \tag{8.27}$$

and

$$\Theta\mathcal{H} + \mathcal{H}^\top\Theta > 0 \tag{8.28}$$

where $\Theta = diag(1/\theta_1, 1/\theta_2, \cdots, 1/\theta_N)$ *and* $\mathcal{H}$ *is an* M*-matrix according to Lemma 4.*

Then, according to [70, 49, 272] the following Assumption is introduced.

Assumption 3 ([70])**.** *Each possible communication topology* $\bar{\mathcal{G}}_\sigma \in \Sigma$ *contains a directed spanning tree with the leader as the root.* ▲

Remark 3. *According to Assumption 3, it follows that each matrix* $\mathcal{H}_\sigma$*, related to the communication topology* $\bar{\mathcal{G}}_\sigma \in \Sigma$*, satisfies Lemma 8.25 and Lemma 8. In so doing, for each communication topology* $\bar{\mathcal{G}}_\sigma \in \Sigma$ *there exists a positive vector* $\theta_\sigma = [\theta_{1,\sigma},\ \ \theta_{2,\sigma},\ \ \cdots,\ \ \theta_{N,\sigma}]^\top$ *such that*

$$\mathcal{H}_\sigma\theta_\sigma = 1_N \tag{8.29}$$

and

$$\Theta_\sigma\mathcal{H}_\sigma + \mathcal{H}_\sigma^\top\Theta_\sigma > 0 \tag{8.30}$$

being $\Theta_\sigma = diag(1/\theta_{1,\sigma}, 1/\theta_{2,\sigma}, \cdots, 1/\theta_{N,\sigma})$*.*

Considering the control input recast as in (8.24), the closed-loop vehicular network in (8.23) can be expressed as

$$\begin{aligned}\dot{\eta}(t) =&(I_N \otimes \bar{A})\eta(t) + (I_N \otimes \bar{B})\tilde{\Delta}f(t) - \alpha_\sigma(I_N \otimes \bar{B})(\mathcal{H}_\sigma \otimes K_\sigma^\top)\eta(t)\\ &- \alpha_\sigma(I_N \otimes \bar{B})\tilde{\Delta}b(t)\underline{b}^{-1}(\mathcal{H}_\sigma \otimes K_\sigma^\top)\eta(t).\end{aligned} \tag{8.31}$$

Now, the stability of the heterogeneous uncertain nonlinear platoon undergoing switching topologies can be proved according to the following Theorem.

Theorem 2. *Consider the uncertain nonlinear closed-loop platoon dynamics in* (8.31) *such that Assumptions 2 is fulfilled. Let Assumption 3 holds and assume there exists a finite dwell-time among consecutive switching instants.*
If, for each given communication topology $\bar{\mathcal{G}}_\sigma \in \Sigma$ $(\sigma = 1, \ldots, m)$*, there exist scalars* α_σ*,* γ_σ*,* c_σ*, a positive vector* $\theta_\sigma \in \mathbb{R}^N$ *and matrices* Θ_σ *as in*

(8.29)-(8.30), *a symmetric and positive definite matrix* $P_\sigma \in \mathbb{R}^{n\times n}$ *such that:*

$$c_\sigma < \underline{\lambda}_\sigma \theta_{0,\sigma}, \tag{8.32}$$

$$\Lambda_\sigma = \begin{bmatrix} \Theta_\sigma \otimes (\bar{A}P_\sigma + P_\sigma \bar{A}^\top - \alpha_\sigma c_\sigma \bar{B}\bar{B}^\top) - \alpha_\sigma \underline{\underline{\lambda}}^\star_\sigma (I_N \otimes \bar{B}\bar{B}^\top) + I_{3N} & \Theta_\sigma \otimes \bar{B} \\ \star & -\gamma_\sigma^2 I_N \end{bmatrix} < 0, \tag{8.33}$$

being $\underline{\lambda}_\sigma = \lambda_{min}(\Theta_\sigma \mathcal{H}_\sigma + \mathcal{H}_\sigma^\top \Theta_\sigma)$, $\theta_{0,\sigma}$ *the minimum value of the positive vector* θ_σ, $\underline{\underline{\lambda}}^\star_\sigma = \lambda_{min}(\underline{\Psi}_\sigma + \underline{\Psi}_\sigma^\top)$, *where* $\underline{\Psi}_\sigma$ *is the value assumed by matrix* $\Psi_\sigma(t) = (\Theta_\sigma \otimes 1)\underline{\tilde{\Delta}}b(t)\underline{b}^{-1}(\mathcal{H}_\sigma \otimes 1)$ *in correspondence the upper-bound of the unknown time-varying uncertainties, then, by choosing control gains as*

$$K_\sigma = \bar{B}^\top P_\sigma^{-1}, \tag{8.34}$$

the robust nonlinear platoon control problem as in Problem 1 is solved.

Proof. Consider the following multiple Lyapunov function [273]

$$V_\sigma(t) = \eta^\top(t)(\Theta_\sigma \otimes P_\sigma^{-1})\eta(t). \tag{8.35}$$

Differentiating (8.35) along the trajectories of the closed-loop system (8.31), after some algebraic manipulation, one has:

$$\begin{aligned} \dot{V}_\sigma(t) =& \eta^\top(t)(\Theta_\sigma \otimes (P_\sigma^{-1}\bar{A}))\eta(t) + \eta^\top(t)(\Theta \otimes (\bar{A}^\top P_\sigma^{-1}))\eta(t) \\ &- 2\alpha_\sigma \eta^\top(t)((\Theta_\sigma \mathcal{H}_\sigma) \otimes (P_\sigma^{-1}\bar{B}K_\sigma^\top))\eta(t) \\ &- 2\alpha_\sigma \eta^\top(t)(\Theta_\sigma \otimes (P_\sigma^{-1}\bar{B}))\underline{\tilde{\Delta}}b(t)\underline{b}^{-1}(\mathcal{H}_\sigma \otimes K_\sigma^\top)\eta(t) \\ &+ 2\eta^\top(t)(\Theta_\sigma \otimes (P_\sigma^{-1}\bar{B}))\tilde{\Delta}f(t). \end{aligned} \tag{8.36}$$

Now, according to Lemma 6, it is possible to obtain:

$$\begin{aligned} \dot{V}_\sigma(t) =& \eta^\top(t)(I_N \otimes P_\sigma^{-1})(\Theta_\sigma \otimes \bar{A})\eta(t) \\ &+ \eta^\top(t)(\Theta_\sigma \otimes \bar{A}^\top)(I_N \otimes P_\sigma^{-1})\eta(t) \\ &- 2\alpha_\sigma \eta^\top(t)((\Theta_\sigma \mathcal{H}_\sigma) \otimes (P_\sigma^{-1}\bar{B}K_\sigma^\top))\eta(t) \\ &- 2\alpha_\sigma \eta^\top(t)(\Theta_\sigma \otimes (P_\sigma^{-1}\bar{B}))\underline{\tilde{\Delta}}b(t)\underline{b}^{-1}(\mathcal{H}_\sigma \otimes K_\sigma^\top)\eta(t) \\ &- 2\eta^\top(t)(\Theta_\sigma \otimes (P_\sigma^{-1}\bar{B}))\tilde{\Delta}f(t). \end{aligned} \tag{8.37}$$

Following the approach in [70], by introducing the following vector transformations:

$$\begin{aligned}&\tilde{\eta}(t) = (I_N \otimes P^{-1})\eta(t) \to \tilde{\eta}^\top(t) = \eta^\top(t)(I_N \otimes P^{-1})\\&\eta(t) = (I_N \otimes P_\sigma)\tilde{\eta}(t) \to \eta^\top(t) = \tilde{\eta}^\top(t)(I_N \otimes P_\sigma),\end{aligned} \tag{8.38}$$

(8.37) can be recast as

$$\begin{aligned}\dot{V}_\sigma(t) =&\tilde{\eta}^\top(t)(\Theta_\sigma \otimes (\bar{A}P_\sigma + P_\sigma\bar{A}^\top))\tilde{\eta}(t)\\&- 2\alpha_\sigma\eta^\top(t)((\Theta_\sigma\mathcal{H}_\sigma) \otimes (P_\sigma^{-1}\bar{B}K_\sigma^\top))\eta(t)\\&- 2\alpha_\sigma\eta^\top(t)(\Theta_\sigma \otimes (P_\sigma^{-1}\bar{B}))\underline{\tilde{\Delta}}b(t)\underline{b}^{-1}(\mathcal{H}_\sigma \otimes K_\sigma^\top)\eta(t)\\&+ 2\eta^\top(t)(\Theta_\sigma \otimes (P_\sigma^{-1}\bar{B}))\tilde{\Delta}f(t).\end{aligned} \tag{8.39}$$

Substituting $K_\sigma^\top = \bar{B}^\top P_\sigma^{-1}$ into (8.39), it yields:

$$\begin{aligned}\dot{V}_\sigma(t) =&\tilde{\eta}^\top(t)(\Theta_\sigma \otimes (\bar{A}P_\sigma + P_\sigma\bar{A}^\top))\tilde{\eta}(t)\\&- 2\alpha_\sigma\eta^\top(t)((\Theta_\sigma\mathcal{H}_\sigma) \otimes (P_\sigma^{-1}\bar{B}\bar{B}^\top P_\sigma^{-1}))\eta(t)\\&- 2\alpha_\sigma\eta^\top(t)(\Theta_\sigma \otimes (P_\sigma^{-1}\bar{B}))\underline{\tilde{\Delta}}b(t)\underline{b}^{-1}(\mathcal{H}_\sigma \otimes \bar{B}^\top P_\sigma^{-1})\eta(t)\\&+ 2\eta^\top(t)(\Theta_\sigma \otimes (P_\sigma^{-1}\bar{B}))\tilde{\Delta}f(t).\end{aligned} \tag{8.40}$$

Considering again Lemma 6, (8.40) can be rewritten as

$$\begin{aligned}\dot{V}_\sigma(t) =&\tilde{\eta}^\top(t)(\Theta_\sigma \otimes (\bar{A}P_\sigma + P_\sigma\bar{A}^\top))\tilde{\eta}(t)\\&- 2\alpha_\sigma\eta^\top(t)(I_N \otimes P_\sigma^{-1})(\Theta_\sigma\mathcal{H} \otimes \bar{B}\bar{B}^\top)(I_N \otimes P_\sigma^{-1})\eta(t)\\&- 2\alpha_\sigma\eta^\top(t)((I_N \otimes P_\sigma^{-1})(\Theta_\sigma \otimes \bar{B}))\underline{\tilde{\Delta}}b(t)\underline{b}^{-1}\\&((\mathcal{H}_\sigma \otimes \bar{B}^\top) \otimes (I_N \otimes P_\sigma^{-1}))\eta(t)\\&+ 2\eta^\top(t)((I_N \otimes P_\sigma^{-1})(\Theta_\sigma \otimes \bar{B}))\tilde{\Delta}f(t).\end{aligned} \tag{8.41}$$

Moreover, taking into account both vector transformation (8.38) and Lemma 8.25, (8.41) can be re-formulated as

$$\begin{aligned}\dot{V}_\sigma(t) =&\tilde{\eta}^\top(t)(\Theta_\sigma \otimes (\bar{A}P_\sigma + P_\sigma\bar{A}^\top))\tilde{\eta}(t)\\&- \alpha_\sigma\tilde{\eta}^\top(t)((\Theta_\sigma\mathcal{H}_\sigma + \mathcal{H}_\sigma^\top\Theta_\sigma) \otimes \bar{B}\bar{B}^\top)\tilde{\eta}(t)\\&- 2\alpha_\sigma\tilde{\eta}^\top(t)(\Theta_\sigma \otimes \bar{B})\underline{\tilde{\Delta}}b(t)\underline{b}^{-1}(\mathcal{H}_\sigma \otimes \bar{B}^\top)\tilde{\eta}(t)\\&+ 2\tilde{\eta}^\top(t)(\Theta_\sigma \otimes \bar{B})\tilde{\Delta}f(t).\end{aligned} \tag{8.42}$$

Then, introducing $\Psi_\sigma(t) = (\Theta_\sigma \otimes 1)\underline{\tilde{\Delta}}b(t)\underline{b}^{-1}(\mathcal{H}_\sigma \otimes 1)$ and applying Lemma 5, after some algebraic manipulations, one has:

$$\begin{aligned}\dot{V}_\sigma(t) =& \tilde{\eta}^\top(t)(\Theta_\sigma \otimes (\bar{A}P_\sigma + P_\sigma \bar{A}^\top))\tilde{\eta}(t) \\ &- \alpha_\sigma \tilde{\eta}^\top(t)((\Theta_\sigma \mathcal{H}_\sigma + \mathcal{H}_\sigma^\top \Theta_\sigma) \otimes \bar{B}\bar{B}^\top)\tilde{\eta}(t) \\ &- \alpha_\sigma \tilde{\eta}^\top(t)(I_N \otimes \bar{B})(\Psi_\sigma(t) + \Psi_\sigma^\top(t))(I_N \otimes \bar{B}^\top)\tilde{\eta}(t) \\ &+ 2\tilde{\eta}^\top(t)(\Theta_\sigma \otimes \bar{B})\tilde{\Delta}f(t).\end{aligned} \tag{8.43}$$

Since $\Psi_\sigma(t) + \Psi_\sigma^\top(t)$ is a symmetric matrix $\forall\sigma$, by applying Lemma 7, one gets:

$$\begin{aligned}\dot{V}_\sigma(t) \leq& \tilde{\eta}^\top(t)(\Theta_\sigma \otimes (\bar{A}P_\sigma + P_\sigma \bar{A}^\top))\tilde{\eta}(t) - \underline{\lambda}_\sigma \alpha_\sigma \tilde{\eta}^\top(t)(I_N \otimes \bar{B}\bar{B}^\top)\tilde{\eta}(t) \\ &- \alpha_\sigma \underline{\underline{\lambda}}_\sigma(t)\tilde{\eta}^\top(t)(I_N \otimes \bar{B}\bar{B}^\top)\tilde{\eta}(t) + 2\tilde{\eta}^\top(t)(\Theta_\sigma \otimes \bar{B})\tilde{\Delta}f(t),\end{aligned} \tag{8.44}$$

where $\underline{\lambda}_\sigma = \lambda_{min}(\Theta_\sigma \mathcal{H}_\sigma + \mathcal{H}_\sigma^\top \Theta_\sigma)$ and $\underline{\underline{\lambda}}_\sigma(t) = \lambda_{min_\sigma}(\Psi_\sigma(t) + \Psi_\sigma^\top(t))$. By explicitly considering the upper bound of the unknown time-varying uncertainties (see (8.8)) and exploiting Lemma 8, one has:

$$\begin{aligned}\dot{V}_\sigma(t) \leq& \tilde{\eta}^\top(t)(\Theta_\sigma \otimes (\bar{A}P_\sigma + P_\sigma \bar{A}^\top))\tilde{\eta}(t) \\ &- \underline{\lambda}_\sigma \alpha_\sigma \theta_{0,\sigma} \tilde{\eta}^\top(t)(\Theta_\sigma \otimes \bar{B}\bar{B}^\top)\tilde{\eta}(t) \\ &- \alpha_\sigma \underline{\underline{\lambda}}_\sigma^\star \tilde{\eta}^\top(t)(I_N \otimes \bar{B}\bar{B}^\top)\tilde{\eta}(t) \\ &+ 2\tilde{\eta}^\top(t)(\Theta_\sigma \otimes \bar{B})\tilde{\Delta}f(t),\end{aligned} \tag{8.45}$$

where $\theta_{0,\sigma}$ is the minimum value of the positive vector $\theta_\sigma(t)$ as defined in Lemma 8, while $\underline{\underline{\lambda}}_\sigma^\star = \lambda_{min}(\overline{\Psi}_\sigma + \overline{\Psi}_\sigma^\top)$ is the minimum eigenvalue of the matrix $(\overline{\Psi}_\sigma + \overline{\Psi}_\sigma^\top)$, being $\overline{\Psi}_\sigma$ the value assumed by the matrix $\Psi_\sigma(t)$ in correspondence of the upper-bound of the unknown time-varying uncertainties.
By defining the parameter $c_\sigma < \underline{\lambda}_\sigma \theta_{0,\sigma}$, (8.45) can be finally recast as

$$\begin{aligned}\dot{V}_\sigma(t) <& \tilde{\eta}^\top(t)\Big(\Theta_\sigma \otimes (\bar{A}P_\sigma + P_\sigma \bar{A}^\top - \alpha_\sigma c_\sigma \bar{B}\bar{B}^\top) \\ &- \alpha_\sigma \underline{\underline{\lambda}}_\sigma^\star (I_N \otimes \bar{B}\bar{B}^\top)\Big)\tilde{\eta}(t) + 2\tilde{\eta}^\top(t)(\Theta_\sigma \otimes \bar{B})\tilde{\Delta}f(t).\end{aligned} \tag{8.46}$$

In order to guarantee robustness w.r.t. vehicle uncertainties, the following performance index are introduced:

$$J_\sigma = \int_0^{+\infty} (\tilde{\eta}^\top(s)\tilde{\eta}(s) - \gamma_\sigma^2 \tilde{\Delta}f^\top(s)\tilde{\Delta}f(s))ds, \tag{8.47}$$

being $\gamma_\sigma \in \mathbb{R}_+$ an attenuation index $\forall\sigma = 1, \ldots, m$.
Now, following the approach [274, 275, 276], in order to minimise J_σ, it s necessary to guarantee

$$J_\sigma \leq \int_0^{+\infty} (\tilde{\eta}^\top(s)\tilde{\eta}(s) - \gamma_\sigma^2 \tilde{\Delta}f^\top(s)\tilde{\Delta}f(s) + \dot{V}(s))ds < 0. \tag{8.48}$$

Thus, according to (8.48), the robust leader-tracking is guaranteed if

$$\dot{V}_\sigma(t) + \tilde{\eta}^\top(t)\tilde{\eta}(t) - \gamma_\sigma^2 \tilde{\Delta}f^\top(t)\tilde{\Delta}f(t) < 0 \tag{8.49}$$

and, therefore, if

$$\begin{aligned}&\tilde{\eta}^\top(t)\Big(\Theta_\sigma \otimes (\bar{A}P_\sigma + P_\sigma\bar{A}^\top - \alpha_\sigma c_\sigma \bar{B}\bar{B}^\top) - \alpha_\sigma \underline{\underline{\lambda}}_\sigma^\star (I_N \otimes \bar{B}\bar{B}^\top)\Big)\tilde{\eta}(t)\\ &+ 2\tilde{\eta}^\top(t)(\Theta_\sigma \otimes \bar{B})\tilde{\Delta}f(t) + \tilde{\eta}^\top(t)\tilde{\eta}(t) - \gamma_\sigma^2 \tilde{\Delta}f^\top(t)\tilde{\Delta}f(t) < 0.\end{aligned} \tag{8.50}$$

Letting the following augmented vector as $\varphi(t) = [\tilde{\eta}^\top(t), \tilde{\Delta}f^\top(t)]^\top \in \mathbb{R}^{4N\times 1}$, inequality (8.50) can be recast in a more compact form as:

$$\varphi^\top(t)\Lambda_\sigma\varphi(t) = [\tilde{\eta}^\top(t) \;\; \tilde{\Delta}f^\top(t)]\Lambda_\sigma \begin{bmatrix}\tilde{\eta}(t)\\ \tilde{\Delta}f(t)\end{bmatrix} < 0, \tag{8.51}$$

where

$$\Lambda_\sigma = \begin{bmatrix}\Lambda_{11,\sigma} & \Lambda_{12,\sigma}\\ \star & \Lambda_{22,\sigma}\end{bmatrix},$$

with

$$\begin{aligned}\Lambda_{11,\sigma} &= \Theta_\sigma \otimes (\bar{A}P_\sigma + P_\sigma\bar{A}^\top - \alpha_\sigma c_\sigma \bar{B}\bar{B}^\top) - \alpha_\sigma \underline{\underline{\lambda}}_\sigma^\star (I_N \otimes \bar{B}\bar{B}^\top) + I_{3N},\\ \Lambda_{12,\sigma} &= \Theta_\sigma \otimes \bar{B},\\ \Lambda_{22,\sigma} &= -\gamma_\sigma^2 I_N.\end{aligned} \tag{8.52}$$

From (8.51), it follows that if (8.33) holds (i.e, if $\Lambda_\sigma < 0\ \forall\ \sigma$), then one has that $\eta(t) \to 0$ as $t \to \infty$ and $\int_0^\infty \|\tilde{\eta}(s)\|^2 ds \leq \gamma^2 \int_0^\infty \|\tilde{\Delta}f(s)\|^2 ds$. In so doing, the robust platoon control problem is solved (see (8.13)) and this completes the proof. □

Remark 4. *Note that the control parameters in* (8.14) *are tailored for each vehicle i since the control gains vector* $K_\sigma^\top = [K_{p,\sigma} \ \ K_{d,\sigma} \ \ K_{i,\sigma}] \in \mathbb{R}^{1\times 3}$ *obtained as in Theorem 2, is weighted for the nominal value of each vehicle mass* $\bar{b}_i$ *(see* (8.6)*).*

Remark 5. *Note that, Theorem 2 provides sufficient conditions ensuring the stability of the overall vehicular network as in* (8.31) *under the hypothesis of a finite dwell-time (interested readers can refer to [277, 271, 278], and references therein, for an overview of the theoretical framework).*

Remark 6. *The LMI in* (8.33) *is feasible and can be solved by using, for example, the interior-point method [275] embedded in the Yalmip Toolbox with SeDuMi solver [279].*

8.5 Numerical Analysis

8.5.1 Driving Scenario and Manoeuvres

The assessment of the proposed control strategy in (8.14) and the evaluation of the achievable performance for different platoon manoeuvres are performed leveraging the Integrated Simulation Environment MiTraS (see Chapter 4). As an exemplary case, a platoon composed of 5 vehicle plus a leader, sharing information via the L-P-F communication topology and travelling along a 5600 $[m]$ long highway segment whose altitude profile is reported in Figure8.1, is considered.

Table 8.1: Heterogeneous Nonlinear Vehicle Parameters

Vehicle Id	m_i $[kg]$	ξ_i $[-]$	r_i $[m]$	μ_i $[-]$	$C_{D,i}$ $[-]$	$A_{f,i}$ $[m^2]$	a_{max} $[m/s^2]$	a_{min} $[m/s^2]$
0	1545	0.89	0.3060	0.020	0.28	2.3315	2.5	-6.0
1	1015	0.89	0.2830	0.022	0.30	2.1900	2.5	-6.0
2	1375	0.89	0.2880	0.019	0.24	2.4000	2.5	-6.0
3	1430	0.89	0.3284	0.021	0.28	2.4600	2.5	-6.0
4	1067	0.89	0.2653	0.023	0.29	2.1400	2.5	-6.0
5	1155	0.89	0.2880	0.024	0.33	2.0400	2.5	-6.0
Uncertainty	±20%	±5%	±2%	±10%	±10%	±10%	-	-

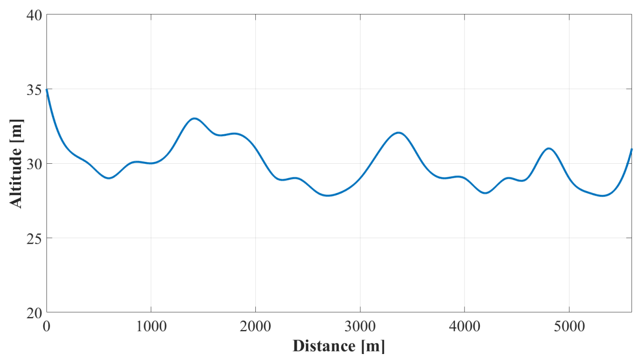

Figure 8.1: Altitude profile for the appraised road network.

Heterogeneous vehicle parameters and their specific range of variation of uncertainty are reported in Tab. 8.1 [255]. To evaluate the performances of the platoon under the action of the proposed control strategy for different values of the unknown time-varying parameters uncertainties, as well as for various combinations of them, the Monte Carlo method is exploited. Accordingly, it is possible to achieve broad test coverage by varying a large number of parameters values in a wide range. Control gains parameters are chosen according to theoretical derivation as in Theorem 2. Specifically, Yalmip Toolbox and the SeDuMi solver are exploited to solve the feasibility problem as in (8.32)-(8.33), tailored for the appraised L-P-F communication topology and for the parameter uncertainties bounds as in Table 8.1.
The analysis involves the following manoeuvres: *i*) platoon formation and maintenance *ii*) leader-tracking; *iii*) join in-the-middle; *iv*) leave from-the-middle. Note that considered platooning manoeuvres [269] are here performed only to emulate variation in the communication topology. Indeed, having a successful platoon manoeuvre requires a higher-level coordination protocol (e.g. see [3, 46, 280]). Since the design of such a high-level coordination controller is outside the scope, only the spread of changes in the control topology is implemented.

8.5.1.1 Platoon Formation and Maintenance

Starting from different initial conditions, vehicles within the platoon must reach and maintain the constant speed reference behaviour imposed by the leader according to the desired spacing policy. Control gains

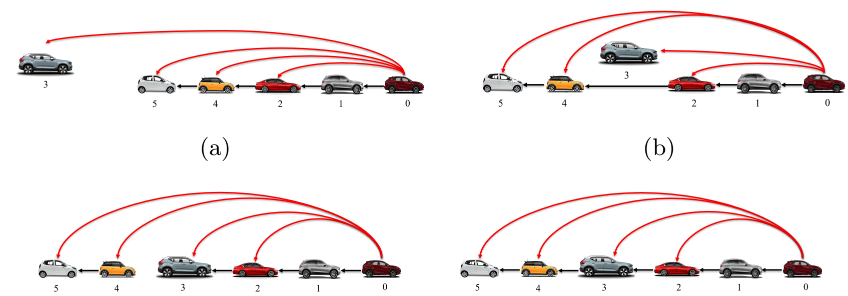

Figure 8.2: Evolution of the communication topology in the *join in the middle* manoeuvre: (a) communication topology $\bar{\mathcal{G}}_1$; (b) communication topology $\bar{\mathcal{G}}_2$; (c) communication topology $\bar{\mathcal{G}}_3$; (d) communication topology $\bar{\mathcal{G}}_4$.

parameters are: $K_\sigma^\top = [K_{p,\sigma} \quad K_{d,\sigma} \quad K_{i,\sigma}] = [0.0246 \quad 0.0044 \quad 0.1209]$, $\alpha = 4.8965$, $\gamma = 2.9195$ and $c = 1.5004$.

8.5.1.2 Leader-Tracking

Each platoon vehicle has to correctly track the time-varying reference speed profile (e.g., a trapezoidal one) imposed by the leader while maintaining the desired inter-vehicle distance. Control gains parameters for this manoeuvre are the ones presented in Sec. 8.5.1.1 since the appraised communication topology is again the L-P-F one.

8.5.1.3 Join in-the-middle Manoeuvre

The join in-the-middle manoeuvre involves four platoon operations as depicted in Figure 8.2. The $\mathcal{H}$ matrices for the switching communication topologies involved during these operations are reported in Tab. 8.2. The platoon is initially composed of 4 vehicles plus a leader and travels on a dedicated lane. The sixth vehicle, travelling on an adjacent lane, requests joining the platoon to the leader (Fig. 8.2(a)). The leader, based on some algorithm, decides first whether the vehicle can join or not and, then, in what position (see, e.g., the exemplary position decision algorithm in [281]). After the leader decides that the requesting vehicle has to

Table 8.2: $\mathcal{H}_\sigma$ matrices for the topologies related to the *join in-the-middle* manoeuvre.

$$\underset{\sigma=1}{\begin{bmatrix} 1 & 0 & 0 & 0 & 0 \\ -1 & 2 & 0 & 0 & 0 \\ 0 & -1 & 2 & 0 & 0 \\ 0 & 0 & -1 & 2 & 0 \\ 0 & 0 & 0 & 0 & 1 \end{bmatrix}} \quad \underset{\sigma=2}{\begin{bmatrix} 1 & 0 & 0 & 0 & 0 \\ -1 & 2 & 0 & 0 & 0 \\ 0 & 0 & 1 & 0 & 0 \\ 0 & -1 & 0 & 2 & 0 \\ 0 & 0 & 0 & -1 & 2 \end{bmatrix}}$$

$$\underset{\sigma=3}{\begin{bmatrix} 1 & 0 & 0 & 0 & 0 \\ -1 & 2 & 0 & 0 & 0 \\ 0 & -1 & 2 & 0 & 0 \\ 0 & 0 & 0 & 1 & 0 \\ 0 & 0 & 0 & -1 & 2 \end{bmatrix}} \quad \underset{\sigma=4}{\begin{bmatrix} 1 & 0 & 0 & 0 & 0 \\ -1 & 2 & 0 & 0 & 0 \\ 0 & -1 & 2 & 0 & 0 \\ 0 & 0 & -1 & 2 & 0 \\ 0 & 0 & 0 & -1 & 2 \end{bmatrix}}$$

join the platoon in the third position, it triggers the manoeuvre and sends to all other vehicles within the platoon the updated adjacency matrices [282] More specifically, to allow the newly sixth vehicle to enter the platoon, it needs to create enough space within the formation. Hence, the leader communicates to vehicles in third and fourth positions to become the vehicles in fourth and fifth positions, respectively, and to change their inter-vehicle distances to accommodate the new vehicle (Fig. 8.2(b)). When the sixth vehicle becomes a platoon member, it establishes communication with both its preceding and following vehicles to create the new platoon formation (Fig. 8.2(c)-(d)).
Control gains parameters for this manoeuvre are reported in Tab. 8.4.

8.5.1.4 Leave from-the-middle Manoeuvre

The leave from-the-middle manoeuvre involves four platoon operations as depicted in Fig. 8.3. The $\mathcal{H}$ matrices for the switching communication topologies involved during these operations are reported in Tab. 8.3. The manoeuvre starts with a platoon composed of 5 vehicles plus a leader; then, the vehicle in the third position decides to leave the platoon (Fig. 8.3(a)). After the request is accepted and the leaving vehicle changes lane (Fig. 8.3(b)-(c)), vehicles in fourth and fifth positions close the gap distance by becoming vehicles three and four respectively, hence, creating a new platoon formation (Fig. 8.3(d)). Control gains parameters for this manoeuvre are reported in Tab. 8.4.

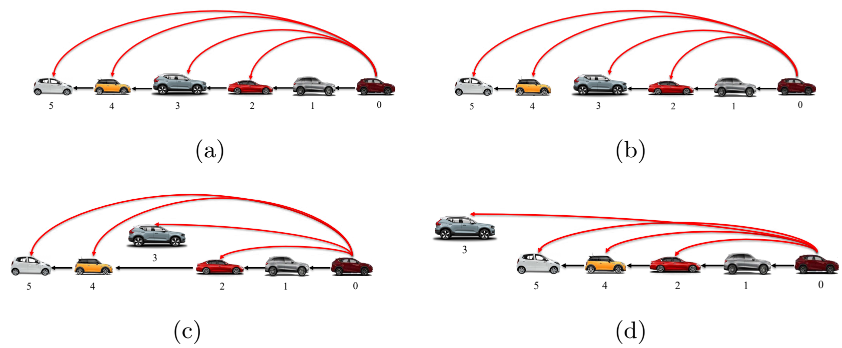

Figure 8.3: Evolution of the communication topology in the *leave from-the-middle* manoeuvre: (a) communication topology $\bar{\mathcal{G}}_4$; (b) communication topology $\bar{\mathcal{G}}_3$; (c) communication topology $\bar{\mathcal{G}}_2$; (d) communication topology $\bar{\mathcal{G}}_1$.

Table 8.3: $\mathcal{H}_\sigma$ matrices for the topologies related to the *leave from-the-middle* manoeuvre.

$$\underset{\sigma=4}{\begin{bmatrix} 1 & 0 & 0 & 0 & 0 \\ -1 & 2 & 0 & 0 & 0 \\ 0 & -1 & 2 & 0 & 0 \\ 0 & 0 & -1 & 2 & 0 \\ 0 & 0 & 0 & -1 & 2 \end{bmatrix}} \quad \underset{\sigma=3}{\begin{bmatrix} 1 & 0 & 0 & 0 & 0 \\ -1 & 2 & 0 & 0 & 0 \\ 0 & -1 & 2 & 0 & 0 \\ 0 & 0 & 0 & 1 & 0 \\ 0 & 0 & 0 & -1 & 2 \end{bmatrix}}$$

$$\underset{\sigma=2}{\begin{bmatrix} 1 & 0 & 0 & 0 & 0 \\ -1 & 2 & 0 & 0 & 0 \\ 0 & 0 & 1 & 0 & 0 \\ 0 & -1 & 0 & 2 & 0 \\ 0 & 0 & 0 & -1 & 2 \end{bmatrix}} \quad \underset{\sigma=1}{\begin{bmatrix} 1 & 0 & 0 & 0 & 0 \\ -1 & 2 & 0 & 0 & 0 \\ 0 & -1 & 2 & 0 & 0 \\ 0 & 0 & -1 & 2 & 0 \\ 0 & 0 & 0 & 0 & 1 \end{bmatrix}}$$

Switching Signal	$K_\sigma^\top = [K_{p,\sigma} \;\; K_{d,\sigma} \;\; K_{i,\sigma}]$	α_σ	γ_σ	c_σ
$\sigma = 1$	[0.0246 0.0048 0.2207]	4.8955	2.9192	1.5012
$\sigma = 2$	[0.0246 0.0047 0.1209]	4.8964	2.9195	1.5012
$\sigma = 3$	[0.0247 0.0045 0.1204]	4.8951	2.9182	1.5189
$\sigma = 4$	[0.0246 0.0044 0.1209]	4.8965	2.9195	1.5004

Table 8.4: Control Parameters for *join in-the-middle* and *leave from-the-middle* manoeuvres.

8.5.2 Simulation Results

Here are discussed the performances obtained via the proposed PID-like control strategy when considering the manoeuvres described Sec. 8.5.1.

8.5.2.1 Platoon Formation and Maintenance

Simulation outputs, depicted in Fig. 8.4, confirm the ability of the proposed approach in creating and maintaining the platoon. Indeed, all vehicles, starting from random initial gap-distances and speed, reach the consensus and converge toward the desired positions (Fig. 8.4(b)-(c)) and the leader speed (Fig. 8.4(d)-(e)) with no collisions (Fig. 8.4(a)) and a comfortable driving experience (Fig. 8.4(f)) [283], despite the presence of the different uncertainties acting on vehicles dynamics.

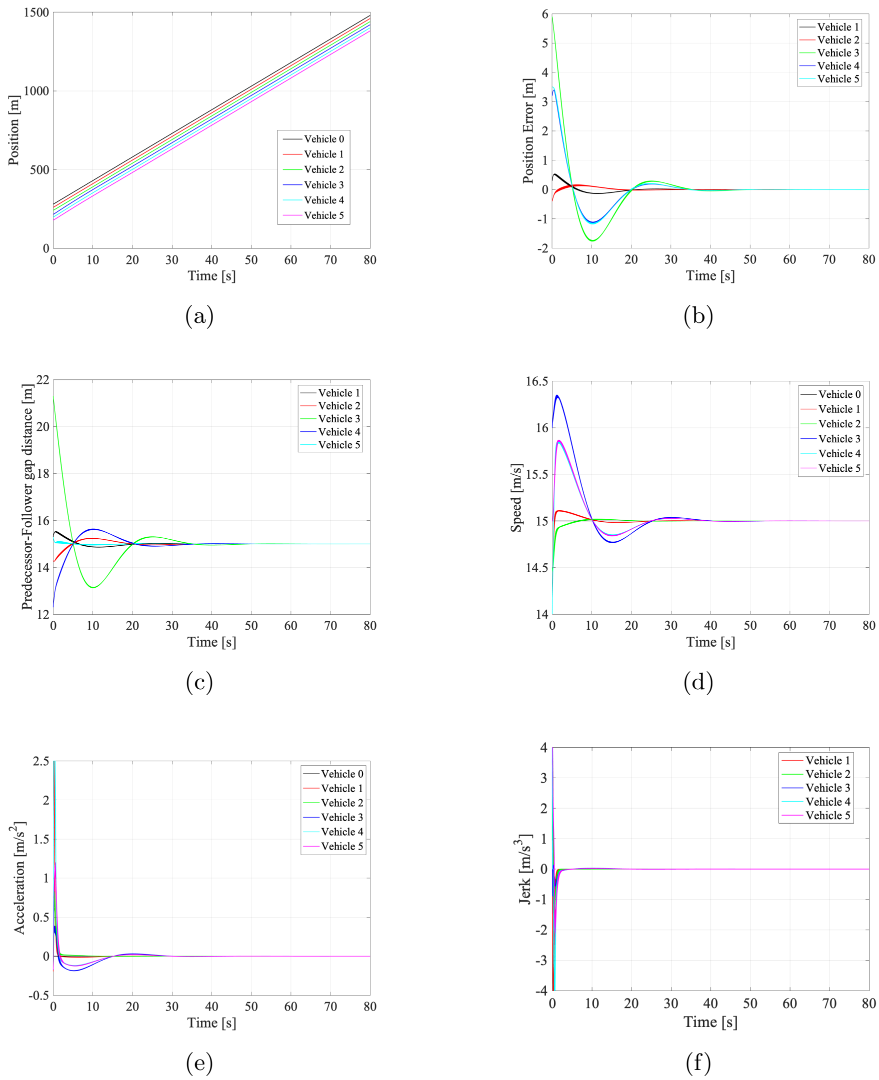

Figure 8.4: Platoon Formation and Maintenance performances. Robustness analysis via the Monte Carlo Method. Time history of: (a) vehicles position $p_i(t)$; (b) vehicles position errors computed $p_i(t) - p_0(t) - d_{i0}$; (c) vehicles inter-vehicle distance computed $p_i(t) - p_{i-1}(t)$; (d) vehicles speed $v_i(t)$; (e) vehicles acceleration $a_i(t)$; (f) vehicles jerk $\dot{a}_i(t)$;

8.5.2.2 Leader Tracking for Trapezoidal Speed Profile

Once the platoon is formed, the proposed control strategy ability to track the leading vehicle when it moves according to a trapezoidal speed profile is tested. Specifically, at $t = 100$ $[s]$, the leader accelerates from 15 $[m/s]$ to 20 $[m/s]$ with a constant acceleration of 1 $[m/s^{-2}]$; then, at $t = 180$ $[s]$, it decelerates to 10 $[m/s]$ with a constant deceleration of -1 $[m/s^{-2}]$; again, at $t = 270$ $[s]$, the leader accelerates from 10 $[m/s]$ to 15 $[m/s]$ with a constant acceleration of 1 $[m/s^{-2}]$.
Results in Fig. 8.5 confirm the theoretical derivation and show how all vehicles, despite the presence of parameters uncertainties, track the leader speed profile (Fig. 8.5(b)-(c)) while preserving at the same time the required mutual positions (Fig. 8.5(a)-(f)). As expected, speed and acceleration plots in Fig. 8.5(b)-(c) disclose that the fast-tracking of the leader motion is achieved with a smooth behaviour (see also Fig. 8.5(g)). Moreover, tiny bounded sudden changes naturally arise in the errors profiles corresponding to transient variations in the reference speed signal (Fig. 8.5(d)-(e)-(f)). Note that instantaneous variations in the acceleration profile are unrealistic since they usually occur within a specific time interval related to the powertrain features. So, results in Fig. 8.5 have to be considered as a test of robustness to challenging variation in the leader acceleration profile. Indeed, even if an instantaneous variation in acceleration profile occurs, the performance of the system is still admissible and does not degrade considerably.

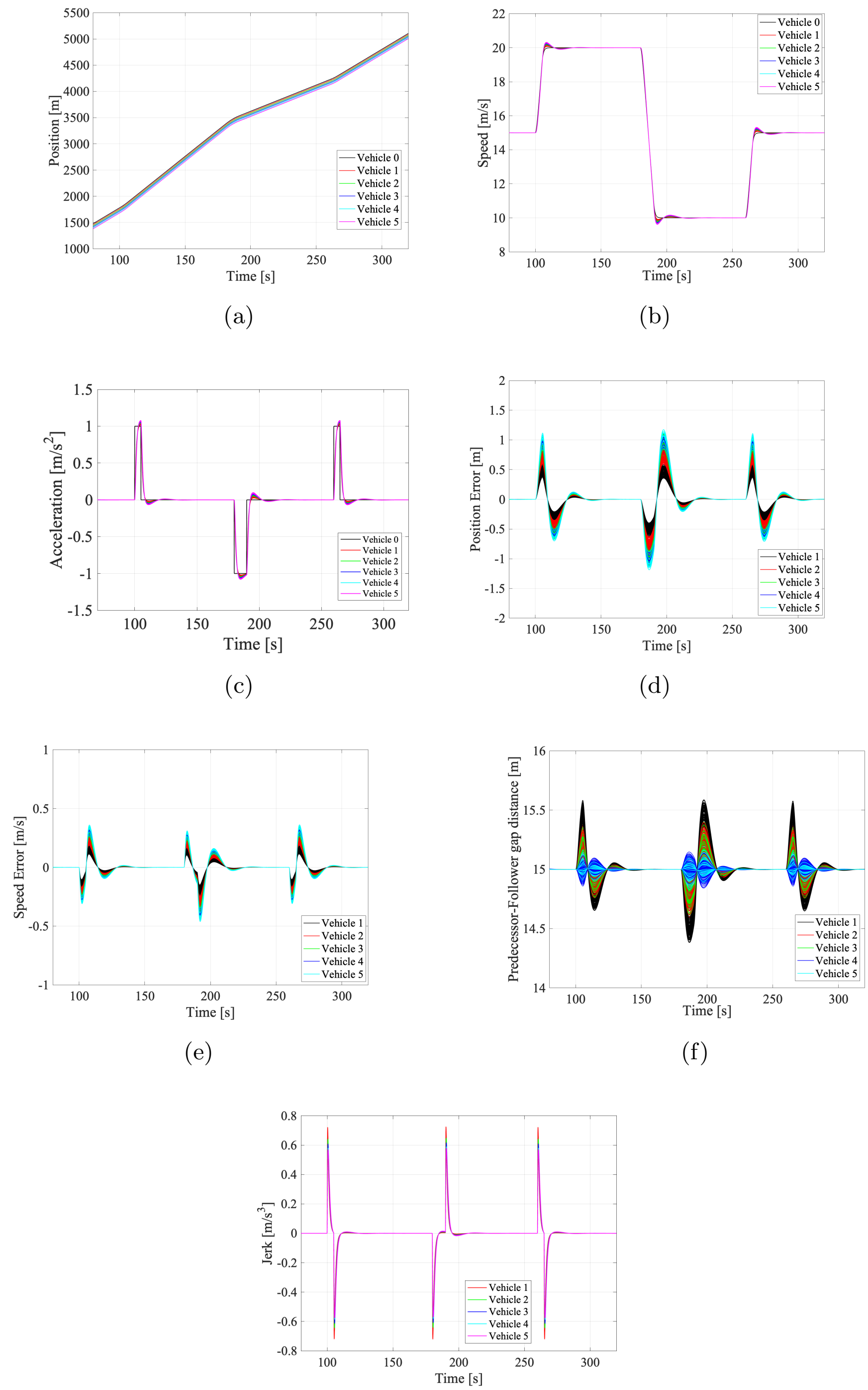

(a) (b) (c) (d) (e) (f) (g)

Figure 8.5: Leader Tracking performance for trapezoidal speed profile. Robustness analysis via the Monte Carlo Method. Time history of: (a) vehicles positions $p_i(t)$; (b) vehicles speed $v_i(t)$; (c) vehicles acceleration $a_i(t)$; (d) vehicles position errors computed $p_i(t) - p_0(t) - d_{i0}$; (e) vehicles speed errors computed $v_i(t) - v_0(t)$; (f) vehicles inter-vehicle distance computed $p_i(t) - p_{i-1}(t)$; (g) vehicles jerk $\dot{a}_i(t)$.

8.5.2.3 Join in-the-middle Manoeuvre

Fig. 8.6 discloses the results for the *join in-the-middle* manoeuvre. The manoeuvre starts with four vehicles (named V_1, V_2, V_4, V_5) plus a leader (i.e., V_0) moving in platoon formation, while the vehicle labelled as V_3 is still not a member of the platoon and travels in an adjacent lane. At $t = 55$ $[s]$, V_3 sends a join request to the leader V_0, which, after accepting it, shares the $\mathcal{H}_2$ matrix (Tab. 8.2) to all the platoon members, indicating that the vehicle V_3 is going to become the new predecessor of vehicle V_4. Accordingly, the desired inter-vehicle distance of V_4 is updated (see the dashed cyan line in Fig. 8.6(b)) and for $t \in [55; 60]$, vehicles V_4 and V_5 decelerate to create the required space to let the vehicle V_3 performing safely its cut-in manoeuvre (Fig. 8.6(a) and Fig. 8.6(d)). It is worth noting that, within this time interval, the vehicle V_3 is still travelling along a different lane from the one occupied by the platoon. Thus, since V_3 and V_4 travel along different lanes, no collisions occur for $t \in [55; 60]$, even if the inter-vehicle distance of vehicle V_4 w.r.t. the vehicle V_3 assumes negative values (see dashed line in Fig. 8.6(b) and Fig. 8.6(c)). At $t = 60$ $[s]$, the safe space has been created, and hence vehicle V_3 is allowed to perform the required cut-in manoeuvre, bringing itself to the correct third platoon position. Afterward, once the new formation is achieved, all vehicles travel as a convoy on the same lane, and the inter-vehicle distance of vehicle V_4 w.r.t. the vehicle V_3 only assumes positive values (Fig. 8.6(b)-(c)).
Finally, it is worth noting that a comfortable driving experience is ensured, as depicted in Fig. 8.6(d).

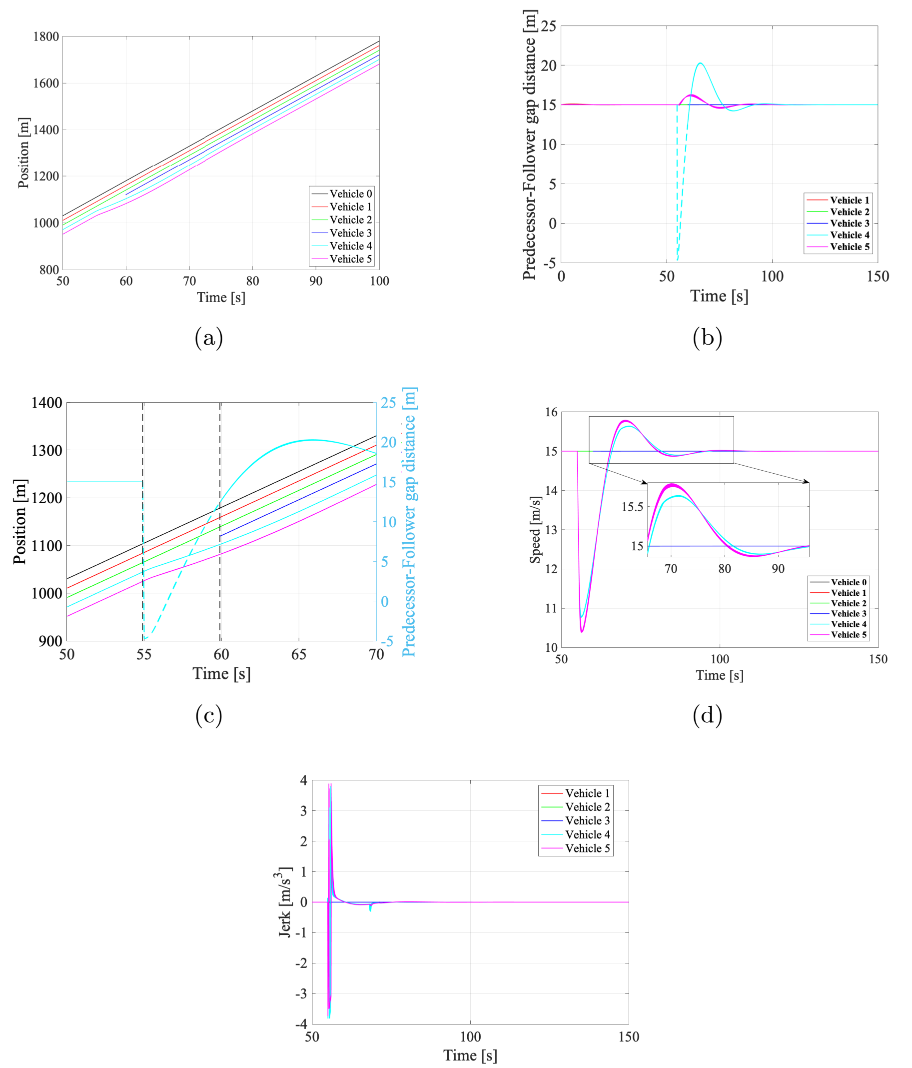

(a) (b) (c) (d) (e)

Figure 8.6: *Join in-the-middle* manoeuvre performances. Robustness analysis via the Monte Carlo Method. Time history of: (a) vehicles position $p_i(t)$; (b) inter-vehicle distance computed as $p_i(t) - p_{i-1}(t)$; (c) vehicles position $p_i(t)$ vs predecessor-follower gap distance for vehicle 4; (d) vehicles speed $v_i(t)$; (e) vehicles jerk $\dot{a}_i(t)$.

8.5.2.4 Leave from-the-middle Manoeuvre

Fig. 8.7 discloses the results for the *leave from-the-middle* manoeuvre. The manoeuvre starts with five vehicles (i.e. V_1, V_2, V_3, V_4, V_5) plus a leader (i.e. V_0) moving in platoon formation. At $t = 55$ $[s]$, the vehicle V_3 send to the leader the request to leave the platoon. After V_3 leaves the platoon, vehicles V_4 and V_5 change their platoon index position from the fourth to third and from fifth to fourth, respectively (Fig. 8.7(a)). Accordingly, they accelerate so to converge towards the desired inter-vehicle gap-distance (Fig. 8.7(b)) and the speed profile imposed by the leader. close the gap distance (Fig. 8.7(c)). Note that the manoeuvre is performed ensuring a comfortable driving experience as depicted in Fig. 8.7(d).

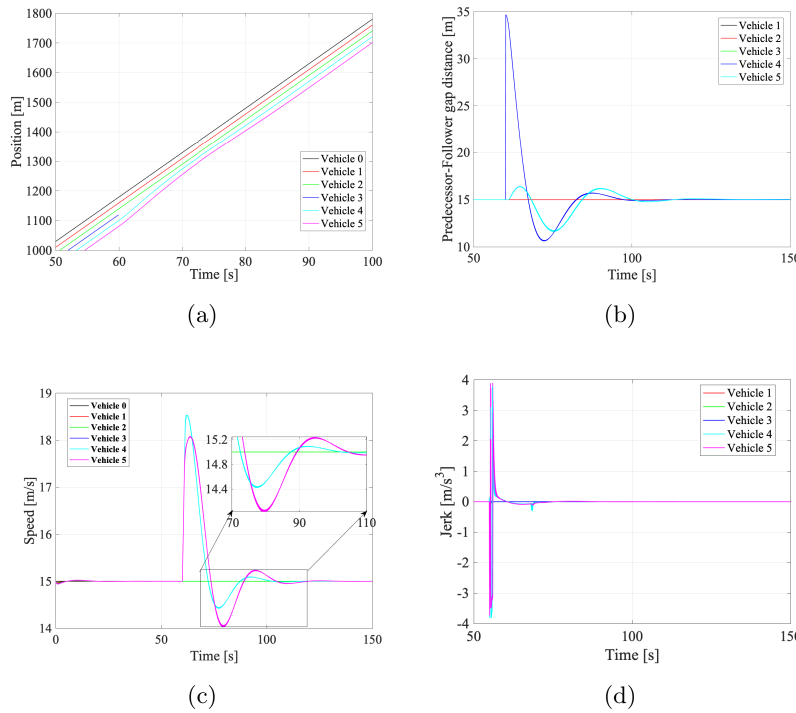

Figure 8.7: *Leave from-the-middle* manoeuvre performances. Robustness analysis via the Monte Carlo Method. Time history of: (a) vehicles position $p_i(t)$; (b) vehicles inter-vehicle distance computed $p_i(t) - p_{i-1}(t)$; (c) vehicles speed $v_i(t)$; (d) vehicles jerk $\dot{a}_i(t)$.

8.5.3 Robustness with respect to Communication Delays

In the real-world, cooperative driving strategies like platooning have to cope with time-varying delays affecting wireless communication. Indeed, CAVs exchange information through a non-ideal wireless channel affected by unavoidable communication impairment [52]. In this perspective, the proposed control strategy is evaluated in a realistic communication environment by considering, as an exemplary driving scenario, the leader-tracking one described in Sec. 8.5.1.2. Specifically, it is assumed that each communicating link, allowing the information sharing between a vehicle i and a vehicle j ($\forall i = 1, \cdots, N$, $\forall j = 0, 1, \cdots, N$ with $i \neq j$), is affected by a different time-varying communication delay whose value is influenced by the actual conditions of communication channels, i.e., $\tau_{ij}(t)$. Since, in practice, the V2V communication delay is bounded [284], each $\tau_{ij}(t)$ is emulated as random variables, uniformly distributed in $[0, 0.1]$ $[s]$ (Fig. 8.8(f)), with an upper bound that is greater than the average end-to-end communication delay typical of the IEEE 802.11p. The appraised communication topology is again the L-P-F one, and, accordingly, control gains parameters are the ones presented in Sec. 8.5.1.1.
The outcomes in Fig. 8.8 show that all vehicles within the platoon, despite the presence of time-varying communication delays, track the leader speed profile (Fig. 8.8(a)-(b)) while preserving at the same time the required inter-vehicle distance (Fig. 8.8(c)). Speed and accelerations profiles in Fig. 8.8(b)-(d) disclose that the fast-tracking of the leader motion is achieved with a smooth behaviour (see also Fig. 8.8(e)), while bounded acceptable variations in the errors profiles (Fig. 8.8(b)-(c), respectively) arise in correspondence of transient variations in the reference speed signal. Summarising, although the tracking performances slightly degrades compared to the nominal case in Fig. 8.5, Fig. 8.8 proves that the robustness of the proposed approach w.r.t. the presence of time-varying communication delays.

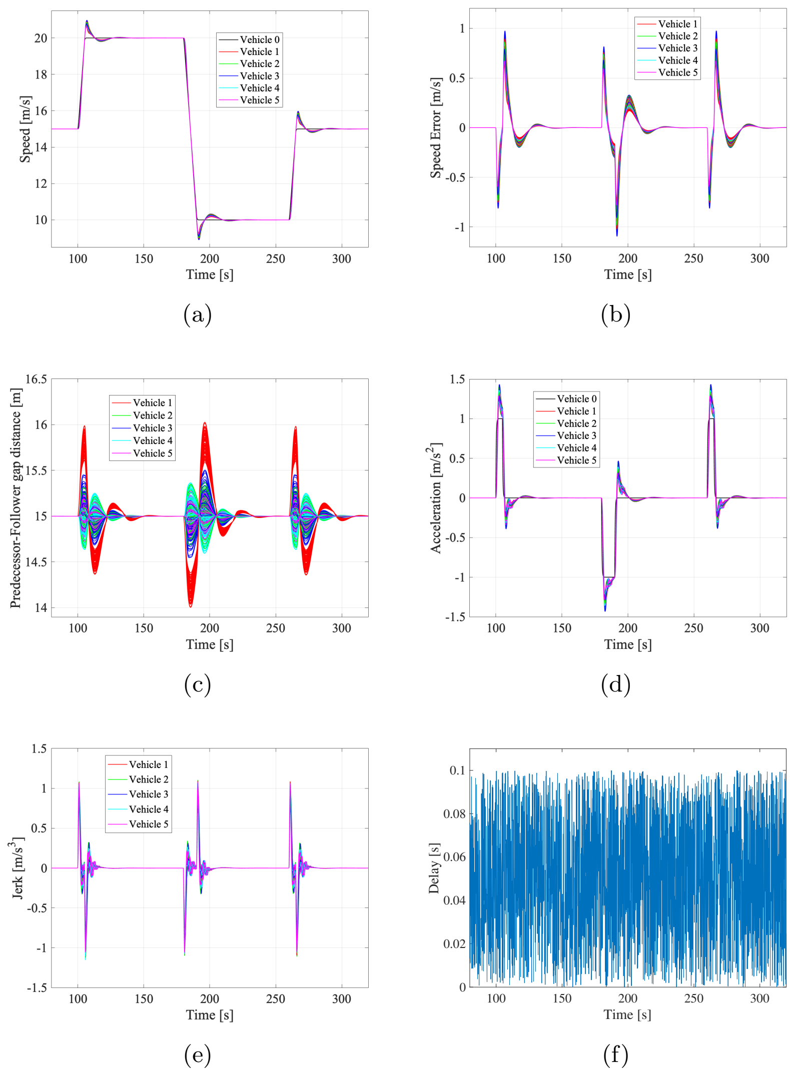

Figure 8.8: Leader Tracking performance for trapezoidal speed profile in presence of time-varying communication delays. Robustness analysis via the Monte Carlo Method. Time history of: (a) vehicles speed $v_i(t)$; (b) vehicles speed errors computed $v_i(t) - v_0(t)$; (c) vehicles inter-vehicle distance computed $p_i(t) - p_{i-1}(t)$; (d) vehicles acceleration $a_i(t)$; (e) vehicles jerk $\dot{a}_i(t)$; (f) communication delays $\tau_{ij}(t)$.

8.6 Concluding Remarks

This chapter addressed the cooperative leader-tracking control problem for uncertain heterogeneous nonlinear vehicles platoon performing cooperative manoeuvres. A distributed robust PID-like control strategy is proposed to deal with this challenging issue. By exploiting the V2V communication, the algorithm tracks the leader behaviour and regulates the gap distance among vehicles during manoeuvres, despite unknown time-varying parameter uncertainties due to varying driving conditions. The effectiveness of the proposed control strategy has been numerically evaluated via MiTraS Integrated Simulation Environment and the Monte Carlo method by carrying out different manoeuvres, including the join in-the-middle and the leave from-the-middle ones. Numerical results have confirmed the theoretical derivation and have disclosed good leader-tracking performances and the control strategy robustness w.r.t. both uncertainties and switching information topologies.

CHAPTER 9

Distributed Fixed-Time Leader-Tracking Control for Heterogeneous Uncertain Autonomous Connected Vehicles Platoons

Longitudinal control for platoons of connected autonomous vehicles is an open research topic in the C-ITS domain. Most existing approaches solve the platooning problem asymptotically without ensuring the achievement of the consensus in a finite settling time. To this aim, in this chapter the problem of guaranteeing the leader-tracking for heterogeneous vehicles platoons in a fixed time despite the presence of external disturbances is addressed. To solve this problem, by exploiting the integral sliding mode ISM approach and the Lyapunov theory, a distributed control strategy ensuring the leader-tracking in a finite settling time independent from any vehicles initial conditions is proposed. The simulation analysis, carried out in two different driving scenarios via MiTraS, confirms the effectiveness of the theoretical derivation..

9.1 Leader-Tracking Control Issues

Over the past decades, the advances in information communication technology have attracted considerable attention in C-ITS domain due to the benefit they could lead in terms of road safety increasing, and the decreasing of the environmental pollution [21]. Specifically, the deployment of connected autonomous vehicles platoons moving in a formation with a joint velocity while keeping a prefixed inter-vehicular distance may significantly improve different aspects of the vehicular traffic flow such as the traffic congestion [285]. In this driving scenario, all vehicles are connected through V2V wireless communication paradigm and exchange information by exploiting different communication protocol (see Sec. 2.4). Leveraging these information, the cooperative control strategies aim to guarantee that each vehicle within the platoon tracks the reference behaviour imposed by the leader, i.e., the first vehicle of the fleet, while achieving the desired formation w.r.t. the communicating vehicles [256].

Exploiting the Multi-Agent Systems (MASs) paradigm [286], in the wide technical literature, different cooperative driving controllers have been proposed both for homogeneous vehicles platoons (see for example [287, 69, 288] and the reference therein) and for heterogeneous ones (see for example [90, 289, 49]). Among them, robust protocols are suggested to counteract both the parameter uncertainties in [262] and the co-presence of parameter uncertainty and time-delays in [71]. Again, resilient strategies able to deal with cyber-attacks have been recently proposed in [256, 287, 290], while adaptive approaches have been designed in [291] and in [289].

However, all the works mentioned above focus on the design of an appropriate distributed control able to achieve consensus asymptotically; however, it is expected that the final prescribed inter-gap formation could be formed in a finite-time interval [271]. Moreover, it has been shown in [292, 293] that finite-time consensus controllers have a faster convergence rate and better disturbance rejection to system uncertainty and external disturbance w.r.t. the typical consensus-based strategies. Despite these crucial aspects, few works have designed finite-time cooperative control for autonomous vehicles platoons. Along this line, nonlinear finite-time consensus protocols are suggested in [271] to solve the platooning

problem over fixed and switching communication topologies and in [294] to guarantee the string-stability of heterogeneous vehicles platoons in finite-time.
Although the consensus is pursued in a finite time, the settling time estimation explicitly relies on the initial conditions of each agent within the MAS [295, 296]. It implies that there might be an applicability limit of the finite-time consensus approaches in those cases when initial states of agents are unknown or unavailable apriori. This brought to the emergence of fixed-time consensus protocols whose stability, as well as the settling time estimation, is entirely independent of initial conditions of agents [297].
To this aim, to the best of the author knowledge, the fixed-time leader-tracking control problem for heterogeneous uncertain autonomous vehicles platoons is addressed here for the first time. To solve this problem, here is proposed a fixed-time control protocol able to: *i*) counteract the vehicles heterogeneity and unknown external disturbances; *ii*) guarantee the leader-tracking in a fixed settling time whose estimation only depends on the proper choice of the control gains, not on any vehicle's initial conditions. The stability of the vehicular network under the action of the proposed distributed control protocol is analytically proved by exploiting the fixed-time stability tools and the Lypaunov theory, and an estimation of the fixed settling time is provided. Numerical analysis, carried out considering two exemplar driving scenarios through MiTraS, confirms the theoretical derivation and discloses the effectiveness of the control strategy in ensuring the robust leader-tracking in a fixed settling time, despite the variation of vehicles initial conditions and the network communication topology.

9.2 Mathematical Preliminaries on Fixed-Time

Here some definitions and lemmas useful for deriving the main result are introduced.

Definition 2 (*Fixed-Time Stability*[298])**.** *Considering the system*

$$\dot{x}(t) = f(x(t)),$$

if there exist a continuous, positive definite function $V(x(t)) : \mathbb{R}^n \to \mathbb{R}$*, such that* $\dot{V}(x(t)) \leq -a\, V^p(x(t)) -\, b\, V^q(x(t))$*,* $\forall x(t) \in \mathbb{R}^n,\ a, b > 0,\ p \in$

$(0,1)$ and $q \in (1,\infty)$, then the system is fixed-time stable and the fixed settling time is bounded by $T \leq \frac{1}{a(1-p)} + \frac{1}{b(q-1)}$.

Lemma 9. *[299] Consider the n ($n \geq 2$) order integrator system $\dot{x}_1(t) = x_2(t)$, $\dot{x}_2(t) = x_3(t)$, $\cdots$, $\dot{x}_n(t) = u(t)$, $x(0) = x_0$, with $x_k(t) \in \mathbb{R}(i = 1,\cdots,n)$ and $u(t) \in \mathbb{R}$. Let k_i ($\forall i = 1,\cdots,n$) positive constants such that the characteristic polynomial, defined with the Laplace operator, $s^n + k_n s^{n-1} + \cdots + k_2 s + k_1$ and $s^n + 3k_n s^{n-1} + \cdots + 3k_2 s + 3k_1$ is Hurwitz. There exists a constant $\epsilon \in \left(\frac{n-2}{n+2}, 1\right)$ such that, for every $\gamma \in (\epsilon, 1)$, the integrator system is stabilised at the origin in fixed-time under the feedback control*

$$u(t) = -\sum_{r=1}^{n} k_r(\lceil x_r(t) \rfloor^{\gamma_r} + \lceil x_r(t) \rfloor + \lceil x_r(t) \rfloor^{\gamma_r^{'}}),$$

with parameters γ_r and $\gamma_r^{'}$ satisfying $\gamma_{n-g} = \frac{\gamma}{(g+1)-g\gamma}$, $\gamma_{n-g}^{'} = \frac{2-\gamma}{g\gamma-(g-1)}$, ($g = 0, 1, \cdots, n-1$).

Lemma 10. *[300] Let $x_1, x_2, \cdots, x_N \geq 0$. If $p \in (0,1]$, one has*

$$\sum_{i=1}^{N} x_i^p \geq \Big(\sum_{i=1}^{N} x_i\Big)^p. \tag{9.1}$$

Instead, if $p \in (1,+\infty)$, one has

$$\sum_{i}^{N} x_i^p \geq N^{1-p}\Big(\sum_{i=1}^{N} x_i\Big)^p. \tag{9.2}$$

For easiness, throughout the section, the following notation is adopted. Given a non-negative value of c, the sig function [301] is indicated as

$$\lceil x \rfloor^c = |x|^c \text{sign}(x),\ \forall x \in \mathbb{R}$$

being $sign(\cdot)$ is the signum function. According the above notation, one has $x\lceil x \rfloor^c = |x|^{c+1}$.

9.3 Platooning Control Problem in Fixed-Time

Consider a platoon composed of N autonomous connected vehicles plus a leader sharing information about their position and velocity through a V2V wireless communication network. The behaviour of each vehicle i ($\forall i = 1, \cdots, N$) can be described by its linearized longitudinal dynamics as [257]

$$\begin{aligned} \dot{p}_i(t) &= v_i(t), \\ \dot{v}_i(t) &= u_i(t) + w_i(t), \end{aligned} \tag{9.3}$$

where $p_i(t)$ $[m]$ and $v_i(t)$ $[m/s]$ are the $i-$th vehicle absolute position (w.r.t. a given reference framework) and longitudinal velocity, respectively; $u_i(t)$ $[m/s^2]$ the desired longitudinal acceleration to be imposed to the vehicle, which can be computed as $\frac{1}{M_i}\tilde{u}_i(t)$, being M_i $[kg]$ the $i-$th vehicle mass and $\tilde{u}_i(t)$ $[kg\ m/s^2]$ the desired driving/brake force; $w_i(t)$ $[m/s^2]$ is the unknown external disturbance acting on the vehicle dynamics arising from environmental factors, such as variations in wind velocity and/or road slope.

Similarly, the leading vehicle, which imposes the reference behaviour for the whole vehicles platoon, is described by the following non-autonomous dynamical system [271]:

$$\begin{aligned} \dot{p}_0(t) &= v_0(t) \\ \dot{v}_0(t) &= u_0(t), \end{aligned} \tag{9.4}$$

where $p_0(t)$ $[m]$ and $v_0(t)$ $[m/s]$ are the leading vehicle absolute position (w.r.t. a given reference framework) and velocity, respectively; $u_0(t)$ $[m/s^2]$ the leader acceleration which can be computed as $\frac{1}{M_0}\tilde{u}_0(t)$, being M_0 $[kg]$ its mass and $\tilde{u}_0(t)$ $[kg\ m/s^2]$ the leader driving/brake force.

Given the autonomous vehicles platoon dynamics as in (9.3) and (9.4), the following assumptions hold.

Assumption 4 ([257])**.** *The unknown disturbances $w_i(t)$, $i = 1, \cdots, N$ are bounded, i.e. $|w_i(t)| < \bar{w}_i < +\infty$, with $\bar{w}_i$ are finite constant known to all vehicles.*

Assumption 5. *The leader behaviour is unknown, but bounded due to physical constraints [270], i.e.* $|u_0(t)| < u_0^{max} < +\infty$*, with the finite constant* u_0^{max} *known to all vehicles.*

Now the platooning control problem can be stated as follows.

Problem 2 (Platooning Control in fixed-time)**.** *Given a platoon composed of* N *connected autonomous vehicles plus a leader imposing the reference behaviour for the whole vehicular network, find a distributed control input* $u_i(t)$ $(\forall i = 1, \cdots, N)$ *such that each vehicle* i*, in a fixed-time* $T^\star$*, tracks the leader motion* $v_0(t)$ *while maintaining a desired inter-vehicular distance* d_{ij} *w.r.t. its neighbours* j $(j = 0, 1, 2, \cdots, N)$*, i.e.*

$$\begin{aligned} \lim_{t \to T^\star} \|p_i(t) - p_j(t) - d_{ij}\| = 0, \\ \lim_{t \to T^\star} \|v_i(t) - v_0(t)\| = 0, \end{aligned} \tag{9.5}$$

where $T^\star < T_{max} < +\infty$*, being* T_{max} $[s]$ *the settling time estimation, independent from the platoon initial conditions and computed according to Definition 2.*

9.4 Distributed Fixed-Time Platooning Control

This section introduces a novel distributed fixed-time control protocol able to solve Problem 2. Then, the fixed-time stability of the vehicular network under the action of the proposed controller is analytically proved.

9.4.1 Control Design

Define for each vehicle i ($\forall i = 1, \cdots, N$) the position and velocity tracking errors vectors as

$$\delta_{pi}(t) = \sum_{j=1}^{N} a_{ij}(p_i(t) - p_j(t) - d_{ij}) + b_i(p_i(t) - p_0(t) - d_{i0}) \tag{9.6}$$

$$\delta_{vi}(t) = \sum_{j=1}^{N} a_{ij}(v_i(t) - v_j(t)) + b_i(v_i(t) - v_0(t)), \tag{9.7}$$

where a_{ij} and b_i model the network communication topology as defined in Sec. 3.1.2.
By introducing the state error of the $i-$th vehicle w.r.t. the leader as

$$\begin{aligned} \tilde{p}_i(t) &= p_i(t) - p_0(t) - d_{i0}, \\ \tilde{v}_i(t) &= v_i(t) - v_0(t), \end{aligned} \tag{9.8}$$

the disagreement vectors in (9.6) and (9.7) can be recast as

$$\delta_{pi}(t) = \sum_{j=1}^{N} a_{ij}(\tilde{p}_i(t) - \tilde{p}_j(t)) + b_i\tilde{p}_i(t) \tag{9.9}$$

$$\delta_{vi}(t) = \sum_{j=1}^{N} a_{ij}(\tilde{v}_i(t) - \tilde{v}_j(t)) + b_i\tilde{v}_i(t). \tag{9.10}$$

Now, taking into account the definition of the disagreement vectors as in (9.9) and (9.10), from (9.3) and (9.4), the error tracking dynamics can be derived as

$$\begin{aligned} \dot{\delta}_{pi}(t) &= \delta_{vi}(t), \\ \dot{\delta}_{vi}(t) &= \sum_{j=1}^{N} a_{ij}\Big(u_i(t) + w_i(t) - u_j(t) - w_j(t)\Big) \\ &\quad + b_i\Big(u_i(t) + w_i(t) - u_0(t)\Big). \end{aligned} \tag{9.11}$$

Now, to solve the fixed-time platooning control as stated in Problem 2, the following integral sliding surface for each vehicle i is introduced:

$$\begin{aligned} \sigma_i(t) = \delta_{iv}(t) + \int_0^t & k_{i1}(\lceil \delta_{p_i}(s) \rfloor^{\gamma_1} + \lceil \delta_{p_i}(s) \rfloor + \lceil \delta_{p_i}(s) \rfloor^{\gamma_1^{'}}) \\ & + k_{i2}(\lceil \delta_{v_i}(s) \rfloor^{\gamma_2} + \lceil \delta_{v_i}(s) \rfloor + \lceil \delta_{v_i}(s) \rfloor^{\gamma_2^{'}}) ds \end{aligned} \tag{9.12}$$

where k_{i1}, k_{i2}, $\gamma_{1,2}$ and $\gamma_{1,2}^{'}$ have to be chosen according to Lemma 9. Specifically, regarding the choice of k_{i1}, k_{i2}, since the error dynamics as in (9.11) is of order $n = 2$, it is sufficient selecting k_{i1} and $k_{i2} \in \mathbb{R}_+$. In view of (9.12), for each vehicle i, the following distributed fixed-time control protocol is proposed:

$$\begin{aligned} u_i(t) = -\Big(\sum_{j=1}^{N} a_{ij} + b_i\Big)^{-1} &(k_{i1}(\lceil \delta_{p_i}(t) \rfloor^{\gamma_1} + \lceil \delta_{p_i}(t) \rfloor \\ &+ \lceil \delta_{p_i}(t) \rfloor^{\gamma_1'}) + k_{i2}(\lceil \delta_{v_i}(t) \rfloor^{\gamma_2} + \lceil \delta_{v_i}(t) \rfloor + \lceil \delta_{v_i}(t) \rfloor^{\gamma_2'} \\ &- \sum_{j=1}^{N} a_{ij} u_j(t) + \lceil \sigma_i(t) \rfloor^{p} + \lceil \sigma_i(t) \rfloor + \lceil \sigma_i(t) \rfloor^{q} \\ &+ \kappa_i \mathrm{sign}(\sigma_i(t))) \end{aligned} \tag{9.13}$$

being $p \in (0,1)$, $q \in (1,\infty)$ and κ_i a control gain to be properly tuned.

9.4.2 Stability Analysis

The fixed-time stability of the heterogeneous autonomous vehicles platoon under the action of the proposed controller in (9.13) is guaranteed by the following theorem.

Theorem 3. *Consider a platoon composed of N heterogeneous vehicles plus a leader imposing the reference behaviour, whose dynamics are as in* (9.3) *and* (9.4)*, respectively. Let Assumptions 4 and 5 hold. The Problem 2 is solved in a fixed-time $T^\star$ by the distributed control input* (9.13) *if one selects the control κ_i, $\forall i$ as:*

$$\kappa_i \geq \sum_{j=1}^{N} a_{ij}(\bar{w}_i + \bar{w}_j) + b_i(\bar{w}_i + u_0^{max}), \tag{9.14}$$

being $\bar{w}_i$ and $\bar{w}_j$ the known upper bound of the external disturbances acting on the vehicles i and j, respectively, and u_0^{max} the maximum known value of the leader acceleration.

Proof. Consider the following candidate Lyapunov function:

$$V = \frac{1}{2}\sum_{i=1}^{N} \sigma_i^2(t). \tag{9.15}$$

Differentiating (9.15), by taking into account the definition of the sliding surface as in (9.12) as well as the error tracking dynamics as in (9.11), it is possible to obtain:

$$\begin{aligned}\dot{V} = &\sum_{i=1}^{N} \sigma_i(t)\Big((\sum_{j=1}^{N} a_{ij} + b_i)u_i(t) - \sum_{j=1}^{N} a_{ij}u_j(t)\\ &+ k_{i1}(\lceil\delta_{p_i}(t)\rfloor^{\gamma_1} + \lceil\delta_{p_i}(t)\rfloor + \lceil\delta_{p_i}(t)\rfloor^{\gamma_1^{'}})\\ &+ k_{i2}(\lceil\delta_{v_i}(t)\rfloor^{\gamma_2} + \lceil\delta_{v_i}(t)\rfloor + \lceil\delta_{v_i}(t)\rfloor^{\gamma_2^{'}})\\ &+ \sum_{j=1}^{N} a_{ij}(w_i(t) - w_j(t)) + b_i(w_i(t) - u_0(t))\Big).\end{aligned} \tag{9.16}$$

Now, substituting the control input (9.13) in (9.16), after some algebraic manipulation, it is possible to write:

$$\begin{aligned}\dot{V} = -&\sum_{i=1}^{N}\Big(|\sigma_i(t)|^{p+1} + |\sigma_i(t)|^2 + |\sigma_i(t)|^{q+1} + \kappa_i|\sigma_i(t)|\\ &- \sum_{j=1}^{N} a_{ij}w_j(t)|\sigma_i(t)| - (\sum_{j=1}^{N} a_{ij} + b_i)w_i(t)|\sigma_i(t)|\\ &- b_i|\sigma_i(t)|u_0(t)\Big).\end{aligned} \tag{9.17}$$

Now, consider the Assumptions 4 and 5, and select the control gains $\kappa_i,\ i = 1, \cdots, N$ as in (9.14). In so doing, leveraging also Lemma 10, (9.17) can be recast as

$$\begin{aligned}\dot{V}(t) &\leq -\sum_{i=1}^{N}\Big(|\sigma_i(t)|^{p+1} + |\sigma_i(t)|^2 + |\sigma_i(t)|^{q+1}\Big)\\ &\leq -\Big(\sum_{i=1}^{N}|\sigma_i(t)|^2\Big)^{\frac{p+1}{2}} - N^{\frac{1-q}{2}}\Big(\sum_{i=1}^{N}|\sigma_i(t)|^2\Big)^{\frac{q+1}{2}}.\end{aligned} \tag{9.18}$$

Considering the Lyapunov function as in (9.15), inequality (9.18) can be finally re-written as

$$\dot{V}(t) \leq -2^{\frac{p+1}{2}}V(t)^{\frac{p+1}{2}} - 2^{\frac{q+1}{2}}N^{\frac{1-q}{2}}V(t)^{\frac{q+1}{2}}. \tag{9.19}$$

Hence, according to the fixed-time stability theory (see Definition 2), the sliding surface $\sigma_i(t)$ ($\forall i = 1, \cdots, N$) converges to zero in a fixed-time

$T_1 \le \frac{1}{2^{\frac{1+q}{2}}(1-p)} + \frac{1}{2^{\frac{q+1}{2}}N^{\frac{1-q}{2}}(q-1)}$.

Note that, during the sliding motion, i.e. when $\sigma_i(t) = 0$, it is possible to obtain $\dot{\sigma}_i(t) = 0$. This implies that, according to (9.11) and (9.12), for $t \ge T_1$, the reduced closed-loop error dynamics can be derived as

$$\begin{aligned} \dot{\delta}_{p_i}(t) &= \delta_{v_i}(t), \\ \dot{\delta}_{v_i}(t) &= -k_{i1}(\lceil \delta_{p_i}(t) \rfloor^{\gamma_1} + \lceil \delta_{p_i}(t) \rfloor + \lceil \delta_{p_i}(t) \rfloor^{\gamma_1'}) \\ &\quad - k_{i2}(\lceil \delta_{v_i}(t) \rfloor^{\gamma_2} + \lceil \delta_{v_i}(t) \rfloor + \lceil \delta_{v_i}(t) \rfloor^{\gamma_2'}). \end{aligned} \tag{9.20}$$

From Lemma 9, the reduced closed-loop error system (9.20) is fixed-time stable at the origin. It follows that $\delta_{pi}(t),\ \delta_{vi}(t) \to 0$ $(\forall i)$ in a settling time T_2 that is independent of any initial condition.

Accordingly, $\tilde{p}_i(t),\ \tilde{v}_i(t) \to 0$ $(\forall i)$. Indeed, by introducing the global error vectors $\delta_p(t) = [\delta_{p1}(t), \delta_{p2}(t), \cdots, \delta_{pN}(t)]^\top \in \mathbb{R}^N$, $\delta_v(t) = [\delta_{v1}(t), \delta_{v2}(t), \cdots, \delta_{vN}(t)]^\top \in \mathbb{R}^N$ $\tilde{p}(t) = [\tilde{p}_1(t), \tilde{p}_2(t), \cdots, \tilde{p}_N(t)]^\top \in \mathbb{R}^N$ and $\tilde{v}(t) = [\tilde{v}_1(t), \tilde{v}_2(t), \cdots, \tilde{v}_N(t)]^\top \in \mathbb{R}^N$, according to (9.9) and (9.10), one can express the disagreement vector as function of (9.8) as

$$\begin{aligned} \delta_p(t) &= (\mathcal{L} + \mathcal{B})\tilde{p}(t), \\ \delta_v(t) &= (\mathcal{L} + \mathcal{B})\tilde{v}(t). \end{aligned} \tag{9.21}$$

Given the Assumption 1, it follows that $\mathcal{L}+\mathcal{B}$ is a non-singular diagonally dominant M-matrix and all its eigenvalues have positive real parts. This assumption holds since $\mathcal{L} + \mathcal{B}$ is a positive definite $M-$matrix, $\delta_p(t),\ \delta_v(t) \to 0$ in a fixed-time implies that $\tilde{p}(t),\ \tilde{v}(t) \to 0$.

Therefore, each vehicle within the platoon tracks the leader behaviour while maintaining the formation in a fixed-time $T^\star \le T_{max} = T_1 + T_2$, depending on the proper choice of the control gains. In so doing the statement is proven. □

9.5 Numerical Analysis

In this section, the effectiveness of the proposed distributed sliding mode control approach in guaranteeing the fixed-time leader-tracking consensus is validated considering an exemplar heterogeneous platoon composed of

$N = 5$ vehicles plus a leader and leveraging MiTraS Integrated Simulation Environment. In the designed scenario, it is assumed that the leading vehicle moves according to a trapezoidal velocity profile. Specifically, it drives at an initial velocity of 15 $[m/s]$. At $t = 15$ $[s]$ it begins accelerating with a constant acceleration of 2 $[m/s^2]$ until reaching the constant velocity of 25 $[m/s]$. Then, at $t = 32$ $[s]$ it starts decelerating with a constant deceleration of -1.9 $[m/s^2]$ until reaching the final constant velocity of 10 $[m/s]$. External disturbances are chosen as

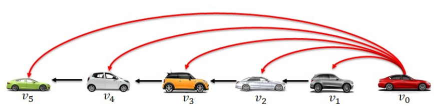

Figure 9.1: Exemplar platoon of five heterogeneous vehicles plus a leader connected via the L-P-F topology.

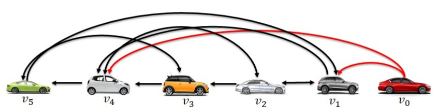

Figure 9.2: Exemplar platoon of five heterogeneous vehicles plus a leader connected via a Random topology.

Mass m_i $[kg]$	$m_0 = 1400,\ m_1 = 1500,\ m_2 = 1445,$ $m_3 = 1550,\ m_4 = 1200,\ m_5 = 1600$
Max acceleration $[ms^{-2}]$	5
Min acceleration $[ms^{-2}]$	-5
Desired spacing policy d_{ij} $[m]$	20
Control parameter p	0.5
Control parameter q	1.5
Control parameter γ_1	0.53
Control parameter $\gamma_1^{'}$	1.85
Control parameter γ_2	0.7
Control parameter $\gamma_2^{'}$	1.3
Control gains k_{i1} $[s^{-2}]$	0.1 $\quad \forall i = 1, \cdots, 5$
Control gains k_{i2} $[s^{-1}]$	1.1 $\quad \forall i = 1, \cdots, 5$

Table 9.1: Vehicle and Control parameters.

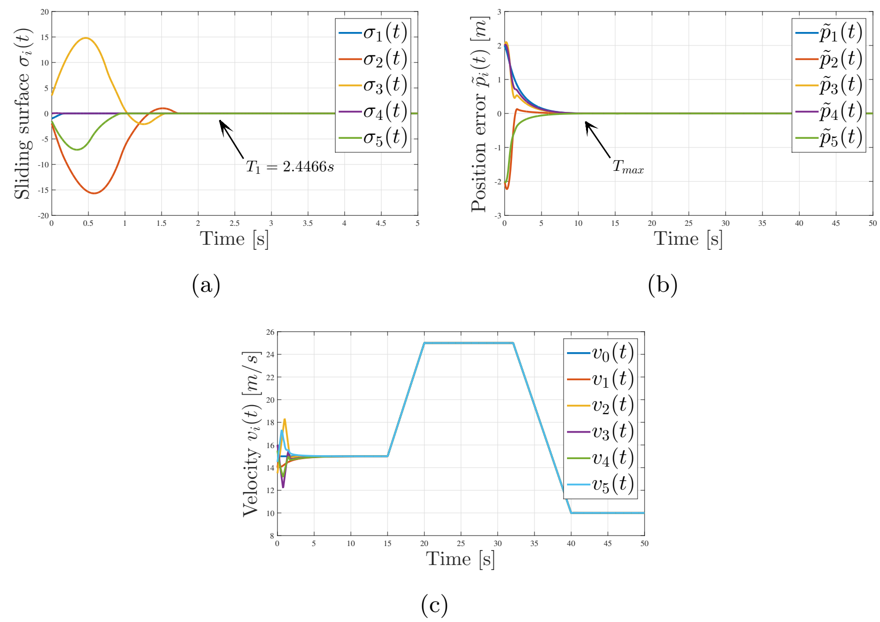

Figure 9.3: Leader-tracking performance under the control in (9.13). Leader-Predecessor-Follower topology scenario. Time history of: (a) sliding surface $\sigma_i(t)$ $(i = 1, 2, 3, 4, 5)$; (b) position error $\tilde{p}_i(t) = p_i(t) - p_0(t) - d_{i0}$ $(i = 1, 2, 3, 4, 5)$; (c) vehicles velocity $v_i(t)$ $(i = 0, 1, 2, 3, 4, 5)$.

$w_1(t) = 0.2\sin(0.5t)$, $w_2(t) = 0.2\sin(0.1t)$, $w_3(t) = 0.3\sin(t)$, $w_4(t) = 0.6\sin(t)$ and $w_5(t) = 0.1\sin(0.1t)$.

The vehicle parameters as well as the control ones, selected according to Definition 2 and Lemma 9, are reported in Tab. 9.1. To disclose the effectiveness of the control strategy and how it can ensure the leader-tracking in a fixed-time (which only depends on the proper choice of the control gains and not on any vehicles initial condition), two representative scenarios are considered where different initial conditions as well as different communication networks are considered, namely: *i*) L-P-F topology case (Fig. 9.1); *ii*) Random topology scenario (Fig. 9.2).

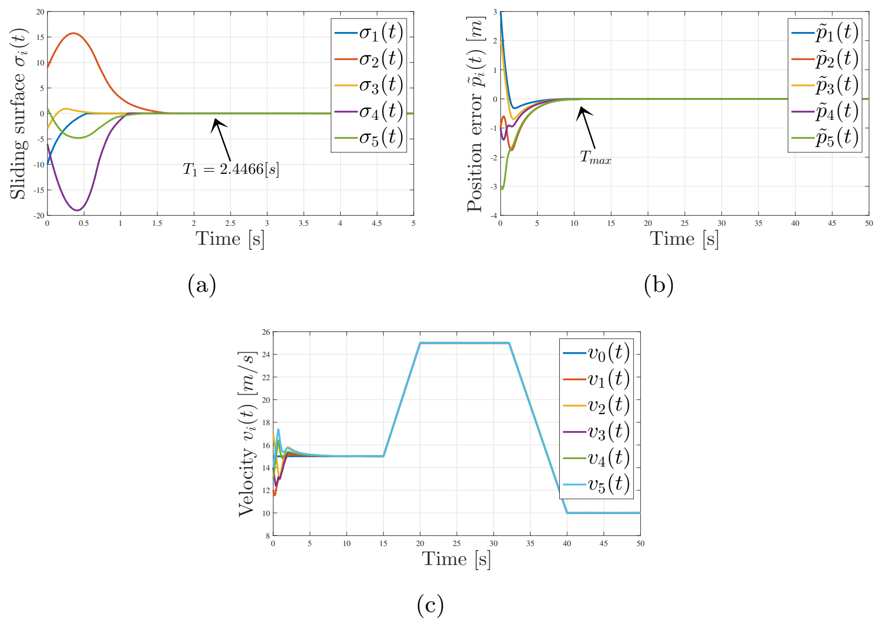

(a) (b) (c)

Figure 9.4: Leader-tracking performance under the control in (9.13). Random topology scenario. Time history of: (a) sliding surface $\sigma_i(t)$ ($i = 1, 2, 3, 4, 5$); (b) position error $\tilde{p}_i(t) = p_i(t) - p_0(t) - d_{i0}$ ($i = 1, 2, 3, 4, 5$); (c) vehicles velocity $v_i(t)$ ($i = 0, 1, 2, 3, 4, 5$).

9.5.1 Leader-Predecessor-Follower Topology Scenario

In the first driving scenario, vehicles are connected through the common L-P-F topology, where each vehicle shares information with its predecessor and the leader. The position/velocity initial conditions for this scenario, as well as the control gains tuned according to Theorem 3 are listed in Tab. 9.2.

Results in Fig. 9.3 confirm the theoretical derivation and disclose the effectiveness of the proposed fixed-time controller in guaranteeing the leader-tracking in a settling time $T^\star \leq T_{max} = T_1 + T_2 \approx 10$ $[s]$. Specifically, Fig. 9.3 (a) shows the time history of the sliding surface which converges to zero in a finite settling time $T_1 \approx 2.45$ $[s]$. Conversely, Fig.s 9.3 (b)-(c), disclosing the time histories of the position error $\tilde{p}_i(t)$ ($\forall i = 1, \cdots, 5$) and the vehicles velocities $v_i(t)$ ($\forall i = 0, 1, \cdots, 5$), highlight that, once the manifold $\gamma_i = 0$ ($\forall i$) is reached, each vehicle tracks the leader motion (Fig. 9.3(c)) while maintaining the desired spacing distance (Fig. 9.3(b)) in $T_2 \approx 7.55$ $[s]$.

9.5.2 Random Topology Scenario

In this operating scenario, it is assumed that vehicles are connected through the random communication topology depicted in Fig. 9.2, where the leader information is available just for a subset of vehicles, i.e. the first and fourth. The position/velocity initial conditions for this scenario, as well as the control gains tuned according to Theorem 3 are listed in Tab. 9.3.

Fig. 9.4 confirms the theoretical derivation also for this operative scenario and disclose how, despite the changing of vehicles initial conditions and the network communication topology, the proposed control approach ensures the leader-tracking in the fixed-time $T^\star \leq T_{max} = T_1 + T_2 \approx 10$ $[s]$ (equal to one obtained into the L-P-F scenario). Note that this result is consistent with the theoretical derivation and proves the ability of the proposed distributed fixed-time controller in solving Problem 2 in a settling time which is fixed and independent from any initial conditions. Specifically, Fig. 9.4 (a) shows the time history of the sliding surface which converges to zero in a finite settling time $T_1 \approx 2.45$ $[s]$, despite the changing of initial conditions and the network connections. Conversely, Fig. 9.4s (b)-(c), disclosing the time histories of the position error $\tilde{p}_i(t)$ $(\forall i = 1, \cdots, 5)$ and the vehicles velocities $v_i(t)$ $(\forall i = 0, 1, \cdots, 5)$, highlight that, once the manifold $\gamma_i = 0$ $(\forall i)$ is reached, each vehicle, under the action of the proposed controller, tracks the leader motion (see Fig. 9.4(c)) while maintaining the desired spacing distance (see Fig. 9.4(b)) in $T_2 \approx 7.55$ $[s]$.

Initial position $[p_0(0), \cdots, p_5(0)]^\top$ $[m]$	$[100, 82, 58, 42, 22, -2]$
Initial velocity $[v_0(0), \cdots, v_5(0)]^\top$ $[ms^{-1}]$	$[15.0, 14.0, 13.5, 16.0, 15.5, 14.5]$
Control gains $[\kappa_1, \cdots, \kappa_5]$ $[s^{-2}]$	$[5.7, 5.94, 6.14, 6.8, 6.06]$

Table 9.2: Simulation parameters for the L-P-F topology scenario.

Initial position $[p_0(0), \cdots, p_5(0)]^\top$ $[m]$	$[103, 86, 62, 45, 21, 0]$
Initial velocity $[v_0(0), \cdots, v_5(0)]^\top$ $[ms^{-1}]$	$[15, 12, 17, 14, 13, 14]$
Control gains $[\kappa_1, \cdots, \kappa_5]$ $[s^{-2}]$	$[6.15, 1.3, 1.15, 8.07, 1.15]$

Table 9.3: Simulation parameters for Random topology scenario.

9.6 Concluding Remarks

This sections has addressed the fixed-time leader-tracking control problem for heterogeneous uncertain autonomous connected vehicles platoons via a distributed sliding-mode based control approach. Leveraging the fixed-time stability tools and the Lyapunov theory, it has analytically proved how the proposed distributed control strategy can ensure the leader-tracking in a fixed-time which only depends on the proper choice of the control gains, and not on any vehicles initial conditions. Moreover an estimation of this settling time has been provided. Numerical analysis, carried out considering two exemplar driving scenarios, have confirmed the theoretical derivation and have disclosed the effectiveness of the distributed fixed-time protocol in solving the leader-tracking problem in a finite settling time.

CHAPTER 10

Distributed Nonlinear Model Predictive Control for Connected Autonomous Electric Vehicles Platoon with Distance-Dependent Air-Drag Formulation

This chapter deals with the leader-tracking problem for a platoon of heterogeneous autonomous, connected, fully-electric vehicles, where the selection of the inter-vehicle distance between adjacent vehicles plays a crucial role in energy consumption reduction. In this framework, a cooperative driving control strategy lets electric vehicles move as a convoy while keeping a variable energy-oriented inter-vehicle distance between adjacent vehicles is designed. To this aim, by exploiting a distance-dependent air drag coefficient formulation, a novel DNMPC is proposed, which cost function is designed to ensure leader-tracking performances and optimise the inter-vehicle distance to reduce energy consumption. Extensive simulation analyses, involving a comparative analysis compared to to the classical CTG spacing policy, are performed to confirm the capability of the DNMPC in guaranteeing energy saving.

10.1 Energy-Saving Challenge in Platooning Applications

Electric Vehicles (EVs) are considered the most promising and viable near-term technology to reduce the exploitation of fossil fuels and resulting greenhouse gas (GHG) emissions produced by ICE vehicles [4]. Although sustainability and environmental benefits may have a significant influence on the EVs adoption, they are usually behind performance in the customers' ranking [302]; it follows that the maximisation of range autonomy of EV is a crucial aspect for their massive market deployment. An efficient solution to improve the energy performance of EVs is to operate along with the road platoons of Connected Autonomous Distributed Electric Vehicles (CADEVs) since they could bring many benefits in terms of driving safety and comfort, as well as the traffic congestion [303]. It is well known that, when in a platoon, vehicles move in a fleet tracking the desired velocity profile (provided by the leading vehicle or by an external infrastructure) while maintaining a small inter-vehicle distance to reduce air resistance and energy consumption [304, 256, 71]. Due to the advantages mentioned above, platooning control problem for ICE vehicles has become a hot research topic during the last decades in automotive and intelligent transportation research fields [305]. For instance, recent control solution have been suggested in [306, 287, 307, 114]. Specifically, a proportional-derivative based CACC controller has been suggested in [306] to address the problem of CAVs platoon under a dynamic information flow topology that allows considering communication failures, while also Denial-of-Service (DoS) attacks phenomena have been tackled in [287] via a sampled-data diffusive control law whose exponential stability analysis is proven by exploiting time-delay system theory. Instead, the coexistence of CAVs and Human-driven Vehicles (HDVs) on the road has been considered in [307, 114], where new modelling for the mimicking of the mixed platoon has been introduced by leveraging MASs theory and car-following model, while consensus controllers have been used to stabilize the overall mixed vehicular network. The problem of heterogeneous vehicle platoons affected by model uncertainties and external disturbances was addressed in [265], where authors developed a tube-based MPC aiming at guaranteeing leader-tracking purpose in the presence of spatial-geometry constraints.

Although the deployment of CADEVs is going to play a crucial role for the eco-intelligent transportation systems, few works explore the energy-saving benefit of EVs platoon consisting of more than two vehicles [308, 309, 310].

In addition to considering a platoon of CADEVs with a comprehensive dynamical model to represent all the required internal components, another crucial issue to be tackled in platooning application for energy-saving purposes is the choice of the spacing policy to impose between adjacent vehicles. Most commonly used spacing policies are described in detail in Sec. 3.1.3.

Based on these facts, it is possible to observe that both the selection of the platoon control protocol and the selection of the spacing policy are pertinent with the aerodynamic interactions among the vehicles belonging to the platoon [311]. The drag force generated on a vehicle consists of two main components, namely: *i*) the skin friction drag; *ii*) the form drag. The skin friction drag depends mainly on the roughness and the total area of the vehicle subjected to the air flow; hence it is not affected by the distance gap between vehicles. On the other hand, the form drag is affected by the distance between consecutive vehicles travelling a platoon/convoy. At steady-state operation, the aerodynamic drag coefficient depends on the specific position of each vehicle within the platoon, and it is usually assumed to be known and constant. Conversely, during the transient phase associated with different manoeuvres (e.g., acceleration or braking), the aerodynamic effects result in significant variations of the air drag coefficient that should be taken into account [311]. Indeed, for each vehicle belonging to the platoon, the coefficient of the air-drag force varies as a function of the distance to the predecessor vehicle. This distance-dependent formulation should be considered from the initial control design phase to explicitly consider the impact of the spacing policy on the aerodynamic forces, especially from an energy-saving point of view [311, 312, 313]. Along this line, [311] addresses the longitudinal platoon control problem with more precise modelling of the effects of the air-drag force via two $\mathcal{H}_\infty$ controller able to guarantee the string stability and the achievement of smaller spacing errors without aggressive manoeuvres, respectively. The same distance-dependent air-drag formulation has been used in [312] for heavy-duty fuel vehicle platoon with the aim of safely and fuel-efficiently coordinating its motion. Again, considering the same air drag formulation, [313] introduces a stochastic optimisation procedure aiming at finding both controller parameters and an optimal CTG spacing policy by taking into account disturbances and transmission time delays.

From the literature overview on platooning control, it is clear that the choice of the spacing policy plays a crucial role in guaranteeing energy-saving requirements, especially in electric vehicle platooning, where battery management strongly affects the vehicle life cycle. Therefore, avoiding energy waste is very crucial for prolonging the life-cycle of the battery [314]. To this end, here, by embedding a distance-dependent air drag formulation into the vehicle prediction model, an energy-saving oriented DNMPC for a heterogeneous platoon of CADEVs to guarantee a threefold control objective is designed: *i*) to ensure that each vehicle tracks the leader speed profile, assumed to be already optimised in terms of energy consumption and directly or indirectly known by each vehicle within the platoon; *ii*) to compute, for each time instant, the optimal variable inter-vehicle distance from the vehicle ahead by taking into account safety and road capacity constraints, as well as electric power saving requirement and distance-dependent air-drag formulation; *iii*) to guarantee the minimisation of the required battery power, thus achieving energy saving objective. Note that the proposed energy-oriented architecture computes a variable inter-vehicle gap-distance that directly impacts the air drag coefficient. In so doing, based on typical values of minimum and maximum values of time-gap [79], inter-vehicle distance constraints are defined to guarantee a trade-off between smaller inter-vehicles distances, which increase the rear-end collisions risk, and larger spacing that, instead, reduce the road capacity. An extensive numerical analysis carried out in MiTraS, involving a comparison analysis compared to a typical CTG spacing policy and a discussion about the computational load, confirms the benefits of the proposed control approach in ensuring energy saving.

10.2 E-Platoon Modelling and Control Objectives

Consider an heterogeneous e-platoon consisting on N vehicles plus a additional one, labelled as 0, acting as a leader in providing the reference behaviour to the whole vehicular network. The platoon is arranged as a convoy, with vehicles travelling along a straight road and able to share their position, speed and acceleration information via V2V wireless communication networks (based on IEEE 802.11p communication standard or 5G communication) [43, 315]. In the appraised technological scenario, each Electric Vehicle (EV) is equipped with on-board inertial sensor and GPS receiver for measuring its state information, as well as with transmitting devices enabling the connectivity among vehicles within the e-platoon [316]. The aim is to guarantee that each EV tracks the leader behaviour while maintaining a safe and energy-saving oriented inter-vehicle distance compared to the predecessor vehicle ahead. Indeed, the desired optimal gap distance is properly computed in order to reduce the energy consumption of each i-th vehicle within the platoon by acting on air-drag coefficient reduction, which varies as a function of inter-vehicle distance.

In the sequel, a detailed model of the EV by describing its nonlinear longitudinal dynamics is given.

10.2.1 Nonlinear Longitudinal EV Model

The longitudinal behaviour of each EV i ($\forall i = 1, \cdots N$) can be depicted by the following nonlinear dynamics [90, 317, 9, 318]:

$$\begin{aligned}
\dot{p}_i(t) &= v_i(t) \\
\dot{v}_i(t) &= \frac{\eta_i}{r_i m_i} u_i(t) - gsin(\theta_i(t)) - gcos(\theta_i(t)) \frac{C_r}{1000}(c_1 v(t) + c_2) \\
&\quad - \frac{\rho_{air}}{2m_i(t)} C_{D_i}(d_{i,i-1}(t)) A_{f_i} v_i^2(t),
\end{aligned} \tag{10.1}$$

being $p_i(t)$ $[m] \in \mathbb{R}$ and $v_i(t)$ $[m/s] \in \mathbb{R}$ the position and the speed of vehicle i; $u_i(t)$ $[Nm]$ is the control input representing the vehicle propulsion torque; m_i $[kg]$ is the mass of vehicle; η_i is the drive-train efficiency; r_i $[m]$ is the radius of the wheel; the parameters C_r, c_1 and c_2

are related to the rolling resistance force and vary on basis of the road surface condition and the type of the vehicle tire; ρ_{air} $[kg/m^3]$ is the air density; A_{f_i} $[m^2]$ is the frontal area of vehicle i; g $[m/s^2]$ is the gravity acceleration, while $\theta_i(t)$ $[rad]$ is the road-track slope. Furthermore, $C_{D_i}(d_{i,i-1}(t))$ is the vehicle drag coefficient of vehicle i, which varies on the basis of the distance compared to the ahead $(i-1)$ vehicle as [313]:

$$C_{D_i}(d_{i,i-1}(t)) = C_a\left(1 - \frac{C_b}{C_c + d_{i,i-1}(t)}\right), \tag{10.2}$$

where C_a is the i-th vehicle air-drag coefficient in the absence of any slipstream, i.e. it represents the leading vehicle air-drag coefficient, while C_b and C_c are positive constants, whose value have been experimental found in [319]. Note that drag coefficient formulation as in (10.2) takes into account the fact that the air-drag force is strictly related to both vehicle shape and airflow around it. Indeed, the aerodynamic resistance depends on how fast and uniformly the air cut by the vehicle rejoins the vehicle downstream, i.e., turbulence level and wake shape. This implies that, when the shape of a vehicle is streamlined or a vehicle follows another one at closer spacing, the aerodynamic resistance is lower (see [45] and references therein). Moreover, some experimental works on the aerodynamic interactions among the vehicles in convoys are presented in the technical literature about automated highway systems [2, 320] and based on them, the air-drag coefficients are found. By exploiting state space formalism and by introducing the state vector for the vehicle i as $x_i(t) = [p_i(t),\ v_i(t)] \in \mathbb{R}^{2\times 1}$, the nonlinear system in (10.1) $\forall i \in \{1, \ldots, N\}$ can be re-written in a more compact notation as [317]:

$$\dot{x}_i(t) = \begin{bmatrix} v_i(t) \\ \varphi_i(v_i(t)) \end{bmatrix} + \begin{bmatrix} 0 \\ b_i \end{bmatrix} u_i(t), \tag{10.3}$$

being $b_i = \eta_i/(m_i R_i)$, while $\varphi_i(v_i(t)) \in \mathbb{R}$ is nonlinear vector field, assumed to be bounded, continuous and differentiable. On the other hand, the leader dynamics acting as a reference for the whole vehicular network is described by the following autonomous nonlinear system:

$$\dot{x}_0(t) = \begin{bmatrix} v_0(t) \\ \varphi_0(v_0(t)) \end{bmatrix} \tag{10.4}$$

where $x_0(t) = [p_0(t),\ v_0(t)] \in \mathbb{R}^{2\times 1}$ the leader state vector, with $p_0(t)$ $[m]$ and $v_0(t)$ $[m/s]$ its position and speed, respectively.

10.3 Design of Distributed Distance-Based Nonlinear Model Predictive Control

E-platoon control aim is to guarantee that each EV i ($\forall i = 1, \dots, N$), in a distributed fashion, tracks the leading vehicle dynamics, which provides an optimal reference behaviour guaranteeing the safety and the energy-saving requirements by explicitly taking into account air-drag reduction due to the presence of distance-dependent air drag coefficient $C_{D_i}(d_{i,i-1}(t))$. More specifically, the objective is to design a distributed controller $u_i(t)$ in (10.3) for each vehicle i such that $\forall i \in \{1, \dots, N\}$:

$$\begin{aligned}
&\lim_{t\to\infty} \|v_i(t) - v_0(t)\| = 0;\\
&\lim_{t\to\infty} \|p_i(t) - p_0(t) - \tilde{d}_{i,0}(t)\| = 0;\\
&u_i = arg\Big(\min_{u_i} P_{req,i}(u_i(t), \tilde{d}_{i,i-1}(t))\Big),
\end{aligned} \tag{10.5}$$

being $\tilde{d}_{i,0}(t)$ the desired spacing policy between vehicle i and vehicle 0 while and $\tilde{d}_{i,i-1}(t)$ is the desired one between vehicle i and its predecessor $i-1$. Note that these desired safe distances are computed by considering safety constraints without assuming a fixed time-headway value.

To fulfil (10.5), the energy-optimal control input $u_i(t)$ is designed via a DNMPC strategy as the solution of the following constrained multiple optimisation problem.

Problem $\mathcal{F}_i$: Let Assumption 1. Given the optimal reference trajectory to be tracked, i.e. $x_0(t)$, and the information sent by neighbouring vehicles

$\mathcal{N}_i$, for each vehicle i, find $u_i(t)$ such that, at each time instant t:

$$\min_{u_i} \mathcal{J}_i = \int_t^{t+T} L_i(x_i^p(\tau,t), x_i^a(\tau,t), x_0(\tau,t), x_j^a(\tau,t), \tilde{d}_{i,i-1}(\tau,t), u_i^p(\tau,t))d\tau$$

$$\begin{aligned} &\text{subject to} \\ &\dot{x}_i = f_i(x_i, u_i) \\ &x_i^p(\tau,t) = x_i(t) \\ &u_i^p(\tau,t) = h_i(v_i^p(t)) \\ &v_{i,\min} \leq v_i(\tau,t) \leq v_{i,\max} \\ &a_{i,\min} \leq a_i(\tau,t) \leq a_{i,\max} \\ &u_{i,\min} \leq u_i(\tau,t) \leq u_{i,\max} \\ &d_{i,i-1}^{min}(t) \leq \tilde{d}_{i,i-1}(\tau,t) \leq d_{i,i-1}^{max}(t) \end{aligned} \tag{10.6}$$

where u_i and u_i^p denote the unknown control input to be optimised and its prediction, respectively; $x_i^p(\tau,t)$ and $x_i^a(\tau,t)$ are the predicted and the assumed state of the EV i, respectively; $x_j^a(\tau,t)$ is the assumed state of the communicating EV j ($\forall j \in \mathcal{N}_i$); $h_i(v_i^p(t)) = \frac{R_i}{\eta_i}\varphi_i(v_i^p(t))$ is used to counterbalance the external forces [89]; $(\cdot)_{max}$ and $(\cdot)_{min}$ stand for the maximum and the minimum bounds for the related variable $(\cdot)$. More specifically, $d_{i,i-1}^{max}(t)$ and $d_{i,i-1}^{min}(t)$ are related to the maximum and minimum allowed inter-vehicle distances between vehicle i and its predecessor. To ensure emergency braking manoeuvres, as well as air drag reduction, they can be computed considering the minimum and maximum value of vehicle time-headway as [74]:

$$d_{i,i-1}^{min} = d_{st} + h_{min}v_i(t), \qquad d_{i,i-1}^{max} = d_{st} + h_{max}v_i(t), \tag{10.7}$$

being d_{st} $[m]$ the standstill distance, while h_{min} $[s]$ and h_{max} $[s]$ the lower and upper time-gap, commonly selected as $h_{min} = 0.4$ $[s]$ and $h_{max} = 1$ $[s]$ [79].
The integral part of the cost function $\mathcal{J}_i$ in (10.8), i.e. L_i, is designed as:

$$L_i = \omega_1 L_{i,1} + \omega_2 L_{i,2} + \omega_3 L_{i,3} + \omega_4 L_{i,4} + \omega_5 L_{i,5} + \omega_6 L_{i,6} + \omega_7 L_{i,7}, \tag{10.8}$$

where $\omega_1, \omega_2, \omega_3, \omega_4, \omega_5, \omega_6, \omega_7$ are positive weights to be properly selected and

$$L_{i,1} = \left(p_i^p(t) - p_0(t) - \tilde{d}_{i,0}(t)\right)^2 \tag{10.9a}$$

$$L_{i,2} = \left(v_i^p(t) - v_0(t)\right)^2 \tag{10.9b}$$

$$L_{i,3} = \sum_{j\in\mathcal{N}_i} \left(p_i^p(t) - p_j^a(t) - \tilde{d}_{i,j}(t)\right)^2 \tag{10.9c}$$

$$L_{i,4} = \sum_{j\in\mathcal{N}_i} \left(v_i^p(t) - v_j^a(t)\right)^2 \tag{10.9d}$$

$$L_{i,5} = \left(x_i^p(t) - x_i^a(t)\right)^2 \tag{10.9e}$$

$$L_{i,6} = \left(u_i^p(t) - h_i(v_i(t))\right)^2, \tag{10.9f}$$

$$L_{i,7} = P_{req,i}(t, u_i(t), \tilde{d}_{i,i-1}(t)) + P_{aux}. \tag{10.9g}$$

Note that, $L_{i,1}$ and $L_{i,2}$ in (10.9a)-(10.9b) guarantee that the i-th EV tracks the leader behaviour, with $L_{i,1} \neq 0$ and $L_{i,2} \neq 0$ if and only if $p_i = 1$, being p_i the pinning matrix element defined in Sec. 3.1.2; conversely if $p_i = 0$ the i-th EV is unable to directly know the leader behaviour so that $L_{i,1} = L_{i,2} = 0$. $L_{i,3}$ and $L_{i,4}$ in (10.9c)-(10.9d) ensure that the i-th EV tries to reach a coordination with the assumed trajectory of the j-th communicating EV and, hence, $L_{i,3} \neq 0$ and $L_{i,4} \neq 0$ for all $j \in \mathcal{N}_i$, being $\mathcal{N}_i$ the set of the neighbours of the i-th EV as defined in Sec. 3.1.2. Term $L_{i,5}$ in (10.9e) weights the deviations of the i-th EV state trajectories compared to the corresponding assumed state, which is its shifted last-step optimal state and sent to the EVs belonging the set $\mathcal{O}_i$; $L_{i,6}$ (10.9f) counterbalances the deviations of the input error from the equilibrium, according to [89]. Finally, $L_{i,7}$ in (10.9g) ensures the minimisation of the instantaneous power consumption.

It is worth noting that the DNMPC allows emulating the typical attitude of a driver by pre-estimating the trajectory that each EV has to maintain for a defined horizon [321]. Besides the advantages of this kind of controller, it is fundamental to choose a proper plant model to ensure coherence between reality and simulations, hence obtaining correct and effective results. However, more detailed vehicle models describing, for instance, both longitudinal and lateral dynamics, as well as the

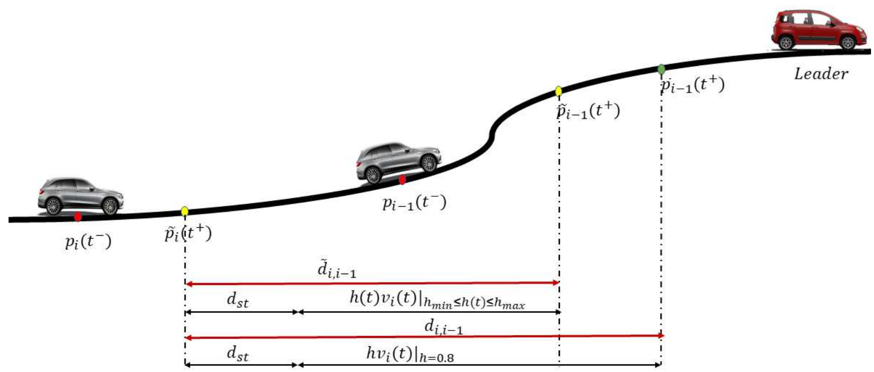

Figure 10.1: Energy-oriented optimal spacing policy for the EV i.

interaction forces [322, 323], require more computational resources and efforts. In this case, the requirement of high-performances architectures arises to deal with this kind of problem (see, e.g., [321]).

Note that, since the formulation of the spacing policy is not fixed, the procedure allows to embed within the architecture an energy oriented variable spacing policy that, unlike the classical CTG (with typical value of $h = 0.8$ $[s]$ [74]), guarantees the minimisation of the inter-vehicle distance between two adjacent EVs while satisfying safety requirements. This results in an air-drag reduction and, hence, in energy consumption improvement. Indeed, in so doing, for each time instant, the inter-vehicle gap distance between the i-th and its $i-1$-th predecessor is found according to constraints in (10.7), while ensuring the power optimisation as well as the air drag reduction.

To better disclose the advantages of exploiting this kind of energy-oriented spacing policy within the control design, the classical CTG spacing policy for the i-th EV with the proposed one is compared in Fig. 10.1. Herein, $p_i(t^-)$ and $p_{i-1}(t^-)$ are the positions of the i-th and $i-1$ EVs at time instant t^-, while $\tilde{p}_i(t^+)$ and $\tilde{p}_{i-1}(t^+)$ are the position of i-th and $i-1$ EVs at time instant t^+ by embedding them with our DNMPC. Instead, $\bar{p}_{i-1}(t^+)$ is the ideal position of the EV $i-1$ at time t^+ under CTG spacing policy with $h = 0.8$ $[s]$. Hence, two inter-vehicle distances can be considered: $\tilde{d}_{i,i-1}$ and $\bar{d}_{i,i-1}$, consisting of a common part, i.e. d_{st}, plus an additional term that depends on the time-headway value. As it is possible to observe, the suggested energy-oriented strategy permits to

Table 10.1: Heterogeneous Nonlinear Vehicles Parameters

Vehicle ID	m_i $[kg]$	η_i $[-]$	r_i $[m]$	$C_{a,i}$ $[-]$	$A_{f,i}$ $[m^2]$	a_{max} $[m/s^2]$	a_{min} $[m/s^2]$	$C_{batt,i}$ $[Ah]$	$n_{b,i}$ $[-]$	$\eta_{batt,i}$ $[-]$
0	1545	0.89	0.3060	0.28	2.3315	2.5	-6.0	65	96	0.97
1	1015	0.89	0.2830	0.30	2.1900	2.5	-6.0	65	96	0.97
2	1375	0.89	0.2880	0.24	2.4000	2.5	-6.0	65	96	0.97
3	1430	0.89	0.3284	0.28	2.4600	2.5	-6.0	65	96	0.97
4	1067	0.89	0.2653	0.29	2.1400	2.5	-6.0	65	96	0.97
5	1155	0.89	0.2880	0.33	2.0400	2.5	-6.0	65	96	0.97

select, whenever it is possible, a value for time-headway that is lower than the one commonly pre-fixed with a typical CTG spacing policy. Of course, this reduction strongly affects energy-saving through the distance-dependent air drag coefficient formulation.

10.4 Numerical Analysis

To show the effectiveness of the proposed DNMPC in (10.6), an exemplar heterogeneous e-platoon consisting of $N = 5$ EVs plus a leader moving along a flat road highway segment and connected among them via a L-P-F topology (see Sec. 3.1.2 and Fig. 3.6) is considered. According to Sec. 3.1.2, the communication topology is described by leveraging graph theory, thus obtaining a static graph whose characteristic matrices are:

$$\mathcal{P} = \begin{bmatrix} 1 & 0 & 0 & 0 & 0 \\ 0 & 1 & 0 & 0 & 0 \\ 0 & 0 & 1 & 0 & 0 \\ 0 & 0 & 0 & 1 & 0 \\ 0 & 0 & 0 & 0 & 1 \end{bmatrix}, \qquad \mathcal{L} = \begin{bmatrix} 0 & 0 & 0 & 0 & 0 \\ -1 & 1 & 0 & 0 & 0 \\ 0 & -1 & 1 & 0 & 0 \\ 0 & 0 & -1 & 1 & 0 \\ 0 & 0 & 0 & -1 & 1 \end{bmatrix}. \tag{10.10}$$

To disclose the benefits of the proposed architecture, two simulation scenarios are considered: *i*) *basic* scenario, where the DNMPC embeds a CTG spacing policy, i.e. $\bar{d}_{i,i-1} = d_{st} + hv_i(t)$, with a constant time-headway $h = 0.8$ $[s]$; *ii*) *energy-oriented* scenario, where the inter-vehicle distance $\tilde{d}_{i,i-1}(t)$ is online computed, for each vehicle i, via the solution of the optimisation problem in (10.6) which explicitly takes into account energy saving requirement, leader-tracking control objectives, as well as the safety constraints (10.7). The aim is to evaluate how the proposed architecture, by embedding distance safety constraints in (10.7), as well as distance-dependent air-drag formulation as in (10.2), can further reduce the energy consumption compared to the case where the pre-fixed time-gap value $h = 0.8$ $[s]$ is considered.

Note that the time-gap values for cooperative platoon systems have to be chosen to avoid vehicles collisions during emergencies. [324].

The numerical analysis is carried out via MiTraS Integrated Simulation Environment, and the EVs parameters are listed in Tab. 10.1. Note that the vehicle dynamics parameters are the one of a typical passenger car and they are selected according to [255]. The battery pack parameters, as well as the electric motor efficiency, are related to a Nissan Leaf-type electric vehicle, and they are chosen according to [4]. The initial leader state is set as $p_0(0) = 2000$ $[m]$, while its energy-optimal speed profile, which has to be imposed on the whole vehicular network, is assumed to be known and it is highlighted in Fig. 10.2(a). Moreover, in both scenarios, the prediction horizon in Problem $\mathcal{F}_i, \forall i$ is set as $N_p = 20$, while the control horizon is $N_c = 2$. The corresponding weights $\omega_z, z \in \{1, \dots, 7\}$ in the cost functional in (10.8) are tuned, according to the trail and error procedure [325, 326], as : $\omega_1 = 10;\ \omega_2 = 10;\ \omega_3 = 20;\ \omega_4 = 20;\ \omega_5 = 0.1;\ \omega_6 = 0.1;\ \omega_7 = 10$.

Note that this choice of selecting the same weighting factors for both the appraised scenario guarantees the fairness of the comparison analysis. Indeed, in so doing, it is possible to focus mainly on the effect the different spacing policies can have on energy-saving requirements.

Table 10.2: Percentage of energy saving in $[kWh/km]$ under Energy-Oriented Architecture compared to *basic* scenario.

Configuration	**Vehicle 1**	**Vehicle 2**	**Vehicle 3**	**Vehicle 4**	**Vehicle 5**	**Mean**
Energy-oriented strategy	-2.1220	-2.1971	-2.2549	-2.2686	-2.2150	-2.2115

Table 10.3: Percentage of energy saving in $[kWh/km]$ under Energy-Oriented Architecture compared to *basic* scenario with proportional controller.

Configuration	**Vehicle 1**	**Vehicle 2**	**Vehicle 3**	**Vehicle 4**	**Vehicle 5**	**Mean**
Energy-oriented strategy	-3.6553	-3.3454	-3.0981	-2.8665	-2.6365	-3.1204

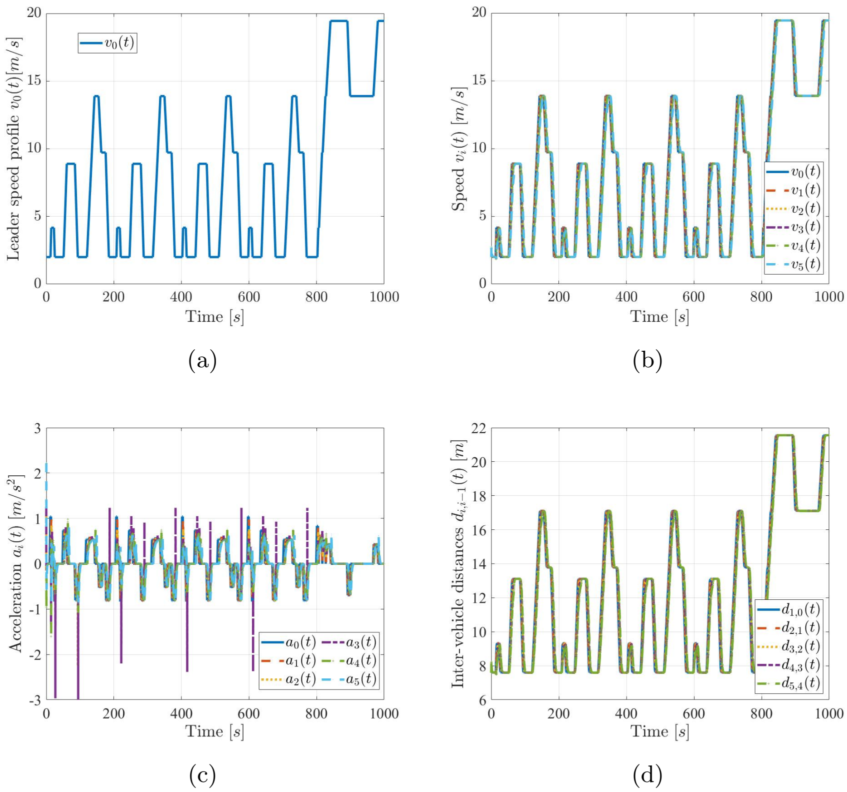

Figure 10.2: *basic* scenario. Tracking performances. Time history of: *a*) Energy-optimal leader speed profile; *b*) vehicles speed $v_i(t)$; *c*) vehicles acceleration $a_i(t)$; *d*) inter-vehicle distances $\bar{d}_{i,i-1}(t)$

Results in Fig. 10.2(b)-(c) show the behaviour of the e-platoon in *basic* scenario, in terms of speed and acceleration profiles respectively, while the inter-vehicle distance of each vehicle within the platoon compared to its predecessor is reported in Fig. 10.2(d).
For the same energy-optimal leader speed profile as in Fig. 10.2(a), Fig. 10.3 discloses the results of *energy-oriented* scenario, where the inter-vehicle distances between two adjacent vehicles, adequately computed by the DNMPC, is shown in Fig. 10.3(d). Good tracking performances in terms of speed and acceleration can also be appreciated in this scenario (Fig. 10.3(b)-(c)), while also the time history of the longitudinal

positions of EVs is shown in Fig. 10.3(a). To disclose the benefits of the proposed DNMPC, the inter-vehicle distance obtained with the proposed approach compared to the basic scenario is compared. In this perspective, Fig. 10.3(e) shows the comparison between the two spacing gap distances in these two simulation scenarios, i.e. $\bar{d}_{i,i-1}(t)$ and $\tilde{d}_{i,i-1}(t)$ in *basic* and *energy-oriented* scenarios, respectively. As it is possible to observe, a smaller inter-vehicle gap-distance can be achieved under the proposed energy-oriented strategy with distance-dependent air drag formulation, thus achieving better performances in terms of energy consumption. Indeed, one can find that the minimum and maximum spacing for the energy-oriented scenario are 6.4 $[m]$ and 16.3 $[m]$, respectively, while in the *basic* scenario these thresholds are 7.6 $[m]$ and 21.5 $[m]$ respectively. To further illustrate the benefits of the proposed energy-oriented architecture in terms of energy savings, the percentage variation of energy consumption in $[kWh/km]$ is computed as in (4.21). Results, reported in Tab. 10.2, confirm how the proposed DNMPC guarantees an average energy reduction of 2.2% for the entire e-platoon.

10.4.1 DNMPC vs Pure Diffusive Controller

In order to highlight the benefits of the proposed DNMPC in guaranteeing leader-tracking performances while ensuring energy-saving requirements, here its performance are compared with the one achievable via the following more classic distributed diffusive linear controller:

$$u_i(t) = -K_P \sum_{j=0}^{N} a_{ij}(p_i(t) - p_j(t) - d_{ij}(t)) - K_V \sum_{j=0}^{N} a_{ij}(v_i(t) - v_j(t)), \tag{10.11}$$

where the control gains are selected as $K_P = 250$ and $K_V = 220$ according to [317]; $d_{ij}(t)$ is the inter-vehicle distance between the i-th and j-th EV, properly selected exploiting CTG spacing policy with $h = 0.8$ $[s]$. The aim is to disclose that, despite the higher computational load required by the proposed control action (10.6), the online computation of $\tilde{d}_{i,i-1}(t)$ allows guaranteeing improved energy-saving and leader-tracking performances, while complying with safety constraints. As an exemplar driving scenario, the one presented in Fig. 10.2(a) is considered, while Simulink Profiler Tool is exploited to compare the two control approaches in terms of computational load.

To this aim, an Intel Core $i5 - 8300H$ processor is exploited, while the Graphics Processing Unit (GPU) is the Nvidia GeForce GTX.
The Pie-charts in Fig. 10.4 summarise the simulation profile reports for the strategies in comparison, while the required total computational times are 572.9731 $[s]$ and 24.057 $[s]$ for the DNMPC approach and (10.11), respectively. Specifically, for both the cases, based on these total times, it is possible to disclose in Fig. 10.4 the time percentage required by each distributed control action $u_i(t), \forall i \in \{1, \ldots, N\}$, while the label *Other* represents the residual computational load requested by the other software parts of the simulation scheme. This analysis reveals the high computational burden required by the DNMPC compared to more classical consensus-based controllers as in (10.11). However, even if these latter ask for a less computational cost, they suffer from the problem of managing multiple variable constraints [321], such as the energy-saving ones appraised in this work.
Indeed, although (10.11) ensures good tracking leader performances (see Fig. 10.5(a)), the inter-vehicle distance $d_{i,i-1}(t)$ the diffusive controller let the vehicles maintain is greater than $\tilde{d}_{i,i-1}(t)$, ensured by the DNMPC (see Fig. 10.5(b)-(c)). This implies that the proposed *energy-oriented* strategy with a distance-dependent drag coefficient allows achieving improved performances in terms of energy consumption, with an average energy reduction of 3.1204% for the entire e-platoon (see Tab. 10.3).
Finally, it is necessary to underline that the higher computational load required by the DNMPC does not preclude its real-time implementation. Indeed there exists an extensive research line devoted to this crucial aspect, and different effective solutions have been found (see, e.g., [327] and references therein).

10.5 Concluding Remarks

In this chapter, the energy-saving and leader-tracking control problem for an heterogeneous platoon of CADEVs with nonlinear dynamics has been explored and solved through a Distributed Nonlinear Model Predictive Control, where the cost function for each vehicle is properly chosen according to both leader-tracking and power minimisation control objectives. Specifically, the energy consumption reduction is ensured via the integration of a distance-dependent air drag formulation, which, for each vehicle, varies in function of the distance from the ahead vehicle. The suggested energy-oriented control architecture allows embedding an optimised variable spacing policy that considers distance constraints aiming at avoiding both smaller, which could lead to rear-end collision risk, and larger inter-vehicle gaps that, instead, could bring to road capacity reduction. Finally, numerical analysis have highlighted the effectiveness and the capability of the DNMPC in guaranteeing an improvement of energy performance for EVs platoon compared to a basic scenario, where traditional CTG spacing policy is used, with an average energy saving of about 2.2%.

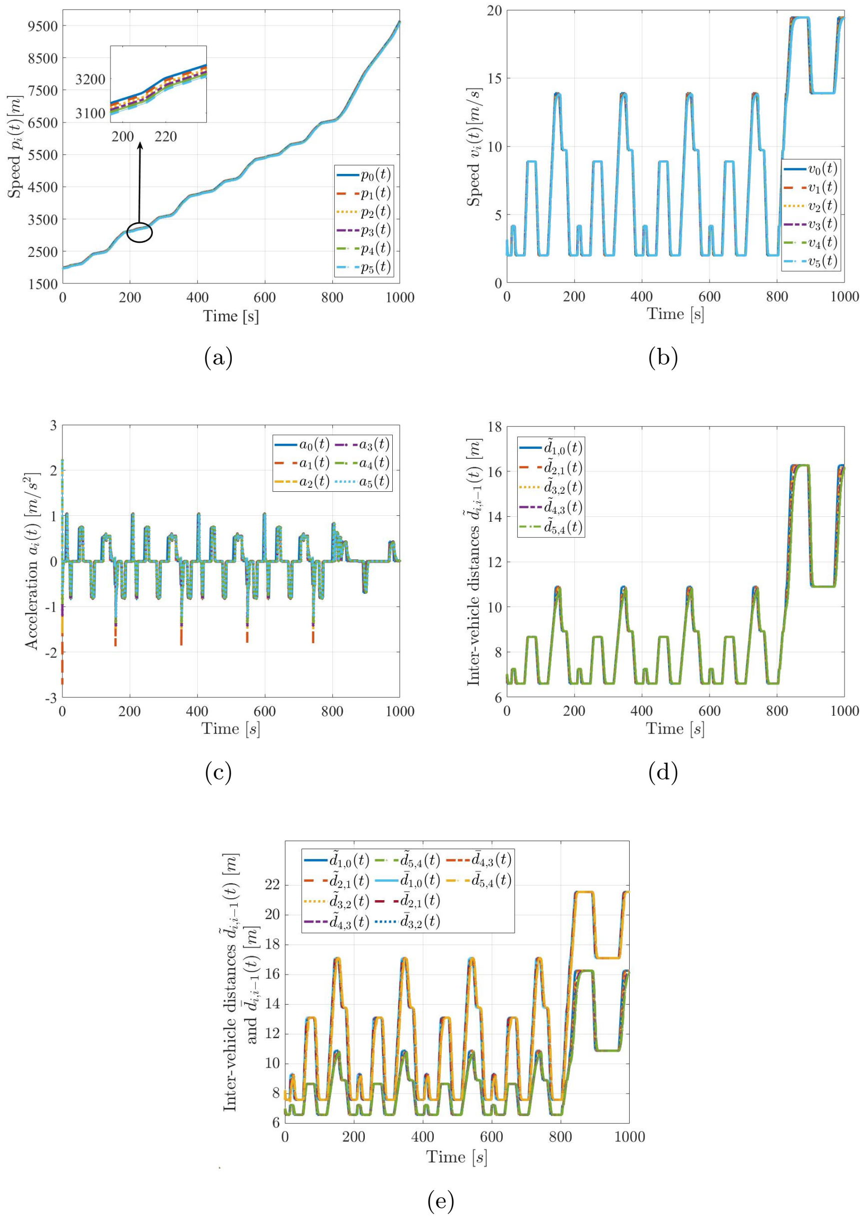

Figure 10.3: *Energy-oriented* scenario. Tracking performances. Time history of: *a*) vehicles longitudinal position $p_i(t)$; *b*) vehicles speed $v_i(t)$; *c*) vehicles acceleration $a_i(t)$5; *d*) inter-vehicle distances $\tilde{d}_{i,i-1}(t)$; *e*) Comparison between inter-vehicle distances $\bar{d}_{i,i-1}(t)$ and $\tilde{d}_{i,i-1}$ in *basic* and *energy-oriented* scenarios.

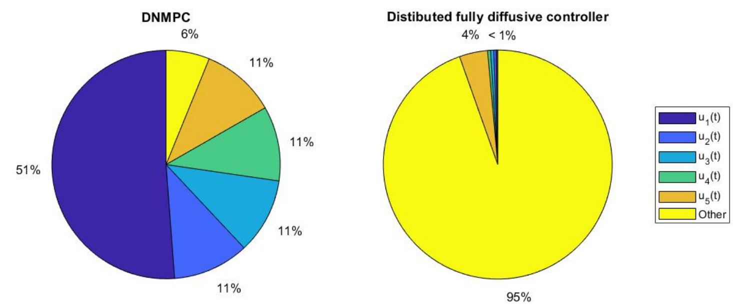

Figure 10.4: Computational load in *energy-oriented* scenario and *basic-scenario* with controller (10.11).

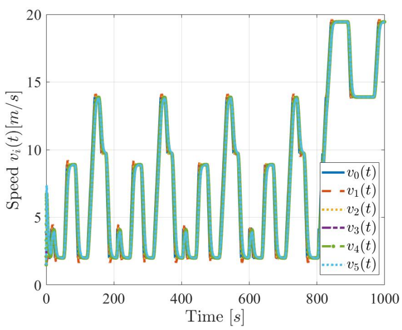

(a)

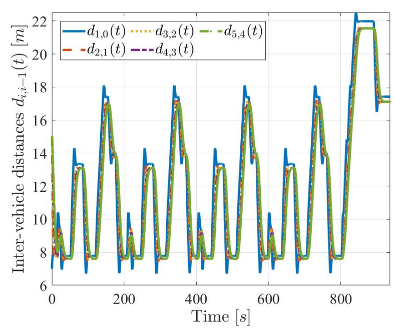

(b)

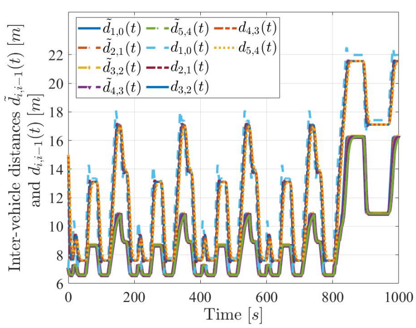

(c)

Figure 10.5: Tracking performances with the classic distributed diffusive control in (10.11). Time history of: *a*) vehicles speed $v_i(t)$; *b*) inter-vehicle distances $d_{i,i-1}(t)$; *c*) Comparison between inter-vehicle distances $d_{i,i-1}(t)$ and $\tilde{d}_{i,i-1}(t)$ in *basic* and *energy-oriented* scenarios.

CHAPTER 11

Conclusions

This thesis has addressed the problem of developing new fully automated and connected C-ITS services to mitigate traffic congestion and improve both road safety and energy performance. The attention has been focused on two different but closely related open challenges in the context of automated and connected driving applications, namely:

1. Research and develop innovative C-ITS strategies based on reliable and resilient control architectures that, exploiting V2X communication, allow to increase the performance of automated and connected driving in both urban and extra-urban traffic environments.

2. Test and validate C-ITS strategies in several complex traffic contexts to develop and deploy flexible, adaptable, and safety services to any traffic situation.

Firstly, a novel virtual, holistic and modular Integrated Simulation Environment, named MiTraS, has been proposed to address challenge 2. It embeds different interacting tools to accurately model both automated/autonomous connected vehicles and surrounding traffic environments. The evaluation assessment of all the strategies proposed through the thesis has been performed by exploiting the proposed platform.
To address the challenge 1, different C-ITS strategies have been proposed within the thesis, for both urban and extra-urban traffic scenarios.
Regarding the urban environment, the first issue that has been addressed

is related to crossing manoeuvres at signalised/unsignalised intersections under mixed-traffic conditions. For signalised intersection, Chapter 5 introduced a GLOSA algorithm aiming at reducing both waiting time and *stop&go* phenomena by computing an optimal speed profile to follow, based on Traffic Light Signals information shared via I2V wireless communication. The algorithm has been embedded on a single connected vehicle, while all other vehicles have been assumed to be human-driven. A more challenging open issue for urban environment is the crossing of unsignalised intersections under mixed-traffic conditions. To deal with this latter problem, in Chapter 7 a novel longitudinal control strategy for CAVs that combines the use of on-board ranging sensors with V2V communications to safely drive vehicles across the intersection, despite the presence of human-driven vehicles, has been proposed.

Another crucial problem in the urban environment is accomplishing different complex driving tasks simultaneously, such as avoiding collisions with obstacles, tracking a path along a curved road, and reducing energy consumption. To this end, in Chapter 6 a double layer control architecture combining the classical ACC with the multi-objective NMPC approach, able to drive the vehicle along a predefined path while keeping a safe distance from the predecessor and ensuring energy-saving consumption, has been designed. Moreover, the cornering effects affecting energy consumption have been explicitly considered.

Regarding extra-urban traffic scenarios, three platooning applications have been considered. In Chapter 8 the cooperative leader-tracking control problem for uncertain heterogeneous nonlinear vehicles platoon performing cooperative manoeuvres has been addressed. A distributed robust PID-like control strategy has been proposed to face the issue mentioned above: exploiting information shared via V2V communication allows tracking the leader behaviour and regulating the longitudinal gap among vehicles during manoeuvres, despite the presence of unknown time-varying parameter uncertainties.

Another crucial issue for leader-tracking is to guarantee the consensus for heterogeneous vehicles platoons in a fixed time despite external disturbances. This problem has been addressed in Chapter 9 where, by exploiting the ISM approach and the Lyapunov theory, a distributed control strategy able to ensure the leader-tracking in a finite settling time which is independent of any initial conditions of vehicles has been

proposed.
In addition to the leader-tracking problem, Chapter 10 addressed the problem of energy-saving for a heterogeneous platoon of electric vehicles with nonlinear dynamics. The problem has been solved through a Distributed Nonlinear Model Predictive Control, where the cost function for each vehicle has been chosen according to both leader-tracking and power minimisation control objectives.

Future works of this thesis could include:

- a further improvement of both the Integrated Simulation Environment in Chapter 4 and the assessment methodology in Chapter 5;
- an improvement of the GLOSA service described in Chapter 5, considering, for instance, a multi-segment approach or the estimation of queue at intersection;
- the stability analysis of the controller proposed in Chapter 7;
- a theoretical theoretical robustness analysis of the distributed robust cooperative control in Chapter 8 in presence of communication impairments originated by the wireless networks;
- a theoretical extension of the framework of the distributed robust cooperative controller, proposed in Chapter 8, to ensure precise leader-tracking performance with a desired transient behaviour;
- a theoretical extension of the framework of the distributed fixed-time controller, discussed in Chapter 9, considering nonlinear vehicle dynamics for control purposes;
- the experimental validation of the controllers proposed in Chapter 7 and Chapter 8.

APPENDIX **A**

Terminology

A description of the terminology used within the thesis is provided to provide a common basis of discussion and make understanding the thesis easier. It is worth noting that the definitions given are not definitive and will undoubtedly evolve

A.1 Autonomous vs. Automated Vehicle

There is some inconsistency in the terminology used in the self-driving car industry; indeed, the words *automated* and *autonomous* are usually used together. A representative definition for automated/autonomous driving can be: *Automated or autonomous driving systems are complex combinations of various components that can be defined as systems where perception, decision making, and operation of the automobile are performed by electronics and machinery instead of a human driver, and as the introduction of automation into road traffic. This includes handling the vehicle, destination, and awareness of surroundings. While the automated system has control over the vehicle, it allows the human operator to leave all responsibilities to the system* [328].
Accordingly, it is possible to deduce that *automated* driving implies that the driver has passed the driven control to the vehicle automation system, being, at the same time, ready to retake the control at any moment in case of necessity [328]. In other words, the automation system is capable

of automated driving, but not for all conditions encountered during regular operation. Instead, *autonomous* driving means self-governing: it implies satisfactory performance under significant uncertainties in the environment, and the ability to compensate for system failures without external intervention, i.e., the vehicle moves autonomously without any driver supervision.

A.2 Platooning

Platooning is a a viable control solution for cooperatively driving a group of vehicles together. The goal is to achieve the fleet of vehicles so that they all converge towards some common target motion specified by a leader vehicle: for instance, follow a reference speed profile while maintain a desired inter-vehicle distance.

A.3 Virtual Environment Components

In the following, some the components of virtual simulation environment are described in detail. Readers interested in deepening the topic can refer to [329].

Ego-Vehicle The term *Ego-Vehicle* is used to describe the set composed of the vehicle itself, the driver, and optional automation. Depending on the research focus, driver action, automation action, or driver and automation action can be predefined.

Use Case Test cases need to be specified for simulating and testing an automated/autonomous vehicle and/or its components. Each of them involves a scenario and criteria to be able to analyse the results of the same. In addition, the functional description of the system (*use case*) must be defined in the early stages of the system design. The term *use case*, therefore, refers to a description of the operating range and the desired behaviour, the specification of the system limits, and the definition of one or more use scenarios. While these scenario descriptions may be approximate and incomplete in the first phase, they can be detailed to achieve fully verifiable test runs in the development process. A possible scheme of *use case* and its components is shown in Fig. A.1.

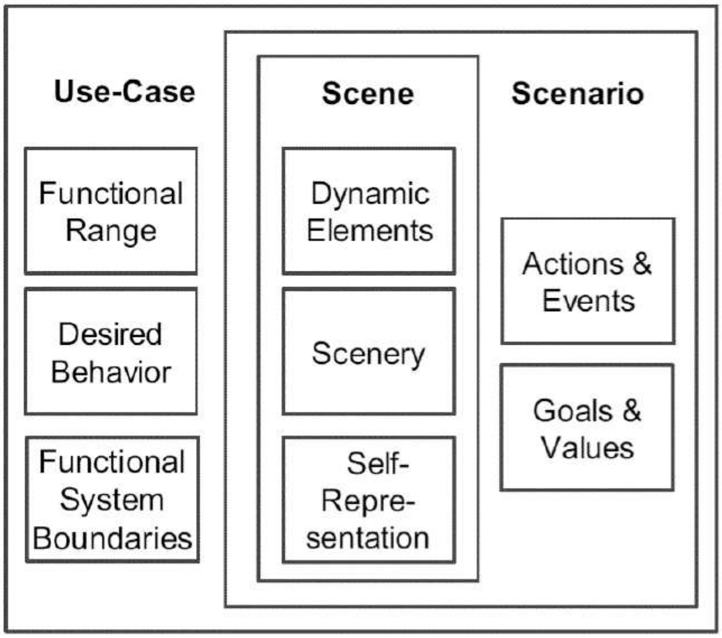

Figure A.1: Exemplary scheme of a Use-Case

Situation A *situation* is the set of circumstances, which must be considered for the selection of an appropriate model of behaviour at a given moment. It includes all conditions, options, and determinants of behaviour. A *situation* arises from the scene and from a process of selecting and augmenting information based on transitory (eg, mission-specific) and/or permanent goals and values. Thus, a *situation* is always subjective, representing the point of view of an element.

Scene A *scene* describes a snapshot of the environment, including the scenic and dynamic elements of which it is composed, as well as the self-representations of all the actors and observers as well as the relationships between these entities. Only a stage representation in a simulated world can be all-encompassing (e.g., objective *scene*). In the real world, it is incomplete, incorrect, uncertain, and from the point of view of one or more observers (subjective *scene*). It can be considered as the representation of a specific environment in a short period and is characterised by several different elements: *i*) background, i.e., the set of static components, such as road geometry, state of the carriageway; location of road signs and traffic lights, static obstacles such as buildings and trees; *ii*) dynamic elements, i.e., elements whose state changes over time, such as vehicles, state of traffic lights, and atmospheric conditions; *iii*) self-representation, i.e., the definition of the abilities of the actors in the scene.

Scenario A *scenario* describes the temporal development between multiple scenes in a sequence of scenes. Each *scenario* begins with an opening scene. Actions and events, as well as goals and values, can be specified to characterise this temporal development in a *scenario*. The scenes that make up a *scenario* are connected by actions and events; consequently, a scenario is to be understood as a temporal sequence of actions/events and scenes. A scenario needs to include at least one (initial) scene and actions and events to specify an end. Hence, a *scenario* spans over a considerable period.

Dynamic Elements *Dynamic elements* describe all objects other than the Ego-Vehicle, that change their state throughout the scenario. These are, for instance, other vehicles, pedestrians, or objects like traffic signals.

Static Elements *Static elements* are objects that are stationary and do not change their state during the scenario; for example, traffic signs, trees, and buildings.

Environment The *environment* describes the road layout and lane network with the lane markings, for example. Additionally, it describes environmental states, such as lighting and weather conditions (i.e., rain, snow, fog, etc.).

APPENDIX B

Typical Architecture of Automated/Autonomous Cars

Here is an overview of the typical architecture of the automation system of automated/autonomous cars. A block diagram of the typical architecture of the automation system, according to [23], is shown in Fig. B.1: it is possible to clearly distinguish Perception and Decision Making systems, as well as each of their subsystems. More detail about the architecture, as well as about its equipment, can be found in [23, 330, 328, 151].

B.1 Vehicle Equipment

State-of-the-art automated driving systems employ a wide selection of on-board sensors. Indeed, high sensor redundancy is needed in most tasks for robustness and reliability. Then, the equipment of a typical automated vehicle is briefly described below.

B.1.1 Proprioceptive Sensors

Proprioceptive sensings are exploited for internal vehicle state monitoring tasks. Indeed, vehicle states such as speed, acceleration, and yaw must

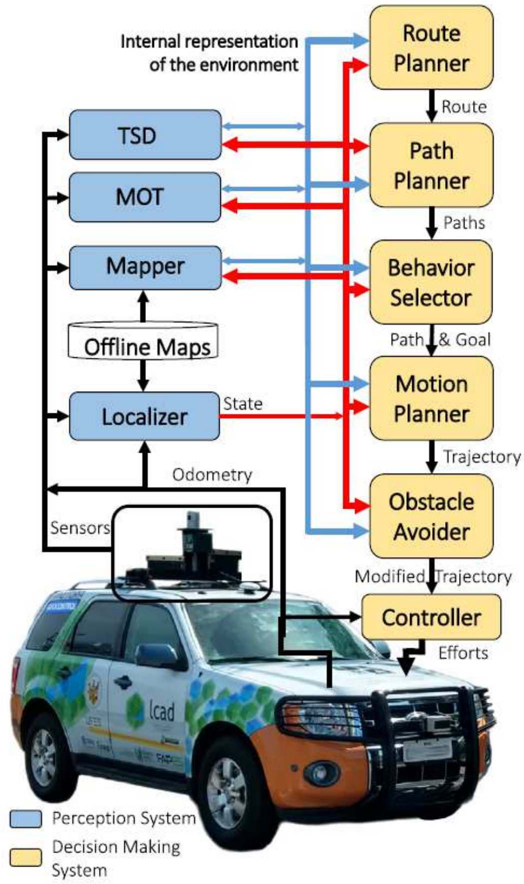

Figure B.1: Overview of the typical architecture of the automation system of automated/autonomous vehicle.

be continuously measured to operate the platform safely with feedback. These signals can be accessed through the Controller Area Network (CAN) protocol of modern cars. CAN bus is a robust vehicle bus standard designed to allow micro-controllers and devices to communicate without a host computer.

Global Positioning System The Global Positioning System (GPS) is a satellite-based radio navigation system owned by the United States government and operated by the United States Space Force. It is one of the global navigation satellite systems (GNSS) that provides geo-location and time information to a GPS receiver. Obstacles (e.g., buildings) can block the relatively weak GPS signals.

Inertial Measurement Unit An inertial measurement unit (IMU) is an electronic device that measures and reports the force, angular rate, and orientation of the vehicle, using a combination of accelerometers, gyroscopes, and sometimes magnetometers. Recent developments allow for the production of IMU-enabled GPS devices: IMU allows a GPS receiver to work when GPS signals are unavailable (e.g., in tunnels).

Accelerometer An accelerometer is a tool that measures the acceleration of the vehicle in its instantaneous rest frame.

Gyroscope A gyroscope is a device used for measuring or maintaining orientation and angular velocity.

Odometer An odometer is a tool used for measuring the distance traveled by a vehicle. The device may be electronic, mechanical, or a combination of the two (electromechanical). Modern cars include a trip meter (trip odometer) that can be reset at any point in a journey, making it possible to record the distance traveled in any particular journey or part of a trip.

B.1.2 Exteroceptive Sensors

Exteroceptive sensors are mainly used to perceive the environment, which includes dynamic and static objects, e.g., drivable areas, buildings, pedestrian crossings, etc.

Monocular Cameras Cameras can sense colours and are passive, i.e., they do not emit any signal for measurements and, accordingly, it does not interfere with other systems. Sensing colours is extremely important for tasks such as traffic light recognition. Furthermore, 2D computer vision is an established field with remarkable state-of-the-art algorithms. However, cameras have certain shortcomings. For instance, illumination conditions affect their performance drastically, and depth information is challenging to obtain from a single camera.

Omnidirectional Cameras Omnidirectional cameras are used as an alternative to camera arrays for 360° 2D vision. They have seen widespread use, with increasingly compact and high-performance hardware being constantly released. Panoramic view is particularly desirable for navigation, localisation, and mapping applications.

Event Cameras Event cameras record data asynchronously for individual pixels concerning visual stimulus. Therefore, the output is an irregular sequence of data points or events triggered by changes in brightness. The main limitation of current event cameras is pixel size and image resolution.

Radar Radar helps cover the shortcomings of cameras. Distance to objects can be measured effectively to retrieve 3D information since it is not affected by illumination conditions. However, they are active sensors. However, being active sensors, radars emit radio waves that bounce back from objects and measure the time of each bounce. Emissions from active sensors can interfere with other systems. Such technology is a well-established technology since it is lightweight and cost-effective. For instance, radars can fit inside side mirrors, are cheaper, and detect objects at longer distances than lidars.

Lidars Lidar operates similarly to radar, but it emits infrared light waves instead of radio waves. It has much higher accuracy than radar under 200 meters. However, weather conditions are negatively affected (e.g., fog or snow). Regarding the sensor size, lidars are generally larger than radars.

B.1.3 Computational Units and Actuators

Besides sensors, actuators are required to manipulate the vehicle and advanced computational units for processing and storing sensor data.

Electronic Control Unit The electronic control unit (ECU) is an embedded system in automotive electronics that controls one or more of the electrical systems or subsystems in a car.

Battery management System A battery management system (BMS) is any electronic system that manages a rechargeable battery (e.g. by protecting the battery from operating outside its safe operating area), monitoring its state and controlling its environment.

B.1.4 Communication Systems

On-board Unit An On-board unit (OBU) is an electronic device that connects vehicles to infrastructure (V2I) and/or to other vehicles (V2V).

B.2 Perception System

Perception system is responsible for estimating the state of the car and for creating an internal representation of the surrounding environment, using data captured by on-board sensors, such as lidar, radar, camera, GPS, IMU, odometer, etc., and prior information about the models of sensors, road network, traffic rules, car dynamics, etc.

Localiser Subsystem The localizer subsystem estimates the state of the car (position, linear and angular velocities, etc.) with static maps of the environment; information regarding the rules and regulations (e.g., direction of traffic, maximum speed, lane demarcation, etc.) are typically embedded in road maps, and are represented using geometrical and topological properties. The subsystem receives the offline maps, sensors data, and the odometry of the automated/autonomous vehicle and returns the state of the vehicle as output. It is worth noting that GPS alone is not enough for proper localisation in urban environments due to interference caused, for instance, by tall trees, buildings, tunnels, etc., that makes GPS positioning unreliable.

Offline Maps Offline maps (or static maps) are computed automatically before the autonomous operation, typically using the sensors of the vehicle itself. One or more offline maps may be used for localisation, such as occupancy grid maps, remission maps, or landmark maps.

Mapper Subsystem The mapper subsystem receives as input both the offline maps and the state of the vehicle, generating the online map as output. This latter is typically a merge of information present in the offline maps and an occupancy grid map computed online using data from sensors and the current state of the car.

Moving Objects Tracker subsystem The Moving Objects Tracker (MOT) subsystem receives the offline maps and the self-driving and the state of the vehicle, then detects and tracks, i.e., calculates the position and velocity of the nearest moving obstacles to avoid collision with them.

Traffic Signalisation Detector subsystem The Traffic Signalisation Detector (TSD) subsystem detects the position of traffic signals and recognises their class or status.

B.3 Decision Making System

The Decision-making system is responsible for navigating the car from its initial position to the final goal defined by the user, considering the current state of the car and the internal representation of the environment, traffic rules, and passengers safety and comfort.

Route Planner Subsystem The route planner subsystem computes a route to follow in the offline maps, starting from the current state of the car to the final goal.

Path Planner Subsystem The path planner subsystem computes, considering the current state of the vehicle and the internal representation of the environment and traffic rules.

Behaviour Selector Subsystem The behaviour selector subsystem chooses the desired driving behaviour, such as lane-keeping, intersection handling, traffic light handling, and so on. The final goal is selected considering the current driving behaviour and avoiding collisions with static and moving obstacles in the environment within the decision horizon time frame (prediction of the future state of both automated/autonomous vehicle and other road actors).

Obstacle Avoidance Subsystem The obstacle avoidance subsystem receives the desired trajectory computed by the motion planner and changes it to avoid collisions.

Controller Subsystem The controller subsystem receives the motion planner trajectory, eventually modified by the obstacle avoidance subsystem, and computes and sends control commands to the actuators of the steering wheel, throttle and brakes in order to follow the desired trajectory as best as the physical features of the car allow.

Motion Planner Subsystem The controller subsystem receives the motion planner trajectory, eventually modified by the obstacle avoidance subsystem, then computes and sends control commands to the actuators of the steering wheel, throttle, and brakes to follow the desired trajectory as best as possible physical features of the car allow.

List of Acronyms

3GPP 3^{rd} Generation Partnership Project

5GAA 5G Automotive Association

5G NR 5G New Radio

ABS Anti-lock Braking System

ACC Adaptive Cruise Control

ADAS Advanced Driver Assistance Systems

B-F Bidirectional-Follower topology

B-L-F Bidirectional-Leader-Follower topology

BR Broadcast or All-to-All topology

C2C-CC Car2Car Communication Consortium

CA Conflicting Area

CACC Cooperative Adaptive Cruise Control

CADEVs Connected Autonomous Distributed Electric Vehicles

CAM Cooperative Awareness Messages

CAV Connected and Automated/Autonomous Vehicle

CAVs Connected and Automated/Autonomous Vehicles

CC Cruise Control

CCAM Cooperative, Connected and Automated Mobility

CCRW Cooperative Collision Risk Warning

CHV Connected Human-driven Vehicle

CHVs Connected Human-driven Vehicles

CSF Constant Safety Factors

CSP Constant Spacing Policy

C-V2X Cellular Vehicle

C-ITS Cooperative Intelligent Transportation Systems

CPEM Comprehensive Power-based EV Energy consumption Mode

CTG Constant Time Gap

CTH Constant Time Headway

CV Connected Vehicle

C-V2X Cellular Vehicle-to-Everything

CZ Cooperative Zone

DENM Decentralized Environmental Notification Message

DGPS Differential GPS

DGPS Differential GPS

DiL Driver-in-the-Loop

DoF Degree-of-Freedom

DoS Denial-of-Service

DMPC Distributed Model Predictive Controller

DNMPC Distributed Nonlinear Model Predictive Controller

DP Dynamic Programming

DSMC Distributed Sliding Mode Control

DSRC Dedicated Short Range Communications

EC European Commission

EM Electric Motor

ESC Electronic stability control

ETSI European Telecommunications Standards Institute

EU European Union

EV Electric Vehicle

EVs Electric Vehicles

EVA Emergency Vehicle Approaching

FAFP (First Arrive First Pass

FCW Forward Collision Warning

FOT Field Operational Test

GHG greenhouse gas

GLOSA Green Light Optimal Speed Advisory

GPS Global Positioning Systems

GPU Graphics Processing Unit

HDB Human Driving Behavior

HDVs Human-driven Vehicles

HiL Hardware-in-the-Loop

I2V Infrastructure-to-Vehicle

ICE Internal Combustion Engine

IEEE Institute of Electrical and Electronic Engineers

IMU Inertial Measurement Unit

IoT Internet-of-Things

ISA Intelligent Speed Assistance

ISM Integral Sliding Mode

ITS Intelligent Transportation Systems

KPI Key Performance Index

KPIs Key Performance Indexes

LDW Lane Departure Warning

LMIs Linear Matrix Inequalities

L-P-F Leader-Predecessor-Follower topology

LTE Long-Term Evolution

LTE-V Long-Term Evolution for vehicles

MASs Multi-Agent Systems

MAC Medium access control layer

MAP Map Data message

MFD Macroscopic Fundamental Diagram

MiL Model-in-the-Loop

MiTraS Mixed Traffic Simulator

MOT Moving Objects Tracker

MPC Model Predictive Controller

NMPC Nonlinear Model Predictive Controller

NLoS Non-Line of Sight

OBU On-Board unit

ODD Operational Design Domain

OEMs Original Equipment Manufacturers

OPC Optimal Control Problem

PF Predecessor-Follower topology

PHY Physical access control layer

PID Proportional-Integral-Derivative

QoS Quality of Service

RSU Road-Side unit

RWW Road Works Warning

SAE Society of Automotive Engineers

SiL Software-in-the-Loop

SMC Sliding Mode Control

SOC State Of Charge

SPaT Signal Phase and Timing Message

SUMO Simulation of Urban Mobility

SWD Shockwave Damping

TEN-T Trans-European Network-Transport

TLS Traffic Light Signal

TLSs Traffic Light Signals

TJW Traffic Jam ahead Warning

TSD Traffic Signalisation Detector

TSR Traffic Sign Recognition

TTC Time-to-Collision

TTI Time-to-Intersection

TTG Time To Green

UE user equipment

VANETs Vehicular-ad-hoc-networks

V2I Vehicle-to-Infrastructure

V2N Vehicle-to-Network

V2P Vehicle-to-Pedestrian

V2V Vehicle-to-Vehicle

V2X Vehicle-to-Everything

ViL Vehicle-in-the-Loop

VSGN In-Vehicle Signage

VSPD In-Vehicle Speed limit

VTG Variable Time-Gap

VT-CPFM Virginia Tech Comprehensive Power-Based Fuel Consumption Model

VTH Variable Time-Headway

WTC Weather Conditions

List of Abbreviations

Fig. Figure

Sec. Section

Tab. Table

w.r.t. with respect to

Bibliography

[1] Y. Wu, S. E. Li, Y. Zheng, and J. K. Hedrick, "Distributed sliding mode control for multi-vehicle systems with positive definite topologies," in *IEEE 55th Conference on Decision and Control (CDC), 2016*. IEEE, 2016, pp. 5213–5219.

[2] M. Zabat, N. Stabile, S. Farascaroli, and F. Browand, "The aerodynamic performance of platoons: A final report," 1995.

[3] T. Sturm, C. Krupitzer, M. Segata, and C. Becker, "A taxonomy of optimization factors for platooning," *IEEE Transactions on Intelligent Transportation Systems*, 2020.

[4] R. Maia, M. Silva, R. Araújo, and U. Nunes, "Electrical vehicle modeling: A fuzzy logic model for regenerative braking," *Expert systems with applications*, vol. 42, no. 22, pp. 8504–8519, 2015.

[5] L. Chen and C. Englund, "Cooperative intersection management: A survey," *IEEE Transactions on Intelligent Transportation Systems*, vol. 17, no. 2, pp. 570–586, 2016.

[6] J. Rios-Torres and A. A. Malikopoulos, "A survey on the coordination of connected and automated vehicles at intersections and merging at highway on-ramps," *IEEE Transactions on Intelligent Transportation Systems*, vol. 18, no. 5, pp. 1066–1077, 2016.

[7] E. Namazi, J. Li, and C. Lu, "Intelligent intersection management systems considering autonomous vehicles: a systematic literature review," *IEEE Access*, vol. 7, pp. 91 946–91 965, 2019.

[8] C. J. Beckers, I. J. Besselink, and H. Nijmeijer, "Assessing the impact of cornering losses on the energy consumption of electric city buses," *Transportation Research Part D: Transport and Environment*, vol. 86, p. 102360, 2020.

[9] L. Pariota, A. Coppola, L. Di Costanzo, A. Di Vico, A. Andolfi, C. D'Aniello, and G. N. Bifulco, "Integrating tools for an effective testing of connected and automated vehicles technologies," *IET Intelligent Transport Systems*, vol. 14, no. 9, pp. 1025–1033, 2020.

[10] A. Coppola, L. Di Costanzo, L. Pariota, S. Santini, and G. N. Bifulco, "An integrated simulation environment to test the effectiveness of glosa services under different working conditions," *Transportation Research Part C: Emerging Technologies*, vol. 134, p. 103455, 2022.

[11] L. Pariota, L. Di Costanzo, A. Coppola, C. Dâ€™Aniello, and G. N. Bifulco, "Green light optimal speed advisory: a c-its to improve mobility and pollution," in *2019 IEEE International Conference on Environment and Electrical Engineering and 2019 IEEE Industrial and Commercial Power Systems Europe (EEEIC/I&CPS Europe)*. IEEE, 2019, pp. 1–6.

[12] G. N. Bifulco, A. Coppola, S. G. Loizou, A. Petrillo, and S. Santini, "Combined energy-oriented path following and collision avoidance approach for autonomous electric vehicles via nonlinear model predictive control." in *2021 IEEE International Conference on Environment and Electrical Engineering and 2021 IEEE Industrial and Commercial Power Systems Europe (EEEIC/I&CPS Europe)*. IEEE, 2021, pp. 1–6.

[13] G. N. Bifulco, B. Caiazzo, A. Coppola, and S. Santini, "Intersection crossing in mixed traffic flow environment leveraging v2x information," in *2019 IEEE International Conference on Connected Vehicles and Expo (ICCVE)*. IEEE, 2019, pp. 1–6.

[14] A. Coppola, D. G. Lui, A. Petrillo, and S. Santini, "Distributed fixed-time leader-tracking control for heterogeneous uncertain autonomous connected vehicles platoons," in *2021 29th Mediterranean*

Conference on Control and Automation (MED). IEEE, 2021, pp. 554–559.

[15] B. Caiazzo, A. Coppola, A. Petrillo, and S. Santini, “Energy-oriented inter-vehicle distance optimization for heterogeneous e-platoons,” in *Optimization and Data Science: Trends and Applications.* Springer, 2021, pp. 113–125.

[16] ——, “Distributed nonlinear model predictive control for connected autonomous electric vehicles platoon with distance-dependent air drag formulation,” *Energies*, vol. 14, no. 16, p. 5122, 2021.

[17] L. Baskar, B. De Schutter, J. Hellendoorn, and Z. Papp, “Traffic control and intelligent vehicle highway systems: a survey,” *Intelligent Transport Systems, IET*, vol. 5, no. 1, pp. 38–52, March 2011.

[18] L. Figueiredo, I. Jesus, J. Machado, J. Ferreira, and J. de Carvalho, “Towards the development of intelligent transportation systems,” in *Intelligent Transportation Systems, 2001. Proceedings. 2001 IEEE*, 2001, pp. 1206–1211.

[19] J. Wang, Y. Shao, Y. Ge, and R. Yu, “A survey of vehicle to everything (v2x) testing,” *Sensors*, vol. 19, no. 2, p. 334, 2019.

[20] P. Papadimitratos, A. La Fortelle, K. Evenssen, R. Brignolo, and S. Cosenza, “Vehicular communication systems: Enabling technologies, applications, and future outlook on intelligent transportation,” *Communications Magazine, IEEE*, vol. 47, no. 11, pp. 84–95, November 2009.

[21] L. Di Costanzo, A. Coppola, L. Pariota, A. Petrillo, S. Santini, and G. N. Bifulco, “Variable speed limits system: A simulation-based case study in the city of naples,” in *2020 IEEE International Conference on Environment and Electrical Engineering and 2020 IEEE Industrial and Commercial Power Systems Europe (EEEIC/I&CPS Europe).* IEEE, 2020, pp. 1–6.

[22] A. Tesone, A. Coppola, L. Di Costanzo, L. Pariota, and G. N. Bifulco, “Route guidance systems based on the macroscopic fundamental diagram concept: a simulation-based case study in the

city of portici," in *2021 IEEE International Conference on Environment and Electrical Engineering and 2021 IEEE Industrial and Commercial Power Systems Europe (EEEIC/I&CPS Europe)*. IEEE, 2021, pp. 1–6.

[23] C. Badue, R. Guidolini, R. V. Carneiro, P. Azevedo, V. B. Cardoso, A. Forechi, L. Jesus, R. Berriel, T. M. Paixao, F. Mutz *et al.*, "Self-driving cars: A survey," *Expert Systems with Applications*, vol. 165, p. 113816, 2021.

[24] S. Zeadally, M. A. Javed, and E. B. Hamida, "Vehicular communications for its: standardization and challenges," *IEEE Communications Standards Magazine*, vol. 4, no. 1, pp. 11–17, 2020.

[25] R. Shrestha, S. Y. Nam, R. Bajracharya, and S. Kim, "Evolution of v2x communication and integration of blockchain for security enhancements," *Electronics*, vol. 9, no. 9, p. 1338, 2020.

[26] 3GPP, "Study on enhancement of 3gpp support for 5g v2x services," 2018.

[27] M. I. Hassan, H. L. Vu, and T. Sakurai, "Performance analysis of the ieee 802.11 mac protocol for dsrc safety applications," *IEEE Transactions on vehicular technology*, vol. 60, no. 8, pp. 3882–3896, 2011.

[28] S. A. A. Shah, E. Ahmed, M. Imran, and S. Zeadally, "5g for vehicular communications," *IEEE Communications Magazine*, vol. 56, no. 1, pp. 111–117, 2018.

[29] G. Naik, B. Choudhury, and J.-M. Park, "Ieee 802.11 bd & 5g nr v2x: Evolution of radio access technologies for v2x communications," *IEEE access*, vol. 7, pp. 70 169–70 184, 2019.

[30] M. PIETRUCH, A. MŁYNIEC, and A. WETULA, "An overview and review of testing methods for the verification and validation of adas, active safety systems, and autonomous driving."

[31] S. Xu, H. Peng, Z. Song, K. Chen, and Y. Tang, "Design and test of speed tracking control for the self-driving lincoln mkz platform," *IEEE Transactions on Intelligent Vehicles*, vol. 5, no. 2, pp. 324–334, 2019.

[32] M. Klomp, M. Jonasson, L. Laine, L. Henderson, E. Regolin, and S. Schumi, “Trends in vehicle motion control for automated driving on public roads,” *Vehicle System Dynamics*, vol. 57, no. 7, pp. 1028–1061, 2019.

[33] Y. Kang, H. Yin, and C. Berger, “Test your self-driving algorithm: An overview of publicly available driving datasets and virtual testing environments,” *IEEE Transactions on Intelligent Vehicles*, vol. 4, no. 2, pp. 171–185, 2019.

[34] V. G. Cerf, “A comprehensive self-driving car test,” *Communications of the ACM*, vol. 61, no. 2, pp. 7–7, 2018.

[35] J. Lai, J. Hu, L. Cui, Z. Chen, and X. Yang, “A generic simulation platform for cooperative adaptive cruise control under partially connected and automated environment,” *Transportation Research Part C: Emerging Technologies*, vol. 121, p. 102874, 2020.

[36] D. Jia, J. Sun, A. Sharma, Z. Zheng, and B. Liu, “Integrated simulation platform for conventional, connected and automated driving: A design from cyber–physical systems perspective,” *Transportation Research Part C: Emerging Technologies*, vol. 124, p. 102984, 2021.

[37] R. M. Murray, “Recent research in cooperative control of multivehicle systems,” *Journal of Dynamic Systems, Measurement, and Control*, vol. 129, no. 5, pp. 571–583, 2007.

[38] L. Alvarez and R. Horowitz, “Safe platooning in automated highway systems,” *California Partners for Advanced Transit and Highways (PATH)*, 1997.

[39] S. Shladover, “Path at 20 history and major milestones,” *Intelligent Transportation Systems, IEEE Transactions on*, vol. 8, no. 4, pp. 584–592, Dec 2007.

[40] R. Kianfar, B. Augusto, A. Ebadighajari, U. Hakeem, J. Nilsson, A. Raza, R. S. Tabar, N. V. Irukulapati, C. Englund, P. Falcone *et al.*, “Design and experimental validation of a cooperative driving system in the grand cooperative driving challenge,” *IEEE Transactions on Intelligent Transportation Systems*, vol. 13, no. 3, pp. 994–1007, 2012.

[41] H. Hao and P. Barooah, "Stability and Robustness of Large Platoons of Vehicles with Double-integrator Models and Nearest Neighbor Interaction," *International Journal of Robust and Nonlinear Control*, pp. 1099 – 1125, 2012.

[42] L. Li and F.-Y. Wang, "Cooperative driving at blind crossings using intervehicle communication," *IEEE Transactions on Vehicular technology*, vol. 55, no. 6, pp. 1712–1724, 2006.

[43] E. Coelingh and S. Solyom, "All aboard the robotic road train," *Ieee Spectrum*, vol. 49, no. 11, pp. 34–39, 2012.

[44] V. Milanés, S. E. Shladover, J. Spring, C. Nowakowski, H. Kawazoe, and M. Nakamura, "Cooperative adaptive cruise control in real traffic situations," *IEEE Transactions on Intelligent Transportation Systems*, vol. 15, no. 1, pp. 296–305, 2014.

[45] A. A. Hussein and H. A. Rakha, "Vehicle platooning impact on drag coefficients and energy/fuel saving implications," *arXiv preprint arXiv:2001.00560*, 2020.

[46] S. Badnava, N. Meskin, A. Gastli, M. Al-Hitmi, J. Ghommam, M. Mesbah, and F. Mnif, "Platoon transitional maneuver control system: A review," *IEEE Access*, 2021.

[47] R. Visser, I. C. van Driel, I. H. Versteegt, and C. Enschede, "Cooperative driving on highways," 2005.

[48] S. Santini, A. Salvi, A. S. Valente, A. Pescapé, M. Segata, and R. L. Cigno, "A consensus-based approach for platooning with intervehicular communications and its validation in realistic scenarios," *IEEE Transactions on Vehicular Technology*, vol. 66, no. 3, pp. 1985–1999, 2017.

[49] A. Salvi, S. Santini, and A. S. Valente, "Design, analysis and performance evaluation of a third order distributed protocol for platooning in the presence of time-varying delays and switching topologies," *Transportation Research Part C: Emerging Technologies*, vol. 80, pp. 360–383, 2017.

[50] R. Olfati-Saber and R. M. Murray, "Consensus problems in networks of agents with switching topology and time-delays," *Automatic Control, IEEE Transactions on*, vol. 49, no. 9, pp. 1520–1533, 2004.

[51] A. Petrillo, A. Pescape, and S. Santini, "A collaborative control strategy for platoons of autonomous vehicles in the presence of message falsification attacks," in *2017 5th IEEE International Conference on Models and Technologies for Intelligent Transportation Systems (MT-ITS)*. IEEE, 2017, pp. 110–115.

[52] A. Petrillo, A. Salvi, S. Santini, and A. S. Valente, "Adaptive multi-agents synchronization for collaborative driving of autonomous vehicles with multiple communication delays," *Transportation research part C: emerging technologies*, vol. 86, pp. 372–392, 2018.

[53] M. Bartels and H. Werner, "Cooperative and consensus-based approaches to formation control of autonomous vehicles," *IFAC Proceedings Volumes*, vol. 47, no. 3, pp. 8079–8084, 2014.

[54] W. Ren and R. W. Beard, *Distributed consensus in multi-vehicle cooperative control*. Springer, 2008.

[55] P. Fernandes and U. Nunes, "Multiplatooning leaders positioning and cooperative behavior algorithms of communicant automated vehicles for high traffic capacity," *IEEE Transactions on Intelligent Transportation Systems*, vol. 16, no. 3, pp. 1172–1187, 2015.

[56] G. S. Seyboth, W. Ren, and F. Allgöwer, "Cooperative control of linear multi-agent systems via distributed output regulation and transient synchronization," *Automatica*, vol. 68, pp. 132–139, 2016.

[57] C. Letter and L. Elefteriadou, "Efficient control of fully automated connected vehicles at freeway merge segments," *Transportation Research Part C: Emerging Technologies*, vol. 80, pp. 190–205, 2017.

[58] G. Fiengo, A. Petrillo, A. Salvi, S. Santini, and M. Tufo, "A control strategy for reducing traffic waves in delayed vehicular networks," in *Decision and Control (CDC), 2016 IEEE 55th Conference on*. IEEE, 2016, pp. 2462–2467.

[59] R. Hult, F. E. Sancar, M. Jalalmaad, A. Vijayan, A. Severinson, M. Di Vaio, P. Falcone, B. Fidan, and S. Santini, “Design and experimental validation of a cooperative driving control architecture for the grand cooperative driving challenge 2016,” *Transactions on Intelligent Transportation Systems*, 2017,to appear in October.

[60] R. Rajamani, *Vehicle dynamics and control.* Springer Science & Business Media, 2011.

[61] S. E. Li, Y. Zheng, K. Li, L.-Y. Wang, and H. Zhang, “Platoon control of connected vehicles from a networked control perspective: Literature review, component modeling, and controller synthesis,” *IEEE Transactions on Vehicular Technology*, 2017.

[62] Y. Zheng, S. E. Li, K. Li, and W. Ren, “Platooning of connected vehicles with undirected topologies: Robustness analysis and distributed h-infinity controller synthesis,” *IEEE Transactions on Intelligent Transportation Systems*, vol. 19, no. 5, pp. 1353–1364, 2018.

[63] A. A. Peters, R. H. Middleton, and O. Mason, “Leader tracking in homogeneous vehicle platoons with broadcast delays,” *Automatica*, vol. 50, no. 1, pp. 64–74, 2014.

[64] L. Xiao and F. Gao, “Practical string stability of platoon of adaptive cruise control vehicles,” *IEEE Transactions on intelligent transportation systems*, vol. 12, no. 4, pp. 1184–1194, 2011.

[65] J. P. Maschuw and D. Abel, “Longitudinal vehicle guidance in networks with changing communication topology,” *IFAC Proceedings Volumes*, vol. 43, no. 7, pp. 785–790, 2010.

[66] S. Lekshmi and L. P. PS, “Mathematical modeling of electric vehicles-a survey,” *Control Engineering Practice*, vol. 92, p. 104138, 2019.

[67] D. Jia, K. Lu, J. Wang, X. Zhang, and X. Shen, “A survey on platoon-based vehicular cyber-physical systems,” *IEEE communications surveys & tutorials*, vol. 18, no. 1, pp. 263–284, 2016.

[68] Y. Zheng, S. E. Li, J. Wang, D. Cao, and K. Li, "Stability and scalability of homogeneous vehicular platoon: Study on the influence of information flow topologies," *IEEE Transactions on Intelligent Transportation Systems*, vol. 17, no. 1, pp. 14–26, 2016.

[69] Y. Zheng, S. E. Li, K. Li, and W. Ren, "Platooning of connected vehicles with undirected topologies: Robustness analysis and distributed h-infinity controller synthesis," *IEEE Transactions on Intelligent Transportation Systems*, vol. 19, no. 5, pp. 1353–1364, 2017.

[70] G. Wen, Z. Duan, G. Chen, and W. Yu, "Consensus tracking of multi-agent systems with lipschitz-type node dynamics and switching topologies," *IEEE Transactions on Circuits and Systems I: Regular Papers*, vol. 61, no. 2, pp. 499–511, 2013.

[71] G. Fiengo, D. G. Lui, A. Petrillo, S. Santini, and M. Tufo, "Distributed robust pid control for leader tracking in uncertain connected ground vehicles with v2v communication delay," *IEEE/ASME Transactions on Mechatronics*, vol. 24, no. 3, pp. 1153–1165, 2019.

[72] R. A. Horn and C. R. Johnson, *Matrix Analisis*. Cambridge: University Press, 1987.

[73] S. E. Li, Y. Zheng, K. Li, and J. Wang, "An overview of vehicular platoon control under the four-component framework," in *2015 IEEE Intelligent Vehicles Symposium (IV)*. IEEE, 2015, pp. 286–291.

[74] C. Wu, Z. Xu, Y. Liu, C. Fu, K. Li, and M. Hu, "Spacing policies for adaptive cruise control: A survey," *IEEE Access*, vol. 8, pp. 50 149–50 162, 2020.

[75] Y. Zheng, S. Eben Li, J. Wang, D. Cao, and K. Li, "Stability and Scalability of Homogeneous Vehicular Platoon: Study on the Influence of Information Flow Topologies," *IEEE Transactions on Intelligent Transportation Systems*, vol. 17, no. 1, pp. 14–26, 2016.

[76] P. A. Ioannou and C.-C. Chien, “Autonomous intelligent cruise control,” *IEEE Transactions on Vehicular technology*, vol. 42, no. 4, pp. 657–672, 1993.

[77] J. Wang and R. Rajamani, “Should adaptive cruise-control systems be designed to maintain a constant time gap between vehicles?” *IEEE Transactions on Vehicular Technology*, vol. 53, no. 5, pp. 1480–1490, 2004.

[78] Y. Bian, Y. Zheng, W. Ren, S. E. Li, J. Wang, and K. Li, “Reducing time headway for platooning of connected vehicles via v2v communication,” *Transportation Research Part C: Emerging Technologies*, vol. 102, pp. 87–105, 2019.

[79] D. Yanakiev and I. Kanellakopoulos, “Nonlinear spacing policies for automated heavy-duty vehicles,” *IEEE Transactions on Vehicular Technology*, vol. 47, no. 4, pp. 1365–1377, 1998.

[80] I. G. Jin and G. Orosz, “Dynamics of connected vehicle systems with delayed acceleration feedback,” *Transportation Research Part C: Emerging Technologies*, vol. 46, pp. 46–64, 2014.

[81] L. Zhang and G. Orosz, “Consensus and disturbance attenuation in multi-agent chains with nonlinear control and time delays,” *International Journal of Robust and Nonlinear Control*, 2016.

[82] J. Schweizer, “Non-linear feedback control for short time headways based on constant-safety vehicle-spacing,” in *IEEE Intelligent Vehicles Symposium, 2004*. IEEE, 2004, pp. 167–172.

[83] H. E. Sungu, M. Inoue, and J.-i. Imura, “Nonlinear spacing policy based vehicle platoon control for local string stability and global traffic flow stability,” in *2015 European Control Conference (ECC)*. IEEE, 2015, pp. 3396–3401.

[84] P. Fancher, “Research on desirable adaptive cruise control behavior in traffic streams,” Tech. Rep., 2003.

[85] E. Shaw and J. K. Hedrick, “String stability analysis for heterogeneous vehicle strings,” in *2007 American control conference*. IEEE, 2007, pp. 3118–3125.

[86] H. Hao, P. Barooah, and P. G. Mehta, "Stability margin scaling laws for distributed formation control as a function of network structure," *IEEE Transactions on Automatic Control*, vol. 56, no. 4, pp. 923–929, 2011.

[87] B. Bamieh, M. R. Jovanovic, P. Mitra, and S. Patterson, "Coherence in large-scale networks: Dimension-dependent limitations of local feedback," *IEEE Transactions on Automatic Control*, vol. 57, no. 9, pp. 2235–2249, 2012.

[88] F. Lin, M. Fardad, and M. R. Jovanovic, "Optimal control of vehicular formations with nearest neighbor interactions," *IEEE Transactions on Automatic Control*, vol. 57, no. 9, pp. 2203–2218, 2012.

[89] Y. Zheng, S. E. Li, K. Li, F. Borrelli, and J. K. Hedrick, "Distributed model predictive control for heterogeneous vehicle platoons under unidirectional topologies," *IEEE Transactions on Control Systems Technology*, vol. 25, no. 3, pp. 899–910, 2016.

[90] Y. Wu, S. E. Li, J. Cortés, and K. Poolla, "Distributed sliding mode control for nonlinear heterogeneous platoon systems with positive definite topologies," *IEEE Transactions on Control Systems Technology*, 2019.

[91] H. Chehardoli and A. Ghasemi, "Adaptive centralized/decentralized control and identification of 1-d heterogeneous vehicular platoons based on constant time headway policy," *IEEE Transactions on Intelligent Transportation Systems*, vol. 19, no. 10, pp. 3376–3386, 2018.

[92] X. Guo, J. Wang, F. Liao, and R. S. H. Teo, "Neuroadaptive quantized pid sliding-mode control for heterogeneous vehicular platoon with unknown actuator deadzone," *International Journal of Robust and Nonlinear Control*, vol. 29, no. 1, pp. 188–208, 2019.

[93] J. Ploeg, D. P. Shukla, N. van de Wouw, and H. Nijmeijer, "Controller synthesis for string stability of vehicle platoons," *IEEE Trans. Intelligent Transportation Systems*, vol. 15, no. 2, pp. 854–865, 2014.

[94] R. Kianfar, P. Falcone, and J. Fredriksson, "A control matching model predictive control approach to string stable vehicle platooning," *Control Engineering Practice*, vol. 45, pp. 163–173, 2015.

[95] Z. Yang, J. Huang, Z. Hu, and Z. Zhong, "Utilising bidirectional inequality constraints in optimal robust control for heterogeneous vehicular platoons," *IET Intelligent Transport Systems*, 2020.

[96] R. Olfati-Saber, J. A. Fax, and R. Murray, "Consensus and Cooperation in Networked Multi-Agent System," in *Proceedings of the IEEE*, vol. 95, no. 1, January 2007, pp. 215–233.

[97] H. Zhang, F. L. Lewis, and A. Das, "Optimal design for synchronization of cooperative systems: state feedback, observer and output feedback," *IEEE Transactions on Automatic Control*, vol. 56, no. 8, pp. 1948–1952, 2011.

[98] Z. Li, G. Wen, Z. Duan, and W. Ren, "Designing fully distributed consensus protocols for linear multi-agent systems with directed graphs," *IEEE Transactions on Automatic Control*, vol. 60, no. 4, pp. 1152–1157, 2015.

[99] C. Li and G. Chen, "Synchronization in general complex dynamical networks with coupling delays," *Physica A: Statistical Mechanics and its Applications*, vol. 343, pp. 263–278, 2004.

[100] S. Dragomir, J. Pecaric, and L. Persson, "Some inequalities of hadamard type," *Soochow J. Math*, vol. 21, no. 3, pp. 335–341, 1995.

[101] K. Gu, V. Kharitonov, and J. Chen, *Stability of Time-Delay Systems*, ser. Control Engineering. Birkhäuser Boston, 2012.

[102] R. A. Horn and C. R. Johnson, *Matrix analysis*. Cambridge university press, 2012.

[103] M. R. Zofka, S. Klemm, F. Kuhnt, T. Schamm, and J. M. Zöllner, "Testing and validating high level components for automated driving: simulation framework for traffic scenarios," in *2016 IEEE intelligent vehicles symposium (IV)*. IEEE, 2016, pp. 144–150.

[104] M. Hadj-Bachir, E. Abenius, J.-C. Kedzia, and P. de Souza, "Full virtual adas testing. application to the typical emergency braking euroncap scenario," 2019.

[105] F. Batsch, S. Kanarachos, M. Cheah, R. Ponticelli, and M. Blundell, "A taxonomy of validation strategies to ensure the safe operation of highly automated vehicles," *Journal of Intelligent Transportation Systems*, pp. 1–20, 2020.

[106] H.-P. Schöner, "Simulation in development and testing of autonomous vehicles," in *18. Internationales Stuttgarter Symposium.* Springer, 2018, pp. 1083–1095.

[107] J. Barceló *et al.*, *Fundamentals of traffic simulation.* Springer, 2010, vol. 145.

[108] M. Fellendorf and P. Vortisch, "Microscopic traffic flow simulator vissim," in *Fundamentals of traffic simulation.* Springer, 2010, pp. 63–93.

[109] J. Barceló and J. Casas, "Dynamic network simulation with aimsun," in *Simulation approaches in transportation analysis.* Springer, 2005, pp. 57–98.

[110] K. W Axhausen, A. Horni, and K. Nagel, *The multi-agent transport simulation MATSim.* Ubiquity Press, 2016.

[111] D. Krajzewicz, J. Erdmann, M. Behrisch, and L. Bieker, "Recent development and applications of sumo-simulation of urban mobility," *International journal on advances in systems and measurements*, vol. 5, no. 3&4, 2012.

[112] G. Song, L. Yu, and Y. Zhang, "Applicability of traffic microsimulation models in vehicle emissions estimates: Case study of vissim," *Transportation research record*, vol. 2270, no. 1, pp. 132–141, 2012.

[113] M. Semrau and J. Erdmann, "Simulation framework for testing adas in chinese traffic situations," *SUMO 2016–Traffic, Mobility, and Logistics*, vol. 30, pp. 103–115, 2016.

[114] M. Di Vaio, G. Fiengo, A. Petrillo, A. Salvi, S. Santini, and M. Tufo, "Cooperative shock waves mitigation in mixed traffic flow environment," *IEEE Transactions on Intelligent Transportation Systems*, vol. 20, no. 12, pp. 4339–4353, 2019.

[115] L. Cui, J. Hu, B. B. Park, and P. Bujanovic, "Development of a simulation platform for safety impact analysis considering vehicle dynamics, sensor errors, and communication latencies: Assessing cooperative adaptive cruise control under cyber attack," *Transportation research part C: emerging technologies*, vol. 97, pp. 1–22, 2018.

[116] J. Wittenburg, *Dynamics of multibody systems.* Springer Science & Business Media, 2007.

[117] J. Zhao, H. Wu, and C. Chang, "Virtual traffic simulator for connected and automated vehicles," SAE Technical Paper, Tech. Rep., 2019.

[118] M. Smith, M. Barton, M. Bass, M. Branschofsky, G. McClellan, D. Stuve, R. Tansley, and J. H. Walker, "Dspace: An open source dynamic digital repository," 2003.

[119] M. Tideman and M. Van Noort, "A simulation tool suite for developing connected vehicle systems," in *2013 IEEE Intelligent Vehicles Symposium (IV).* IEEE, 2013, pp. 713–718.

[120] S. Dupuy, A. Egges, V. Legendre, and P. Nugues, "Generating a 3d simulation of a car accident from a written description in natural language: The carsim system," *arXiv preprint cs/0105023*, 2001.

[121] B. Wymann, E. Espié, C. Guionneau, C. Dimitrakakis, R. Coulom, and A. Sumner, "Torcs, the open racing car simulator," *Software available at http://torcs. sourceforge. net*, vol. 4, no. 6, 2000.

[122] M. Naumann, F. Poggenhans, M. Lauer, and C. Stiller, "Coincarsim: An open-source simulation framework for cooperatively interacting automobiles," in *2018 IEEE Intelligent Vehicles Symposium (IV).* IEEE, 2018, pp. 1–6.

[123] A. Dosovitskiy, G. Ros, F. Codevilla, A. Lopez, and V. Koltun, "Carla: An open urban driving simulator," *arXiv preprint arXiv:1711.03938*, 2017.

[124] S. Shah, D. Dey, C. Lovett, and A. Kapoor, "Airsim: High-fidelity visual and physical simulation for autonomous vehicles," in *Field and service robotics*. Springer, 2018, pp. 621–635.

[125] M. Bojarski, D. Del Testa, D. Dworakowski, B. Firner, B. Flepp, P. Goyal, L. D. Jackel, M. Monfort, U. Muller, J. Zhang *et al.*, "End to end learning for self-driving cars," *arXiv preprint arXiv:1604.07316*, 2016.

[126] F. Rosique, P. J. Navarro, C. Fernández, and A. Padilla, "A systematic review of perception system and simulators for autonomous vehicles research," *Sensors*, vol. 19, no. 3, p. 648, 2019.

[127] M. Piorkowski, M. Raya, A. L. Lugo, P. Papadimitratos, M. Grossglauser, and J.-P. Hubaux, "Trans: realistic joint traffic and network simulator for vanets," *ACM SIGMOBILE mobile computing and communications review*, vol. 12, no. 1, pp. 31–33, 2008.

[128] D. Krajzewicz, L. Bieker, J. Härri, and R. Blokpoel, "Simulation of v2x applications with the itetris system," *Procedia-Social and Behavioral Sciences*, vol. 48, pp. 1482–1492, 2012.

[129] C. Sommer, R. German, and F. Dressler, "Bidirectionally coupled network and road traffic simulation for improved ivc analysis," *IEEE Transactions on mobile computing*, vol. 10, no. 1, pp. 3–15, 2010.

[130] T. Issariyakul and E. Hossain, "Introduction to network simulator 2 (ns2)," in *Introduction to network simulator NS2*. Springer, 2009, pp. 1–18.

[131] G. F. Riley and T. R. Henderson, "The ns-3 network simulator," in *Modeling and tools for network simulation*. Springer, 2010, pp. 15–34.

[132] A. Varga, "Omnet++," in *Modeling and tools for network simulation*. Springer, 2010, pp. 35–59.

[133] M. Segata, S. Joerer, B. Bloessl, C. Sommer, F. Dressler, and R. L. Cigno, “Plexe: A platooning extension for veins,” in *2014 IEEE Vehicular Networking Conference (VNC)*, 2014, pp. 53–60.

[134] C. Sommer, O. K. Tonguz, and F. Dressler, “Traffic information systems: efficient message dissemination via adaptive beaconing,” *IEEE Communications Magazine*, vol. 49, no. 5, pp. 173–179, 2011.

[135] A. Cottignies, M. Daley, E. Newton, and H. Parker, “rfpro & sumo: the road to a complete real-time simulation of urban environments for dil, adas and autonomous testing,” *SUMO 2017–Towards Simulation for Autonomous Mobility*, vol. 31, p. 62, 2017.

[136] J. So, N. Motamedidehkordi, Y. Wu, F. Busch, and K. Choi, “Estimating emissions based on the integration of microscopic traffic simulation and vehicle dynamics model,” *International Journal of Sustainable Transportation*, vol. 12, no. 4, pp. 286–298, 2018.

[137] E. M. Campaña, N. Müllner, and S. Mubeen, “Interfacing a brake-by-wire simulink model with sumo,” in *2018 International Conference on Intelligent and Innovative Computing Applications (ICONIC)*. IEEE, 2018, pp. 1–6.

[138] B. Hegde, A. V. Rajendran, Q. Ahmed, and G. Rizzoni, “On quantifying the utility of look-ahead data for energy management,” *IFAC-PapersOnLine*, vol. 51, no. 31, pp. 57–62, 2018.

[139] A. V. Rajendran, B. Hegde, Q. Ahmed, and G. Rizzoni, “Design and development of traffic-in-loop powertrain simulation,” in *2017 IEEE Conference on Control Technology and Applications (CCTA)*. IEEE, 2017, pp. 261–266.

[140] O. Michel, “Cyberbotics ltd. webotsâ„¢: professional mobile robot simulation,” *International Journal of Advanced Robotic Systems*, vol. 1, no. 1, p. 5, 2004.

[141] P. A. Lopez, M. Behrisch, L. Bieker-Walz, J. Erdmann, Y.-P. Flötteröd, R. Hilbrich, L. Lücken, J. Rummel, P. Wagner, and E. Wießner, “Microscopic traffic simulation using sumo,” in *2018 21st International Conference on Intelligent Transportation Systems (ITSC)*. IEEE, 2018, pp. 2575–2582.

[142] W. Alasmary and W. Zhuang, “Mobility impact in ieee 802.11p infrastructureless vehicular networks,” *Ad Hoc Networks*, vol. 10, no. 2, pp. 222 – 230, 2012.

[143] A. F. Acosta, J. E. Espinosa, and J. Espinosa, “Traci4matlab: Enabling the integration of the sumo road traffic simulator and matlab® through a software re-engineering process,” in *Modeling Mobility with Open Data*. Springer, 2015, pp. 155–170.

[144] H. A. Rakha, K. Ahn, K. Moran, B. Saerens, and E. Van den Bulck, “Virginia tech comprehensive power-based fuel consumption model: model development and testing,” *Transportation Research Part D: Transport and Environment*, vol. 16, no. 7, pp. 492–503, 2011.

[145] J. Y. Wong, “Theory of ground vehicles john wiley & sons,” *Inc., New York*, 2001.

[146] C. Fiori, K. Ahn, and H. A. Rakha, “Power-based electric vehicle energy consumption model: Model development and validation,” *Applied Energy*, vol. 168, pp. 257–268, 2016.

[147] Y. Li, Z. Zhong, K. Zhang, and T. Zheng, “A car-following model for electric vehicle traffic flow based on optimal energy consumption,” *Physica A: Statistical Mechanics and its Applications*, vol. 533, p. 122022, 2019.

[148] S. Edwards, G. Hill, P. Goodman, P. Blythe, P. Mitchell, and Y. Huebner, “Quantifying the impact of a real world cooperative-its deployment across multiple cities,” *Transportation Research Part A: Policy and Practice*, vol. 115, pp. 102–113, 2018.

[149] E. Mintsis, E. I. Vlahogianni, and E. Mitsakis, “Dynamic eco-driving near signalized intersections: Systematic review and future research directions,” *Journal of Transportation Engineering, Part A: Systems*, vol. 146, no. 4, p. 04020018, 2020.

[150] M. Kloeppel, J. Grimm, S. Strobl, and R. Auerswald, “Performance evaluation of glosa-algorithms under realistic traffic conditions using c2i-communication,” in *The 4th Conference on Sustainable Urban Mobility*. Springer, 2018, pp. 44–52.

[151] R. Hussain and S. Zeadally, "Autonomous cars: Research results, issues, and future challenges," *IEEE Communications Surveys & Tutorials*, vol. 21, no. 2, pp. 1275–1313, 2018.

[152] S. Mandava, K. Boriboonsomsin, and M. Barth, "Arterial velocity planning based on traffic signal information under light traffic conditions," in *2009 12th International IEEE Conference on Intelligent Transportation Systems*. IEEE, 2009, pp. 1–6.

[153] T. Tielert, M. Killat, H. Hartenstein, R. Luz, S. Hausberger, and T. Benz, "The impact of traffic-light-to-vehicle communication on fuel consumption and emissions," in *2010 Internet of Things (IOT)*. IEEE, 2010, pp. 1–8.

[154] K. Katsaros, R. Kernchen, M. Dianati, and D. Rieck, "Performance study of a green light optimized speed advisory (glosa) application using an integrated cooperative its simulation platform," in *2011 7th International Wireless Communications and Mobile Computing Conference*. IEEE, 2011, pp. 918–923.

[155] D. Krajzewicz, L. Bieker, and J. Erdmann, "Preparing simulative evaluation of the glosa application," in *Proceedings CD ROM 19th ITS World Congress 2012 Wien, Österreich, Paper ID: EU-00630*, 2012.

[156] H. Rakha and R. K. Kamalanathsharma, "Eco-driving at signalized intersections using v2i communication," in *2011 14th international IEEE conference on intelligent transportation systems (ITSC)*. IEEE, 2011, pp. 341–346.

[157] R. K. Kamalanathsharma and H. A. Rakha, "Multi-stage dynamic programming algorithm for eco-speed control at traffic signalized intersections," in *16th International IEEE Conference on Intelligent Transportation Systems (ITSC 2013)*. IEEE, 2013, pp. 2094–2099.

[158] D. Eckhoff, B. Halmos, and R. German, "Potentials and limitations of green light optimal speed advisory systems," in *2013 IEEE Vehicular Networking Conference*. IEEE, 2013, pp. 103–110.

[159] A. Stevanovic, J. Stevanovic, and C. Kergaye, “Green light optimized speed advisory systems: Impact of signal phasing information accuracy,” *Transportation research record*, vol. 2390, no. 1, pp. 53–59, 2013.

[160] M. Seredynski, W. Mazurczyk, and D. Khadraoui, “Multi-segment green light optimal speed advisory,” in *2013 IEEE International Symposium on Parallel & Distributed Processing, Workshops and Phd Forum.* IEEE, 2013, pp. 459–465.

[161] J. Li, M. Dridi, and A. El-Moudni, “Multi-vehicles green light optimal speed advisory based on the augmented lagrangian genetic algorithm,” in *17th International IEEE Conference on Intelligent Transportation Systems (ITSC).* IEEE, 2014, pp. 2434–2439.

[162] M. Staubach, N. Schebitz, F. Köster, and D. Kuck, “Evaluation of an eco-driving support system,” *Transportation research part F: traffic psychology and behaviour*, vol. 27, pp. 11–21, 2014.

[163] R. T. van Katwijk and S. Gabriel, “Optimising a vehicle’s approach towards an adaptively controlled intersection,” *IET Intelligent Transport Systems*, vol. 9, no. 5, pp. 479–487, 2015.

[164] S. Stebbins, J. Kim, M. Hickman, and H. L. Vu, “Combining model predictive intersection control with green light optimal speed advisory in a connected vehicle environment,” in *Australasian Transport Research Forum (ATRF), 38th, 2016, Melbourne, Victoria, Australia*, 2016.

[165] N. Wan, A. Vahidi, and A. Luckow, “Optimal speed advisory for connected vehicles in arterial roads and the impact on mixed traffic,” *Transportation Research Part C: Emerging Technologies*, vol. 69, pp. 548 – 563, 2016.

[166] G. De Nunzio, C. C. De Wit, P. Moulin, and D. Di Domenico, “Ecodriving in urban traffic networks using traffic signals information,” *International Journal of Robust and Nonlinear Control*, vol. 26, no. 6, pp. 1307–1324, 2016.

[167] S. Stebbins, M. Hickman, J. Kim, and H. L. Vu, "Characterising green light optimal speed advisory trajectories for platoon-based optimisation," *Transportation Research Part C: Emerging Technologies*, vol. 82, pp. 43–62, 2017.

[168] G. Njobelo, T. Sando, S. Sajjadi, E. Mtoi, M. A. Dulebenets, and J. Sobanjo, "Enhancing the green light optimized speed advisory system to incorporate queue formation," Tech. Rep., 2018.

[169] H. Suzuki and Y. Marumo, "A new approach to green light optimal speed advisory (glosa) systems and its limitations in traffic flows," in *International Conference on Human Systems Engineering and Design: Future Trends and Applications.* Springer, 2018, pp. 776–782.

[170] ——, "Evaluating green light optimum speed advisory (glosa) system in traffic flow with information distance variations," in *International Conference on Human Interaction and Emerging Technologies.* Springer, 2019, pp. 502–508.

[171] K. McConky and V. Rungta, "Donâ€™t pass the automated vehicles!: System level impacts of multi-vehicle cav control strategies," *Transportation Research Part C: Emerging Technologies*, vol. 100, pp. 289–305, 2019.

[172] C. Guardiola, B. Pla, V. Pandey, and R. Burke, "On the potential of traffic light information availability for reducing fuel consumption and nox emissions of a diesel light-duty vehicle," *Proceedings of the Institution of Mechanical Engineers, Part D: Journal of Automobile Engineering*, p. 0954407019867167, 2019.

[173] C. Masera, M. Imprialou, L. Budd, and C. Morton, "Estimating the traffic impacts of green light optimal speed advisory systems using microsimulation," *International Journal of Transport and Vehicle Engineering*, vol. 13, no. 1, pp. 22–29, 2019.

[174] L. Simchon and R. Rabinovici, "Real-time implementation of green light optimal speed advisory for electric vehicles," *Vehicles*, vol. 2, no. 1, pp. 35–54, 2020.

[175] Z. Zhang, Y. Zou, X. Zhang, and T. Zhang, "Green light optimal speed advisory system designed for electric vehicles considering queuing effect and driverâ€™s speed tracking error," *IEEE Access*, 2020.

[176] G. Scora and M. Barth, "Comprehensive modal emissions model (cmem), version 3.01," *User guide. Centre for environmental research and technology. University of California, Riverside*, vol. 1070, 2006.

[177] D. Biggs and R. Akcelik, "An energy-related model of instantaneous fuel consumption," *Traffic engineering and control*, vol. 27, pp. 320–325, 1986.

[178] K. Ahn, H. Rakha, A. Trani, and M. Van Aerde, "Estimating vehicle fuel consumption and emissions based on instantaneous speed and acceleration levels," *Journal of transportation engineering*, vol. 128, no. 2, pp. 182–190, 2002.

[179] M. Sharara, M. Ibrahim, and G. Chalhoub, "Impact of network performance on glosa," in *2019 16th IEEE Annual Consumer Communications & Networking Conference (CCNC)*. IEEE, 2019, pp. 1–6.

[180] W. Tian, "A review of sensitivity analysis methods in building energy analysis," *Renewable and Sustainable Energy Reviews*, vol. 20, pp. 411–419, 2013.

[181] S. Hausberger, M. Rexeis, M. Zallinger, and R. Luz, "Emission factors from the model phem for the hbefa version 3. report nr," I-20/2009 Haus-Em 33/08/679 from 07.12, Tech. Rep., 2009.

[182] N. Geroliminis and C. F. Daganzo, "Existence of urban-scale macroscopic fundamental diagrams: Some experimental findings," *Transportation Research Part B: Methodological*, vol. 42, no. 9, pp. 759–770, 2008.

[183] D. Ni, *Traffic flow theory: Characteristics, experimental methods, and numerical techniques*. Butterworth-Heinemann, 2015.

[184] F. V. Webster, "Traffic signal settings," Tech. Rep., 1958.

[185] Y. Huang, E. C. Ng, J. L. Zhou, N. C. Surawski, E. F. Chan, and G. Hong, "Eco-driving technology for sustainable road transport: A review," *Renewable and Sustainable Energy Reviews*, vol. 93, pp. 596–609, 2018.

[186] C. J. Wu and M. S. Hamada, *Experiments: planning, analysis, and optimization.* John Wiley & Sons, 2011, vol. 552.

[187] M. Xu, D. Fralick, J. Z. Zheng, B. Wang, X. M. Tu, and C. Feng, "The differences and similarities between two-sample t-test and paired t-test," *Shanghai archives of psychiatry*, vol. 29, no. 3, p. 184, 2017.

[188] W. H. Kruskal and W. A. Wallis, "Use of ranks in one-criterion variance analysis," *Journal of the American statistical Association*, vol. 47, no. 260, pp. 583–621, 1952.

[189] F. Murena, M. V. Prati, and M. A. Costagliola, "Real driving emissions of a scooter and a passenger car in naples city," *Transportation Research Part D: Transport and Environment*, vol. 73, pp. 46–55, 2019.

[190] M. Weiss, K. C. Cloos, and E. Helmers, "Energy efficiency trade-offs in small to large electric vehicles," *Environmental Sciences Europe*, vol. 32, no. 1, pp. 1–17, 2020.

[191] T. Kurczveil, P. Á. López, and E. Schnieder, "Implementation of an energy model and a charging infrastructure in sumo," in *Simulation of Urban MObility User Conference.* Springer, 2013, pp. 33–43.

[192] D. Krajzewicz, M. Behrisch, P. Wagner, R. Luz, and M. Krumnow, "Second generation of pollutant emission models for sumo," in *Modeling mobility with open data.* Springer, 2015, pp. 203–221.

[193] I. Sagaama, A. Kchiche, W. Trojet, and F. Kamoun, "Evaluation of the energy consumption model performance for electric vehicles in sumo," in *2019 IEEE/ACM 23rd International Symposium on Distributed Simulation and Real Time Applications (DS-RT).* IEEE, 2019, pp. 1–8.

[194] R. M. Harrison, T. Van Vu, H. Jafar, and Z. Shi, "More mileage in reducing urban air pollution from road traffic," *Environment International*, vol. 149, p. 106329, 2021.

[195] J. F. Paredes, G. P. Cazar, and M. Donkers, "A shrinking horizon approach to eco-driving for electric city buses: Implementation and experimental results," *IFAC-PapersOnLine*, vol. 52, no. 5, pp. 556–561, 2019.

[196] I. Jeffreys, G. Graves, and M. Roth, "Evaluation of eco-driving training for vehicle fuel use and emission reduction: A case study in australia," *Transportation Research Part D: Transport and Environment*, vol. 60, pp. 85–91, 2018.

[197] A. Sciarretta, G. De Nunzio, and L. L. Ojeda, "Optimal ecodriving control: Energy-efficient driving of road vehicles as an optimal control problem," *IEEE Control Systems Magazine*, vol. 35, no. 5, pp. 71–90, 2015.

[198] E. Ozatay, S. Onori, J. Wollaeger, U. Ozguner, G. Rizzoni, D. Filev, J. Michelini, and S. Di Cairano, "Cloud-based velocity profile optimization for everyday driving: A dynamic-programming-based solution," *IEEE Transactions on Intelligent Transportation Systems*, vol. 15, no. 6, pp. 2491–2505, 2014.

[199] T. Schwickart, H. Voos, J.-R. Hadji-Minaglou, and M. Darouach, "A fast model-predictive speed controller for minimised charge consumption of electric vehicles," *Asian Journal of Control*, vol. 18, no. 1, pp. 133–149, 2016.

[200] M. Batra, J. McPhee, and N. L. Azad, "Anti-jerk model predictive cruise control for connected electric vehicles with changing road conditions," in *2017 11th Asian Control Conference (ASCC)*. IEEE, 2017, pp. 49–54.

[201] S. A. Sajadi-Alamdari, H. Voos, and M. Darouach, "Nonlinear model predictive control for ecological driver assistance systems in electric vehicles," *Robotics and Autonomous Systems*, vol. 112, pp. 291–303, 2019.

[202] M. Amodeo, M. Di Vaio, A. Petrillo, A. Salvi, and S. Santini, "Optimization of fuel consumption and battery life cycle in a fleet of connected hybrid electric vehicles via distributed nonlinear model predictive control," in *2018 European Control Conference (ECC)*. IEEE, 2018, pp. 947–952.

[203] E. Kim, J. Kim, and M. Sunwoo, "Model predictive control strategy for smooth path tracking of autonomous vehicles with steering actuator dynamics," *International Journal of Automotive Technology*, vol. 15, no. 7, pp. 1155–1164, 2014.

[204] J. Ji, A. Khajepour, W. W. Melek, and Y. Huang, "Path planning and tracking for vehicle collision avoidance based on model predictive control with multiconstraints," *IEEE Transactions on Vehicular Technology*, vol. 66, no. 2, pp. 952–964, 2016.

[205] S. Cheng, L. Li, H.-Q. Guo, Z.-G. Chen, and P. Song, "Longitudinal collision avoidance and lateral stability adaptive control system based on mpc of autonomous vehicles," *IEEE Transactions on Intelligent Transportation Systems*, vol. 21, no. 6, pp. 2376–2385, 2019.

[206] M. A. Daoud, M. Osman, M. W. Mehrez, and W. W. Melek, "Path-following and adjustable driving behavior of autonomous vehicles using dual-objective nonlinear mpc," in *2019 IEEE International Conference on Vehicular Electronics and Safety (ICVES)*. IEEE, 2019, pp. 1–6.

[207] "Integrated vehicle dynamics control via coordination of active front steering and rear braking," *European Journal of Control*, vol. 19, no. 2, pp. 121 – 143, 2013.

[208] M. Canale, L. Fagiano, M. Milanese, and P. Borodani, "Robust vehicle yaw control using active differential and internal model control techniques," in *2006 American Control Conference*, 2006.

[209] T. D. Gillespie, *Fundamentals of vehicle dynamics*. Society of automotive engineers Warrendale, PA, 1992, vol. 400.

[210] V. Milanés and S. E. Shladover, "Modeling cooperative and autonomous adaptive cruise control dynamic responses using experimental data," *Transportation Research Part C: Emerging Technologies*, vol. 48, pp. 285–300, 2014.

[211] G. N. Bifulco, B. Caiazzo, A. Coppola, and S. Santini, "Intersection crossing in mixed traffic flow environment leveraging v2x information," in *2019 IEEE International Conference on Connected Vehicles and Expo (ICCVE)*, 2019, pp. 1–6.

[212] G. Padilla, C. Pelosi, C. Beckers, and M. Donkers, "Eco-driving for energy efficient cornering of electric vehicles in urban scenarios," *IFAC-PapersOnLine*, vol. 53, no. 2, pp. 13 816–13 821, 2020.

[213] T. Litman, *Autonomous vehicle implementation predictions.* Victoria Transport Policy Institute Victoria, Canada, 2017.

[214] Gartner.

[215] D. Hajdu, I. G. Jin, T. Insperger, and G. Orosz, "Robust design of connected cruise control among human-driven vehicles," *IEEE Transactions on Intelligent Transportation Systems*, vol. 21, no. 2, pp. 749–761, 2019.

[216] I. G. Jin and G. Orosz, "Connected cruise control among human-driven vehicles: Experiment-based parameter estimation and optimal control design," *Transportation research part C: emerging technologies*, vol. 95, pp. 445–459, 2018.

[217] W. B. Qin and G. Orosz, "Experimental validation on connected cruise control with flexible connectivity topologies," *IEEE/ASME Transactions on Mechatronics*, vol. 24, no. 6, pp. 2791–2802, 2019.

[218] E. Benalia, S. Bitam, and A. Mellouk, "Data dissemination for internet of vehicle based on 5g communications: A survey," *Transactions on Emerging Telecommunications Technologies*, vol. 31, no. 5, p. e3881, 2020.

[219] J. Howell, "Number of connected iot devices will surge to 125 billion by 2030, ihs markit says," *IHS Markit Technology, Oct*, vol. 24, 2017.

[220] Z. Mahmood, *Connected Vehicles in the Internet of Things*. Springer, 2020.

[221] A. Kashevnik, I. Lashkov, A. Ponomarev, N. Teslya, and A. Gurtov, "Cloud-based driver monitoring system using a smartphone," *IEEE Sensors Journal*, vol. 20, no. 12, pp. 6701–6715, 2020.

[222] E.-H. Choi, "Crash factors in intersection-related crashes: An on-scene perspective," Tech. Rep., 2010.

[223] Q. Guo, L. Li, and X. J. Ban, "Urban traffic signal control with connected and automated vehicles: A survey," *Transportation research part C: emerging technologies*, 2019.

[224] T. Board, "Hcm 2010-highway capacity manual," *National Research Council*, 2010.

[225] Z. Wang, G. Wu, and M. J. Barth, "Cooperative eco-driving at signalized intersections in a partially connected and automated vehicle environment," *IEEE Transactions on Intelligent Transportation Systems*, 2019.

[226] A. Validi, T. Ludwig, A. Hussein, and C. Olaverri-Monreal, "Examining the impact on road safety of different penetration rates of vehicle-to-vehicle communication and adaptive cruise control," *IEEE Intelligent Transportation Systems Magazine*, vol. 10, no. 4, pp. 24–34, 2018.

[227] P. Chen, J. Sun, and H. Qi, "Estimation of delay variability at signalized intersections for urban arterial performance evaluation," *Journal of Intelligent Transportation Systems*, vol. 21, no. 2, pp. 94–110, 2017.

[228] Y. Chen, J. Zha, and J. Wang, "An autonomous t-intersection driving strategy considering oncoming vehicles based on connected vehicle technology," *IEEE/ASME Transactions on Mechatronics*, vol. 24, no. 6, pp. 2779–2790, 2019.

[229] Y. Zhang and C. G. Cassandras, "An impact study of integrating connected automated vehicles with conventional traffic," *Annual Reviews in Control*, 2019.

[230] J. Dahl, G. R. de Campos, C. Olsson, and J. Fredriksson, "Collision avoidance: a literature review on threat-assessment techniques," *IEEE Transactions on Intelligent Vehicles*, vol. 4, no. 1, pp. 101–113, 2018.

[231] R. Sengupta, S. Rezaei, S. E. Shladover, D. Cody, S. Dickey, and H. Krishnan, "Cooperative collision warning systems: Concept definition and experimental implementation," *Journal of Intelligent Transportation Systems*, vol. 11, no. 3, pp. 143–155, 2007.

[232] J. M. Scanlon, R. Sherony, and H. C. Gabler, "Earliest sensor detection opportunity for left turn across path opposite direction crashes," *IEEE Transactions on Intelligent Vehicles*, vol. 2, no. 1, pp. 62–70, 2017.

[233] I. Mahdinia, A. Mohammadnazar, R. Arvin, and A. J. Khattak, "Integration of automated vehicles in mixed traffic: Evaluating changes in performance of following human-driven vehicles," *Accident Analysis & Prevention*, vol. 152, p. 106006, 2021.

[234] A. Sinha, S. Chand, K. P. Wijayaratna, N. Virdi, and V. Dixit, "Comprehensive safety assessment in mixed fleets with connected and automated vehicles: A crash severity and rate evaluation of conventional vehicles," *Accident Analysis & Prevention*, vol. 142, p. 105567, 2020.

[235] R. J. Harrington, C. Senatore, J. M. Scanlon, and R. M. Yee, "The role of infrastructure in an automated vehicle future," *The Bridge*, vol. 48, no. 2, 2018.

[236] K. Gao, S. Huang, J. Xie, N. N. Xiong, and R. Du, "A review of research on intersection control based on connected vehicles and data-driven intelligent approaches," *Electronics*, vol. 9, no. 6, p. 885, 2020.

[237] K. Zhang, C. Xie, Y. Wang, M. Wang, A. de La Fortelle, W. Zhang, and Z. Duan, "Service-oriented cooperation policies for intelligent ground vehicles approaching intersections," *Applied Sciences*, vol. 8, no. 9, p. 1647, 2018.

[238] J. Khoury, J. Khoury, G. Zouein, and J.-P. Arnaout, "A practical decentralized access protocol for autonomous vehicles at isolated under-saturated intersections," *Journal of Intelligent Transportation Systems*, vol. 23, no. 5, pp. 427–440, 2019.

[239] H. C. Manual, "Hcm2010," *Transportation Research Board, National Research Council, Washington, DC*, p. 1207, 2010.

[240] S. Krauß, P. Wagner, and C. Gawron, "Metastable states in a microscopic model of traffic flow," *Physical Review E*, vol. 55, no. 5, p. 5597, 1997.

[241] L. Zhang and G. Orosz, "Motif-based design for connected vehicle systems in presence of heterogeneous connectivity structures and time delays," *IEEE Transactions on Intelligent Transportation Systems*, vol. 17, no. 6, pp. 1638–1651, 2016.

[242] D. Ngoduy and T. Li, "Hopf bifurcation structure of a generic car-following model with multiple time delays," *Transportmetrica A: Transport Science*, pp. 1–19, 2020.

[243] J. Kaths and S. Krause, "Integrated simulation of microscopic traffic flow and vehicle dynamics," in *IPG Apply & Innovate 2016*, 2016.

[244] M. Doumiati, O. Sename, L. Dugard, J.-J. Martinez-Molina, P. Gaspar, and Z. Szabo, "Integrated vehicle dynamics control via coordination of active front steering and rear braking," *European Journal of Control*, vol. 19, no. 2, pp. 121–143, 2013.

[245] M. Di Vaio, P. Falcone, R. Hult, A. Petrillo, A. Salvi, and S. Santini, "Design and experimental validation of a distributed interaction protocol for connected autonomous vehicles at a road intersection," *IEEE Transactions on Vehicular Technology*, vol. 68, no. 10, pp. 9451–9465, 2019.

[246] L. Hu, J. Ou, J. Huang, Y. Chen, and D. Cao, "A review of research on traffic conflicts based on intelligent vehicles," *Ieee Access*, vol. 8, pp. 24 471–24 483, 2020.

[247] A. Arikere, D. Yang, and M. Klomp, "Optimal motion control for collision avoidance at left turn across path/opposite direction intersection scenarios using electric propulsion," *Vehicle system dynamics*, vol. 57, no. 5, pp. 637–664, 2019.

[248] C. Backfrieder and G. Ostermayer, "Modeling a continuous and accident-free intersection control for vehicular traffic in traffsim," in *2014 European Modelling Symposium*. IEEE, 2014, pp. 332–337.

[249] G. M. Hoffmann, C. J. Tomlin, M. Montemerlo, and S. Thrun, "Autonomous automobile trajectory tracking for off-road driving: Controller design, experimental validation and racing," in *2007 American Control Conference*. IEEE, 2007, pp. 2296–2301.

[250] E. Borhaug and K. Y. Pettersen, "Cross-track control for underactuated autonomous vehicles," in *Proceedings of the 44th IEEE Conference on Decision and Control*. IEEE, 2005, pp. 602–608.

[251] A. Mirheli, M. Tajalli, L. Hajibabai, and A. Hajbabaie, "A consensus-based distributed trajectory control in a signal-free intersection," *Transportation research part C: emerging technologies*, vol. 100, pp. 161–176, 2019.

[252] S. S. Mahmud, L. Ferreira, M. S. Hoque, and A. Tavassoli, "Application of proximal surrogate indicators for safety evaluation: A review of recent developments and research needs," *IATSS research*, vol. 41, no. 4, pp. 153–163, 2017.

[253] D. Jia and D. Ngoduy, "Platoon based cooperative driving model with consideration of realistic inter-vehicle communication," *Transportation Research Part C: Emerging Technologies*, vol. 68, pp. 245–264, 2016.

[254] P. Liu, U. Ozguner, and Y. Zhang, "Distributed mpc for cooperative highway driving and energy-economy validation via microscopic simulations," *Transportation Research Part C: Emerging Technologies*, vol. 77, pp. 80–95, 2017.

[255] K. Li, F. Gao, S. E. Li, Y. Zheng, and H. Gao, "Robust cooperation of connected vehicle systems with eigenvalue-bounded interaction

topologies in the presence of uncertain dynamics," *Frontiers of Mechanical Engineering*, vol. 13, no. 3, pp. 354–367, 2018.

[256] A. Petrillo, A. Pescape, and S. Santini, "A secure adaptive control for cooperative driving of autonomous connected vehicles in the presence of heterogeneous communication delays and cyberattacks," *IEEE transactions on cybernetics*, 2020.

[257] Y. Zhu, J. Wu, and H. Su, "V2v-based cooperative control of uncertain, disturbed and constrained nonlinear cavs platoon," *IEEE Transactions on Intelligent Transportation Systems*, 2020.

[258] J. Hu, P. Bhowmick, F. Arvin, A. Lanzon, and B. Lennox, "Cooperative control of heterogeneous connected vehicle platoons: An adaptive leader-following approach," *IEEE Robotics and Automation Letters*, vol. 5, no. 2, pp. 977–984, 2020.

[259] W. Yue, G. Guo, L. Wang, and W. Wang, "Nonlinear platoon control of arduino cars with range-limited sensors," *International Journal of Control*, vol. 88, no. 5, pp. 1037–1050, 2015.

[260] Y. Zhu and F. Zhu, "Barrier-function-based distributed adaptive control of nonlinear cavs with parametric uncertainty and full-state constraint," *Transportation Research Part C: Emerging Technologies*, vol. 104, pp. 249–264, 2019.

[261] M. Yan, J. Song, L. Zuo, and P. Yang, "Neural adaptive sliding-mode control of a vehicle platoon using output feedback," *Energies*, vol. 10, no. 11, p. 1906, 2017.

[262] S. E. Li, X. Qin, K. Li, J. Wang, and B. Xie, "Robustness analysis and controller synthesis of homogeneous vehicular platoons with bounded parameter uncertainty," *IEEE/ASME Transactions on Mechatronics*, vol. 22, no. 2, pp. 1014–1025, 2017.

[263] C. K. Verginis, C. P. Bechlioulis, D. V. Dimarogonas, and K. J. Kyriakopoulos, "Robust distributed control protocols for large vehicular platoons with prescribed transient and steady-state performance," *IEEE Transactions on Control Systems Technology*, vol. 26, no. 1, pp. 299–304, 2017.

[264] G. Feng, D. Dang, and Y. He, "Robust coordinated control of nonlinear heterogeneous platoon interacted by uncertain topology," *IEEE Transactions on Intelligent Transportation Systems*, 2020.

[265] Q. Luo, A.-T. Nguyen, J. Fleming, and H. Zhang, "Unknown input observer based approach for distributed tube-based model predictive control of heterogeneous vehicle platoons," *IEEE Transactions on Vehicular Technology*, 2021.

[266] S. Santini, A. Salvi, A. S. Valente, A. Pescapè, M. Segata, and R. L. Cigno, "Platooning maneuvers in vehicular networks: A distributed and consensus-based approach," *IEEE Transactions on Intelligent Vehicles*, vol. 4, no. 1, pp. 59–72, 2018.

[267] Z. Wang, G. Wu, and M. J. Barth, "Developing a distributed consensus-based cooperative adaptive cruise control system for heterogeneous vehicles with predecessor following topology," *Journal of Advanced Transportation*, vol. 2017, 2017.

[268] S. Baldi, M. R. Rosa, P. Frasca, and E. B. Kosmatopoulos, "Platooning merging maneuvers in the presence of parametric uncertainty," *IFAC-PapersOnLine*, vol. 51, no. 23, pp. 148–153, 2018.

[269] D. Bevly, X. Cao, M. Gordon, G. Ozbilgin, D. Kari, B. Nelson, J. Woodruff, M. Barth, C. Murray, A. Kurt *et al.*, "Lane change and merge maneuvers for connected and automated vehicles: A survey," *IEEE Transactions on Intelligent Vehicles*, vol. 1, no. 1, pp. 105–120, 2016.

[270] D. Li and G. Guo, "Prescribed performance concurrent control of connected vehicles with nonlinear third-order dynamics," *IEEE Transactions on Vehicular Technology*, 2020.

[271] Y. Li, C. Tang, K. Li, S. Peeta, X. He, and Y. Wang, "Nonlinear finite-time consensus-based connected vehicle platoon control under fixed and switching communication topologies," *Transportation Research Part C: Emerging Technologies*, vol. 93, pp. 525–543, 2018.

[272] Z. Yu, H. Jiang, D. Huang, and C. Hu, "Consensus of nonlinear multi-agent systems with directed switching graphs: a directed spanning tree based error system approach," *Nonlinear Analysis: Hybrid Systems*, vol. 28, pp. 123–140, 2018.

[273] D. Liberzon, *Switching in systems and control.* Springer Science & Business Media, 2003.

[274] A. Shariati, H. Taghirad, and A. Fatehi, "A neutral system approach to H_∞ PD/PI controller design of processes with uncertain input delay," *J. Process Contr.*, vol. 24, no. 3, pp. 144–157, 2014.

[275] S. Boyd, L. El Ghaoui, E. Feron, and V. Balakrishnan, *Linear matrix inequalities in system and control theory.* Siam, 1994, vol. 15.

[276] S. Xu, J. Lam, and Y. Zou, "New results on delay-dependent robust hâˆž control for systems with time-varying delays," *Automatica*, vol. 42, no. 2, pp. 343–348, 2006.

[277] H. Lin and P. J. Antsaklis, "Stability and stabilizability of switched linear systems: a survey of recent results," *IEEE Transactions on Automatic control*, vol. 54, no. 2, pp. 308–322, 2009.

[278] A. S. Morse, "Supervisory control of families of linear set-point controllers-part i. exact matching," *IEEE transactions on Automatic Control*, vol. 41, no. 10, pp. 1413–1431, 1996.

[279] J. Lofberg, "Yalmip: A toolbox for modeling and optimization in matlab," in *2004 IEEE international conference on robotics and automation (IEEE Cat. No. 04CH37508).* IEEE, 2004, pp. 284–289.

[280] R. Firoozi, X. Zhang, and F. Borrelli, "Formation and reconfiguration of tight multi-lane platoons," *Control Engineering Practice*, vol. 108, p. 104714, 2021.

[281] A. Paranjothi, M. Atiquzzaman, and M. S. Khan, "Pmcd: Platoon-merging approach for cooperative driving," *Internet Technology Letters*, vol. 3, no. 1, p. e139, 2020.

[282] M. Segata, B. Bloessl, S. Joerer, F. Dressler, and R. L. Cigno, "Supporting platooning maneuvers through ivc: An initial protocol analysis for the join maneuver," in *2014 11th Annual conference on wireless on-demand network systems and services (WONS)*. IEEE, 2014, pp. 130–137.

[283] W. Zhao, D. Ngoduy, S. Shepherd, R. Liu, and M. Papageorgiou, "A platoon based cooperative eco-driving model for mixed automated and human-driven vehicles at a signalised intersection," *Transportation Research Part C: Emerging Technologies*, vol. 95, pp. 802–821, 2018.

[284] W. Alasmary and W. Zhuang, "Mobility impact in ieee 802.11 p infrastructureless vehicular networks," *Ad Hoc Networks*, vol. 10, no. 2, pp. 222–230, 2012.

[285] D. Jia, K. Lu, J. Wang, X. Zhang, and X. Shen, "A survey on platoon-based vehicular cyber-physical systems," *IEEE communications surveys & tutorials*, vol. 18, no. 1, pp. 263–284, 2015.

[286] D. G. Lui, A. Petrillo, and S. Santini, "An optimal distributed pid-like control for the output containment and leader-following of heterogeneous high-order multi-agent systems," *Information Sciences*, vol. 541, pp. 166–184, 2020.

[287] D. Zhang, Y.-P. Shen, S.-Q. Zhou, X.-W. Dong, and L. Yu, "Distributed secure platoon control of connected vehicles subject to dos attack: theory and application," *IEEE Transactions on Systems, Man, and Cybernetics: Systems*, 2020.

[288] G. Fiengo, D. G. Lui, A. Petrillo, and S. Santini, "Distributed robust output consensus for linear multi-agent systems with input time-varying delays and parameter uncertainties," *IET Control Theory & Applications*, vol. 13, no. 2, pp. 203–212, 2018.

[289] Y. Zhu and F. Zhu, "Distributed adaptive longitudinal control for uncertain third-order vehicle platoon in a networked environment," *IEEE Transactions on Vehicular Technology*, vol. 67, no. 10, pp. 9183–9197, 2018.

[290] Z. Ju, H. Zhang, and Y. Tan, "Distributed deception attack detection in platoon-based connected vehicle systems," *IEEE Transactions on Vehicular Technology*, vol. 69, no. 5, pp. 4609–4620, 2020.

[291] Y. Abou Harfouch, S. Yuan, and S. Baldi, "An adaptive switched control approach to heterogeneous platooning with intervehicle communication losses," *IEEE Transactions on Control of Network Systems*, vol. 5, no. 3, pp. 1434–1444, 2017.

[292] Y. Cao and W. Ren, "Finite-time consensus for multi-agent networks with unknown inherent nonlinear dynamics," *Automatica*, vol. 50, no. 10, pp. 2648–2656, 2014.

[293] X. Lu, Y. Wang, X. Yu, and J. Lai, "Finite-time control for robust tracking consensus in mass with an uncertain leader," *IEEE transactions on cybernetics*, vol. 47, no. 5, pp. 1210–1223, 2016.

[294] X.-G. Guo, J.-L. Wang, F. Liao, and R. S. H. Teo, "String stability of heterogeneous leader-following vehicle platoons based on constant spacing policy," in *2016 IEEE Intelligent Vehicles Symposium (IV)*. IEEE, 2016, pp. 761–766.

[295] Z.-H. Guan, F.-L. Sun, Y.-W. Wang, and T. Li, "Finite-time consensus for leader-following second-order multi-agent networks," *IEEE Transactions on Circuits and Systems I: Regular Papers*, vol. 59, no. 11, pp. 2646–2654, 2012.

[296] L. Wang and F. Xiao, "Finite-time consensus problems for networks of dynamic agents," *IEEE Transactions on Automatic Control*, vol. 55, no. 4, pp. 950–955, 2010.

[297] Z. Zuo, Q.-L. Han, B. Ning, X. Ge, and X.-M. Zhang, "An overview of recent advances in fixed-time cooperative control of multiagent systems," *IEEE Transactions on Industrial Informatics*, vol. 14, no. 6, pp. 2322–2334, 2018.

[298] A. Polyakov, "Nonlinear feedback design for fixed-time stabilization of linear control systems," *IEEE Transactions on Automatic Control*, vol. 57, no. 8, pp. 2106–2110, 2011.

[299] B. Tian, Z. Zuo, and H. Wang, "Leader–follower fixed-time consensus of multi-agent systems with high-order integrator dynamics," *International Journal of Control*, vol. 90, no. 7, pp. 1420–1427, 2017.

[300] Z. Zuo, "Nonsingular fixed-time consensus tracking for second-order multi-agent networks," *Automatica*, vol. 54, pp. 305–309, 2015.

[301] S. P. Bhat and D. S. Bernstein, "Finite-time stability of continuous autonomous systems," *SIAM Journal on Control and Optimization*, vol. 38, no. 3, pp. 751–766, 2000.

[302] O. Egbue and S. Long, "Barriers to widespread adoption of electric vehicles: An analysis of consumer attitudes and perceptions," *Energy policy*, vol. 48, pp. 717–729, 2012.

[303] J. Guo, W. Jingyao, K. Li, and Y. Luo, "Adaptive non-linear coordinated optimal dynamic platoon control of connected autonomous distributed electric vehicles on curved roads," *IET Intelligent Transport Systems*, vol. 14, no. 12, pp. 1626–1637, 2020.

[304] X. He and X. Wu, "Eco-driving advisory strategies for a platoon of mixed gasoline and electric vehicles in a connected vehicle system," *Transportation Research Part D: Transport and Environment*, vol. 63, pp. 907–922, 2018.

[305] W. J. Lee, S. I. Kwag, and Y. D. Ko, "The optimal eco-friendly platoon formation strategy for a heterogeneous fleet of vehicles," *Transportation Research Part D: Transport and Environment*, vol. 90, p. 102664, 2021.

[306] S. Gong, A. Zhou, and S. Peeta, "Cooperative adaptive cruise control for a platoon of connected and autonomous vehicles considering dynamic information flow topology," *Transportation Research Record*, vol. 2673, no. 10, pp. 185–198, 2019.

[307] J. Chen, H. Liang, J. Li, and Z. Xu, "A novel distributed cooperative approach for mixed platoon consisting of connected and automated vehicles and human-driven vehicles," *Physica A: Statistical Mechanics and its Applications*, vol. 573, p. 125939, 2021.

[308] F. Ma, Y. Yang, J. Wang, Z. Liu, J. Li, J. Nie, Y. Shen, and L. Wu, "Predictive energy-saving optimization based on nonlinear model predictive control for cooperative connected vehicles platoon with v2v communication," *Energy*, vol. 189, p. 116120, 2019.

[309] L. Xu, W. Zhuang, G. Yin, and C. Bian, "Energy-oriented cruising strategy design of vehicle platoon considering communication delay and disturbance," *Transportation Research Part C: Emerging Technologies*, vol. 107, pp. 34–53, 2019.

[310] F. Ma, Y. Yang, J. Wang, X. Li, G. Wu, Y. Zhao, L. Wu, B. Aksun-Guvenc, and L. Guvenc, "Eco-driving-based cooperative adaptive cruise control of connected vehicles platoon at signalized intersections," *Transportation Research Part D: Transport and Environment*, vol. 92, p. 102746, 2021.

[311] H. Köroğlu, M. Mirzaei, P. Falcone, and S. Krajnović, "Platoon control under a novel leader and predecessor following scheme with the use of an advanced aerodynamic model," *Journal of Dynamic Systems, Measurement, and Control*, vol. 140, no. 4, 2018.

[312] V. Turri, "Look-ahead control for fuel-efficient and safe heavy-duty vehicle platooning," Ph.D. dissertation, KTH Royal Institute of Technology, 2018.

[313] A. Wasserburger, A. Schirrer, and C. Hametner, "Stochastic optimization for energy-efficient cooperative platooning," in *2019 IEEE Vehicle Power and Propulsion Conference (VPPC)*. IEEE, 2019, pp. 1–6.

[314] S. F. Tie and C. W. Tan, "A review of energy sources and energy management system in electric vehicles," *Renewable and sustainable energy reviews*, vol. 20, pp. 82–102, 2013.

[315] L. M. Castiglione, P. Falcone, A. Petrillo, S. P. Romano, and S. Santini, "Cooperative intersection crossing over 5g," *IEEE/ACM Transactions on Networking*, vol. 29, no. 1, pp. 303–317, 2020.

[316] J. Ryu and J. C. Gerdes, "Integrating inertial sensors with global positioning system (gps) for vehicle dynamics control," *Journal of*

Dynamic Systems, Measurement, and Control, vol. 126, no. 2, pp. 243–254, 2004.

[317] S. Manfredi, A. Petrillo, and S. Santini, "Distributed pi control for heterogeneous nonlinear platoon of autonomous connected vehicles," *IFAC-PapersOnLine*, vol. 53, no. 2, pp. 15 229–15 234, 2020.

[318] A. Coppola, A. Petrillo, R. Rizzo, and S. Santini, "Adaptive cruise control for autonomous electric vehicles based on q-learning algorithm," in *2021 AEIT International Annual Conference (AEIT)*. IEEE, 2021, pp. 1–6.

[319] W. Hucho and G. Sovran, "Aerodynamics of road vehicles," *Annual review of fluid mechanics*, vol. 25, no. 1, pp. 485–537, 1993.

[320] M. Mirzaei and S. Krajnović, "Numerical simulation of two vehicles at short distances in a platoon," in *First International Conference in Numerical and Experimental Aerodynamics of Road Vehicles and Trains (Aerovehicles 1), Bordeaux, France, June*, 2014, pp. 23–25.

[321] F. Cosimi, P. Dini, S. Giannetti, M. Petrelli, and S. Saponara, "Analysis and design of a non-linear mpc algorithm for vehicle trajectory tracking and obstacle avoidance," in *International Conference on Applications in Electronics Pervading Industry, Environment and Society*. Springer, 2020, pp. 229–234.

[322] E. Siampis, E. Velenis, S. Gariuolo, and S. Longo, "A real-time nonlinear model predictive control strategy for stabilization of an electric vehicle at the limits of handling," *IEEE Transactions on Control Systems Technology*, vol. 26, no. 6, pp. 1982–1994, 2017.

[323] R. N. Jazar, *Vehicle dynamics: theory and application*. Springer, 2017.

[324] C. Nowakowski, J. O'Connell, S. E. Shladover, and D. Cody, "Cooperative adaptive cruise control: Driver acceptance of following gap settings less than one second," in *Proceedings of the Human Factors and Ergonomics Society Annual Meeting*, vol. 54, no. 24. SAGE Publications Sage CA: Los Angeles, CA, 2010, pp. 2033–2037.

[325] M. Alhajeri and M. Soroush, "Tuning guidelines for model-predictive control," *Industrial & Engineering Chemistry Research*, vol. 59, no. 10, pp. 4177–4191, 2020.

[326] E. Ali, "Heuristic on-line tuning for nonlinear model predictive controllers using fuzzy logic," *Journal of Process Control*, vol. 13, no. 5, pp. 383–396, 2003.

[327] D. Burk, A. Völz, and K. Graichen, "A modular framework for distributed model predictive control of nonlinear continuous-time systems (grampc-d)," *Optimization and Engineering*, pp. 1–25, 2021.

[328] F. J. Belmonte, S. Martín, E. Sancristobal, J. A. Ruiperez-Valiente, and M. Castro, "Overview of embedded systems to build reliable and safe adas and ad systems," *IEEE Intelligent Transportation Systems Magazine*, 2020.

[329] E. De Gelder, J.-P. Paardekooper, A. K. Saberi, H. Elrofai, J. Ploeg, L. Friedmann, B. De Schutter *et al.*, "Ontology for scenarios for the assessment of automated vehicles," *arXiv preprint arXiv:2001.11507*, 2020.

[330] E. Yurtsever, J. Lambert, A. Carballo, and K. Takeda, "A survey of autonomous driving: Common practices and emerging technologies," *IEEE access*, vol. 8, pp. 58 443–58 469, 2020.